Universidade do Minho
Escola de Engenharia

João Alberto Pinheiro Pereira de Almeida

Innovative and sustainable masonry strengthening system for the rehabilitation and improvement of urban resilience

July 2025

Fundação para a Ciência e a Tecnologia

Innovative and sustainable masonry strengthening system for the rehabilitation and improvement of urban resilience

João Alberto Pinheiro Pereira de Almeida

UMinho | 2025

Universidade do Minho
Escola de Engenharia

João Alberto Pinheiro Pereira de Almeida

Innovative and sustainable masonry strengthening system for the rehabilitation and improvement of urban resilience

Doctoral thesis

Civil engineering

Work performed under the supervision of:
Eduardo Nuno Borges Pereira
Joaquim António de Oliveira Barros

July 2025

Copyright and Terms of Use for Third Party Work.

This dissertation reports on academic work that can be used by third parties as long as the internationally accepted standards and good practices are respected concerning copyright and related rights.

This work can thereafter be used under the terms established in the license below.

Readers needing authorization conditions not provided for in the indicated licensing should contact the author through the RepositóriUM of the University of Minho

License granted to users of this work:



Atribuição-NãoComercial-SemDerivações
CC BY-NC-ND

https://creativecommons.org/licenses/by-nc-nd/4.0/

"O caos é uma ordem por decifrar"

"Chaos is merely order waiting to be deciphered."

José Saramago

ACKNOWLEDGMENTS

This Thesis could not have been accomplished without the contributions of numerous people who have been involved in the process, both directly and indirectly. I am deeply grateful to all of them and would like to express my thanks.

This research was conducted at the Civil Engineering Department of the University of Minho, Portugal, under the supervision of Professor Eduardo Nuno Borges Pereira and co-supervised by Professor Joaquim António de Oliveira Barros. The Portuguese Foundation for the Science and Technology (Fundação para a Ciência e a Tecnologia, FCT) financially supported this work under grant number SFRH/BD/ 115090/2016, grateful acknowledge. This work would not have been possible without the financial support of this institution. I would also like to acknowledge the Institute for Sustainability and Innovation in Structural Engineering (ISISE) for providing facilities and resources.

Above all, I would like to thank my supervisors for their essential assistance, their commitment, and encouragement. For my supervisor Professor Eduardo Pereira I must have a special word of gratitude and appreciation for the scientific guidance, patience and for giving me a push when I needed it. I acknowledge also my co-supervisor Professor Joaquim Barros for all the support and assistance which were crucial for this work. For both I must thank the opportunities to participate in workshops and conferences during this period.

My special thanks for all the support, good advice and training given during these years goes for the technicians from LEST laboratories at the University of Minho, specially to Marco Jorge, António Matos and César Gonçalves and to Carlos Jesus from the LMC laboratory for all the help with the experimental work.

I would like to thank friends and colleagues that I had the pleasure to meet during these PhD years: Leonardo, Susana, Giorgos, Chandan, Fede, Chrysl, Javier, Ton, Angelo, Carlos Barroso and so many others.... A special mention to my friend Reza, thanks for the good Iranian food. I am also very grateful for all the help, inputs and support from my colleagues and friends Ana Rita Neves, Fábio Cruz, Filipa Monteiro, Norma Gaibor, Behzad Zahabizadeh, Isabel Pereira and Rafael Santos.

Finally, I would like to dedicate this work to my family and to my wife Joana. Without love and support, it would have been impossible. I will be eternally grateful to you.

STATEMENT OF INTEGRITY

I hereby declare having conducted this academic work with integrity. I confirm that I have not used plagiarism or any form of undue use of information or falsification of results along the process leading to its elaboration.

I further declare that I have fully acknowledged the Code of Ethical Conduct of the University of Minho.

University of Minho, July 25, 2025



João Alberto Pinheiro Pereira de Almeida

ABSTRACT

The rehabilitation of existing buildings and the enhancement of their architectural quality are pressing challenges in contemporary construction. Many traditional structures, especially in Portugal, were not designed to withstand seismic events, revealing a critical need for efficient and sustainable strengthening systems. At the same time, conventional reinforcement methods are often invasive or incompatible with masonry. In this context, the development of innovative materials and systems, such as fibre-reinforced mortars (FRMs), textile-reinforced mortars (TRMs), and fibre-reinforced cementitious matrices (FRCMs), opens new possibilities. However, key knowledge gaps remain regarding the performance, durability, and adaptability of these systems, particularly when applied to ceramic infill and structural masonry.

This thesis proposes a rehabilitation strategy based on thin overlays of fibre-reinforced mortars (FRMs) as a simple, effective, and sustainable TRM strengthening technique for masonry elements. The research followed a twofold approach: first, developing alternative FRM formulations using sustainable materials, such as recycled aggregates and recycled fibres; second, experimentally characterising these mortars and their effectiveness in reinforcing masonry elements. The study involved extensive testing of fresh and hardened properties of mortars, with a focus on toughness and residual strength, particularly under high temperature exposure. At the structural level, new diagonal tensile test setups were designed to assess the in-plane performance of strengthened masonry under cyclic and biaxial loading, simulating cyclic actions.

The results demonstrate that the proposed FRM system offers significant improvements in mechanical performance and resilience of masonry structures, while maintaining compatibility with masonry substrates. The adaptability of the matrix and fibre components allows tailoring the solution to the needs of different intervention scenarios. Overall, this work contributes to the development of more sustainable and versatile reinforcement techniques for existing masonry buildings, offering a viable path toward increased urban resilience. Nevertheless, future work is needed to address long-term durability and system performance at the urban scale.

KEYWORDS: Alternative binders; Analysis of constructive typologies; In-plane cyclic tests; Masonry strengthening; Textile reinforced mortar

RESUMO

A reabilitação dos edifícios existentes e a valorização da sua qualidade arquitetónica constituem desafios prementes na construção contemporânea. Muitas estruturas tradicionais, especialmente em Portugal, não foram concebidas para resistir a ações sísmicas, revelando a necessidade crítica de sistemas de reforço eficientes e sustentáveis. Simultaneamente, os métodos convencionais de reforço são frequentemente invasivos ou incompatíveis com alvenarias. Neste contexto, o desenvolvimento de materiais e sistemas inovadores, como as argamassas reforçadas com fibras (FRM), as argamassas têxteis reforçadas (TRM) e as matrizes cimentícias reforçadas com fibras (FRCM), abre novas possibilidades. No entanto, persistem lacunas no que diz respeito ao desempenho, durabilidade, particularmente quando aplicados a alvenarias estruturais ou de enchimento.

Esta tese propõe uma estratégia de reabilitação baseada na aplicação de finas camadas de argamassas reforçadas com fibras (FRM), como uma técnica TRM de reforço simples, eficaz e sustentável para elementos de alvenaria. A investigação seguiu uma abordagem em duas fases: por um lado, o desenvolvimento de formulações alternativas de FRM com materiais sustentáveis, incluindo agregados e fibras recicladas; por outro, a caracterização experimental dos sistemas de reforço e da sua eficácia no reforço de elementos de alvenaria. O estudo incluiu ensaios extensivos às propriedades no estado fresco e endurecido das argamassas, com especial enfoque na tenacidade e na resistência residual, nomeadamente após exposição a altas temperaturas. Ao nível estrutural, foram concebidas novas configurações de ensaios de tração diagonal para avaliar o comportamento no plano da alvenaria reforçada sob solicitações cíclicas e biaxiais.

Os resultados demonstram que o sistema FRM proposto proporciona melhorias significativas no desempenho mecânico e na resiliência das estruturas em alvenaria, mantendo a compatibilidade com os substratos existentes. A adaptabilidade da matriz e do conteúdo de fibras permite ajustar a solução às necessidades específicas de diferentes cenários de intervenção. De forma geral, este trabalho contribui para o desenvolvimento de técnicas de reforço mais sustentáveis e versáteis aplicáveis à reabilitação de edifícios em alvenaria, oferecendo um caminho viável para o aumento da resiliência urbana. Ainda assim, será necessário aprofundar o estudo da durabilidade a longo prazo e do desempenho destes sistemas à escala urbana.

KEYWORDS: Argamassa reforçada com malhas; Análise de tipologias construtivas; Ensaios cíclicos no plano; Ligantes alternativos; Reforço de alvenaria

TABLE OF CONTENTS

ACKNOWLEDGMENTS ..... **iv**

ABSTRACT ..... **vi**

RESUMO ..... **vii**

TABLE OF CONTENTS ..... **viii**

LIST OF TABLES ..... **xi**

LIST OF FIGURES ..... **xiv**

LIST OF ABBREVIATIONS AND SYMBOLS ..... **xxii**

1. INTRODUCTION **1**

1.1. BACKGROUND AND MOTIVATION 1

1.2. OBJECTIVES AND RESEARCH METHODOLOGY 3

1.3. OUTLINE OF THE DISSERTATION 4

1.4. REFERENCES 7

2. MASONRY: CHARACTERIZATION, PERFORMANCE AND STRENGHTENING SYSTEMS **9**

2.1. CHARACTERIZATION OF THE BUILDING STOCK: PORTUGAL AND EUROPE 9

2.1.1. Masonry in Portugal: Past, Present and Future 10

2.1.2. Masonry in Europe 13

2.2. SEIMIC RISK AND PUBLIC POLICIES FOR THE SEISMIC STRENGTHENING OF EXISTING BUILDINGS 14

2.3. STRUCTURAL STRENGTHENING OF MASONRY WALLS 19

2.3.1. Scope of Interventions 19

2.3.2. Consolidation, Protection and Strengthening Solutions 21

2.4. EXPERIMENTAL ASSESSMENT OF MASONRY 25

2.4.1. Characterization of in-plane behaviour: compressive behaviour 25

2.4.2. Characterization of in-plane behaviour: shear Behaviour 26
2.4.3. Characterization of the out-of-plane behaviour 29
2.5. FINAL CONSIDERATIONS 31
2.6. REFERENCES 32
3. TEXTILE REINFORCED MORTAR FOR THE STRENGTHENING OF MASONRY 35
3.1. TEXTILE REINFORCED MORTARS 35
3.2. MORTARS 36
3.2.1. Alternative binder matrices 36
3.2.2. Properties after exposure to high temperatures 39
3.3. FIBRES, FABRIC AND MESHES FOR REINFORCEMENT 42
3.3.1. Man-made Fibres 42
3.3.2. Natural Fibres 45
3.3.3. Microfibres 47
3.3.4. Fabric and Meshes 49
3.4. CHARACTERIZATION OF TEXTILE REINFORCED MORTAR (TRM) 50
3.4.1. Bond behaviour characterization 50
3.4.2. Mechanical behaviour of TRM 54
3.5. DURABILITY 57
3.6. TRM STRENGTHENING EFFICIENCY 59
3.6.1. Experimental In-plane efficiency evaluation 59
3.6.2. Analytical formulation 62
3.7. FINAL CONSIDERATIONS 63
3.8. REFERENCES 64
4. SUMMARY OF APPENDED PAPERS 77
4.1. PAPER I 78

4.2. PAPER II 79
4.3. PAPER III 79
4.4. PAPER IV 80
4.5. PAPER V 81
5. CONCLUSIONS AND FUTURE WORK 82
5.1. CONCLUSIONS 82
5.2. FUTURE WORK 84
6. TOUGHNESS OF NATURAL HYDRAULIC LIME FIBRE REINFORCED MORTARS FOR MASONRY STRENGTHENING OVERLAY SYSTEMS 86
7. HYBRID FIBRE REINFORCED MORTAR FOR OVERLAY MASONRY STRENGTHENING 118
8. ASSESSMENT OF THE PROPERTIES TO CHARACTERIZE THE INTERFACE BETWEEN CLAY BRICK SUBSTRATE AND STRENGTHENING MORTAR 141
9. ASSESSMENT OF OVERLAY MASONRY STRENGTHENING SYSTEM UNDER IN-PLANE MONOTONIC AND CYCLIC LOADING USING THE DIAGONAL TENSILE TEST 185
10. CHARACTERIZATION OF OVERLAY STRENGTHENING OF MASONRY BY MEANS OF BIAXIAL CYCLIC DIAGONAL TENSILE TESTS 219

LIST OF TABLES

Table 2.1: Structural characteristics of buildings as a function of the construction period, Lisbon area [8]. 11

Table 2.2: Seismic retrofit policies of earthquake-prone countries, according to [20]. 18

Table 2.3: Non-intrusive options for structural rehabilitation [10]. 20

Table 2.4: Common types of techniques applied in masonry walls. 22

Table 2.5: Values for plane of failure parallel to bed joints, f_{xk1} [30]. 30

Table 2.6: Values for plane of failure perpendicular to bed joints, f_{xk2} [30]. 30

Table 3.1: List of changes taking place in concrete during heating according to Hager [63]. 40

Table 3.2: Physical properties of man-made fibres [62,76,77]. 43

Table 3.3: Physical properties of natural fibres. 46

Table 3.4: Mechanical properties of meshes [99]. 50

Table 3.5: Clamping methods and instrumentation used in the laboratories to perform the direct tensile tests [99]. 55

Table 3.6: Environmental durability tests, [123]. 59

Table 3.7: Summary of diagonal tensile test results on strengthened URM specimens obtained from authors. 61

Table I.1: Properties from the commercially available NHL5.0. 90

Table I.2: Properties of PAN fibres. 91

Table I.3: Composition of the mortars. 91

Table I.4: Results from uniaxial compression tests to specimens cured in 60% RH and 85% RH. 95

Table I.5: Flexure test results of specimens cured at 85% RH for 7 days. 96

Table I.6: Flexural test results of specimens cured at 85% RH and 60% RH for 28 days. 96

Table I.7: Flexural test results of specimens cured at 85% RH for 90 days. 97

Table II.1: Recommended molar ratios for geopolymer [21]. 120

Table II.2: Properties from the natural hydraulic lime, commercially available as Secil NHL5.0. 125

Table II.3: Properties of the activators used for the geopolymeric binder. 125

Table II.4: Properties of fibres. 126

Table II.5: Composition of the mortars, weight of materials per m^3. 126

Table II.6: Results obtained from flexural and compressive tests of different FRM's at 28 days. 133

Table III.1: Strength parameters for different types of interfaces. 147
Table III.2: Summary of experimental results. 151
Table III.3: Summary of the samples tested for each mortar batch. 153
Table III.4: Experimental results. 159
Table III.5: Estimation of the friction angle for lower and higher normal stresses based on the linear regressions. 167
Table III.6: Estimated peak parameters for each loading direction. 169
Table III.7: Optimized peak values of Mohr criterion parameters for each loading direction. 170
Table III.8: Optimized residual values of Mohr criterion parameters for each loading direction. . 170
Table III.9: Estimated parameters considering the Mohr-Coulomb criterion and the peak shear stress results. 174
Table III.10: Estimated parameters considering the Mohr-Coulomb criterion for the residual shear stress results. 175
Table III.11: Summary of the $R2$ values obtained for each testing direction. 177

Table IV.1: Summary of previous diagonal tensile test results on strengthened URM. 190
Table IV.2: Properties of the masonry components. 194
Table IV.3: Properties of the PFRM. 195
Table IV.4: Properties of the CFM, [32]. 196
Table IV.5: Monotonic diagonal tensile test results. 200
Table IV.6: Cyclic diagonal compression test results. 200
Table IV.7: Average of the limit values of the shear stress, shearing strain and shear modulus obtained for the reference and the strengthened specimens. 204
Table IV.8: Increase of capacity in terms of shear stress, shearing strain and increment of shear modulus obtained after strengthening. 204
Table IV.9: Variation of the Shear modulus during cyclic tests. 205
Table IV.10: Evolution of the stiffness of the load vs horizontal displacement response from reference specimens under cyclic loading. 207
Table IV.11: Values used in the analytical model to obtain the shear capacity of the specimens. 212
Table IV.12: Shear capacity obtained for reference and strengthened specimens. 214

Table V.1: Properties of mortars used to assemble, render and strengthen the masonry specimens. 224
Table V.2: Results from the uniaxial compressive tests. 230
Table V.3: Results from the uniaxial compressive tests. 233
Table V.4: Results from the biaxial cyclic diagonal compressive tests. 246

LIST OF FIGURES

Figure 1.1: Distribution of classical buildings by conservation status in 2021, adapted from [7].... 2

Figure 2.1: Evolution from type of masonry walls in Portugal [7]. 11

Figure 2.2: Distribution of classical buildings for structural system in 2011, adapted from [10]. . 12

Figure 2.3: Distribution of classical buildings by conservation level considering the year of implementation, adapted from [10]. 12

Figure 2.4: Buildings distribution in Portugal, adapted from [11]. 13

Figure 2.5: Distribution of most used infill elements based on quantitative and qualitative data according to Landolfo et al. [14]. 14

Figure 2.6: Representation of the European Seismic Hazard Map, considering the mean peak ground acceleration (PGA) for 10% exceedance probability in 50 years [16]. 16

Figure 2.7: Evolution of seismic design codes from 1900 to 2020 across European countries [18]. The code design level is presented as CDN for no seismic design code, CDL for low level, CDM for medium level and CDH for high level. 17

Figure 2.8: ISO 15686-7 model for analysing the level of interventions throughout the life cycle of a building [23]. 21

Figure 2.9: Overlay strengthening system. 23

Figure 2.10: Layout of FRP strips in strengthening situations [27]. 23

Figure 2.11: Strengthening of structural walls with “jacketing” technique [24]. 24

Figure 2.12: Jacketing of shear walls [28]. 25

Figure 2.13: Geometry of the specimen to characterize the compressive strength of masonry elements [31]. 26

Figure 2.14: Typical in-plane failure mechanisms for unreinforced masonry walls or piers: a) rocking; b) sliding; c) sliding-shear; d) shear. Adapted from [32]. 27

Figure 2.15: Diagonal tensile test set-up. 27

Figure 2.16: Set-up for shear tests with pre- compression [35]. 29

Figure 2.17: Planes of failure of masonry in flexure [30]. 29

Figure 2.18: Planes of failure of masonry in flexural [36]. 31

Figure 3.1: Evolution of the use of inorganic binders during history. Adapted from [23]. 37

Figure 3.2: Lime and hydraulic lime cycle, adapted from [24]. 38

Figure 3.3: Colour change of concrete surface after exposure to temperatures from 20 to 1000°C [63]. 40
Figure 3.4: PAN fibres [76]: a) "dog-bone" shape; b) "kidney" shape. 43
Figure 3.5: Fibre-matrix interaction [80]: a) fracture surface of reinforced mortar with PVA; b) detail of fibre-matrix interaction; c) detail of the fibre. 44
Figure 3.6: Basalt fibres: a) chopped; b) roving; c) mesh [81]. 45
Figure 3.7: Natural fibres, adapted from [82]. 46
Figure 3.8: Surface of sisal fibre with different treatments after pull-out test [92]. 47
Figure 3.9: Microstructure of a composite with steel and PVA fibres, and CaCO3 whiskers): a) and b) interaction of steel and PVA fibres in the matrix; c) detail of enlarged image of the circle area in b); d) enlarged image of the rectangular area in c). Adapted from [95]. 48
Figure 3.10: SEM micrograph of wollastonite microfibres: a) distribution of fibres[96]; b) detail of single fibre [98]. 49
Figure 3.11: Textile fibre reinforcements, adapted from [101]. 49
Figure 3.12: Rupture modes obtained in Pull-off tests [103]. 51
Figure 3.13: Evaluation of the bond in a brick masonry model with TRM/FRP: a) TRM and FRC systems with pull-heads plates applied; b) pull-off test set-up with dynamometer. Adapted from [104]. 52
Figure 3.14: Pull-out tests: a) textile embedded in epoxy resin; b) textile embedded in mortar block; c) typical load versus slip response curve of monotonic pull-out test. Adapted from [108]. 52
Figure 3.15: Schemes of experimental setups for bond tests: a) single lap; b) double-lap single-prism; c) double-lap double-prism. Adapted from [109]. 53
Figure 3.16: Failure modes in shear bond tests and Stress vs. Slip responses. Adapted from [109]. 54
Figure 3.17: Test commonly used to evaluate the flexural behaviour of TRM: a) Four-point bending test [114]; b) Three-point bending tests [113]. 55
Figure 3.18: TRM direct tensile tests: a) test set-up; b) tensile response and stages obtained. Adapted from [100,109]. 57
Figure 3.19: Experimental setup used for Diagonal Compression Tests: a) Laboratory set-up with no reaction frame, [138]; b) In-situ set-up with no reaction frame [129]; c) Laboratory set-up with reaction frame. 60

Figure I.1: Flexural and compressive strength of FRM´s developed by different authors. 88
Figure I.2: Grading curve for the limestone sand and CEN Reference sand. 90
Figure I.3: Mixing procedure of the FRM. 91
Figure I.4: Equipment used to characterize the fresh behaviour of the mixtures: a) flow table; b) container to determine the air content of FRM. 92
Figure I.5: Images showing the setup used for: a) elasticity modulus in compression; b) compressive strength; and c) flexural strength. 93
Figure I.6: Flow table test results obtained for the different mixtures after 15 strokes. 93
Figure I.7: a) Flow values obtained for different amounts of fibres; b) fresh density and air content values obtained for different fibre fractions. 94
Figure I.8: Typical compressive stress-strain responses obtained for mortars with different fibre fractions and curing conditions. 98
Figure I.9: Compressive behaviour of mixtures in two different curing environments: a) compressive strength; b) elastic modulus. 99
Figure I.10: Schematics of the flexural response and approach adopted to correct the experimental setup adjustments during loading [37]. 100
Figure I.11: Typical flexural stress vs displacement responses obtained from flexure tests for specimens cured at 60%RH and 80%RH. 101
Figure I.12: RH 60 and 85% curing conditions: a) Modulus of rupture; b) Limit of proportionality 102
Figure I.13: Method to calculate the work of fracture in compression [50],[51]. 103
Figure I.14: Compression fracture energy for different curing conditions: a) RH 60 b) RH 85. .. 103
Figure I.15: Definition of compressive toughness ratio [52], [53]. 104
Figure I.16: Toughness ratio for RH 60 and 85 curing conditions: a) $TR_{c,3}$; b) $TR_{c,5}$. 105
Figure I.17: Relation between compressive strength and toughness ratio, $TR_{c,3}$ and $TR_{c,5}$ for RH60 and RH85. 105
Figure I.18: Definition of flexural toughness ratio, [57]. 106
Figure I.19: Toughness values for RH 60% and 85% curing conditions: a) flexural toughness (FT); b) flexural toughness factor Re(l/150). 107
Figure I.20: Relation between flexural strength and toughness ratio. 107
Figure I.21: Efficiency of fibre reinforcement on the normalized flexure strength. 108
Figure I.22: Efficiency of fibre reinforcement on the flexural toughness ratio. 109

Figure I.23: Flexural strength vs. flexural toughness ratio from FRM. 110

Figure II.1: Ternary diagram of the most common cementitious materials, adapted from [21], [24]. 121

Figure II.2: Thermogravimetric curves of the different type of materials. 122

Figure II.3: Phases of brick aggregate processing: a) original material collected from masonry elements; b) jaw crusher mill; c) drum mill with used milling material. 123

Figure II.4: Red Brick Powder processing and analysis: a) Disc mill used; b) particle size distribution by sedimentation. 123

Figure II.5: Particle size distribution of materials: a) processed brick aggregate after each step and CEN reference curve; b) – Metakoalin and processed red brick powder after 6 and 12 minutes. . 124

Figure II.6: Mixing procedure of the FRM. 127

Figure II.7: Thermal analysis of pastes: thermogravimetry at a) 7 days and b) 90 days; differential thermogravimetry at c) 7 days and d) 90 days; heat flow at f) 7 days and e) 90 days. 130

Figure II.8: Compressive behaviour of the pastes: a) compressive strength; b) ratio between the compressive strength at room temperature and residual compressive strength after 600°C 131

Figure II.9: Average load vs displacement at mid-span curves and envelope obtained from the flexural tests to FRM's 132

Figure II.10: Flexural toughness from FRM´s: a) flexural toughness factor, FT; b) flexural toughness factor ratio, Re_2. 134

Figure II.11: Compressive behaviour of the FRM: a) fracture energy in compression; b) compressive toughness ratio $TR_{c0.75Fmax}$ 135

Figure III.1: Triplet test Shubert arrangement, adapted from [25]. 145

Figure III.2: Couplet test Hofmann arrangement, adapted from [25]. 146

Figure III.3: Couplet test DIN arrangement, adapted from [25. 146

Figure III.4: Test setup used to perform cyclic direct shear tests, adapted from [18]. 147

Figure III.5: Schematics of Mohr-Coulomb and Mohr failure criteria for positive tangential stresses. 149

Figure III.6: Ceramic brick used to mount the specimens: a) ceramic brick; b) detail of grooves, dimensions in mm. 150

Figure III.7: Evolution of the hardened state properties of the PFRM: a) equivalent tensile strength in flexure vs curing age; b) compressive strength vs curing age. 151
Figure III.8: Pull-off test: a) detached PFRM layer; b) surface of the bricks after testing; c) pull-off device. 152
Figure III.9: Representation of the loading directions investigated. 153
Figure III.10: Preparation of specimens: a) cutting the bricks; b) pouring mortar to create a compact and regular unit; c) demoulding and turning the unit upside down d) brick samples after casting; e) detailing of the cutting lines for obtaining the final specimens; f) final preparations on the specimens, including the execution of the lateral notches. Dimensions in mm. 154
Figure III.11: Test setup global view. 155
Figure III.12: Detail of the setup developed for the direct shear test. 156
Figure III.13: Position of LVDTs in the specimen: a) Front face, position of LVDT#1 and LVDT#3; b) Rear face, position of LVDT#2 and LVDT#4. 157
Figure III.14: Setup of the direct shear test: a) general view; b) detail of the specimen during testing. 157
Figure III.15: τ-s responses for direction 1 (0 °): a) and b) responses for lower imposed normal stresses; c) and d) responses for higher imposed normal stresses; b) and d) detail of the initial stage up to an average slip of 0.3 mm. 161
Figure III.16: τ-s responses for direction 2 (45 °): a) and b) responses for lower imposed normal stresses; c) and d) responses for higher imposed normal stresses; b) and d) detail of the initial stage up to an average slip of 0.3 mm. 162
Figure III.17: τ-s responses for direction 3 (90 °): a) and b) responses for lower imposed normal stresses; c) and d) responses for higher imposed normal stresses; b) and d) detail of the initial stage up to an average slip of 0.3 mm. 163
Figure III.18: Front view of the ruptured specimens after testing. 164
Figure III.19: Opposite faces of the failure surfaces obtained after testing. 164
Figure III.20: Linear regressions for direction 1 (0 °) considering peak and residual shear stress values. 166
Figure III.21: Linear regressions for direction 2 (45 °) considering peak and residual shear stress values. 166
Figure III.22: Linear regressions for direction 3 (90 °) considering peak and residual shear stress values. 167

Figure III.23: Representation of the Mohr failure criterion when used to characterize the interaction between the normal stress and both the peak and residual values for positive tangential stresses. The subscript 'p' identifies the 'peak' failure surface parameters, and the subscript 'r' identifies the 'residual' parameters. 168
Figure III.24: Failure criteria for 0° loading direction. 171
Figure III.25: Failure criteria for 45° loading direction. 171
Figure III.26: Failure criteria for 90° loading direction. 172
Figure III.27: Representation of the Mohr-Coulomb failure criteria for the peak and the residual shear stress results. 173
Figure III.28: Linear regression of the peak shear stress results for all orientations. 174
Figure III.29: Linear regression of the residual shear stress results for all orientations. 175
Figure III.30: Experimental versus criterion estimations for 0° loading direction: a) peak shear stresses; b) residual stresses. 176
Figure III.31: Experimental versus criterion estimation for 45° loading direction: a) peak shear stresses; b) residual shear stresses. 177
Figure III.32: Experimental versus criterion estimations for 90° loading direction: a) peak shear stresses; b) residual shear stresses. 177
Figure III.33: Failure criteria for peak and residual shear stress. 178
Figure III.34: Combined failure criteria for all directions: a) representation of the peak and residual values for 0, 0.5 and 1.0 MPa normal stresses; b) 3D orthotropic representation of the peak and residual loading/failure criteria 179
Figure IV.1: Diagonal tensile test, general set-up 192
Figure IV.2: Mohr's representation of the stress state assumed in the central area of the specimen. 193
Figure IV.3: General layout of specimens: a) Procedure adopted in the production of the specimens; b) Section of the specimens and detail of the FRMCom system. (Legend: a - masonry; b - roughcast mortar, mortar 1:4:2; c - render layer 1.5 cm thick, mortar 1:5:2; d - PFRM 1.2 cm; e - CFM; f - PFRM 1.2 cm. Dimensions in cm) 197
Figure IV.4: Test set-up of the direct tensile test: a) Geometry of specimens and position of LVDTs (dimensions in mm); b) Detail of the positioning of the specimen and of the test set-up 198
Figure IV.5: Displacement laws imposed during the cyclic tests. 199

Figure IV.6: Load vs displacement responses of the strengthened specimens: (a) global response; (b) detail of the response until peak. 201
Figure IV.7: Image of the specimens after testing: (a) Crack pattern in reference specimen, ref-02 side B; (b) Crack pattern in strengthened specimen, FRMCom-03 side B; (c) Detachment between the strengthening overlay and substrate, FRMCom-03. 202
Figure IV.8: Shear stress vs shear strain response of the specimens. 203
Figure IV.9: Schematics of the different mechanisms leading to structural degradation during the diagonal tensile tests: (a) Type A; (b) Type B; (c) Type C; (d) Type D. 206
Figure IV.10: Identification of the onset of the different types of damage mechanisms. 207
Figure IV.11: Crack patterns of reference specimens after testing: (a) ref_01_side A; (b) ref_02_side A; (c) ref_03_side A. 208
Figure IV.12: Crack patterns of strengthened specimens after testing: (a) FRMCom_01_side A; (b) FRMCom_02_side A; (c) FRMCom_03_side A. 208
Figure V.1: Schematics of the experimental set-ups: a) diagonal tensile test; b) biaxial tensile test. 221
Figure V.2: Sequence of procedures during the preparation of the masonry elements: a) unreinforced ceramic brick specimen mounted, with one layer of screed mortar applied; b) rendering process; c) finish specimen of unreinforced ceramic brick masonry with render, corresponding to the URMR.225
Figure V.3: Sequence of procedures during the strengthening of COM and FRM specimens: a) specimen with one small layer of strengthening mortar and overlayed carbon fibre mesh; b) covering of the carbon fibre mesh with the rendering layer; c) finished COM specimen. 225
Figure V.4: Test set-up used for the uniaxial compression tests. 226
Figure V.5: Test set-up adopted for bidirectional diagonal tensile tests: a) general view of the set-up; b) detail of one of the specimens. 227
Figure V.6: Speckle pattern used for the DIC produced at the surface of the specimens used for the uniaxial compression tests. 229
Figure V.7: Evolution of the ratios $f_c/f_{c,URMR}$ and E/E_{URMR} obtained for the uniaxial compressive tests. 231
Figure V.8: Failure modes obtained under compression: a) URM specimen, crushing of ceramic brick; b) failure of the ceramic brick septs in COM specimen; c) sudden failure of FRM specimen. 232

Figure V.9: Load vs displacement response obtained for FRM-01 under vertical and horizontal monotonic loading. 234
Figure V.10: Load vs displacement response obtained for COM-03 under vertical and horizontal cyclic loading. 234
Figure V.11: Maximum shear stress obtained for vertical and horizontal loading cycles, and corresponding ratios. 235
Figure V.12: Stress vs Strain curves obtained for the biaxial diagonal tests on specimen FRM - 01: vertical and horizontal strain for vertical and horizontal stages of the monotonic loading. 236
Figure V.13: Stress vs Strain curves obtained for the biaxial cyclic diagonal tests on specimen COM - 03: vertical and horizontal strain for each cycle. 239
Figure V.14: Stress vs strain responses obtained for the biaxial cyclic diagonal tests of specimen FRM - 03: vertical (V1 to V7)) and horizontal (H1 to H7) strains vs stress obtained for loading cycles 1 to 7. 242
Figure V.15: Cracking evolution at the surface of URM-01: crack pattern after 5th vertical loading cycle; b) crack pattern after 5th horizontal loading cycle; c) crack pattern after 6th and last vertical loading cycle. 243
Figure V.16: Cracking evolution at the surface of URMR specimen: crack pattern at peak load of 5th vertical loading cycle; b) pattern at the peak load of the 5th horizontal loading cycle. 243
Figure V.17: Evolution of the crack pattern of FRM-02 specimen: a) pattern at the peak load of the vertical monotonic solicitation; b) pattern at the onset of the monotonic horizontal loading cycle; c) pattern at the peak load of the horizontal loading cycle. 244
Figure V.18: Evolution of the crack pattern of COM-03 specimen obtained with DIC: a) crack pattern at the peak load of the 5th vertical loading cycle; b) crack pattern at the peak load of the 5th horizontal loading cycle; c) crack pattern at the peak load of the 6th vertical loading cycle. 244
Figure V.19: Crack opening evolution from monotonic test to COM-01. 246
Figure V.20: Crack opening evolution from monotonic test to FRM-01 247
Figure V.21: Crack opening evolution from cyclic test to COM-03, only the last two vertical cycles and the last horizontal cycle are represented. 247
Figure V.22: Crack opening evolution from cyclic test to FRM-03, only the last two vertical and horizontal cycles are represented. 248

LIST OF ABBREVIATIONS AND SYMBOLS

A_f	Area of the mesh reinforcement by unit width
A_m	Interface loading area between the steel shoe and the specimen
A_n	Net area of the specimen cross section
$A_{n,r}$	Net area of the render cross section
$A_{n,PFRM}$	Net area of the PFRM cross section
E_f	Tensile modulus of elasticity of the cracked FRCM specimen
f_{fv}	Design tensile strength of FRCM reinforcement
$f_{fv,ult}$	Ultimate tensile strength of FRCM reinforcement
f'_m	Compressive strength of the masonry
f'_t	Tensile strength of the masonry
FRCM	Fabric reinforced cementitious matrix
g	Vertical gage length
G	Modulus of stiffness in shear
Geo	Geopolymer
h	Height of the brick units
L	Length of the wall in the direction of the shear force
NHL	Natural hydraulic Lime
n	Number of fabric layers
n^*	Percentage of the net area
P	Applied load
PAN	Polyacrilonitrile
S_s	Shear stress
t	Thickness of the specimen
TRM	Textile reinforced mortar
V_{ref}^{exp}	Shear capacity of the reference specimens obtained experimentally
V_{str}^{exp}	Shear capacity of the strengthened specimens obtained experimentally
V_{ACI}^{an}	Shear capacity of the specimen calculated following the ACI549.4R-13

$V_{ACI+PFRM}^{an}$ Shear capacity of the specimen calculated following ACI549.4R-13 plus the contribution of the PFRM layers

V_{Sup}^{an} Shear capacity of the specimen considering ultimate strain of the FRCM plus the contribution of the PFRM layers

V_{dt} Shear capacity due to diagonal tension failure

V_f Shear capacity of the FRCM system

V_m Shear capacity of the masonry specimen

V_{sf} Shear capacity due to shear friction failure

V_{ss} Shear capacity due to shear sliding failure

$V_{f,ult}$ Shear capacity of the FRCM system considering ultimate tensile strain

V_r Shear capacity of the render layer

V_{PFRM} Shear capacity of the PFRM layer

u_v Vertical shortening

u_h Horizontal elongation

w Length of brick units

γ Shearing strain

ε_{fv} Design value of the tensile strain of FRCM reinforcement

$\varepsilon_{fv,ult}$ Tensile strain ultimate value of FRCM reinforcement

μ_0 Coefficient of internal shear friction in mortar joint

μ_m Modified coefficient of internal shear friction in mortar joint

τ_0 Shear bond strength of the mortar joint

$\tau_{0,m}$ Modified shear bond strength of the mortar joint

θ Angle between horizontal and main diagonal of the wall

CHAPTER 1

INTRODUCTION

This chapter presents the background of the research, aim and objectives, research scope, methodology and outlines of the thesis.

1.1. BACKGROUND AND MOTIVATION

Masonry structures are one of the oldest legacies that survived until our time. Two main reasons can be named to explain this achievement: soundness and durability. Considering this heritage, the scientific community dedicated attention to understand, characterize and, when necessary, develop strengthening solutions for this type of structures. The maintenance of masonry buildings and structures is a concerning issue in the decades to come, given its economic impact in the society.

A major drawback of masonry performing as main structural element is the weak monolithic behaviour in the out-of-plane direction. This weakness can be revealed, for instance, when walls are made from stones or by two external layers well-ordered but not mutually connected and containing a rubble infill. This makes the wall to become brittle, particularly when external forces act in the horizontal direction due to earthquakes [1]. The same problem can happen under vertical loads if these act eccentrically [2]. When used as infill element in reinforced concrete frames, masonry can also suffer high damage after seismic actions. Important level of damage is reported for these elements in the in-plane direction [1,3]. In the out-of-plane direction major damage and collapse are also observed in the infill panels, [4,5] as well as in other elements as parapets [1]. Moreover, there are several reports of damage resulting from the interaction between in-plane and out-of-plane failure modes [5,6].

Considering the national territory, the final data from Portuguese Census 2021 [7] reveals the existence of 3.57 million buildings whose structure and materials are of a non-precarious nature, also referred to as classical buildings. Among those, 0.34 million need medium repairing and 0.16 million need full scale repairing. The conservation level of buildings in Portuguese territory in 2021 is presented in **Figure 1.1**. Census 2021 does not provide information about the structural elements but the previous Census 2011 [8] concluded that approximately 1.7 million of the buildings were made of reinforced concrete structures, mainly using infill masonry elements, and about 1.77 million were made of structural masonry walls. The Southern European countries adopt similar structural systems, being the masonry used mainly as infill in most of the countries. Landolfo et al. [9] present data from several European census and national sources and identify four materials used in structural systems: timber; reinforced concrete; rubble masonry and brick masonry. From the countries under study, all presented reinforced concrete as the most used, followed by brick masonry.

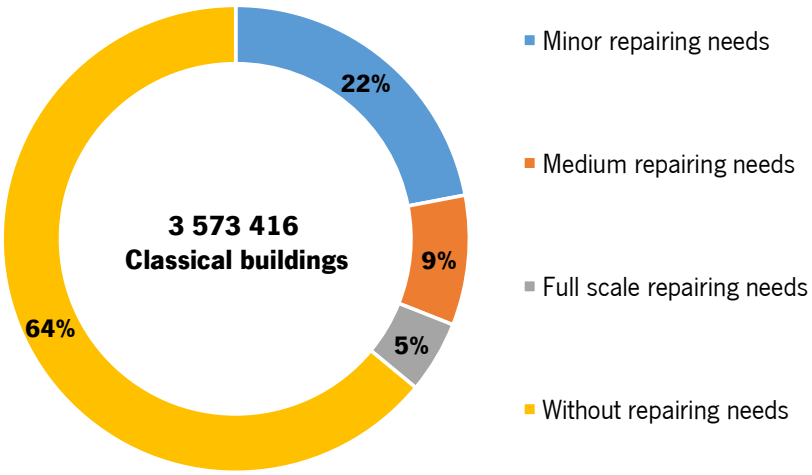


Figure 1.1: Distribution of classical buildings by conservation status in 2021, adapted from [7].

Textile reinforced mortar (TRM), also referred as Fiber reinforced cementitious matrix (FRCM) is a composite material consisting of a fibre-reinforced mortar matrix and one or more layers of textile reinforcement [10–16]. This system has shown great potential in the strengthening and rehabilitation of masonry structures, offering significant advantages over traditional techniques. In the last decade TRM has been used extensively in Italy and implemented in other Southern European countries and seismic areas, where masonry structures are widespread and require frequent maintenance and repair. The advances in TRM technology have been significant in recent years, with numerous studies confirming its effectiveness in enhancing the strength, durability, and seismic resistance of masonry structures [14–19]. In Italy, the use of TRM in the rehabilitation and strengthening of historic masonry

structures has gained significant attention and is interlinked with the most recent earthquakes, L'Aquilla (2009), Emilliana (2012) and Central Italy (2016). TRM has been used to strengthen churches, and other heritage buildings, providing a sustainable and cost-effective solution. Extensive research was conducted by universities and research institutes on TRM, developing innovative materials and optimizing its performance, reducing its costs and environmental impact. Also, in other European countries and Middle East region [20], TRM is becoming an alternative technique for the rehabilitation of masonry structures due to its ease of application and its effectiveness in enhancing the seismic resistance of masonry structures.

The increasing knowledge about the performance of TRM strengthening systems and their use led to the development of standards and guidelines for the correct design and application in the construction sector. The ACI 549.4R-13 [21] was one of the first guiding documents for the design of TRM systems followed by the recommendation documents from RILEM, TC 232-TDT [22] related to the test methods to quantify the performance and the design of TRM systems and TC 250-CSM [23] related with the mortar to substrate bond characterization. In Italy the LG 2018 [24] qualifies the TRM or FRCM composites based on predefined mechanical properties evaluated by means of homologated tensile and debonding tests performed by the manufacturer through accredited laboratories.

1.2. OBJECTIVES AND RESEARCH METHODOLOGY

The main objective of the present work was to develop a strengthening system designed to feature high ductility and proper compatibility and adhesion to masonry substrates, as part of a simple process of application that allows versatility to architectural solutions. This system is meant to be applied to structural masonry and infill masonry showing deficient behaviour against seismic actions and masonry elements with low load carrying capacity. Cement matrix composites are a relatively recent class of materials that show mechanical properties adequate for this application. Additionally, they can be tuned to present self-healing features and improved behaviour when exposed to elevated temperatures.

To develop such type of overlay strengthening system successfully, the following research questions (RQ) should be answered:

RQ 1. Is it possible to combine simplicity of application, mechanical and thermal resistance, and durability in an overlay strengthening system?

RQ 2. In which way it is possible to improve the sustainability of masonry strengthening systems?

RQ 3. What are the advantages and disadvantages of an overlay strengthening system when comparing with alternative systems and how it can be improved?

RQ 4. How to characterize the performance of new masonry overlay strengthening systems in the laboratory?

RQ 5. How are experimental results related to design procedures and guidelines for engineering practice?

In order to answer the research questions, specific objectives or tasks (O/T) where proposed:

O/T 1. Investigate new strengthening systems using fibre reinforced mortar (FRM).

O/T 2. Explore additional functionalities, such as the ability of the systems to withstand high temperatures.

O/T 3. Characterize and understand the bonding behaviour between the strengthening overlays and masonry substrates.

O/T 4. Investigate the experimental procedures to estimate the global efficiency of the strengthening systems when applied to different masonry elements.

O/T 5. Develop additional testing procedures considering the different contributions of the components, specific properties of the materials and systems to be studied to the overall mechanical and functional performance.

1.3. OUTLINE OF THE DISSERTATION

The content of this work, which is presented as a collection of papers published or submitted to peer-review international journals, is organized in five chapters and appended papers, as follows:

- **Chapter 1** provides a general introduction to the research topic, describes the general objectives and overall methodology and, finally, presents the outline of the present work.
- **Chapter 2** introduces a general perspective on the type of structural systems used in the building stock at Portuguese and European level, and points some of the public policies for promoting the seismic retrofit of existing buildings. This chapter also analyses the most common types of structural strengthening methods and techniques used in masonry elements. The chapter ends with some final considerations on the need for fast and effective

strengthening solutions that can be applied in the vast number of seismically vulnerable buildings.

- **Chapter 3** is dedicated to a deeper insight on the overlay strengthening of masonry using textiles, presenting the most significant guidelines and standards currently in use and showing the most important experimental works developed for its characterization. Additionally, alternative materials for the system are introduced and discussed as well as the strengthening efficiency and durability.
- **Chapter 4** presents a brief summary of the papers that constitute this PhD thesis. The structured alignment of papers relates to the research questions, reinforcing the coherence of the doctoral research and highlights its contribution to the field of material development and masonry strengthening. Paper I, III, and IV are already published and Paper II and V are under submission process.
    - Paper I: This paper evaluates the use of PAN fibres in natural hydraulic lime-based mortars, revealing that fibre-reinforced mortars (FRMs) can be designed to maintain workability and be applied easily, while significantly enhancing toughness and ductility (RQ1). The study also characterizes the mortar's fresh and hardened states through standardized mechanical tests, contributing to methodologies for assessing FRM performance in the lab (RQ4).
    - Paper II: This study presents a hybrid mortar incorporating recycled PAN and carbon fibres alongside geopolymeric and cementitious binders, aiming to balance mechanical performance before and after exposure to elevated temperatures and ease of application (RQ1). The incorporation of recycled materials and construction residues is aligned with sustainable construction practices, addressing the goal of improving the environmental profile of strengthening systems (RQ2). The study also includes a comprehensive experimental campaign to assess mechanical performance, aiding in laboratory characterization (RQ4).
    - Paper III: This paper addresses a critical limitation of overlay systems: the vulnerability at the interface between the strengthening mortar and masonry substrate. Through direct shear tests on orthotropic brick substrates, the study identifies key mechanical properties like peak and residual shear stress, which influence interfacial performance and inform potential improvements (RQ3). The experimental methodology enables systematic laboratory assessment of the interface behaviour

(RQ4), and the results are translated into constitutive laws for numerical simulation, providing design-relevant insights for engineering practice (RQ5).

- Paper IV: This paper investigates a FRCM strengthening system that enhances ductility and load-carrying capacity, aligning with the goal of simplicity, mechanical resistance, and durability (RQ1). It demonstrates the advantages of overlay systems for seismic retrofitting, particularly their stiffness and energy dissipation capabilities, while also identifying potential areas for improvement under cyclic loads (RQ3). The research validates diagonal tensile testing under both monotonic and cyclic conditions as a reliable laboratory procedure for simulating seismic effects (RQ4). Furthermore, analytical evaluation is presented offering design-relevant metrics that support structural assessments (RQ5).
- Paper V: This paper investigates the use of TRM for strengthening masonry and highlights their contribution to improving shear and compressive capacity while maintaining ease of application, addressing RQ1. It also reveals performance advantages under biaxial loading and provides insights into cracking and failure modes that support improvements in system design (RQ3). By developing a biaxial cyclic diagonal tensile testing procedure, the study fills a gap in existing laboratory methods, offering a robust approach for characterizing structural behaviour under complex loading (RQ4).

- **Chapter 5** summarizes the main conclusions of the developed work and presents recommendations for future work.
- **Appended Papers** are presented as:

Paper I. Toughness of Natural Hydraulic Lime Fibre-Reinforced Mortars for Masonry Strengthening Overlay Systems.

Paper II. Hybrid Fibre-Reinforced Mortar for Overlay Masonry Strengthening

Paper III. Assessment of the Properties to Characterize the Interface Between Clay Brick Substrate and Strengthening Mortar

Paper IV. Assessment of Overlay Masonry Strengthening System Under In-Plane Monotonic and Cyclic Loading Using the Diagonal Tensile Test

Paper V. Characterization of Overlay Strengthening of Masonry by Means of Biaxial Cyclic Diagonal Tensile Tests

1.4. REFERENCES

[1] Romão X, Costa AA, Paupério E, Rodrigues H, Vicente R, Varum H, et al. Field observations and interpretation of the structural performance of constructions after the 11 May 2011 Lorca earthquake. Eng Fail Anal 2013;34:670–92. https://doi.org/10.1016/j.engfailanal.2013.01.040.

[2] Binda L, Saisi a., Tiraboschi C. Investigation procedures for the diagnosis of historic masonries. Constr Build Mater 2000;14:199–233. https://doi.org/10.1016/S0950-0618(00)00018-0.

[3] Furtado A, Ramos T, Rodrigues H, Arêde A, Varum H, Tavares P. In-plane Response of Masonry Infill Walls: Experimental Study using Digital Image Correlation. Procedia Eng 2015;114:870–6. https://doi.org/10.1016/J.PROENG.2015.08.042.

[4] Furtado A, Rodrigues H, Arêde A, Varum H. Influence of the In-Plane and Out-of-Plane Masonry Infill Walls' Interaction in the Structural Response of RC Buildings. Procedia Eng 2015;114:722–9. https://doi.org/10.1016/J.PROENG.2015.08.016.

[5] Mazza F, Donnici A. In-plane and out-of-plane seismic damage of masonry infills in existing r.c. structures: the case study of De Gasperi-Battaglia school in Norcia. Bulletin of Earthquake Engineering 2021;19. https://doi.org/10.1007/s10518-020-00981-2.

[6] Cavaleri L, Zizzo M, Asteris PG. Residual out-of-plane capacity of infills damaged by in-plane cyclic loads. Eng Struct 2020;209:109957. https://doi.org/10.1016/J.ENGSTRUCT.2019.109957.

[7] Instituto Nacional de Estatística IP. Censos 2021 Resultados Definitivos - Portugal. Lisboa: Instituto Nacional de Estatística, I.P; 2022.

[8] INE. Parque Habitacional em Portugal : Evolução na última década 2012:1–10.

[9] Landolfo R, Formisano A, Di Lorenzo G, Di Filippo A. Classification of european building stock in technological and typological classes. Journal of Building Engineering 2022;45:103482. https://doi.org/10.1016/J.JOBE.2021.103482.

[10] Carozzi FG, Poggi C. Mechanical properties and debonding strength of Fabric Reinforced Cementitious Matrix (FRCM) systems for masonry strengthening. Compos B Eng 2015;70:215–30. https://doi.org/10.1016/j.compositesb.2014.10.056.

[11] Carozzi FG, Milani G, Poggi C. Mechanical properties and numerical modeling of Fabric Reinforced Cementitious Matrix (FRCM) systems for strengthening of masonry structures. Compos Struct 2014;107:711–25. https://doi.org/10.1016/j.compstruct.2013.08.026.

[12] Arboleda D, Carozzi FG, Nanni A, Poggi C. Testing procedures for the uniaxial tensile characterization of fabric-reinforced cementitious matrix composites. Journal of Composites for Construction 2015;1:11. https://doi.org/10.1061/(ASCE)CC.1943-5614.0000626.

[13] Bertolesi E, Carozzi FG, Milani G, Poggi C. Numerical modeling of Fabric Reinforce Cementitious Matrix composites (FRCM) in tension. Constr Build Mater 2014;70:531–48. https://doi.org/10.1016/j.conbuildmat.2014.08.006.

[14] Dalalbashi A, Ghiassi B, Oliveira D V. A multi-level investigation on the mechanical response of TRM-strengthened masonry. Mater Struct 2021;54:224. https://doi.org/10.1617/s11527-021-01817-4.

[15] Allahvirdizadeh R, Oliveira D V., Silva RA. Numerical modeling of the seismic out-of-plane response of a plain and TRM-strengthened rammed earth subassembly. Eng Struct 2019;193:43–56. https://doi.org/10.1016/J.ENGSTRUCT.2019.05.022.

[16] Boem I. Masonry Elements Strengthened with TRM: A Review of Experimental, Design and Numerical Methods. Buildings 2022;12. https://doi.org/10.3390/buildings12091307.

[17] Mininno G. Modelling of the behaviour of TRM-strengthened masonry walls 2016.

[18] Dalalbashi A, Ghiassi B, Oliveira D V. Freeze-thaw effects on the performance of TRM-strengthened masonry. Journal of Building Engineering 2022;59. https://doi.org/10.1016/j.jobe.2022.105077.

[19] García D, Díez J. Stone masonry walls: Strengthening with TRM (I). In: Ayala DFD, Fodde E, editors. Structural Analysis of Historic Construction, London: Taylor & Francis Group; 2008, p. 851–9.

[20] Mezrea PE, Ispir M, Balci IA, Bal IE, Ilki A. Diagonal tensile tests on historical brick masonry wallets strengthened with fabric reinforced cementitious mortar. Structures 2021;33:935–46. https://doi.org/10.1016/J.ISTRUC.2021.04.076.

[21] ACI Committee 549. ACI 549.4R-13: Guide to Design and Construction of Externally Bonded Fabric- Reinforced Cementitious Matrix (FRCM) Systems for Repair and Strengthening Concrete and Masonry Structures. Farmington Hills, Michigan: 2013.

[22] RILEM TC 232-TDT. Recommendation of RILEM TC 232-TDT: test methods and design of textile reinforced concrete. Mater Struct 2016;49:4923–7. https://doi.org/10.1617/s11527-016-0839-z.

[23] de Felice G, Aiello MA, Caggegi C, Ceroni F, De Santis S, Garbin E, et al. Recommendation of RILEM Technical Committee 250-CSM: Test method for Textile Reinforced Mortar to substrate bond characterization. Mater Struct 2018;51:95. https://doi.org/10.1617/s11527-018-1216-x.

[24] Consiglio Superiore dei Lavori Pubblici. Linea Guida per la identificazione, la qualificazione ed il controllo di accettazione di compositi fibrorinforzati a matrice inorganica (FRCM) da utilizzarsi per il consolidamento strutturale di costruzioni esistenti. 2018.

CHAPTER 2

MASONRY: CHARACTERIZATION, PERFORMANCE AND STRENGHTENING SYSTEMS

The legacy of previous cultures provided Portugal with a diverse architectural heritage, and with a range of masonry construction techniques. However, in the last decades reinforced concrete became prevalent, leading to the present masonry infill methods. The 2021 Census data reveals that around 50 % of the buildings in Portugal have structural masonry walls. A considerable portion of these structures requires rehabilitation, especially those constructed before 1945. Also In Europe, most of the buildings featured reinforced concrete, with structural masonry walls and infill elements including sound and hollow brick walls, concrete blocks and timber panels. This chapter deals with the characterization of the Portuguese and European building stock, the seismic risk at European level and public policies for the seismic strengthening. Additionally, structural strengthening techniques commonly used in masonry elements are discussed as well as the experimental evaluation of masonry elements.

2.1. CHARACTERIZATION OF THE BUILDING STOCK: PORTUGAL AND EUROPE

Masonry is widely used as infill and as structural element, not only Portugal and Europe, but also in several other regions. In this section the main focus is on masonry construction in Portuguese and European territory.

2.1.1. Masonry in Portugal: Past, Present and Future

Romans spread their construction techniques around all regions under their domain. In the Portuguese territory there are many traces and examples of constructions such as roads, bridges and temples, in masonry or stonework. With the collapse of the Roman Empire other communities occupied the Central and Northern regions of Portugal. The Sueves and Visigoths remained in these regions between the 3th and 8th century, having built several stone masonry buildings. The southern region was occupied by the Arabs between the 8th and 12th century. That influence is still present by the use of adobe masonry and rammed earth constructions, as well as the practices of whitewashing the walls of the buildings [1].

Scientific developments lead to the increase in knowledge about constructive techniques during the following centuries, leading to the improvement of the response of buildings to seismic actions, shortly after the occurrence of the earthquake of Lisbon in 1755. The “Gaiola Pombalina" construction system was aimed at increasing the flexibility of buildings and improve the behaviour against seismic action. According to this concept, the structures are composed of three-dimensional wood trusses filled by stone masonry [2–5]. In regions with lower seismic activity, the buildings continued to be erected with structural masonry walls, sometimes combining several materials. Often masonry composed of low-quality natural stone and ceramic brick was used. In the Central Coast region of Portugal, typically adobe masonry was used, being nowadays possible to observe a vast built heritage based on this technique [6].

With the arrival of reinforced concrete construction, traditional structural masonry walls were gradually replaced by the "modern" system based on reinforced concrete frames and slabs and infill masonry hollow brick walls, see **Figure 2.1. Table 2.1** summarizes the most important stages of evolution experienced by buildings in Lisbon between these two moments that have marked the history of construction in Portugal: the Lisbon earthquake and the appearance of reinforced concrete.

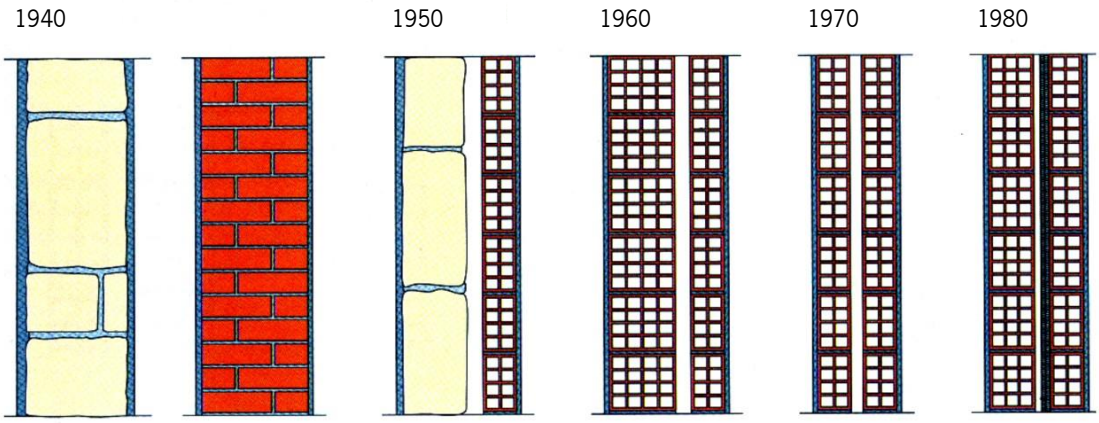


Figure 2.1: Evolution from type of masonry walls in Portugal [7].

Table 2.1: Structural characteristics of buildings as a function of the construction period, Lisbon area [8].

Construction period	Structural characteristics
Before 1755	Stone Masonry
From 1755 to 1870	"Gaiola Pombalina"
From 1870 to 1930	"Gaioleiro" Masonry
From 1930 to 1940	Reinforced concrete and masonry mixed structures
From 1940 to 1960	Reinforced concrete and brick masonry
After 1960	Reinforced concrete with infill masonry walls

The data collected in Census 2021 [9] reveals the existence of 3.6 million buildings whose structure and materials are of a non-precarious nature, with an expected service duration of at least 10 years, also referred to as classical buildings, see **Figure 1.1**. Considering the more detailed data referring to the structural elements from the previous Census 2011 [10], about 1.7 million were made of reinforced concrete structures, 1.1 million had structures with masonry walls and concrete slabs, 480 thousand presented structures with masonry walls (without slab), 189 thousand featured structures with rubble masonry walls or adobe and, finally, the category other included wooden, metallic structures, etc., with 29 thousand buildings. From this data it is possible to infer that there are about 1.77 million buildings whose walls are made of structural masonry. In **Figure 2.2** the type of structural system distribution is presented in percentage.

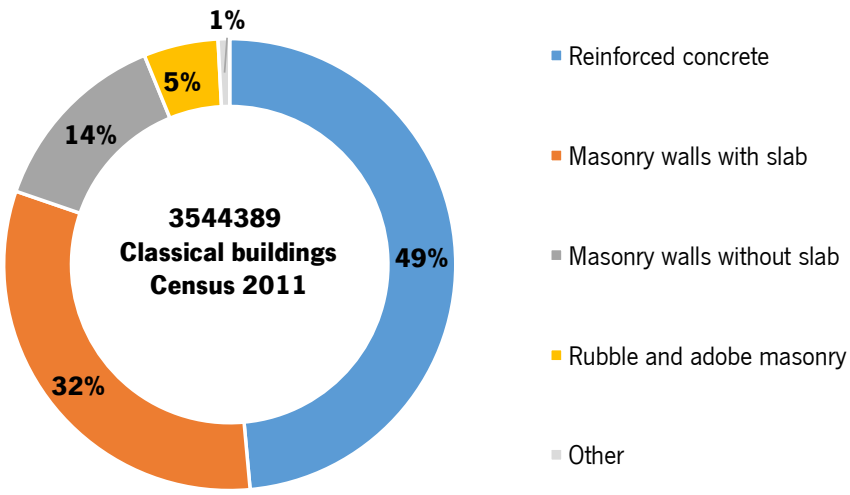


Figure 2.2: Distribution of classical buildings for structural system in 2011, adapted from [10].

Considering the values given in Census 2011 a total of 10% of buildings require repairs from medium to full scale, representing a total of 354 thousand buildings to be targeted for rehabilitation within the next few years. When the conservation level considering the implementation year is analysed (see **Figure 2.3**), it turns out that about 8% of the total number of classic buildings constructed until 1945 were much degraded. This value refers to buildings with structural masonry, since this was the only constructive technique with expression at that time. The number of buildings showing high degradation and repair needs in the Portuguese territory is present in **Figure 2.4**.

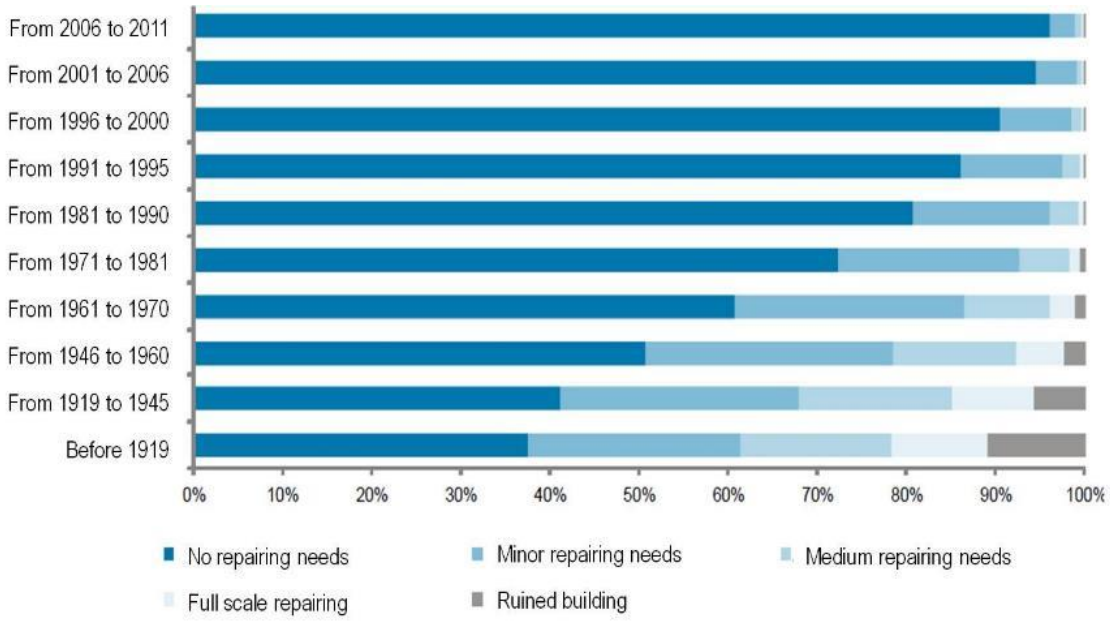
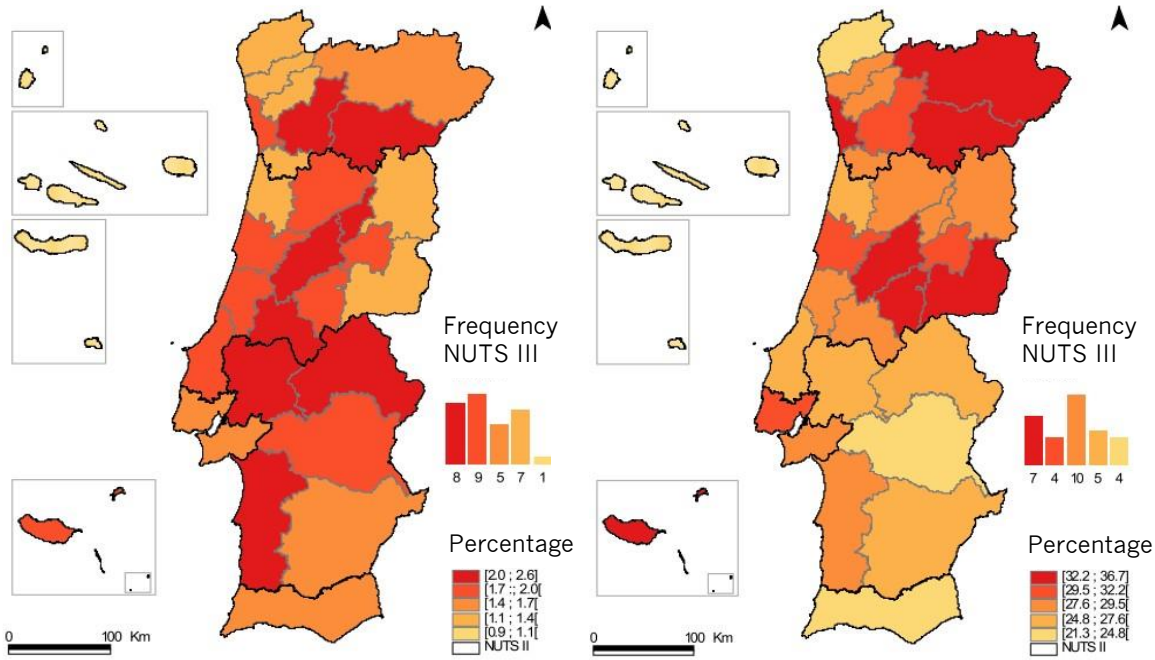


Figure 2.3: Distribution of classical buildings by conservation level considering the year of implementation, adapted from [10].



a) Buildings with high degradation level

b) Buildings with repair needs

Figure 2.4: Buildings distribution in Portugal, adapted from [11].

Considering the Portuguese built heritage, which comprises over 1,200 sites inventoried as National Monuments, Public Interest, Municipal Value or under classification, existing studies estimate the value of the rehabilitation market within this sector at approximately 30.6 billion euros, at 2008 prices [12]. This value serves as an estimate, as the inventory in this segment is still deficient, thus challenging the perception of its real dimension.

2.1.2. Masonry in Europe

The structural systems identified in European countries present some regional variations, in part due to historical events such as the World War II (WWII) but also due to cultural and climatic reasons. After WWII there was an increase in the construction of new buildings, especially in central and eastern European countries, and Butenweg et al. point that 80% of the buildings in the EU countries were built before 1990 [13]. Additionally, Landolfo et al. [14] presented reinforced concrete as the most used structural system followed by structural masonry walls. The infill elements are normally composed of single-layered or double-layered with air chamber hollow brick walls, solid brick or stone masonry, also different infills such as timber panels or solid or hollow concrete blocks can be found. The distribution

of infill walls in different European countries is illustrated in **Figure 2.5**, from this picture, it is evident that the most diffused infill wall type is represented by brick and hollow brick masonry walls.

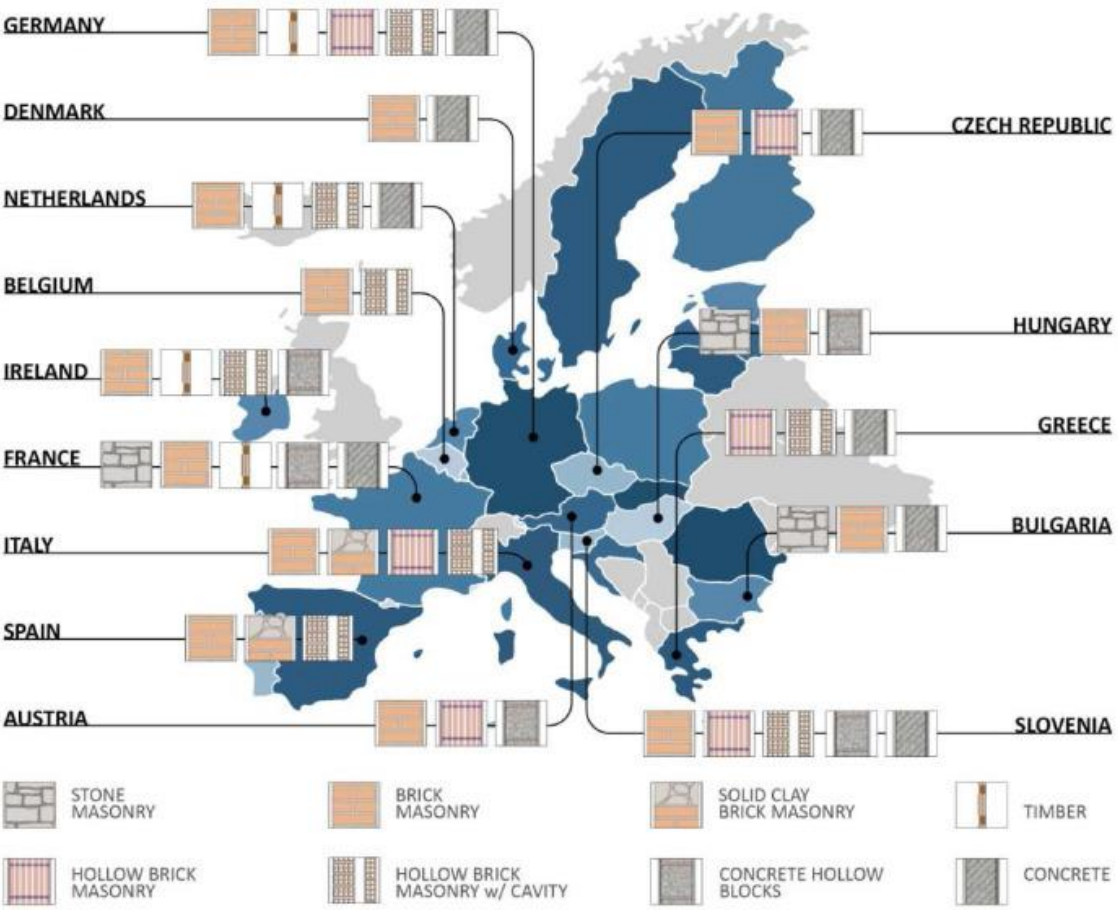


Figure 2.5: Distribution of most used infill elements based on quantitative and qualitative data according to Landolfo et al. [14].

2.2. SEIMIC RISK AND PUBLIC POLICIES FOR THE SEISMIC STRENGTHENING OF EXISTING BUILDINGS

Earthquakes pose a significant risk in some of the world's most seismically active regions, such as Southern Europe, the Middle East and the Circumpolar Belt. These natural disasters are not only highly destructive but also have a significant financial impact. To meet this challenge, seismic design codes play a crucial role in the construction of new buildings and the assessment of the vulnerability of existing structures. Pavel et al. [15] studied the impact of seismic design codes on seismic risk reduction, and used as case study four countries: Italy, Turkey, Greece and Romania. The European

Seismic Risk Model 2020 [16] identifies these countries as having the highest expected average annual losses due to earthquakes. An examination of seismic exposure in these four countries reveals a disquieting fact: out of a total population of more than 170 million people, approximately 130 million live in buildings that are not adequately designed for seismic events or have minimal provisions. This underscores the urgent need for comprehensive seismic design measures to mitigate the potential consequences of future earthquakes. Risk-reduction strategies used for the enhancement of structural and infrastructural earthquake safety and resilience are also discussed by Freddi et al. [17]. In their study the authors divide the risk-reduction strategies in two categories: soft, referring to novel modelling methods/frameworks, early warning systems, disaster financing and parametric insurance; hard, referring to novel structural systems/devices for new structures and retrofitting of existing structures.

The mean peak ground acceleration (PGA) in units of gravity (g) and a 10% exceedance probability in 50 years for the European territory is presented in **Figure 2.6**. The areas in white indicate regions with no seismic hazard, while blue colours indicate comparatively low hazard areas (PGA≤0.1g) and red colours indicate high-hazard areas (PGA≥0.25g). The areas observed to have a higher seismicity are in the Mediterranean, Balkan and central European countries [13]. These areas coincide with areas where masonry buildings have a sound implementation and are also part of the valuable heritage, additionally infill masonry is a common solution in RC frame buildings.

The mean annual expected economic losses caused by earthquakes are lower than 0.2% of the national GDP and large earthquakes in Europe from the past 50 years have produced more than 10 billion Euros in losses and several hundred thousand people affected [15]. Given this, the population should be aware of the importance of the seismic design and retrofitting of existing buildings. However, this perception only exists in the aftermath of a seismic event, better communication of seismic risk would increase seismic risk perception of populations and should be promoted by institutions. In the case of seismic vulnerability, the use of clear language, like inhabitable or uninhabitable, and the associated occurrence probabilities in a certain time frame, might be a solution according to Pavel et al. [15].

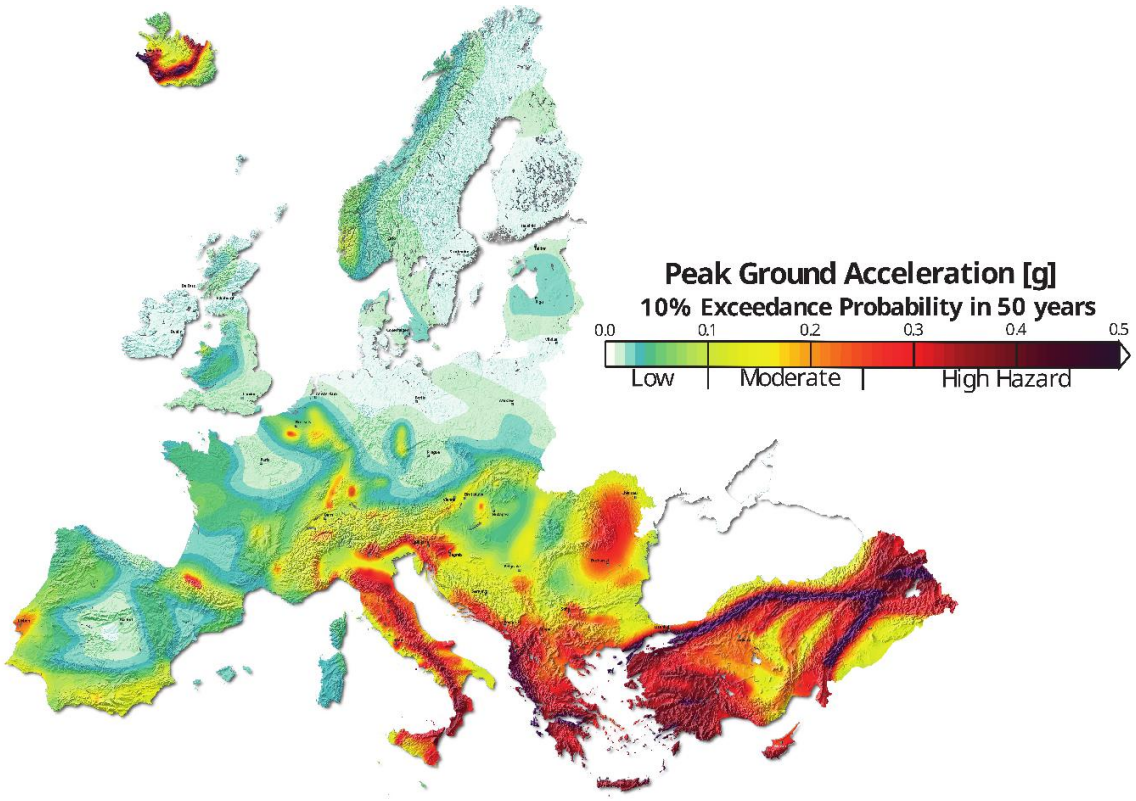


Figure 2.6: Representation of the European Seismic Hazard Map, considering the mean peak ground acceleration (PGA) for 10% exceedance probability in 50 years [16].

The promotion of public policies planned for the seismic retrofit of existing buildings vary among countries. As ultimate goal, they tend to improve the structural integrity of buildings, enhance safety, and reduce the potential damage and casualties caused by earthquakes. These policies often involve a combination of regulations, standards, financial incentives, and educational initiatives. The implementation of regulations and standards are the most common in regions with higher seismic vulnerability. Additionally in countries with better economic situation, financial incentives are promoted more often.

Crowley et al. [18] developed a harmonised classification of seismic design codes across Europe, from no code to high level code. The timeline evolution of seismic codes for each country is presented in **Figure 2.7**, where the vertical black lines represent important updates within a category of design code. Also, earthquakes which have influenced European seismic design are shown [18]. Normally the buildings with no seismic design code are before 1960's, using allowable stresses, very low material strength values and considering mostly the gravity loads. The higher code design level refers to modern seismic design principles that account for capacity design and local ductility measures, like EN 1998-1 [19].

The EN 1998-1 [19] commonly referred as EC8, is the most important standard related with the seismic retrofitting of the existing buildings in seismic regions. The scope of EC8 is to provide the criteria for the evaluation of the seismic performance of existing structures and additionally to depict the methodology to be implemented when strengthening measures are required. Moreover, EC8 provides specific criteria for the design of retrofitting elements and connections to existing structural elements [13].

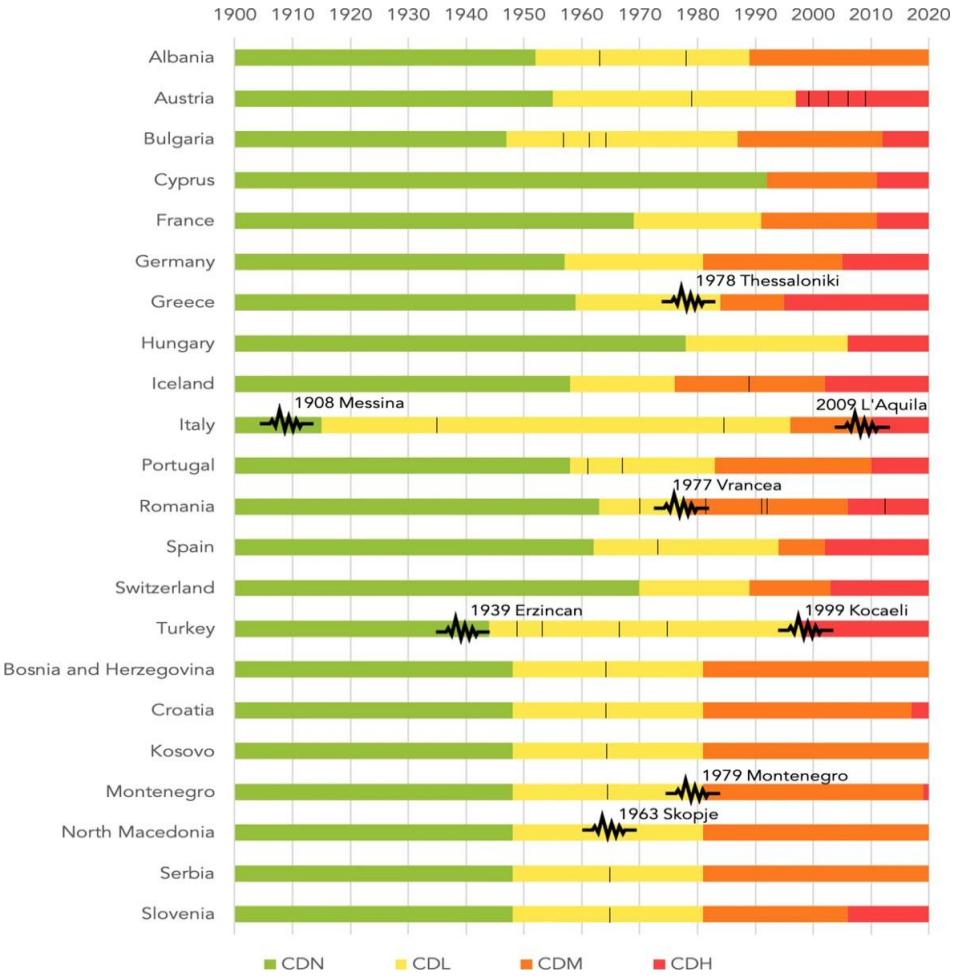


Figure 2.7: Evolution of seismic design codes from 1900 to 2020 across European countries [18]. The code design level is presented as CDN for no seismic design code, CDL for low level, CDM for medium level and CDH for high level.

The policies based on financial incentives are very useful for promoting the strengthening and retrofitting of existing buildings and structures. These have been implemented in several countries at different levels [20], see **Table 2.2**. In Europe, several countries have implemented several public policies to address seismic risks [13]. The policies developed in Italy were very successful and are still being applied. The SISMABONUS program [21], introduced in 2017 and renewed in 2023, provides

financial incentives in the form of tax deductions for seismic and energy renovations of buildings, including residential and social housing. The program aims to encourage homeowners to invest in retrofitting measures that improve the seismic behaviour of their properties in seismic zones 1, 2 and 3. Additionally, building codes and regulations in Italy require new constructions to meet specific seismic design standards.

Table 2.2: Seismic retrofit policies of earthquake-prone countries, according to [20].

Country	Typical vulnerable buildings	Retrofit policies	Mechanisms for financing retrofits
Italy	-URM and RC buildings constructed before 1980	-Compulsory earthquake insurance for residential buildings	-Sponsored or reinsured by the government
Romania	-Buildings constructed before 1941, RC buildings with three or more stories constructed before 1978	-Voluntary retrofit for residential buildings	-Supported by Ministry of Regional Development and Public Administration
Turkey	-Masonry and RC buildings constructed before 1980	-Retrofit or reconstruction for schools, hospitals, and other priority public buildings -Compulsory earthquake insurance for residential buildings	-Financed by the World Bank, European Investment Bank, Council of Europe Development Bank -Sponsored or reinsured by the government
Iran	-Adobe, masonry, and RC buildings from before 1990	-Voluntary retrofit for residential buildings	-Supported by Iranian Housing Foundation
India	-Buildings constructed before 1962, RC buildings with open ground floors or soft stories, non-engineered structures	-Mandatory seismic retrofit for government-owned buildings and selected privately owned buildings (e.g., hospitals, schools), voluntary retrofit for other privately-owned buildings	-Supported by National Disaster Management Authority
Nepal	-Adobe, masonry, and RC buildings constructed before 2004	-Retrofit or reconstruction for schools -Voluntary retrofit for residential buildings	-Financed by Asian Development Bank, World Bank, Australian aid -Supported by Nepal Ministry of Urban Development
China	-Masonry and RC buildings constructed before 1989	-Retrofit work planned and conducted by local governments	-Fully funded by local governments
Japan	-Masonry and RC buildings constructed before 1981	-Mandatory retrofit for large-scale buildings and public buildings, voluntary retrofit for small- and medium-size residential buildings	**Regular incentive**: governmental subsidy covering 66.6% of seismic diagnosis cost and 23% of the seismic retrofit cost **Limited-time promotion:** governmental subsidy covering 83.4–100% of diagnosing cost and 45.8–66.7% of retrofit cost

Country	Typical vulnerable buildings	Retrofit policies	Mechanisms for financing retrofits
United States	-URM buildings, wood-frame soft-story buildings constructed before 1978, RC buildings constructed before 1976, pre-Northridge steel moment frame buildings	**Policies at local government level:** **California State:** mandatory retrofit for URM buildings in regions of the highest seismicity; mandatory retrofit for wood-frame soft-story buildings in San Francisco Bay area and Los Angeles metropolitan region; mandatory retrofit for RC and steel moment frame buildings in Los Angeles metropolitan region.	-Retrofit grants from the Federal Emergency Management Agency, California Earthquake Authority, or the City Council
		Oregon State: mandatory retrofit for URM buildings in the Portland City, Building Class I to V, voluntary retrofit for URM buildings in other regions	-Fee waiver for plan review, building permits, or both -Long-term loans with a low-interest rate, sponsored by the city government
		Washington State: preparing a mandatory retrofit policy for URM buildings	-Pass retrofit cost to tenant
New Zealand	-URM buildings, any buildings with three or more stories constructed before 1976, any buildings with one or two stories constructed before 1935	-73% of territorial authorities adopting seismic retrofit levels between 33% and 67% of new building standards, and 27% of them approving 67% -45% of local authorities choosing an active approach to implement retrofit policies, 32% of them using a passive approach, and 23% of them employing combined active-passive approach	-Funded by the government if the building is recognized as a heritage

2.3. STRUCTURAL STRENGTHENING OF MASONRY WALLS

2.3.1. Scope of Interventions

Prior to any intervention or structural strengthening, a careful and detailed assessment should be made to understand the real level of degradation and the most unfavourable changes to the structure that the intervention might introduce. According to Lourenço et al. [22], the approach should take similar steps to the ones used in medicine:

- study of the historical evolution of the building and overview of the relevant data;
- identification of possible causes and degradation; choice and application of intervention techniques;
- monitoring the effectiveness of the intervention.

Most of the times the structural rehabilitation of masonry structures modifies its original balance, representing a risk for older structural masonry but also in newer infill masonry. Therefore, the extent of interventions should follow the principle of minimizing intrusive approaches and consequently must be the minimum required to achieve the desired goals. A list of interventions to improve the overall

structural behaviour and perform a structural rehabilitation of masonry elements is given in **Table 2.3**.

Materials used nowadays are predominantly different from the original, therefore it is essential to ensure compatibility between the strengthening solution and the original structure. The materials selected for structural reinforcement should not introduce new pathologies, nor have completely different physical or chemical behaviours. Finally, durability should be an aspect to consider in the choice of materials, especially in interventions in historic buildings.

Table 2.3: Non-intrusive options for structural rehabilitation [10].

Scope of structural intervention	Options
Increasing the overall structural behaviour	Introduction of new bracing elements
	Improving the link between structural components
	Introduction of devices that alter the dynamic characteristics of the structure
Structural rehabilitation of masonry	Increase the resistance of the element by confinement
	Increase of the resistance of element by adding a new material
	Reconstruction of the section using the same material
	Reconstruction of the section by reusing or using other material

Illustrating the concepts of conservation and rehabilitation in the life cycle of a building, **Figure 2.8** presents a model of analysis of the state of conservation and the need for maintenance, of improvement or recovery interventions throughout the useful life, presented by ISO 15686-7 [23].

The performance levels of the construction and its components change during the life cycle of the construction (see **Figure 2.8**). The in-use conditions can also be subject to change. Therefore, a proper assessment of the service life should include a thorough assessment of the existing in-use conditions and record any changes to the actions used in the design process, if applicable. **Figure 2.8** illustrates scenarios in the development of the performance (bold line) of construction works from delivery through the maintenance and operation phase. There is a deviation in performance from the client's expectations and requirements from the brief (initial) phase until the delivery ("as built") phase, often due to failures or damage during fabrication. The expectation gap is increased further due to the continuous rise in new requirements and upgrading, business development, etc.

After the delivery, performance decreases during operation, due to wear and tear, or simply due to the age factor, if left with no maintenance. Therefore, the construction and its components are subjected to various corrective actions, or maintenance operations, to keep up with required performance. These actions can be proactive, which is preferred, or reactive, which is largely the current practice. In both cases, inspections and performance assessments should be the basis for maintenance planning. This applies to all functionalities.

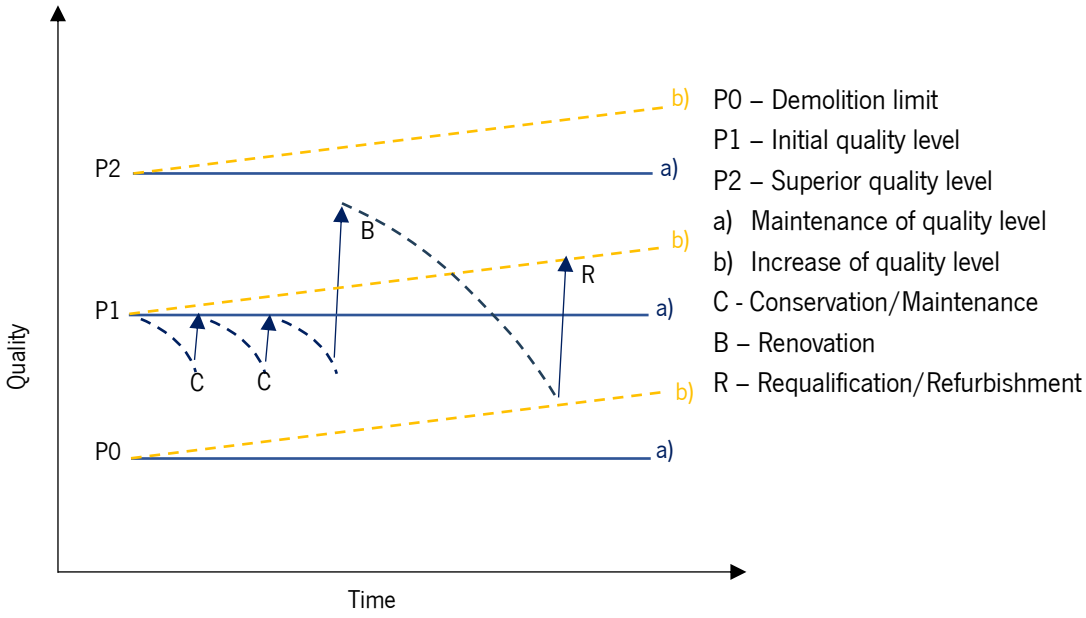


Figure 2.8: ISO 15686-7 model for analysing the level of interventions throughout the life cycle of a building [23].

Conservation refers to preventive maintenance of a building, that is, actions aimed at maintaining its current condition, preventing deterioration or premature aging. These actions may include cleaning, repairs, and replacement of worn or faulty parts or components. Rehabilitation, on the other hand, is a more comprehensive intervention aimed at recovering or improving the conditions of a building that already has problems, such as structural failures, infiltration, among others. Rehabilitation may be necessary when preventive maintenance was not enough to preserve the integrity of the building.

2.3.2. Consolidation, Protection and Strengthening Solutions

Knowing the different anomalies and causes that affect masonry structures, it is necessary to define the level of intervention and proceed to an intervention strategy. In some cases, there is the need to restore part of its initial resistant capacity, this is when consolidation techniques are adopted. In other cases, there is the need to increase the load carrying capacity or reduce the deformation to acceptable

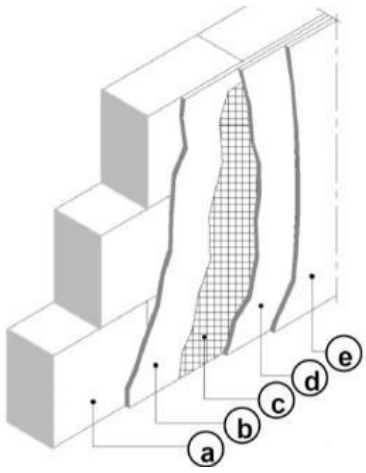
service levels, and strengthening techniques are adopted. Phenomena related to humidity are in general one of the biggest concerns of interventions in old buildings. These phenomena can be associated to the appearance of several anomalies, leading to harmful situations to the structure's durability, see **Table 2.4**.

Table 2.4: Common types of techniques applied in masonry walls.

Consolidation techniques	Strengthening techniques	Protection against humidity
- Consolidation with grout injection - Replacement of degraded material	- Repointing - Sprayed mortar overlay - Strengthening with FRP composites - "Jacketing" - Post-tensioning systems	- Chemical barrier against uptake humidity - Water repellent treatments

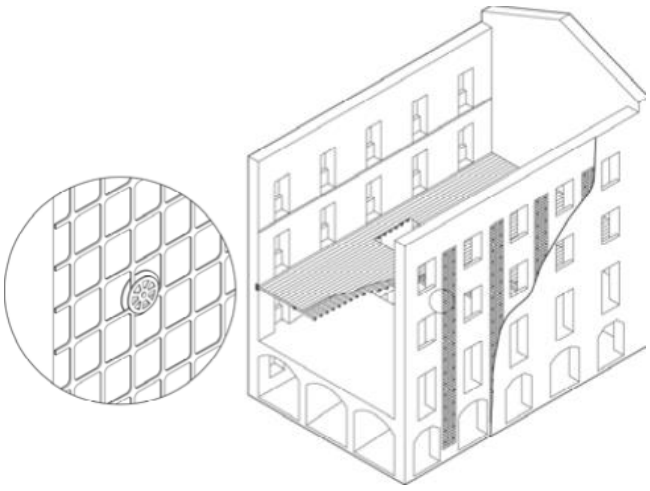
2.3.2.1. Reinforcement by overlaying a strengthening system

The reinforcement through the application of a mortar overlay reinforced with a mesh is one of the most used techniques in recent years [24]. It consists of setting a reinforcement mesh (fibreglass, polypropylene mesh, etc.) by nailing small diameter pins to strengthen the structure, and subsequently shotcreting or manually applying a hydraulic lime or cement mortar, see **Figure 2.9**. It can be applied to one or both sides of the wall, in some cases transverse connectors are also applied. Its implementation is performed on walls in good condition but with high surface degradation or damaged by changes in temperature or low-intensity earthquakes. The advantage of the application of this technique is the use of low modulus of elasticity and high ductility reinforcement, not susceptible to corrosion. Analytical and shaking table tests have demonstrated the effectiveness of this technique, [25]. It should be stressed, though, that this technique should be limited to elements whose aesthetic value is reduced, since it "hides" the original wall.



(a) masonry (b) 1st mortar layer (c) strengthening mesh; (d) 2nd mortar layer; (e) finishing plaster layer

a) Application detail [26].

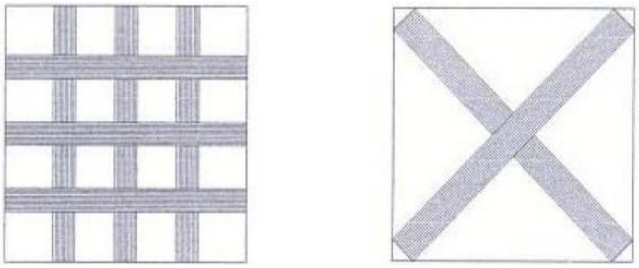


b) System with connectors applied to a building, [25].

Figure 2.9: Overlay strengthening system.

2.3.2.2. Reinforcement with composite materials, FRP

The use of composite FRP (Fibre Reinforced Polymer) in a wall reinforcement comprises the application of a polymeric matrix material reinforced with continuous carbon (CFRP), glass (GFRP) or aramid fibres (AFRP) through gluing with high performance resins or adhesives. These reinforcements can take the form of rolled straps, arranged horizontally, vertically or diagonally (see **Figure 2.10**). The main goal is to confine walls and counter the flexural stresses associated with horizontal loads perpendicular to the plane (earthquakes), and contribute to the shear strength. The applicability of this technique is constrained by the irregularity of the wall that makes it difficult to bond. Other drawbacks of FRP are their susceptibility to fire scenarios, high costs and brittle behaviour (except for aramid fibres) [27].



(a) Orthogonal grid layout (b) Diagonal layout

Figure 2.10: Layout of FRP strips in strengthening situations [27].

2.3.2.3. Reinforcement with "Jacketing" technique

In case of masonry with low compressive strength or heavily damaged, presenting large irregularities or combining different materials with weak bonding, the "jacketing" can be a useful technique. Once it is a very invasive technique it should be prescribed only in cases where no alternatives are possible, [27]. This technique consists of applying a layer of concrete reinforced with steel mesh prefixed with nails to one or both sides of the wall, similarly to the case of the overlay strengthening technique. The result is a coating with a thickness higher than a conventional plaster and with better mechanical characteristics, especially in terms of shear behaviour (see **Figure 2.11**). Details of this solution may be found in **Figure 2.12**.

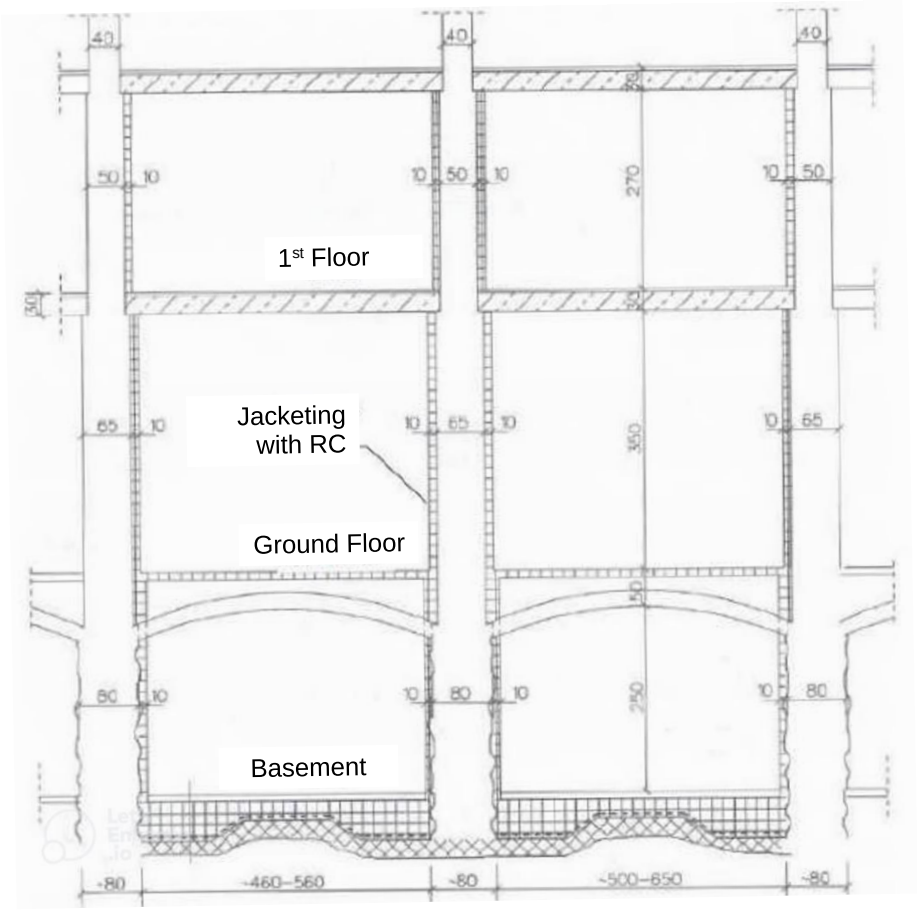


Figure 2.11: Strengthening of structural walls with “jacketing” technique [24].



(a) Reinforcement photo (b) detail

Figure 2.12: Jacketing of shear walls [28].

2.4. EXPERIMENTAL ASSESSMENT OF MASONRY

The characterization of the behaviour of a masonry element should consider several factors according to Binda et al, [29]: geometry; characteristics of masonry texture; physical, chemical and mechanical characteristics of the components (bricks, stones, mortar); and characteristics of masonry as a composite material. In the case of brickwork structures, codes can be used to obtain an approximate estimation of the strength of masonry as a function of the components (bricks, render, etc). In the case of natural stone masonry, the problem is more complex, and some questions can be asked [29]:

- Can the masonry texture be easily identified?
- Can mechanical characteristics of stones and mortars be determined or be considered statistically reliable?;
- Can strength and deformability parameters be used to extrapolate the global strength and deformability of masonry?.

Depending on the answers to these questions the confidence on the characterization of the masonry elements may change, thus leading to a variation to the coefficient given in the Italian codes.

2.4.1. Characterization of in-plane behaviour: compressive behaviour

According to the formulation from EC6 [30], the compressive strength of masonry walls with general purpose mortar can be estimated as follows in **Eq. (2.1)**.

$$f_k = k \times {f_b}^{0.7} \times {f_m}^{0.3} \quad \textbf{(2.1)}$$

where: f_k is the characteristic compressive strength of the masonry, in N/mm²; k is a constant; f_b is the normalized mean compressive strength of the units, in the direction of the applied action effect, in N/mm²; f_m is the compressive strength of the mortar, in N/mm².

For the estimation of the elasticity modulus of masonry, EC6 [30] recommends the adoption of a general value varying between 700 and 1000 times the compressive strength.

The experimental evaluation of masonry elements can be performed following the EN1052-1 [31], see **Figure 2.13**. The method to obtain the strength of masonry in compression without considering the effects of loading restraint, slenderness or eccentricity of loading, follows **Eq. (2.2)**

$$f_i = \frac{F_{i,max}}{A_i} \quad \textbf{(2.2)}$$

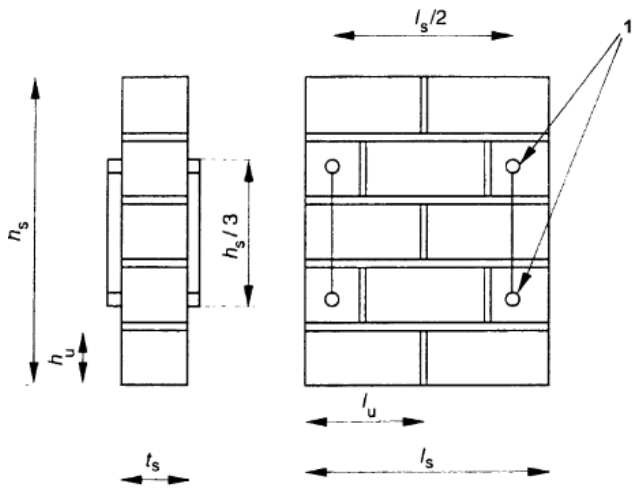


Figure 2.13: Geometry of the specimen to characterize the compressive strength of masonry elements [31].

2.4.2. Characterization of in-plane behaviour: shear Behaviour

The typical in-plane failure modes of masonry walls and piers are clearly characterised and are mostly determined by the element's aspect ratio, axial stress level, and shear capacity. **Figure 2.14** shows common in-plane failure modes. The two main types of in-plane failure mechanisms are the shear failure and the flexural failure. The flexural failure can happen for low axial loads due to the overturning of the wall with simultaneous crushing of the compressed corner, also known as rocking, or toe-crushing due to the attainment of compression strength of masonry, see **Figure 2.14**a). Alternatively with the increase of the axial load the shear failure modes evolve to sliding due to a lower normal force along horizontal joints, see **Figure 2.14**b) failure due to sliding along the bed joints, see

Figure 2.14c), and the failure due to diagonal cracking, usually associated with the attainment of the tensile strength of masonry see **Figure 2.14**d).

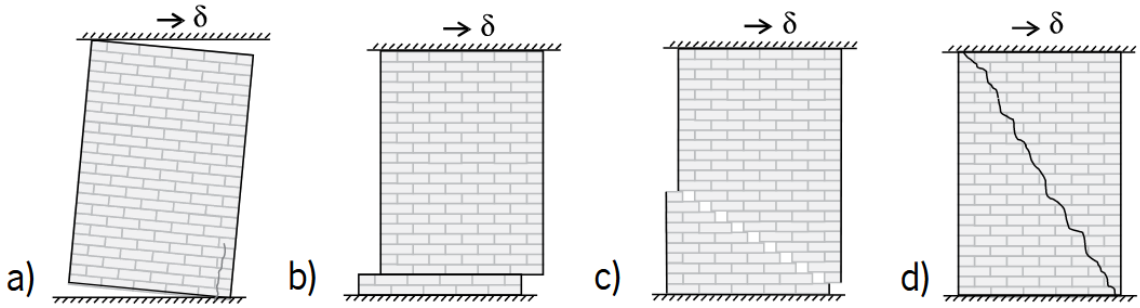


Figure 2.14: Typical in-plane failure mechanisms for unreinforced masonry walls or piers: a) rocking; b) sliding; c) sliding-shear; d) shear. Adapted from [32].

The failure due to diagonal cracking, linked with the tensile strength of masonry, can be evaluated by diagonal tensile tests following the procedures from ASTM E519-15 [33], that induces pure shear stress in the centre of the specimen, see **Figure 2.14**d) and **Figure 2.15**.

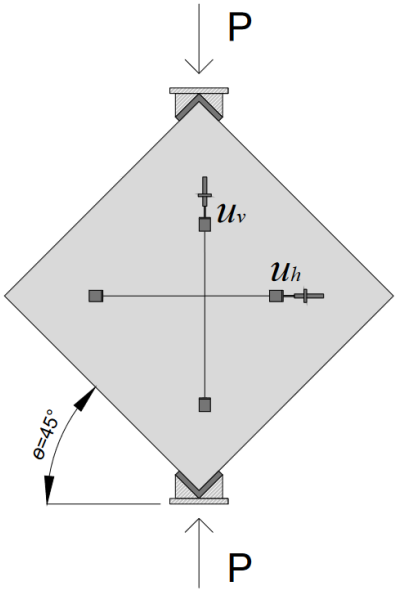


Figure 2.15: Diagonal tensile test set-up.

The values of the shear stress, shear strain and modulus of shear stiffness in the centre of the panel are also obtained experimentally according to the procedures indicated in ASTM E519-15 [33]. The shear stress is obtained by **Eq. (2.3)**.

$$S_s = \frac{0.707 \times P}{A_n} \qquad \textbf{(2.3)}$$

where P is the applied load, A_n is the net area of the specimen's cross-section calculated according to **Eq. (2.4)**:

$$A_n = \left(\frac{w+h}{2}\right) \times t \times n^* \quad \textbf{(2.4)}$$

where w, h and t are, respectively, the width, the height, and the total thickness of the specimen, and n^* is the percentage of the gross area of the unit that is solid, expressed as a decimal.

The shear strain is computed as shown in **Eq. (2.5)**:

$$\gamma = \frac{u_v + u_h}{g} \quad \textbf{(2.5)}$$

where γ is the shearing strain, u_v is the vertical shortening, u_h is the horizontal elongation and g is the vertical gage length.

Finally, the modulus of stiffness in shear is calculated as shown in **Eq. (2.6)**:

$$G = \frac{S_s}{\gamma} \quad \textbf{(2.6)}$$

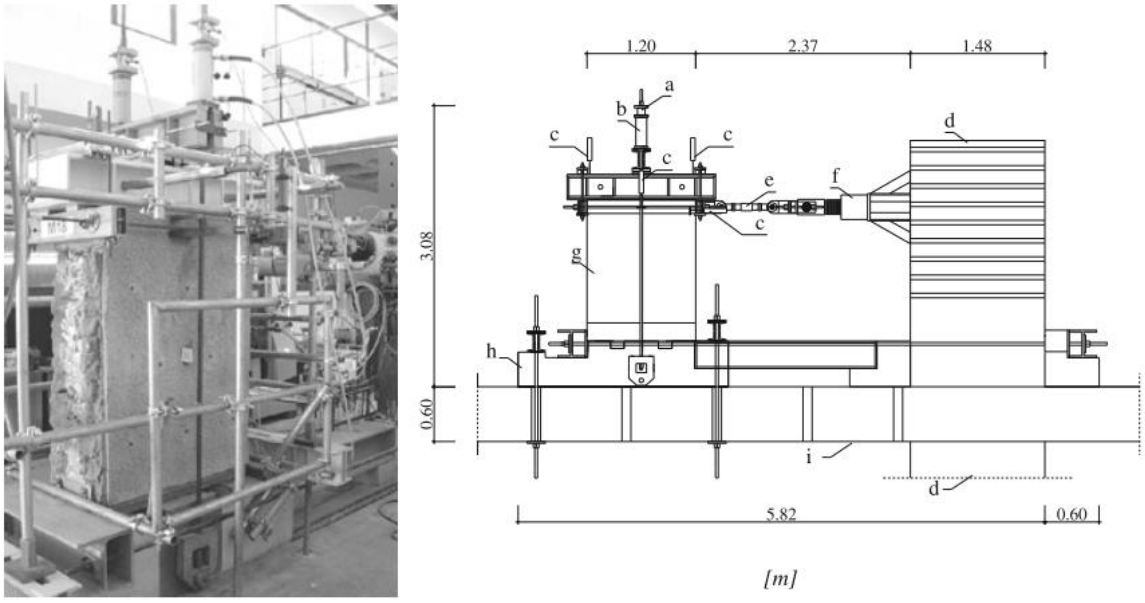
The shear modulus of masonry elements according to the EC 6 [30], can be evaluated by experimentally determining the modulus of elasticity, E, see **Eq. (2.7)**, or by estimating it based on the equations which relate this property with the compressive strength of units and mortar, see in **Eq. (2.1)**.

$$G = 0.4 \times E \quad \textbf{(2.7)}$$

Nevertheless, it was concluded by Tomaževič, [34], that the compression-shear experiments indicate quite different relationships because of inelastic, non-homogeneous and anisotropic characteristics of masonry. Suggesting that G can be evaluated based on lateral displacements, measured during the lateral resistance tests of wall specimens. If not possible to characterize it experimentally, the G/E ratio should be adopted with a more conservative value of around 0.10.

Pinho et al. [35] studied the compression-shear performance of reference specimens and one strengthening solution in walls made of stone masonry. The "set-up" adopted allowed to apply monotonic loads, cyclic loads, or the first two alternated, according to the selected criteria. Solicitations were applied in two stages: a predetermined vertical load was applied first, then a law of variable displacement was imposed by a horizontal actuator until rupture was achieved. The vertical and

horizontal displacements were measured using 7 LVDT's fixed to the base of the specimens. The set - up used for the compression-shear tests is shown in **Figure 2.16**.

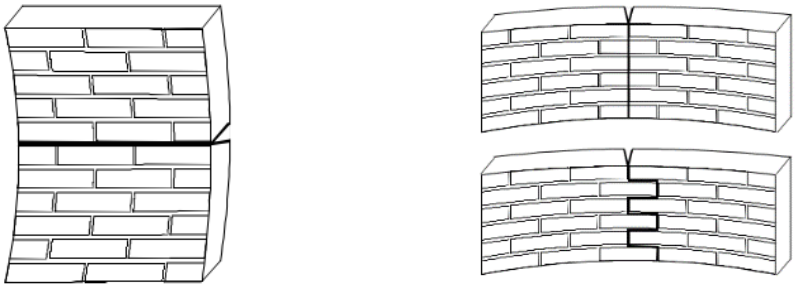


a – load cell; b – vertical actuator; c - LVDTs; d – reaction wall; e – horizontal load cell; f – horizontal actuator; g - specimen; h – reaction slab;

Figure 2.16: Set-up for shear tests with pre- compression [35].

2.4.3. Characterization of the out-of-plane behaviour

The out-of-plane resistance of elements under out-of-plane actions can be directly obtained from the EC6 [30]. The values for different types of masonry are given as a function of the mortar compressive strength, f_m. The out-of-plane resistance is given for two different planes of failure, parallel and perpendicular to bed joints, see **Figure 2.17**, **Table 2.5** and **Table 2.6**.



a) plane of failure parallel to bed joints, f_{xk1} b) plane of failure perpendicular to bed joints, f_{xk2}

Figure 2.17: Planes of failure of masonry in flexure [30].

Table 2.5: Values for plane of failure parallel to bed joints, f_{xk1} [30].

Masonry Unit	f_{xk1} (N/mm²)			
	General purpose mortar		Thin layer mortar	Lightweight mortar
	fm<5N/mm²	fm≥5N/mm²		
Clay	0.10	0.10	0.15	0.10
Calcium silicate	0.05	0.10	0.20	not used
Aggregate concrete	0.05	0.10	0.20	not used
Autoclaved aerated concrete	0.05	0.10	0.15	0.10
Manufactured stone	0.05	0.10	not used	not used
Dimensioned natural stone	0.05	0.10	0.15	not used

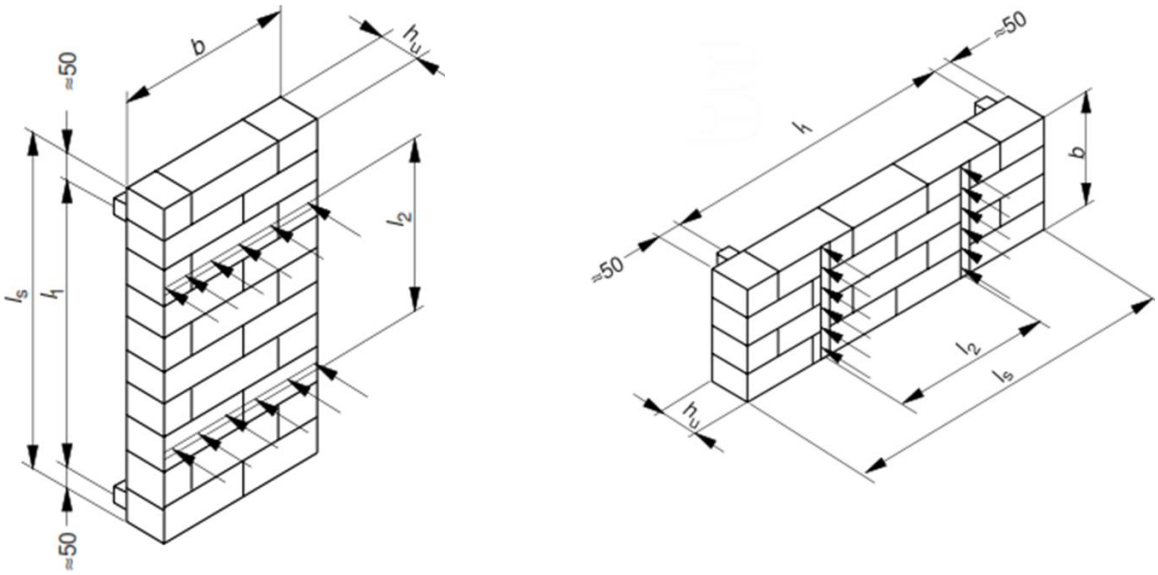
Table 2.6: Values for plane of failure perpendicular to bed joints, f_{xk2} [30].

Masonry Unit		f_{xk2} (N/mm²)			
		General purpose mortar		Thin layer mortar	Lightweight mortar
		fm<5N/mm²	fm≥5N/mm²		
Clay		0.20	0.40	0.15	0.10
Calcium silicate		0.20	0.40	0.30	not used
Aggregate concrete		0.20	0.40	0.30	not used
Autoclaved aerated concrete	ρ<400kg/m3	0.20	0.40	0.20	0.15
	ρ≥400kg/m3	0.20	0.20	0.30	0.15
Manufactured stone		0.20	0.40	not used	not used
Dimensioned natural stone		0.20	0.40	0.15	not used

Alternatively, a more detailed experimental characterization can be performed following the method presented in EN1052-2 [36]. In this case the characterization of the out-of-plane resistance of masonry specimens is based on flexural tests considering the parallel and perpendicular direction to the bed joints. The values obtained, f_{xk1} and f_{xk2} represent the flexural strength of masonry, considering the failure in the parallel and perpendicular direction to the bed joints, see **Eq. (2.8)** and **Figure 2.18**.

$$f_{xi} = \frac{3F_{imax}(l_1 - l_2)}{2b{h_u}^2} \quad \textbf{(2.8)}$$

where: f_{xi} is the flexural strength in the tested direction; F_{imax} is the maximum load obtained; b is the width of the element and h_u is the thickness.



a) plane of failure parallel to bed joints, f_{xk1} b) plane of failure perpendicular to bed joints, f_{xk2}

Figure 2.18: Planes of failure of masonry in flexural [36].

2.5. FINAL CONSIDERATIONS

Portugal has a diverse architectural heritage, presenting a range of masonry construction techniques. Following the devastating 1755 earthquake, Lisbon adopted the "Gaiola Pombalina" system featuring wood trusses and stone masonry. Subsequently, reinforced concrete became prevalent, leading to modern masonry infill methods. The 2021 Census data reveals that around 50 % of the buildings in Portugal have structural masonry walls. A considerable portion of these structures requires rehabilitation, especially those constructed before 1945. Also In Europe, the structural systems evolved and nowadays most of the buildings feature reinforced concrete, with structural masonry walls and infill elements including sound and hollow brick walls, concrete blocks and timber panels.

The seismic risk is higher in seismically active regions like Southern Europe and Middle East. Countries such as Italy, Turkey, Greece, and Romania face high earthquake risks, with 130 million people living in inadequately designed buildings. Seismic design codes, like EN 1998-1 (EC8) [19], play a crucial role in reducing risks, guiding both new constructions and retrofitting efforts. Financial incentives, such as Italy's SISMABONUS program, promote retrofitting and seismic safety improvements, also an effective risk communication and public policies are key to enhancing seismic resilience and reducing future economic losses and casualties.

Before any structural strengthening design, a detailed assessment is essential to understand the building's degradation, this involves studying the building's history, identifying causes of deterioration and ensuring compatibility of materials. Furthermore, to achieve a proper strengthening processes, the behaviour of the elements to strengthen and their contribution to the final capacity of the solution must be understood. In the case of the characterization of masonry behaviour several factors should be involved, namely: geometry, texture, and the physical, chemical, and mechanical properties of its components (bricks, stones, mortar). The strength estimation of masonry can be derived from codes, but for a more reliable assessment the identification of mechanical properties by experimental testing should be performed.

Several knowledge gaps and research needs have been identified throughout this chapter. Current methods for characterizing masonry strength are limited in their ability to account for the contribution of masonry elements within reinforcement solutions. Additionally, there is a critical need to develop simplified experimental methods for predicting the biaxial diagonal behaviour of infill masonry elements. Existing standards provide only limited procedures for diagonal monotonic testing and fail to propose cyclic loading protocols that could yield valuable information about stiffness degradation patterns.

2.6. REFERENCES

[1] Correia JEF. Análise experimental de um murete de alvenaria de pedra tradicional de grandes dimensões. Universidade Nova de Lisboa, 2011.

[2] Lourenço PB. Dimensionamento de Alvenarias Estruturais. Guimarães: 1999.

[3] Ortega J, Vasconcelos G, Rodrigues H, Correia M. Local seismic cultures: The use of timber frame structures in the south of Portugal. Lecture Notes in Civil Engineering 2016;1:101–11. https://doi.org/10.1007/978-3-319-39492-3_8/COVER.

[4] Duarte C, Morais A, Morais A, Fialho C, Diogo B, Ivanova S. Structural efficiency of the 'Pombalino Frontal' infilled with mortar. IOP Conf Ser Mater Sci Eng 2021;1148:012007. https://doi.org/10.1088/1757-899X/1148/1/012007.

[5] Kouris LAS, Meireles H, Bento R, Kappos AJ. Simple and complex modelling of timber-framed masonry walls in Pombalino buildings. Bulletin of Earthquake Engineering 2014;12:1777–803. https://doi.org/10.1007/S10518-014-9586-0/TABLES/6.

[6] Silveira D, Varum H, Costa A, Martins T, Pereira H, Almeida JAPP de. Mechanical properties of adobe bricks in ancient constructions. Constr Build Mater 2012;28:36–44. https://doi.org/10.1016/j.conbuildmat.2011.08.046.

[7] Pacheco Torgal F, Jalali S. Future trends in the sustainability of masonry units. Teoria e Prática Na Engenharia Civil 2010;16:19–28.

[8] Pinho FF da S. Sistematização do estudo sobre paredes de edifícios antigos. Ingenium, No 19 (in Portuguese) 1997:49–59.

[9] Instituto Nacional de Estatística IP. Censos 2021 Resultados Definitivos - Portugal. Lisboa: Instituto Nacional de Estatística, I.P; 2022.

[10] INE. Parque Habitacional em Portugal : Evolução na última década 2012:1–10.

[11] INE. Censos 2011 Resultados Definitivos - Portugal 2012:1–560.

[12] Afonso FP, Martins B, Vital C, Adão D, Neves F das, Martins L, et al. O Mercado da Reabilitação: Enquadramento, Relevância e Perspectivas 2009:109.

[13] Butenweg C, Gervasio H, Gkatzogias K, Manfredi V, Masi A, Pohoryles D, et al. Policy measures for seismic and energy upgrading of buildings in EU Member States. Publications Office of the European Union; 2022. https://doi.org//10.2760/518982.

[14] Landolfo R, Formisano A, Di Lorenzo G, Di Filippo A. Classification of european building stock in technological and typological classes. Journal of Building Engineering 2022;45:103482. https://doi.org/10.1016/J.JOBE.2021.103482.

[15] Pavel F. Seismic Design Codes—Key Elements for Seismic Risk Perception and Reduction in Europe. Buildings 2023;13. https://doi.org/10.3390/BUILDINGS13010158.

[16] Crowley H;, Dabbeek J;, Despotaki V;, Rodrigues D;, Martins L;, Silva V;, et al. European Seismic Risk Model (ESRM20). 2021. https://doi.org/10.3929/ethz-b-000590388.

[17] Freddi F, Galasso C, Cremen G, Dall'Asta A, Di Sarno L, Giaralis A, et al. Innovations in earthquake risk reduction for resilience: Recent advances and challenges. International Journal of Disaster Risk Reduction 2021;60:102267. https://doi.org/10.1016/J.IJDRR.2021.102267.

[18] Crowley H, Despotaki V, Silva V, Dabbeek J, Romão X, Pereira N, et al. Model of seismic design lateral force levels for the existing reinforced concrete European building stock. Bulletin of Earthquake Engineering 2021;19. https://doi.org/10.1007/s10518-021-01083-3.

[19] CEN. EN 1998-1:2004 Eurocode 8: Design of structures for earthquake resistance - Part 1: General rules, seismic actions and rules for buildings. Brussels: COMITÉ EUROPÉEN DE NORMALISATION; 2004.

[20] Zhang Y, Fung JF, Johnson KJ, Sattar S. Review of Seismic Risk Mitigation Policies in Earthquake-Prone Countries: Lessons for Earthquake Resilience in the United States. Journal of Earthquake Engineering 2022;26. https://doi.org/10.1080/13632469.2021.1911889.

[21] European Comission. Superbonus - Strengthening of the Ecobonus and Sismabonus for energy efficiency and building safety (Italy) n.d. https://commission.europa.eu/projects/superbonus-strengthening-ecobonus-and-sismabonus-energy-efficiency-and-building-safety_en (accessed April 18, 2024).

[22] Lourenço PB, Oliveira D V. Conservation of ancient constructions and application to a masonry arch bridge 2006.

[23] ISO. ISO 15686-7:2017 Buildings and constructed assets —Service-life planning - Part 7: Performance evaluation for feedback of service life data from practice. vol. 7. Switzerland: 2017.

[24] Azevedo HD de S. Reforço de Estruturas de Alvenaria de Pedra, Taipa e Adobe com Elementos de Madeira Maciça. Universidade do Porto, 2010.

[25] Cóias V. Reabilitação estrutural de edificios antigos. Lisboa: Argumentum; 2007.

[26] Pereira DF de SM. Estudo Sísmico de Edifícios Antigos: Reforço e análise não linear. Universidade Técnica de Lisboa, 2009.

[27] Roque JCA. Reabilitação estrutural de paredes antigas de alvenaria. Universidade do Minho, 2002.

[28] Mustafaraj E, Corradi M, Yardim Y, Luga E, Codur MY. Ferrocement, Carbon, and Polypropylene Fibers for Strengthening Masonry Shear Walls. Materials 2023;16. https://doi.org/10.3390/ma16134597.

[29] Binda L, Saisi a., Tiraboschi C. Investigation procedures for the diagnosis of historic masonries. Constr Build Mater 2000;14:199–233. https://doi.org/10.1016/S0950-0618(00)00018-0.

[30] CEN. EN 1996-1-1:1995 Eurocode 6 - Design of masonry structures - Part 1-1: General rules for reinforced and unreinforced masonry structures 2005.

[31] CEN. EN 1052-1 Methods of test for masonry - Part 1: Determination of compressive strength 1998.

[32] Elghazouli A, editor. Seismic Design of Buildings to Eurocode 8. CRC Press. CRC Press; 2016. https://doi.org/10.1201/9781315368221.

[33] American Society for Testing and Materials. E 519 – 02: Test Method for Diagonal Tension (Shear) in Masonry Assemblages 2022. https://doi.org/10.1520/E0519_E0519M-22.

[34] Tomaževič M. Shear resistance of masonry walls and Eurocode 6: shear versus tensile strength of masonry. Mater Struct 2009;42:889–907. https://doi.org/10.1617/s11527-008-9430-6.

[35] Pinho FFS, Lúcio VJG, Baião MFC. Rubble stone masonry walls in Portugal strengthened with reinforced micro-concrete layers. Bulletin of Earthquake Engineering 2011;10:161–80. https://doi.org/10.1007/s10518-011-9280-4.

[36] Comité Européen de Normalisation. EN 1052-2:1999 Technical Methods of test for masonry - Part 2: Determination of flexural strength ;1999.

CHAPTER 3

TEXTILE REINFORCED MORTAR FOR THE STRENGTHENING OF MASONRY

This chapter discusses the different types of matrices, fibres and meshes used in the TRM systems. It also discusses the different types of tests adopted for the experimental characterization (pull-out, tensile, bond shear, etc...) the procedures and type of information obtained from these tests. Finally, the most important tests proposed by standards for durability and strengthening efficiency characterization of TRM are discussed.

3.1. TEXTILE REINFORCED MORTARS

TRM systems have emerged as an innovative solution for the strengthening and retrofitting of existing masonry structures, particularly in seismic-prone regions. The typical configuration consists of a cementitious mortar matrix and an open mesh textile reinforcement, often made from materials such as glass, carbon, basalt, or aramid fibres [1–5]. This combination results in a composite material that exploits the advantageous properties of both components: the mortar provides compressive strength and compatibility with traditional masonry, while the textile mesh provides tensile strength and crack-bridging capabilities. When applied to infill walls and load-bearing masonry elements, TRM systems significantly enhance seismic performance. Experimental and analytical studies have consistently demonstrated that TRM retrofitting increases the lateral load capacity, ductility, and energy dissipation of masonry panels subjected to in-plane and out-of-plane loading. This improvement is primarily

attributed to the effect provided by the textile mesh, which delays the cracking and prevents the propagation of major failure mechanisms such as diagonal shear and out-of-plane bending [6–9].

Moreover, TRM systems can be valued for their minimal invasiveness and low added weight, which means that the overall mass and dynamic characteristics of the structure are not substantially altered. This is particularly important in seismic retrofitting, where excessive mass can adversely affect the seismic response. TRM systems represent a versatile, durable, and compatible strengthening technique for masonry structures, offering enhanced mechanical performance and improved seismic resilience. Their growing adoption in both research and practice underscores their potential as a preferred solution for the preservation and safety upgrade of vulnerable masonry constructions.

3.2. MORTARS

The improvement of the properties of mortars applied as overlay by addition of natural fibres is well-known and has been used empirically for centuries [10]. In recent years, various fibre reinforced mortars (FRM) have been developed by adding natural [11–14] or man-made fibres, presenting good mechanical properties [15–17]. These FRM's can be used to upgrade the in-plane and the out-of-plane loading and deformation capacity of the original elements. Additionally, when used as external overlays they constitute a protection system to the reinforced walls from weathering agents. The FRM's developed in the recent past were frequently composed by Portland cement binder, which has been shown to lead to compatibility problems with old masonry elements, namely by the crystallization of salts that damage natural stone. Additionally, the low flexibility of the Portland cement-based mortars may cause structural problems in older ceramic brick or natural stone masonry when the building is subject to movements [18], and delamination of the strengthening layers in the case of infill masonry [7]. The use of natural hydraulic lime (NHL) and alternative binders are believed to show better compatibility with masonry in terms of strength and hygroscopic behaviour [19–22].

3.2.1. Alternative binder matrices

The evolution of the use of inorganic binders in mortars is marked by two major events. The development of lime in the antiquity and the development and use of Portland cement in the end of the 19th century, see **Figure 3.1**.

Lime is a commonly used binder for the preparation of mortars for restoration purposes. However, these mortars in general present poor mechanical performance. The use of Natural Hydraulic Lime

(NHL) in fibre reinforced mortars presents advantages when compared with the use of aerial lime. The mechanical strength of mortars with NHL is higher and is obtained at earlier ages.

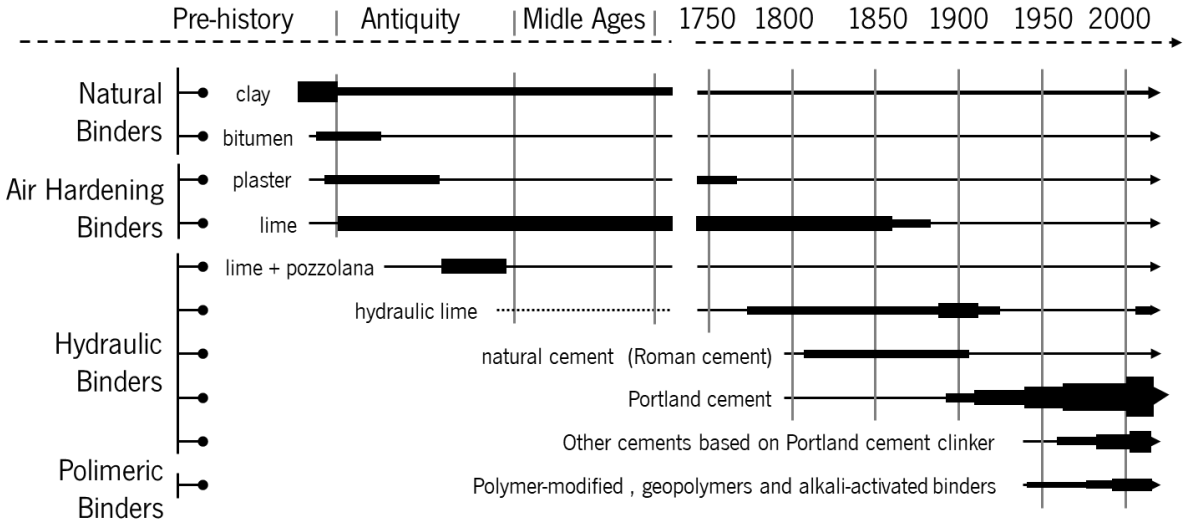


Figure 3.1: Evolution of the use of inorganic binders during history. Adapted from [23].

3.2.1.1. Natural Hydraulic Lime

NHL is a hydraulic binder in the form of powder, obtained from the calcination of limestone containing between 15% and 20% of clay and other impurities, also denominated marls. During the calcination process that occurs at approx. 1200°C (a lower firing temperature than in Portland cement), calcium reacts in the kiln with clay minerals producing silicates, aluminates and ferro-aluminates enabling the NHL to have a faster setting time than quicklime or slaked lime, without the need of exposure to air, occurring also under water. The unreacted calcium is transformed into calcium hydroxide. This part of the lime reacts non-hydraulically in the presence of environmental humidity and carbon dioxide, see **Figure 3.2**. These reactions vary according to the hydraulic index of the NHL and are responsible for the increase of the resistance with time [24].

The revised EN 459 [25] standardised a new group of limes, the Formulated Limes (FL). Formulated Limes are limes with hydraulic properties mainly consisting of air lime (CL) and/or natural hydraulic lime (NHL) with added hydraulic and/or pozzolanic material. According to EN 459 [25] the mixing of FL allows the blending or CL or NHL with the following main constituents: Portland cement including Portland cement clinker, natural pozzolana, natural calcined pozzolana, limestone and/or granulated blast furnace slag. The available lime in FL in the form of $Ca(OH)_2$ should be between 15 to 80% by mass, which means that it is possible to prepare standardised limes with a huge diversity of amounts of natural and artificial hydraulic components. These FL allow a very dedicated mix design of mortars

and plasters with custom-made properties, although their interactions between historic masonry remain unpredictable [24].

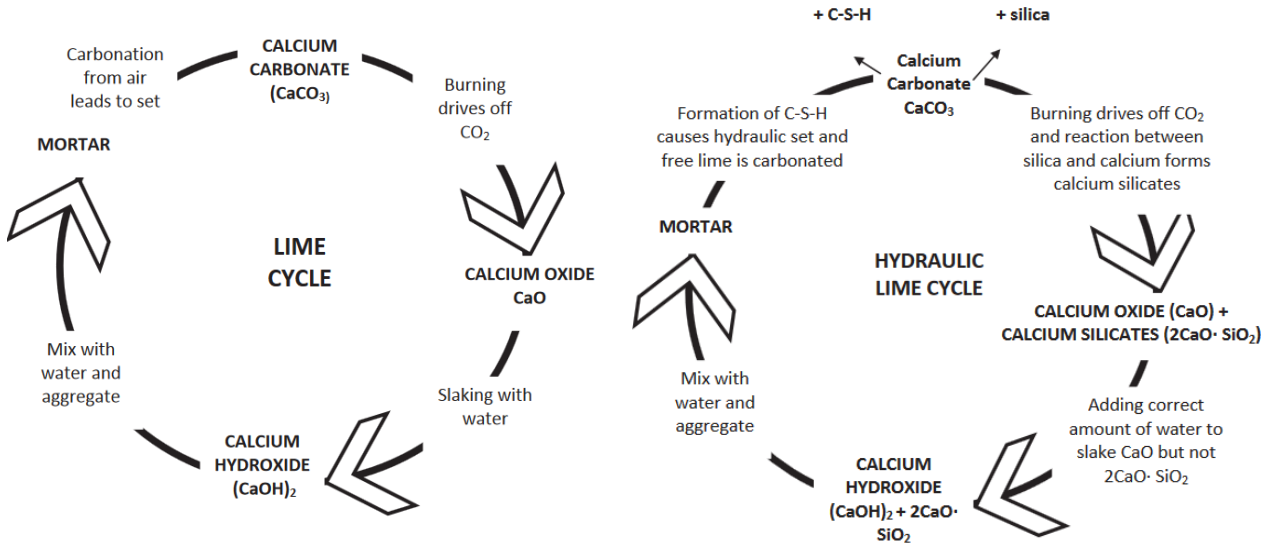


Figure 3.2: Lime and hydraulic lime cycle, adapted from [24].

3.2.1.2. Alkali-activated materials and geopolymeric binders

Geopolymeric and alkali activation is a complex reaction taking place in alkaline solution with aluminosilicate materials. First the alkaline solution has the role of dissolving Si-O and Al-O bonding. Later it promotes their incorporation in the geopolymer network by charge-balancing the alkali-metal cations. Alkali activator promotes the reaction, and for higher molar ratios of SiO_2/Al_2O_3 and Na_2O/Al_2O_3 higher mechanical strength and density are achieved [26].

AAM's have gained an enormous attention, with numerous studies in recent years [26–47], partially due to their potential for reducing greenhouse gas emissions associated with traditional cement production and at the same time to using as precursors materials that are normally considered as by-products [32,48]. The most used sources of aluminosilicate precursors for AAM and geopolymer formulations include fly ash, rice husk ash, blast furnace slag, metakaolin, natural pozzolans, mining tales and construction and demolition wastes. The use of these source materials can provide a sustainable and ecologically friendly alternative to traditional cement manufacturing, and their usage in AAM and geopolymer production is projected to increase. Recent investigations on alternative binders like AAM's have shown substantial success, with numerous uses ranging from structural applications to coatings for fire protection or conservation, and also in façade components [49–53]. Additionally, AMM's are being used in additive manufacturing solutions, with geopolymer mortar printed from 3D CAD models [54,55]. However, when considering infill and structural masonry

elements, Abulencia et al. [56] consider that more studies should be development on the use of geopolymers as strengthening material in overlay systems.

3.2.2. Properties after exposure to high temperatures

Heating cementitious composites to high temperatures causes the dehydration of the cement paste and the conversion of calcium hydroxide into calcium oxide, in which chemically bound water is gradually released to become free water, see **Table 3.1**. Additionally, aggregates also lose their evaporable water, dehydrate and undergo crystalline transformation accompanied by a significant volume expansion [57]. All these transformations make the visual aspect of concrete to change with the evolution of the temperature, see **Figure 3.3**.

The main parameters controlling the high temperature behaviour of aggregates are: i) the chemical and mineralogical composition associated with granular texture and crystallinity of quartz; ii) trapped water and silica hydrates content that may increase the internal pore pressure; iii) porosity combined with cracks evolution [58]. Concrete containing light-weight aggregates tends to show much better mechanical properties, after high temperature exposure, than concrete containing ordinary aggregates [59]. When the rate of heating is high, and the permeability of the cement paste is low, damage to concrete may take place in the form of surface spalling. Spalling occurs when the vapour pressure of steam inside the material increases at a rate faster than the pressure relief in the form of steam into the atmosphere [60].

The single distinction between siliceous and calcareous aggregates does not allow to predict the thermal stability of aggregates at high temperatures, this behaviour is different for different temperature levels [58]. However, concrete containing siliceous aggregate (e.g., granite) tends to show slightly lower strength ratios, f^{r}_{cu}/f_{cu}, when compared with concrete containing calcium aggregates (e.g., limestone) at the same temperature. The difference between these is approximately 6% when T>700°C [59]. Limestone aggregates exhibit better thermal structural stability up to 600°C. Limestone aggregates, quartz vein/quartzite and quartz-feldspathic rock did not show any evidence of micro-crack before 500°C. Other rocks like basalts, rhyolite and granites display short length micro-cracks. In flints, the density and opening of cracks increase with the temperature from 300°C [58].

Considering the effect of aggregate size, concrete spalling tends to decrease when the maximum aggregate size decreases [61]. To improve shrinkage control in high temperature applications, fine

aggregates with dimension lower than 53 μm, such as wollastonite, chamotte, and α-alumina that are stable beyond 1000 °C, can be used as fillers [62].

Table 3.1: List of changes taking place in concrete during heating according to Hager [63].

Temperature range	Changes
20-200°C	- slow capillary water loss and reduction in cohesive forces as water expands; - 80-150°C: ettringite dehydration; C-S-H gel dehydration; - 150-170°C: gypsum decomposition ($CaSO_4.2H_2O$); - physically bound water loss;
300-400°C	- approx. 350°C: break up of some siliceous aggregates (flint); - 374°C: critical temperature of water;
400-500°C	- 460-540°C: portlandite decomposition, $Ca(OH)_2 \rightarrow CaO+H2O$;
500-600°C	- 573°C: quartz phase change ß - α in aggregates and sands;
600-800°C	- second phase of the C-S-H decomposition, formation of ß-C_2S;
800-1000°C	- 840°C: C dolomite decomposition; - 930–960°C: calcite decomposition, $CaCO_3 \rightarrow CaO+CO_2$, carbon dioxide release; - ceramic binding initiation which replaces hydraulic bonds;
1000-1200°C	- 1050°C basalt melting;
1300°C	- total decomposition of concrete, melting.

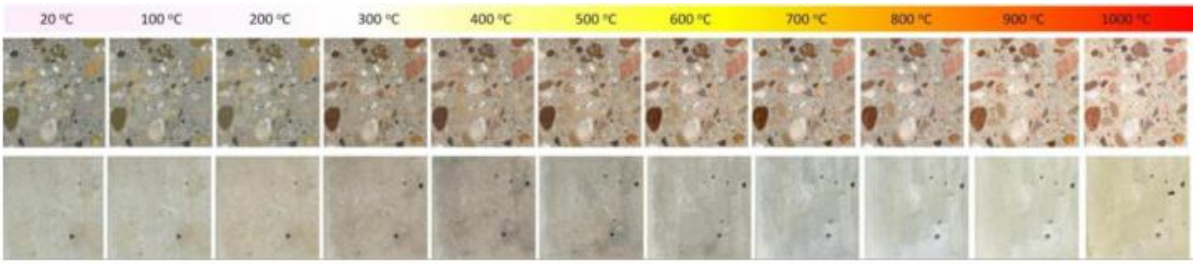


Figure 3.3: Colour change of concrete surface after exposure to temperatures from 20 to 1000°C [63].

Most of the experimental investigations in the topic are conducted to assess the residual behaviour after high temperature exposure, and only in a few cases testing is performed during heating of the specimens. When tests are done at high temperatures the observed findings are as follows: Steel fibres in concrete lead to an improvement in both tensile and compressive strength and heating effects,

like spalling. However, higher contents of steel fibres do not improve the compressive strength of concrete composites at elevated temperatures [64].

The effect of the incorporation of synthetic fibres like polypropylene, was studied by Ezziane et al [65]. At room temperature and after heating up to 500 °C, the flexural strength was improved by the presences of fibres. The residual Young's modulus was slightly higher for the fibre reinforced samples. As the temperature increased, the strength gain due to fibres inclusion was reduced. Beyond 500 °C, the flexural strength was lower for the fibre reinforced cementitious material compared to those without fibres. Fracture energy was also improved for the fibre mortars at room temperature. At 400 °C this improvement decreased gradually with the introduction of polypropylene fibres. Beyond this temperature and due to the introduction of polypropylene fibres, the fracture energy was reduced [65]. The effect of different fibres on the residual compressive strength, ultimate load and flexural toughness, failure patterns and fracture energy of self-compacting high-performance concrete (SCHPC) after exposure to high temperatures was analysed by Ding et al [66]. Their conclusion was that synthetic micro polypropylene fibre (PP fibre) could mitigate the spalling of SCHPC significantly but did not show clear effect on the mechanical properties of concrete. On the other hand, macro steel fibre (SF) reinforced SCHPC showed both higher flexural toughness and ultimate load before and after high temperature exposure. The mechanical properties of hybrid fibre reinforced SCHPC after heating were better than that of mono fibre reinforced SCHPC. The failure mode changed from pull-out of steel fibres for lower temperature to fracture of steel fibres for higher temperature. The use of hybrid fibre reinforcements can be effective in providing the adequate residual strength and failure mode, as well as in improving the toughness and fracture energy of SCHPC after the exposure to high temperatures [66].

In recent years several authors have studied the influence of elevated temperatures on the behaviour of geopolymers (GP) [67–70] and alkali-activated materials (AAM's) [71–74]. Kong et al. [67] used GP's synthesized from metakaolin and combinations of sodium/potassium silicate and sodium/potassium hydroxide as activators and studied: Si/Al ratios; activator/metakaolin ratio; curing temperature; and alkali cation type. After exposure to 800 °C. the samples were subjected to compressive strength, thermogravimetry, and scanning electron microscopy tests. The main results showed that Si/Al ratio have a significant influence on deterioration after exposure to elevated temperatures with lower strength loss observed in geopolymer with high Si/Al ratios (>1.5). Additionally, GP binders with potassium-based activators showed an enhanced performance after

exposure, comparing to sodium-based systems [67]. In a different investigation Kong et al. [70] attributes strength loss in geopolymer concrete at elevated temperatures to the thermal mismatch between the geopolymer matrix and the aggregates.

Ternary AAM's mixes were developed by Huseien et al. [73] using waste ceramic powder (WCP), ground blast furnace slag (GBFS), fly ash (FA) and a low concentration of alkaline activators. The mechanical and microstructure properties after exposure to elevated temperatures (900 °C) show an enhancement of the resistance with the increase of WCP contents from 50 to 70%. Also, the replacement of GBFS by FA in the ternary blends led to the reduction of the mortar deterioration at 900 °C [73]. Çelikten et al. [74] investigated the changes in the mechanical and microstructural properties of alkali-activated blast furnace slag (BFS) and BFS+(FA) blended mortars exposed to temperatures up to 800 °C. They concluded that FA substitution by BFS increases the residual resistance after high temperature exposure of BFS AAM's. The effect of high temperature up to 800 °C, and exposure duration, 1 and 2 h, on the flexural behaviour and microstructure of hybrid basalt textile and steel fibre reinforced alkali-activated slag panels was carried by Li et al. [71]. A decrease in flexural performance occurred as temperature and duration increased, resulting from the decomposition of the alkali-activated slag mortar (AASM) matrix and the deterioration of the bonding performance between the basalt textile and the matrix. Changes of the Ca/Si ratio, the Al/Si ratio, and the crystalline phase of the AASM matrix indicated that after exposure at 800 °C a phase transformation occurred.

3.3. FIBRES, FABRIC AND MESHES FOR REINFORCEMENT

3.3.1. Man-made Fibres

The mechanical properties of the fibres used in the reinforcement of cementitious composites can vary significantly depending on the typology of the fibre, see **Table 3.2**. Additionally, also the type of treatment/finishing applied on the fibres changes the mechanical behaviour of the composite. In general, composites including the addition of fibres with high elasticity modulus (glass or carbon fibres, among others) present high tensile strength and stiffness. On the contrary, composites with the addition of low elasticity modulus fibres and high deformability (polypropylene, polyethylene, polyacrylonitrile, etc.), seem to result in lower capacity to absorb high amounts of energy. Additionally, often the composites show high resistance to impact and tenacity, but do not achieve high resistance [75].

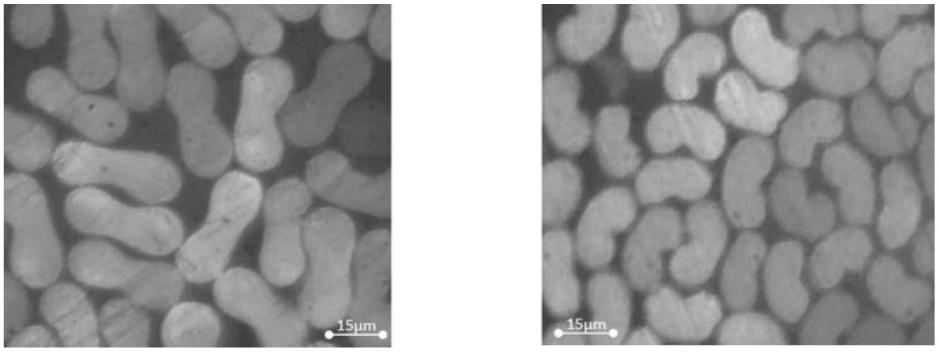
Table 3.2: Physical properties of man-made fibres [62,76,77].

Type of Fibre	Diameter (μm)	Density (g/cm³)	Elastic Modulus (GPa)	Tensile strength (GPa)	Elongation at break (%)
Steel (MTF)	5-500	7.84	200	0.5-2.0	0.5-3.5
Glass (GF)	9-15	2.60	70-80	2-4	2.0-3.5
Polypropylene (PP)	20-400	0.90-0.95	3-10	0.50-0.75	15-25
Aramid (AR)	10-12	1.44	62-120	2.3-3.5	24.5
Carbon (CF)	7-18	1.6-1.95	230-600	3.0-6.0	0.5-2.4
PVA	10-670	1.3	25-41	0.88-1.9	6-10
Acrylic (PAN)	10-50	1.18	14.0-19.5	0.3-1.0	3.0
Basalt (BF)	9-13	2.8-2.9	79.3–93.1	3.0-4.84	3.1
Polyethylene (PE)	25-1000	0.95	1.4-5	0.25-0.6	3-100

3.3.1.1. Polyacrylonitrile fibres (PAN)

Acrylic fibres (polyacrylonitrile, PAN) contain at least 85% of their weight in acrylonitrile units. Some of the properties of the acrylic fibres are shown in **Table 3.2**. Usually, these fibres are used in the textile industry and presents a tensile strength ranging between 207 and 345 MPa. For the use as a construction material, special acrylic fibres of high tenacity and tensile strength - up to 1000 MPa - were developed, replacing the asbestos fibres previously used in several products, [43], [44].

The fibre shows good adhesion to the cementitious matrix due to the shape of the individual filaments cross section, characterized by the “kidney” or “dog bone” shape, see **Figure 3.4**. The values of adhesion stress of about 4 MPa to the cementitious matrix were achieved through "pull-out" tests on filaments of 105 μm diameter and lengths between 2 and 6 mm. Regarding the durability, acrylic fibres reveal stability in alkaline environments [76].



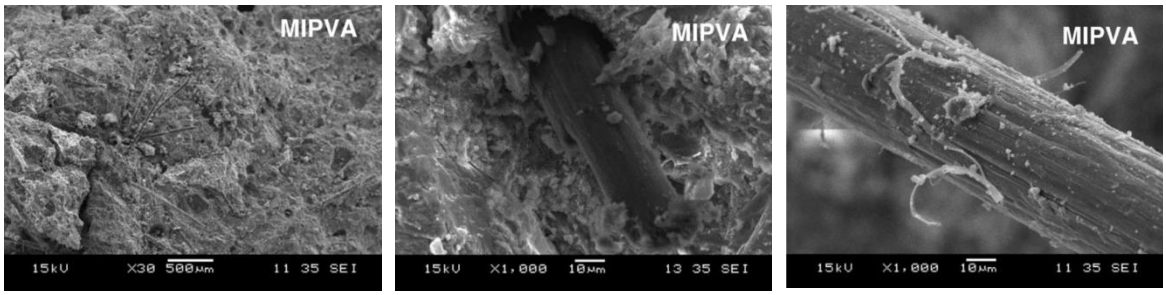
a) b)

Figure 3.4: PAN fibres [76]: a) “dog-bone” shape; b) “kidney” shape.

3.3.1.2. Polyvinyl alcohol fibres (PVA)

PVA fibres were mainly developed for the replacement of asbestos, which were previously used in many products. This type of fibre has high resistance and stiffness due to the addition of boron, which

causes the formation of intermolecular bonds. The fibre surface is treated to increase their compatibility with the matrix and allow for more efficient dispersion. The surface treatment combined with the inherent affinity of this polymer with water, leads not only to efficient dispersion, but also to a strong connection between the fibre and the matrix, see **Figure 3.5**. PVA fibres tend to rupture when pulled out from the cementitious matrix, because of the strong chemical bonding and the sliding/hardening effect that takes place during the "pull-out" [76]. The behaviour in environments with freeze-thaw cycles shows that composites with PVA fibres have greater durability compared to asbestos composites [76].

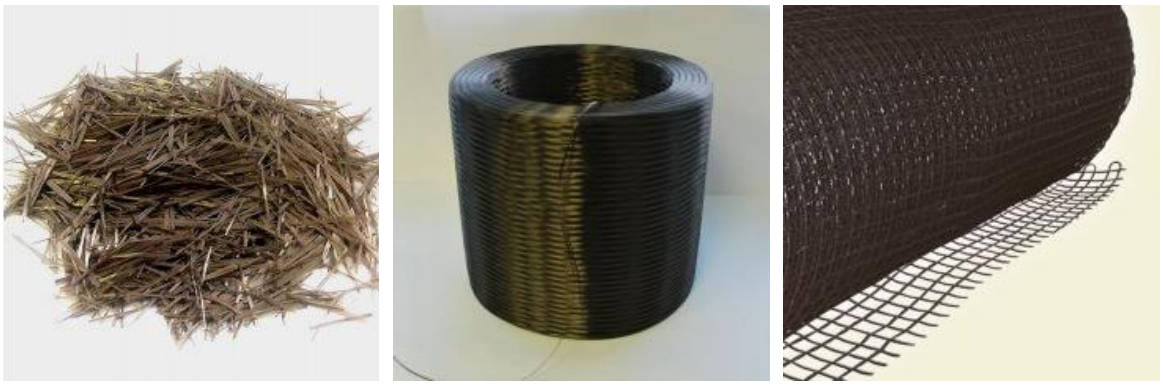


a) b) c)

Figure 3.5: Fibre-matrix interaction [80]: a) fracture surface of reinforced mortar with PVA; b) detail of fibre-matrix interaction; c) detail of the fibre.

3.3.1.3. Basalt Fibres (BF)

Basalt fibres were developed, and the production process patented in 1991. The production of basalt fibres is a continuous process like the production of glass fibres. The extracted basalt rock is crushed, washed, and then transferred to melting baths in gas furnaces heated to 1300°C-1700°C. The molten rock is then extruded through a spinneret of small nozzles, drawn, and subsequently cooled to produce hardened, continuous filaments in the form of rovings containing varying numbers of elementary fibres [77]. Basalt fibres can exhibit high moduli and high strengths, high corrosion and temperature resistance. They are cheaper than carbon fibres and show higher strength than glass fibres, see **Figure 3.6**. The moisture regains, and moisture content of basalt fibres are both less than 1%. Additionally, these fibres can withstand alkaline environment with pH values up to 13 or 14. Basalt fibres have excellent thermal properties compared to glass fibres (E-type) and can withstand for short periods temperatures up to 1000°C without suffering any physical damage [81].



a) b) c)

Figure 3.6: Basalt fibres: a) chopped; b) roving; c) mesh [81].

3.3.2. Natural Fibres

The use of natural fibres is widespread among several types of composites. In the industry they are used together with resin matrices, and in the construction, they are used mainly with inorganic binders [82,83]. The visual appearance and the physical properties of some of the most used natural fibres are shown in **Figure 3.7** and **Table 3.3**. These natural fibres present some important advantages when compared to synthetic ones: i) their extraction from renewable resources; ii) their production requires low energy consumption; iii) their production involves CO_2 absorption and release of oxygen to the atmosphere; iv) they are low-cost; v) they involve low hazard manufacturing processes; vi) they represent low emissions of toxic fumes at end of life; vii) they result in less abrasive damage to processing equipment.

Experimental results show, according to Di Bella et al. [84], that natural fibres, as kenaf and sisal, can be considered as a valid alternative to polypropylene as reinforcement of lime plasters. Under flexural loading conditions, the decrease of the mechanical properties due to freeze/thaw cycles is essentially similar for the three types of plasters studied. Furthermore, after the freeze /thaw cycles the decrease of compressive strength shown by plasters reinforced with sisal fibres was lower than the mortars with kenaf and polypropylene [84].

As disadvantages, natural fibres are in general less durable than synthetic fibres. Additionally, they exhibit high moisture absorption, resulting in performance deterioration. Other disadvantages are lower strength, particularly the impact strength, and greater variability of properties [85].



Flax hemp jute



sisal kenaf

Figure 3.7: Natural fibres, adapted from [82].

Table 3.3: Physical properties of natural fibres.

Fibre	Density (g/cm³)	Young Modulus (GPa)	Tensile strength (MPa)	Elongation at break (%)
Bamboo	0.6-1.1	11-17	140-230	-
Flax	1.5	27.6	345-1035	2.7-3.2
Hemp	1.48	70	690	1.6
Jute	1.3	26.5	393-773	1.5-1.8
Kenaf	-	53	930	1.6
Sisal	1.5	9.4-22	511-635	2.0-2.5
Pineapple	0.8-1.6	1.44	400-627	3.2
Coir	1.2	4-6	175	30

Toledo et al. [86], concluded that durability problems lead to the increase in fibre fracture. This is due to a combination of weakening of the fibres by alkali attack that dissolves the lignin and hemicellulose phases, thus weakening the fibres' structure. Additionally, fibre mineralisation due to the migration of hydration products to lumens and spaces, as well as volume variations due to their high-water absorption, also contribute to the observed degradation [86]. Rogiros et al. [87] explored the challenges in using natural fibres for textile-reinforced mortar (TRM) composites, emphasizing the

need to address durability, tensile response and dimensional stability issues, concluding that treatment protocols are vital to enhance performance.

Fibre treatments and surface modification methods can be performed to improve some drawbacks of natural fibres, see **Figure 3.8**. An effective treatment for natural fibres used by several authors is the hornification, that can be described as a sequence of wetting–drying cycles [13,88–90]. Surface modifications are applied to the fibre surface to improve adhesion properties with different matrices [91].

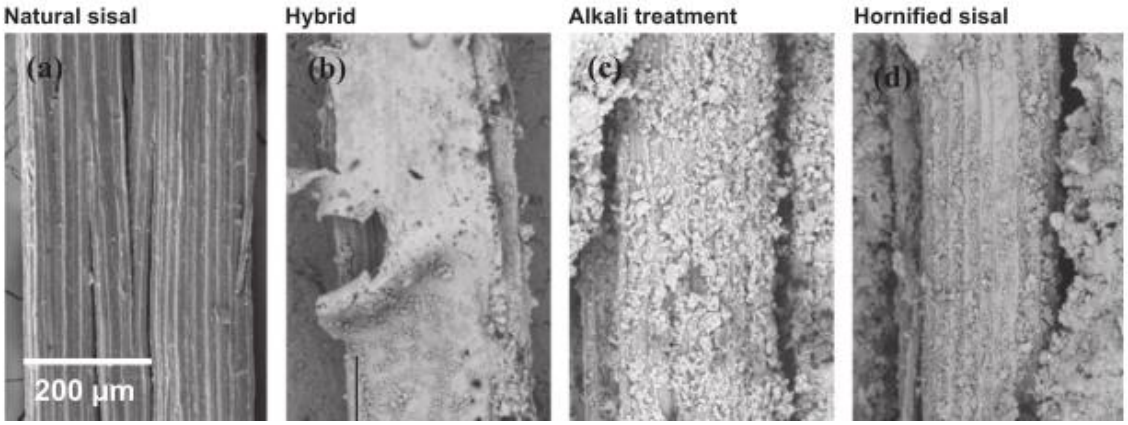


Figure 3.8: Surface of sisal fibre with different treatments after pull-out test [92].

3.3.3. Microfibres

3.3.3.1. Calcium carbonate microfibres (whiskers)

Calcium carbonate ($CaCO_3$) whiskers are microfibres with a micron-scale acicular structure, with high aspect ratio and excellent mechanical properties. Their use in cementitious composites provides excellent effect on strengthening and toughening [93–95]. According to Cao et al. [93] the yield stress and plastic viscosity increased with an increasing content of $CaCO_3$ whisker and a decreasing water-cement ratio. Also, the rheological properties were affected by the distribution of $CaCO_3$ whisker in the matrix. The largest increment in flexural strength was around 27% for mortars with $CaCO_3$ whisker content of 2.0%.

The multiscale cracking behaviour of cementitious composite determines its micro-, meso- and macro-performance. Liu et al. [95] developed a new kind of fibre hybridization containing steel fibre, polyvinyl alcohol (PVA) fibre, and affordable calcium carbonate $CaCO_3$ whisker. The mechanical properties, reinforcing mechanisms and economic efficiency of this designed hybrid fibre-reinforced composite were significantly improved by adding $CaCO_3$ whisker. Scanning electron microscopy images and

fracture tests confirmed that the interaction of different fibres and cracks at multiple scales contributed to enhancing the mechanical properties of the cementitious composite, which was also reflected in its deflection hardening performance and multiple cracking behaviour [95], see **Figure 3.9**.

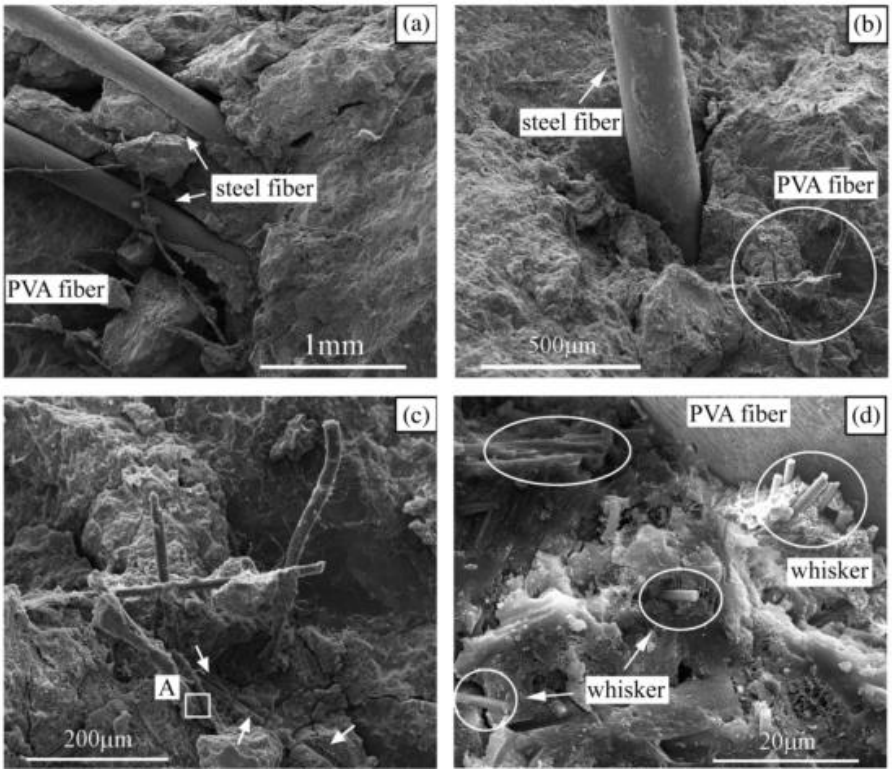
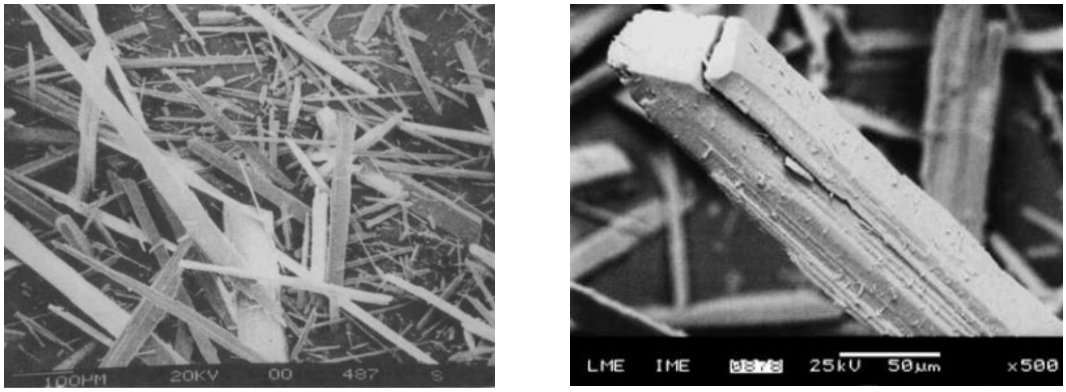


Figure 3.9: Microstructure of a composite with steel and PVA fibres, and CaCO3 whiskers): a) and b) interaction of steel and PVA fibres in the matrix; c) detail of enlarged image of the circle area in b); d) enlarged image of the rectangular area in c). Adapted from [95].

3.3.3.2. Wollastonite microfibres

Wollastonite can be found in acicular or powder form. These natural inorganic microfibres present 400 to 600 μm in length, 25 to 30 μm in cross section, a tensile strength of up to 4100 MPa and an elastic modulus from 300 to 530 GPa, see **Figure 3.10** [96,97]. Natural wollastonite micro-fibres are an effective reinforcement for improving the flexural strength characteristics of the cement systems. The relatively low cost of the wollastonite micro-fibres compared to other micro-fibres may result in more widespread use of this natural mineral in the construction industry [96]. Kwon et al. [97] reported a particularly remarkable effect in the strain hardening process that occurs after initial cracking. The higher ratio of wollastonite microfibers increases the tensile strength, strain capacity, and energy absorption capacity. Additionally, wollastonite microfibers are effective in reducing the scatter obtained in the stress-strain experimental responses. The multiscale fibre reinforcement system examined by the author was successful in bridging microcracks through the incorporation of

wollastonite microfibers, which proved to be very effective in improving the mechanical properties of the UHP-FRCC [97].



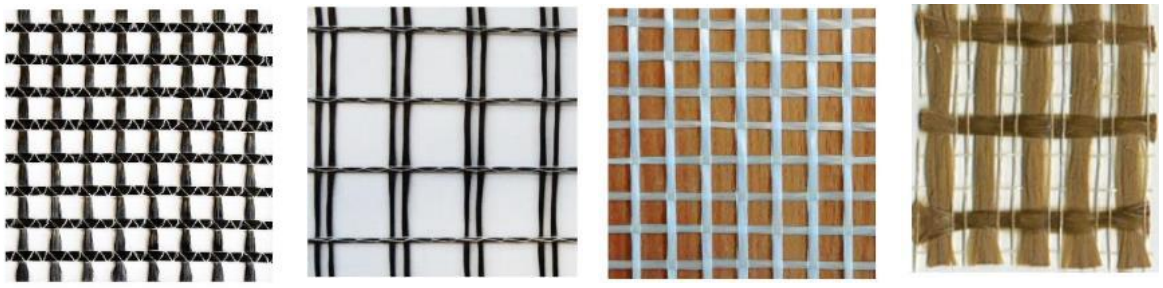
a) b)

Figure 3.10: SEM micrograph of wollastonite microfibres: a) distribution of fibres[96]; b) detail of single fibre [98].

3.3.4. Fabric and Meshes

The two main components of the TRM systems are the matrix mortar and the embedded textile fabric or meshes These reinforcing textiles are frequently composed of steel, carbon, basalt, glass, polyparaphenylene benzobisoxazole (PBO) [99–101], see **Figure 3.11**. The mechanical parameters of mesh materials are presented in **Table 3.4**.

The mechanical properties of the meshes used in TRM systems can considerably impact their performance. The tensile strength has a major influence once materials with high tensile strength can enhance the overall strength of the TRM system. Normally the meshes used in TRM present high elastic modulus, comparing to the matrix materials. Higher elastic modulus results in stiffer TRM systems, as opposed to lower elastic modulus which can provide more flexibility. TRM deformation capacity can promote the enhancement of the ductility of the strengthening system, allowing it to absorb more energy during seismic events.



carbon-fibre textile basalt-fibre textile glass -fibre textile PBO-fibre textile

Figure 3.11: Textile fibre reinforcements, adapted from [101].

Table 3.4: Mechanical properties of meshes [99].

Type of fibre	Tensile strength [MPa]	Modulus of elasticity [GPa]
PBO (P-phenylene benzobisoxazole)	1800	227
Carbon	3400	240
Glass	1800	227
Basalt	1944–1890	203-197
Aramid	2500	230
Steel	1876–1890	187-219

3.4. CHARACTERIZATION OF TEXTILE REINFORCED MORTAR (TRM)

The experimental characterization of the TRM behaviour is focused on the interaction between the overlay mortar and the strengthening mesh, the interaction between the overlay mortar and the substrate, and finally the mechanical behaviour of the TRM composite. The tests and procedures normally used to perform the experimental characterization are presented and discussed in the next sub-sections.

3.4.1. Bond behaviour characterization

Understanding the impact of the mortar/mesh and TRM/substrate bond mechanisms is essential to TRM performance optimisation. This complex interaction depends on several variables, including the chemical compatibility of the materials, the geometrical features of the fabric as texture and configuration, and the mechanical properties such as strength and elastic modulus of the fabric, the mortar and the substrate [102]. The bond behaviour governs the interaction mortar/mesh and mortar/substrate and can be assessed by performing shear bonding, pull-off and pull-out tests.

3.4.1.1. Pull-off tests

An expedite assessment of bond between layers or overlay materials can be achieved by executing pull-off tests [103]. This technique uses a perpendicular load applied to the pull-head glued to a defined circular or polygonal area on the overlay, isolated by a shallow cut in the substrate. This test provides a basic measure of interfacial strength and type of failure mode. This rapid assessment helps to inform the overall performance of the layered system. The failure modes described in EN 1015-12 tests [103] are shown in **Figure 3.12** and can be interpreted as follows:

a) Fracture adhesion: Fracture at the interface between TRM mortar and substrate. Resistance value equal to the adhesion strength.

b) Fracture by cohesion: Fracture in the mortar. The adhesive strength is greater than the test value.

c) Fracture by cohesion: Fracture in the substrate. The adhesive strength is greater than the test value.

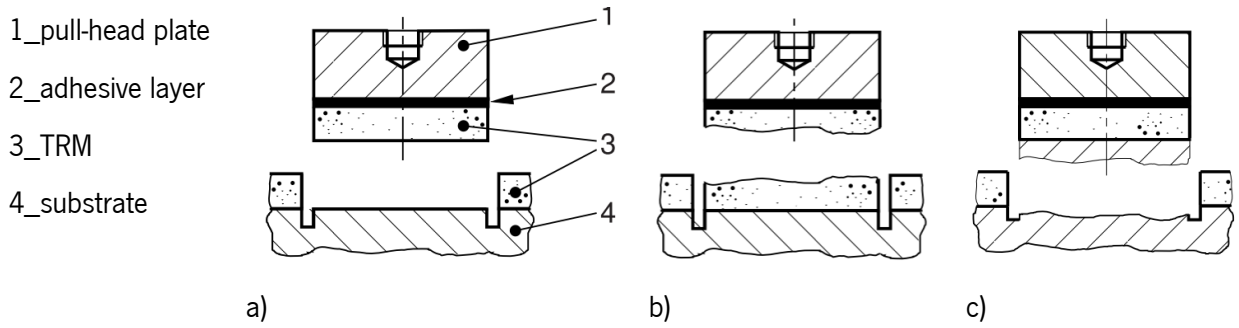


Figure 3.12: Rupture modes obtained in Pull-off tests [103].

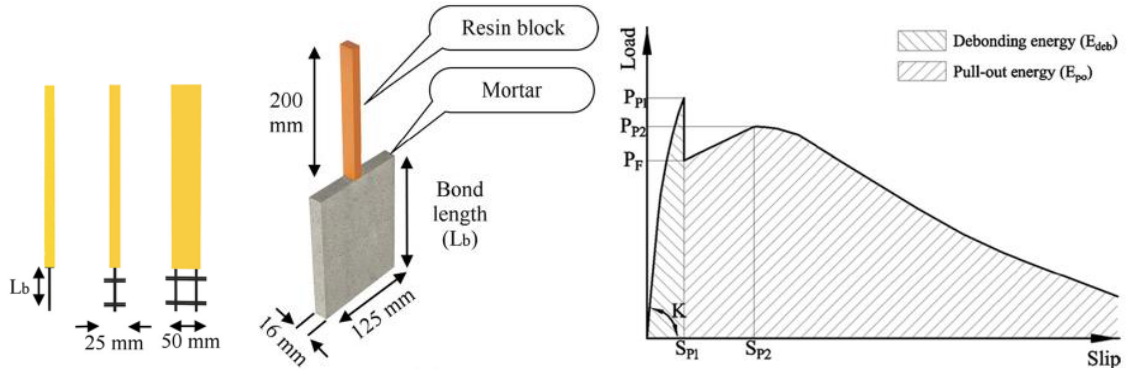
Experimental pull-off tests carried by Cardani et. al [104], were performed as part of an on-site campaign in full-scale brickwork and stonework masonry models strengthened with a pozzolanic lime-based mortar TRM system, a cement polymer modified mortar TRM system and an organic matrix FRC system, see **Figure 3.13**. The first system showed failure within the mortar layer for both substrates. The second showed different performance on the two masonry substrates, with better bonding on brickwork, where the low bond on stonework may be due to the low porosity and to an inadequate saturation of the substrate. The third showed a good bond in both masonry substrates and in this case the values showed the influence of the moisture content, salt crystallization and surface decay [104]. The bond between and existing concrete substrate and an applied TRM layer was studied by Shrestha et al. [105], by investigating the significance of concrete surface preparation before the strengthening process. The obtained results revealed that roughened surfaces promoted the bond between concrete substrate and TRM layer, and additionally PBO-TRM system exhibited better bonding behaviour than carbon-TRM system.



Figure 3.13: Evaluation of the bond in a brick masonry model with TRM/FRP: a) TRM and FRC systems with pull-heads plates applied; b) pull-off test set-up with dynamometer. Adapted from [104].

3.4.1.2. Pull-out tests

Pull-out tests are commonly used for the characterization of the bond behaviour between fibres and matrix [106,107]. The tests can be developed to characterize the interaction of a single yarn or a small portion of mesh with the mortar [108], by embedding the yarns in a mortar block as presented in **Figure 3.14**a) and b). The typical load vs slip response is also presented in **Figure 3.14**c). Tests carried by Dalalbashi et al. [108] revealed that the slip rate until 5 mm/min influenced the peak load, with higher peak loads obtained for higher slip rates. However, for higher rates the peak load was not influenced by the slip rate. Additionally, the load decrease after the full debonding, point (P_{P1};S_{P1}) to point (P_F;S_{P1}) in **Figure 3.14**c) was independent of the applied load rate. The area under the load vs slip can be divided into two parts representing the debonding energy (E_{deb}) and the pull-out energy (E_{po}).



a) b) c)

Figure 3.14: Pull-out tests: a) textile embedded in epoxy resin; b) textile embedded in mortar block; c) typical load versus slip response curve of monotonic pull-out test. Adapted from [108].

3.4.1.3. Shear bond tests

Shear bond tests can be performed in different configurations: single-sided, double-sided and double-sided double prism, see **Figure 3.15** a) b) and c) respectively [109,110]. Each test configuration offers distinct benefits and drawbacks. Single-sided tests are easier to prepare and exhibit lower result variability. Double-sided tests provide more realistic boundary conditions. Direct comparison of results from these setups requires caution due to the different boundary conditions and stress distributions. Double-sided tests typically yield higher peak loads and toughness than single-sided tests [102].

The single-sided shear bond test method, similar to the one presented in **Figure 3.15** a), is proposed by RILEM 250-CM [5] to determine the peak axial stress, related with the maximum capacity of the externally bonded TRM reinforced element, the stress–slip relationship and the failure mode that governs the TRM/substrate load transfer capacity. These guidelines additionally indicate details on the specimen manufacturing, experimental setup and test execution, and analysis of the test results.

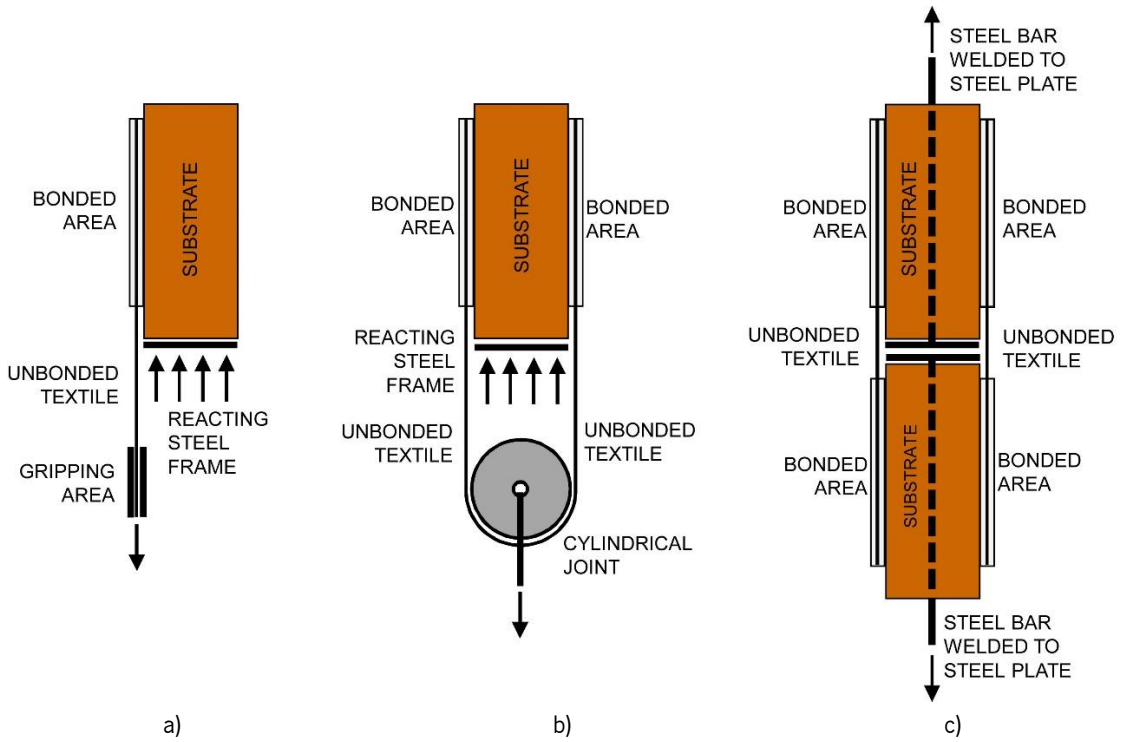


Figure 3.15: Schemes of experimental setups for bond tests: a) single lap; b) double-lap single-prism; c) double-lap double-prism. Adapted from [109].

The different failure types obtained by Santis et al. [109] for TRM shear bond tests and the respective stress vs slip responses are presented in **Figure 3.16** were:

(A) debonding with cohesive failure in the substrate
(B) debonding at the reinforcement-to-substrate interface

(C) debonding at the textile-to-matrix interface
(D) sliding of the textile within the reinforcement thickness
(E) tensile rupture of the textile

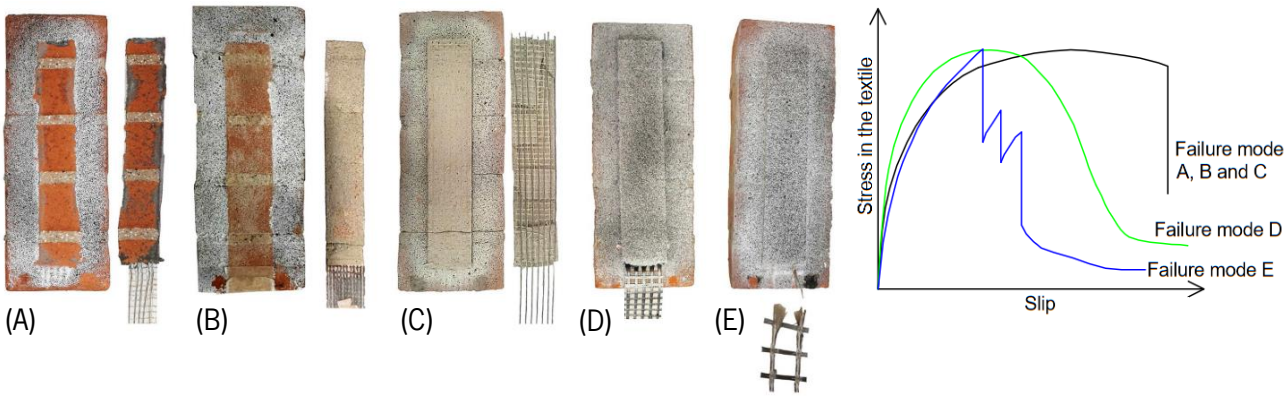


Figure 3.16: Failure modes in shear bond tests and Stress vs. Slip responses. Adapted from [109].

3.4.2. Mechanical behaviour of TRM

The recommendation document TC 232-TDT [111] from RILEM presents test methods to quantify the performance and the design of TRM systems. In Italy the LG2018 [112] qualifies the TRM composites based on predefined mechanical properties evaluated by means of homologated tensile and debonding tests performed by the manufacturer through accredited laboratories. The mechanical behaviour of the TRM is governed by the tensile properties of the composite material, normally assessed by means of tensile tests on TRM coupons.

3.4.2.1. Flexural tests

Flexural tests can be used to evaluate the mechanical behaviour of TRM. However, they have received less attention being normally performed at early stage of development of the strengthening systems [113,114]. The three-point or four-point bending tests are easier to perform, with a less demanding test set-up when comparing to direct tensile tests, see **Figure 3.17**. The information these tests provide is related to the out-of-plane behaviour of the TRM systems. Analytical models must be deployed to adjust it to the tensile characteristics of the system.

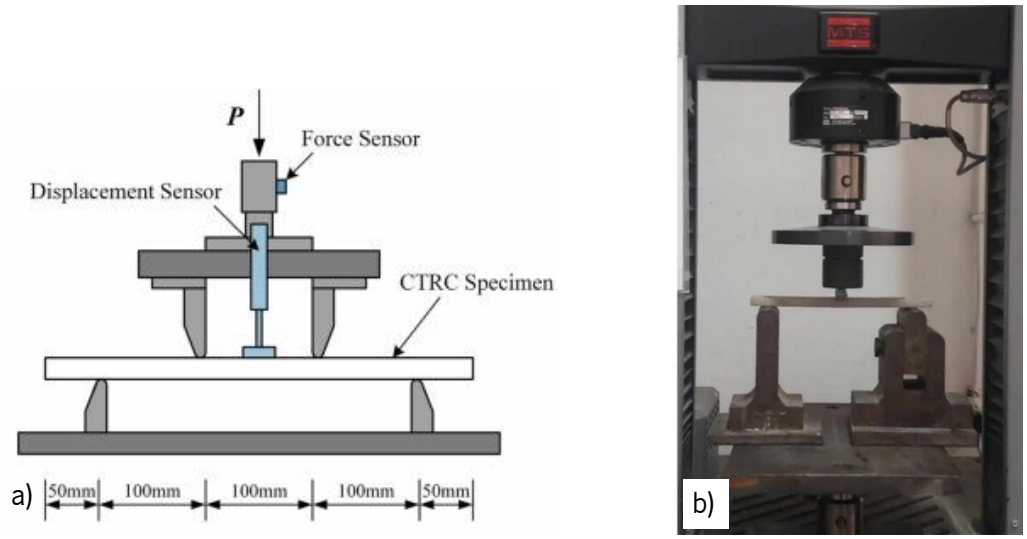


Figure 3.17: Test commonly used to evaluate the flexural behaviour of TRM: a) Four-point bending test [114]; b) Three-point bending tests [113].

3.4.2.2. Direct tensile tests

Direct tensile tests are the most common method used for evaluating the mechanical response of TRM composites [100,109,111,115,116], see **Figure 3.18** a). These Tensile tests provide useful information on the global mechanical response of the strengthening system (deformation capacity, strength and crack spacing) and can also be used for validation of the bond-slip laws extracted from the pull-out tests [102].

In **Table 3.5** the set-up conditions used to perform the direct tensile tests in the TRM coupons in different laboratories are presented, namely the type of clamping systems, type of instrumentation for monitoring and testing rate [99]. In alternative to the monitoring systems shown in **Table 3.5** Bertolesi et al. [117] used optical sensors installed in the central part of the fabric used in the tensile test coupon. From these works it was possible to infer the existence of a vast range of conditions and monitoring systems that differ from one laboratory to the other.

Table 3.5: Clamping methods and instrumentation used in the laboratories to perform the direct tensile tests [99].

University	Clamping method	Instrumentation	Test rate [mm/min]
CERTIMAC	Knurled plates (width 120 mm; height 115 mm)	Extensometer (gauge L = 200 mm)	0.30 (un-cracked phase) /0.50 (cracked phase)
UPATRAS	CFRP wraps and hydraulic clamping system of the testing machine	LVDTs (gauge L = 200 mm)	0.24
UNIBO	FRP tabs and hydraulic clamping system of the testing machine	Extensometer (gauge L = 200 mm) DIC	0.2

University	Clamping method	Instrumentation	Test rate [mm/min]
CUT	The ends of the specimens were embedded in polymer layer (150 mm) and clamped with two bolted steel plates	LVDT (gauge L = 200 mm)	0.3
UNILYON	Aluminium tabs glued to the specimen ends and inserted inside hydraulic grips	LVDT (gauge L = 200 mm)	0.3
POLIMI	FRP tabs (length = 60 mm) and hydraulic clamping system of the testing machine	Extensometer (gauge L = 100 mm)	0.10 (un-cracked phase) 0.20 (cracked phase)
UNIeCAMPUS	GFRP tabs and hydraulic clamping system of the testing machine	LVDT of the testing machine Digital Image Correlation	1
UNIPD	Clevis Type: Two couples of steel plates glued to the ends with quick-setting resin, then bolted	Potentiometer (gauge L = 200 mm)	0.30 (un-cracked phase) 0.30–0.60 (cracked phase)
UNISALENTO	Tabs applied on dry textile and hydraulic clamping system of the testing machine	LVDT of the testing machine	0.3
UNIRM3	GFRP wraps (length = 110 mm) and hydraulic clamping system of the testing machine	Extensometer (gauge length = 50 mm) Potentiometer (gauge length = 200 mm) DIC	0.6

The tensile stress-strain behaviour resulting from the extensive direct tensile test campaigns can be characterized by three different response stages shown in **Figure 3.18** b), and are described as follows:

- Stage I, the mortar is uncracked and significantly contributes to both the stiffness and the load bearing capacity of the composite. The tensile modulus of elasticity of the TRM (EI) can be estimated referring to an equivalent homogenised cross section, assuming a perfect matrix-to-textile bond.
- Stage II starts when the first crack is identified in the matrix, with the crack pattern progressively developing along this stage. The formation of new cracks is associated with load drops, therefore the response curve in this stage is uneven and the stiffness EII needs to be derived through a linear interpolation in a suitable range of data.
- In Stage III, after the crack pattern has completely developed, a stiffer response is observed and the increase of applied envelope displacement produces a nearly linear stress growth.

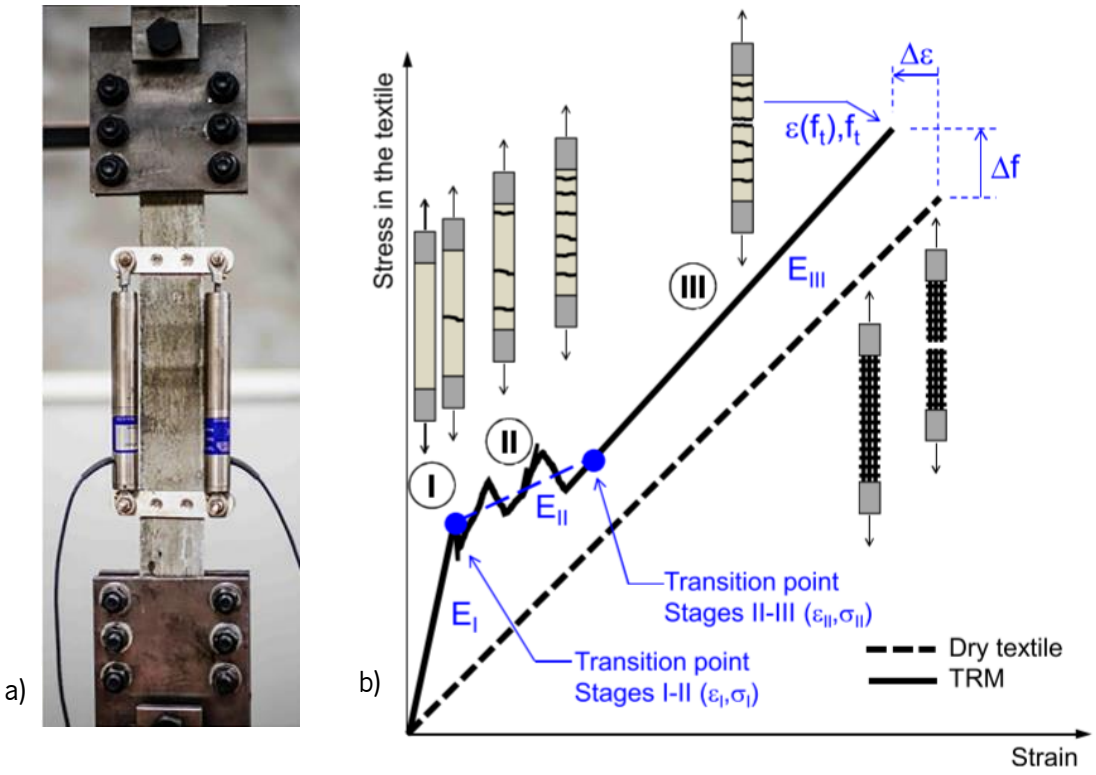


Figure 3.18: TRM direct tensile tests: a) test set-up; b) tensile response and stages obtained. Adapted from [100,109].

3.5. DURABILITY

The research that currently exists on the durability of textile-reinforced mortars (TRM) is still scarce, as indicated in references [102,113,118–120]. There is a gap in knowledge regarding the primary degradation processes in TRM systems, long-term performance when subjected to real conditions or controlled laboratory environments, and the establishment of accelerated ageing tests and configurations to assess the durability. These deficiencies delay not only the development of resilient TRM systems, but also developments in standards and regulatory design codes that consider the impact of ageing on the performance of TRM composites. Achieving durable TRM systems requires a multi-scale evaluation framework to assess the degradation mechanisms and stability of individual components (fibers, matrix, meshes) and the entire TRM composite under various loading scenarios. This includes mechanical stresses, environmental exposures (water, high temperatures, freeze-thaw), and their potentially synergistic effects [102].

Al-Lami et al. [118] reported contradictory results regarding the durability of FRCM lime-based matrices exposed to saline environments. The differences identified were attributed to the variation in the porosity and pore radius of the matrix, and concluded that further studies are required to correlate

the physical properties of the matrix with its durability against various environments [118]. The results obtained by Dalalbashi et al [121] show that the long-term behaviour of TRM composites for different ages is significantly determined by the mortar and fibre combination, remarkably changing between different TRM systems. It was also noted that lime-based systems could not reach their full mechanical properties under indoor conditions even after 3 years, with outdoor conditions leading to significantly higher mechanical properties. Durability and ductility were studied by Gunes et al. [113], for different types of fabrics (glass, basalt and carbon textiles) and natural hydraulic lime-based matrix, the flexural capacities were compared at ambient conditions and then through hot water ageing tests (immersion at 50 °C during 10 days). The interaction between fibres and the matrix was concluded to be of higher importance for long term behaviour. Dalalbashi et al. [122] showed that the freezing-thawing exposure conditions considered in their study didn't show detrimental effects on the mortar strength. However, the fibre-to-mortar bond can weaken, and the deterioration level depends on the fibre type, embedment length, and fibre configuration [122].

The standard AC434 [123] presents acceptance criteria and establishes requirements for recognition of TRM composite systems used for the strengthening of masonry and concrete structures. **Table 3.6** shows the main environmental conditions and performance retention factors. To regulate durability assessment, the Technical Committee 290-IMC from RILEM [124] is currently developing consistent experimental procedures and modelling methods to characterize material properties and structural behaviour in the long-term. This RILEM-TC is additionally elaborating a proposal for guidelines on TRM systems with focus on durability aspects and long-term structural reliability. Attention will be given to the constituent materials, fibres and mortar for FRCM/TRM systems, as well as to the:

- Durability tests on the textiles (fabrics) with focus on the chemical/physical vulnerability of the textiles, and on obtaining the properties retention of aged textiles.
- Durability tests on mortar matrices with the goal of obtaining properties retention ratios of aged inorganic mortars.
- Durability tests on FRCM/TRM systems with the goal of obtaining properties retention ratios of aged FRCM/TRM Systems.
- Durability bond tests with the goal of obtaining bond properties of aged strengthening systems.

Table 3.6: Environmental durability tests, [123].

Environmental durability tests	Relevant standard	Test condition	Test duration	Percent retention Hours	
				1000	3000
Water resistance	ASTM D 2247 ASTM E 104	100%, 100 ± 2°F	1000 and 3000 hours	85	80
Saltwater resistance	ASTM D 1141 ASTM C 581	Immersion at 73 ± 2°F			
Alkali resistance		Immersion in solution with pH = 9.5 or higher and 73 ± 3°F			

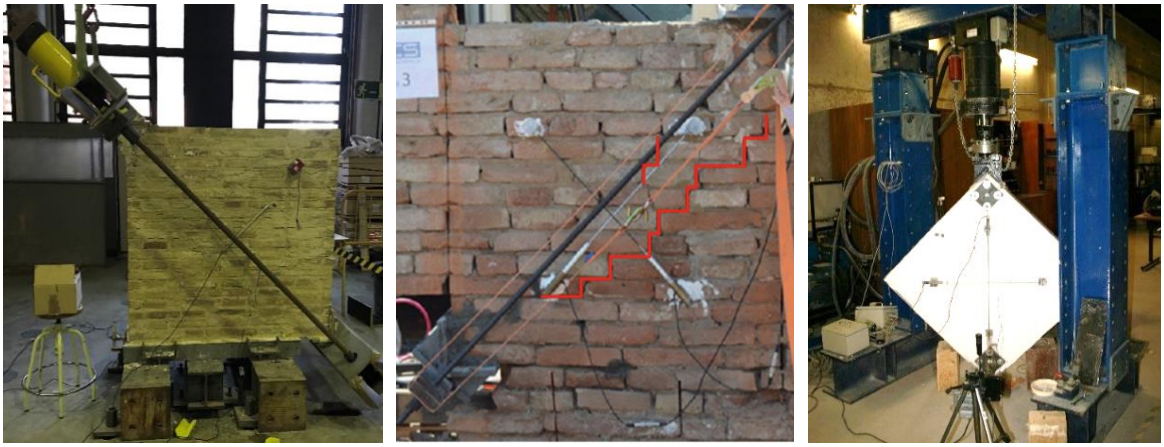
3.6. TRM STRENGTHENING EFFICIENCY

TRM is widely recognised as a successful system for enhancing the structural performance of masonry. Current studies indicate that TRM composites are generally successful in increasing the strength and flexibility of masonry walls, without significantly impacting their stiffness. However, given the broad array of TRM systems and masonry types available, more extensive studies are required to fully comprehend their performance. It's also worth noting that most of the results are derived from static tests conducted on individual wall panels in laboratory environments. Natural seismic events involve dynamic actions, and there is a lack of research involving shaking table tests on entire walls or even buildings, which is essential for understanding how these systems react to earthquakes [102,125,126]. Although the set-ups for the dynamic characterisation are complex and expensive, there are simpler ways to assess the cyclic behaviour of these strengthening systems such as performing quasi-static cyclic tests [127]. The TRM in-plane strengthening efficiency of masonry panels can be assessed by performing uniaxial compressive tests, diagonal compression tests [128–135], and shear compression tests [136–140].

3.6.1. Experimental In-plane efficiency evaluation

Regarding the in-plane efficiency quantification, the shear capacity is often assessed by means of the diagonal tensile tests, using masonry specimens built in the laboratory [141,142], or in-situ [134,143], see **Figure 3.19**. Different types of strengthening systems have already been evaluated using cyclic diagonal compressive tests, [134,144–146]. As discussed in previous publications, Brignola et al [143] conducted force controlled cyclic tests, with a load gradient of 200 N/s in each cycle, with the loading procedure defined to obtain four or five cyclic load steps for each masonry panel. Also, Angiolilli et al. [147] developed an in-situ campaign with cyclic diagonal compression tests performed on stone masonry specimens isolated from the original walls. Two reference panels and two TRM strengthened panels were tested. The TRM system was composed of a glass-fibre grid embedded in NHL-based

mortar and carbon shear connectors TRM to provide also the reference value of the unreinforced masonry. The tests were performed using force-control procedure by applying 20 kN at each load cycle, with a 0.1 kN/s load rate, up to failure. In the experimental campaign presented by Santa-Maria et al [148], the test procedure started with the first diagonal loading and unloading, followed by the loading of the second diagonal and unloading. Two cycles were performed at each load level, the load increments at each level were of 25 kN.



a) b) c)

Figure 3.19: Experimental setup used for Diagonal Compression Tests: a) Laboratory set-up with no reaction frame, [138]; b) In-situ set-up with no reaction frame [129]; c) Laboratory set-up with reaction frame.

A summary of data available in the literature referring to diagonal tensile tests on unreinforced clay brick masonry strengthened with additional overlays or composite materials is presented in **Table 3.7**. Different types of masonry and strengthening systems are presented, although in general the authors use a reduced number of specimens for the characterization of a specific layout. However, whenever possible, the coefficient of variation was calculated and the results obtained are in general quite low, especially for strengthened panels. Therefore, the use of a reduced number of specimens seems to lead to sufficiently representative experimental results.

Table 3.7: Summary of diagonal tensile test results on strengthened URM specimens obtained from authors.

Reference	Type of masonry	Type of reinforcement	F_{max}	Ss	Capacity increment
			(kN)	(MPa)	(%)
Santa-Maria et al. [148]	HCBM	–	132	–	–
		2 diagonal 150 mm-wide CFRP laminate	226	–	71
		2 diagonal CFRP fabric	196	–	48
		2 horizontal 150 mm-wide CFRP laminate	144	–	9
		2 horizontal CFRP fabric	182	–	38
Gabor et al. [149]	HCBM+CM	–	234	–	–
		unidirectional glass fibre, RFV	332	–	42
		unidirectional carbon fibre, RFC	361	–	54
		bidirectional glass fibre, RFW	384	–	64
Lucchini et al. [131]	HCBM + CM	–	35		–
	HCBM + CM	Engineered Cementitious Composites	220		632
Ozsayin et al. [150]	PCBM +CLM	–	–	0.95	–
		CFRP, strips	–	1.98	108
		CFRP, full surface	–	2.25	137
	PCBM +CM	–	–	0.92	–
		CFRP, strips	–	1.29	40
		CFRP, full surface	–	2.38	159
	PCBM +CLM	–	–	0.6	–
		CFRP, strips	–	1.39	132
		CFRP, full surface	–	1.16	93
Kadam et al. [151]	SCBM 1-wythe +CM	–	25	–	–
		unidirectionally anchored welded wire mesh	164	–	561
		bidirectionally anchored welded wire mesh	174	–	602
	SCBM 2-wythe +CM	–	46	–	–
		unidirectionally anchored welded wire mesh	236	–	413
		bidirectionally anchored welded wire mesh	223	–	385
Dehghani et al.[144]	SCBM+CM	–	51	–	
		Engineered Cementitious Composites LT:10 mm	70-	–	37
		Engineered Cementitious Composites LT:15 mm	142		178
Borri et al. [152]	SCBM + LM	–	27		–
	SCBM + LM	Stainless Steel Strip	53		94
	SM + LM	–	45		–
	SM + LM	Stainless Steel Strip	69		54
D'antino et al. [153]	SCBM + LM	–	87		–
	SCBM + LM	Glass Composite Reinforced Mortar	217		149
	SCBM + LM	–	104		–
	SCBM + LM	Glass Composite Reinforced Mortar	230		121
Gattesco et al. [133]]	SCBM + LM	–	192		–
	SCBM + LM	Glass Composite Reinforced Mortar	396		106
	SCBM + LM	Steel Reinforced Plaster	332		73
	SCBM + LM	–	286		–
	SCBM + LM	Glass Composite Reinforced Mortar	482		69
	SCBM + LM	Steel Reinforced Plaster	451		58
Lin et al. [154]	SCBM + CM	–	30		–
	SCBM + CM	Engineered Cementitious Composites	159		432
Mustafaraj [155]	SCBM + CM	–	179		–
	SCBM + CM	Glass Composite Reinforced Mortar	226		26

Where: PCBM = Perforated Clay Brick Masonry; HCBM = Hollow Clay Brick Masonry; SCBM = Solid Clay Brick Masonry; PM = Pebble Masonry; SM = Stone Masonry; CM = Cement Mortar; CLM = Cement and Lime Mortar; LM = Lime Mortar; LT = Layer Thickness

The diagonal tensile test is regarded as a simple and expedite procedure for the in-plane behaviour characterization. However, it is important to stress that the capability of this type of test to disclose all the failure modes of masonry walls is limited. For example, the rocking/crushing mechanism cannot be evaluated, [134]. For the evaluation of those mechanisms, compression shear tests must be performed following experimental procedures that consider the vertical load imposed to the masonry element and the effect of the horizontal displacements imposed by actuators [136,156].

3.6.2. Analytical formulation

The analytical formulation of the contribution of TRM systems to the in-plane shear capacity can be calculated following the analytical methodology presented in ACI 549.4R-13 [157], where the nominal shear capacity, V_n, is computed according to **Eq. (3.1)**:

$$V_n = V_m + V_f \quad \textbf{(3.1)}$$

where V_m represents the contribution of the masonry wall, and V_f represents the contribution of the TRM system. The contribution of the masonry wall can be obtained according to the methodology presented by Li et al. [158], and applied by Babaeidarabad et al. [159]. The following equations are used to compute the shear capacity for each of the four types of failure mechanisms that can occur:

- Shear capacity due to shear sliding failure, V_{ss}, calculated according to **Eq. (3.2)**:

$$V_{ss} = \frac{\tau_0}{1 - \mu_0 \times tan\,\theta} \times A_n \quad \textbf{(3.2)}$$

where τ_0 is the shear bond strength of the mortar joint (MPa), μ_0 is the coefficient of internal shear friction in mortar joints, θ is the angle between horizontal and main diagonal of the wall (degrees), and A_n is the net area of the cross section of the masonry wall (mm²).

- Shear capacity due to shear friction failure, V_{sf}, calculated according to **Eq. (3.3)**:

$$V_{sf} = \frac{\tau_{0,m}}{1 - \mu_m \times tan\,\theta} \times A_n \quad \textbf{(3.3)}$$

$$\tau_{0,m} = \frac{\tau_0}{1 + 1.5 \times \mu_0 \times \frac{h}{w}} \quad \textbf{(3.4)}$$

$$\mu_m = \frac{\mu_0}{1 + 1.5 \times \mu_0 \times \frac{h}{w}} \quad \textbf{(3.5)}$$

where $\tau_{0,\mathrm{m}}$ is the modified shear bond strength in mortar joint (MPa), with h and w being the height and length of the bricks (mm), respectively, and μ_{m} is the modified coefficient of internal shear friction in mortar joint.

- Shear capacity due to the diagonal tension failure, V_{dt}, calculated according to Eq. **(3.6)**:

$$V_{dt} = \frac{tan\,\theta + \sqrt{21.16 + tan\,\theta^2}}{10.58} \times f'_t \times A_n \quad \textbf{(3.6)}$$

where f'_t is the tensile strength of masonry, $f'_t = 0.67 \times \sqrt[2]{f'_m}$,(MPa), with f'_m being the compressive strength of the masonry (MPa)

- Shear capacity due to the crushing failure at the loading end, V_c, calculated according to **Eq. (3.7)**:

$$V_c = \frac{2 \times w \times f'_m}{3 \times h + 2 \times w \times tan\,\theta} \times A_m \quad \textbf{(3.7)}$$

where A_m (mm^2) is de interface loading area between the steel shoe and the wall.

Finally, the shear capacity of the unreinforced or plain wall, V_m, is the minimum value of previous expressions, see **Eq. (3.8)**:

$$V_m = min\{V_{ss}; V_{sf}; V_{dt}; V_c\} \quad \textbf{(3.8)}$$

The contribution of the TRM system for the shear capacity, V_f, is obtained according to Eq. **(3.9)**:

$$V_f = 2 \times n \times A_f \times L \times f_{fv} \quad \textbf{(3.9)}$$

where n is the number of fabric layers, A_f is the area of mesh reinforcement by unit width (mm^2/mm), L is the length of the wall in the direction of the shear force (mm); f_{fv} is the tensile strength of TRM shear reinforcement, $f_{fv} = E_f \times \varepsilon_{fv}$, (MPa), E_f is the tensile modulus of elasticity of the cracked FRM specimen, (MPa), and ε_{fv} is the design tensile strain of FRM shear reinforcement (mm/mm).

3.7. FINAL CONSIDERATIONS

In this chapter different types of mortar matrices, fibres and meshes used for TRM systems were analysed and discussed. Namely, mortars composed by alternative binders, which have been gathering great attention in recent years, as natural hydraulic lime and geopolymeric binders. Also, the thermomechanical properties of aggregates and cementitious and geopolymeric mortars were discussed. Geopolymeric materials have been studied by several authors showing good performance after exposure to high temperatures, up to 800°C. Also, the spalling behaviour of FRM tend to be better than plain mortar or concrete due the channels that can be formed by the combustion of fibre material allowing the vapour pressure to be dissipated. The technology related to the development

and accessibility of fibres provided new options to FRM. It was shown that a great variety of solutions are now available, e.g., from glass fibres to carbon fibres or natural fibres, in addition, a vast option of fabrics and meshes can be found commercially available. Different types of tests are normally performed for the experimental characterization of overlay systems (pull-out, tensile, bond shear, etc...), procedures and type of information obtained from each test were presented and discussed in the chapter. Finally, the most relevant durability tests and procedures proposed by standards were presented and the strengthening efficiency of the TRM composites evaluated by experimental characterization and analytical formulation where discussed.

The literature review carried within this chapter contributed to the proposal of potential solutions using FRM, addressing a knowledge gap by integrating hybrid binders and recycled fibres and aggregates. These hybrid binders are expected to be effective in overcoming certain limitations that individual binders encounter in specific situations, e.g., high temperature from fire after seismic. Furthermore, the rising use of fibres in high-value industries has led to an increased availability of recycled fibres once they have completed their service life. Fibres from components in the wind energy sector, like aspen, or carbon fibres from aviation materials, can now be reintroduced into the market at a reduced cost while still retaining their high mechanical properties.

3.8. REFERENCES

[1] Felice G De, Santis S De, Garmendia L. Mortar-based systems for externally bonded strengthening of masonry. Mater Struct 2014:2021–37. https://doi.org/10.1617/s11527-014-0360-1.

[2] García D, Díez J. Stone masonry walls: Strengthening with TRM (I). In: Ayala DFD, Fodde E, editors. Structural Analysis of Historic Construction, London: Taylor & Francis Group; 2008, p. 851–9.

[3] Garmendia L, Larrinaga P, García D, Marcos I. Textile-reinforced mortar as strengthening material for masonry arches. International Journal of Architectural Heritage 2014;8:627–48. https://doi.org/10.1080/15583058.2012.704480.

[4] Kouris LAS, Triantafillou TC. State-of-the-art on strengthening of masonry structures with textile reinforced mortar (TRM). Constr Build Mater 2018;188:1221–33. https://doi.org/10.1016/j.conbuildmat.2018.08.039.

[5] de Felice G, Aiello MA, Caggegi C, Ceroni F, De Santis S, Garbin E, et al. Recommendation of RILEM Technical Committee 250-CSM: Test method for Textile Reinforced Mortar to substrate

bond characterization. Mater Struct 2018;51:95. https://doi.org/10.1617/s11527-018-1216-x.

[6] Papanicolaou C, Triantafillou TC, Lekka M. Externally bonded grids as strengthening and seismic retrofitting materials of masonry panels. Constr Build Mater 2011;25:504–14. https://doi.org/10.1016/j.conbuildmat.2010.07.018.

[7] Almeida JAPP, Pereira EB, Barros JAO. Assessment of overlay masonry strengthening system under in-plane monotonic and cyclic loading using the diagonal tensile test. Constr Build Mater 2015;94:851–65. https://doi.org/http://dx.doi.org/10.1016/j.conbuildmat.2015.07.040.

[8] Kyriakides MA, Billington SL. Seismic Retrofit Of Masonry-Infilled Non-Ductile Reinforced Concrete Frames Using Sprayable Ductile Fiber-Reinforced Cementitious Composites. The 14 World Conference on Earthquake Engineering, Beijing, China: 2008.

[9] Dehghani A, Fischer G, Nateghi Alahi F. Strengthening masonry infill panels using engineered cementitious composites. Mater Struct 2013:1–20. https://doi.org/10.1617/s11527-013-0176-4.

[10] Stefanidou M, Papayianni I, Pachta V. Evaluation of inclusions in mortars of different historical periods from greek monuments. Archaeometry 2012;54:737–51. https://doi.org/10.1111/j.1475-4754.2011.00645.x.

[11] Mansur MA, Aziz MA. A study of jute fibre reinforced cement composites. International Journal of Cement Composites and Lightweight Concrete 1982;4:75–82. https://doi.org/10.1016/0262-5075(82)90011-2.

[12] Toledo Filho RD, Scrivener K, England GL, Ghavami K. Durability of alkali-sensitive sisal and coconut fibres in cement mortar composites. Cem Concr Compos 2000;22:127–43.

[13] Claramunt J, Ardanuy M, García-Hortal JA, Toledo Filho RD. The hornification of vegetable fibers to improve the durability of cement mortar composites. Cem Concr Compos 2011;33:586–95. https://doi.org/10.1016/j.cemconcomp.2011.03.003.

[14] Fidelis MEA, Toledo Filho RD, Silva F de A, Mechtcherine V, Butler M, Hempel S. The effect of accelerated aging on the interface of jute textile reinforced concrete. Cem Concr Compos 2016;74:7–15. https://doi.org/10.1016/j.cemconcomp.2016.09.002.

[15] Kim D joo, Naaman AE, El-Tawil S. Comparative flexural behavior of four fiber reinforced cementitious composites. Cem Concr Compos 2008. https://doi.org/10.1016/j.cemconcomp.2008.08.002.

[16] Ralegaonkar R, Gavali H, Aswath P, Abolmaali S. Application of chopped basalt fibers in reinforced mortar: A review. Constr Build Mater 2018;164:589–602. https://doi.org/10.1016/j.conbuildmat.2017.12.245.

[17] Skourup BN, Erdogmus E. Characteristics of PVA fiber-reinforced mortars. Proceedings of the 2009 Structures Congress - Don't Mess with Structural Engineers: Expanding Our Role, Leslie E. Robertson Associates, New York, NY, United States: 2009, p. 1622–31.

[18] Silva BA, Ferreira Pinto AP, Gomes A. Natural hydraulic lime versus cement for blended lime mortars for restoration works. Constr Build Mater 2015;94:346–60. https://doi.org/10.1016/j.conbuildmat.2015.06.058.

[19] Pavía S, Hanley R. Flexural bond strength of natural hydraulic lime mortar and clay brick. Mater Struct 2010;43:913–22. https://doi.org/10.1617/s11527-009-9555-2.

[20] Pozo-Antonio JS. Evolution of mechanical properties and drying shrinkage in lime-based and lime cement-based mortars with pure limestone aggregate. Constr Build Mater 2015;77:472–8. https://doi.org/10.1016/j.conbuildmat.2014.12.115.

[21] Kalagri A, Karatasios I, Kilikoglou V. The effect of aggregate size and type of binder on microstructure and mechanical properties of NHL mortars. Constr Build Mater 2014;53:467–74. https://doi.org/10.1016/j.conbuildmat.2013.11.111.

[22] Gulotta D, Goidanich S, Tedeschi C, Toniolo L. Commercial NHL-containing mortars for the preservation of historical architecture. Part 2: Durability to salt decay. Constr Build Mater 2015;96:198–208. https://doi.org/10.1016/j.conbuildmat.2015.08.006.

[23] Bookseries R. Historic Mortars: Characterization, Assessment and Repair. Prague: 2012. https://doi.org/10.1007/978-94-007-4635-0.

[24] Middendorf B, Klein D, Hogewoning S, Schmidt S-O. The New Groups of Formulated Limes (FL) of Lime Standard EN 459 - Bane or Boon ? 2nd Historic Mortars Conference HMC2010 and RILEM TC 203-RHM Final Workshop, Prague: 2010, p. 1087–95.

[25] Comité Européen de Normalisation. EN 459-1:2010 Building lime- Part 1: Definitions, specifications and conformity criteria 2010.

[26] Nodehi M, Vahid &, Taghvaee M. Alkali-Activated Materials and Geopolymer: a Review of Common Precursors and Activators Addressing Circular Economy. Circular Economy and Sustainability 2021 2:1 2021;2:165–96. https://doi.org/10.1007/S43615-021-00029-W.

[27] Pacheco-Torgal F, Castro-Gomes J, Jalali S. Alkali-activated binders: A review: Part 1. Historical background, terminology, reaction mechanisms and hydration products. Constr Build Mater 2008;22:1305–14. https://doi.org/10.1016/J.CONBUILDMAT.2007.10.015.

[28] Pacheco-Torgal F, Castro-Gomes J, Jalali S. Alkali-activated binders: A review. Part 2. About materials and binders manufacture. Constr Build Mater 2008;22:1315–22. https://doi.org/10.1016/J.CONBUILDMAT.2007.03.019.

[29] Shi Z, Shi C, Wan S, Zhang Z. Effects of alkali dosage and silicate modulus on alkali-silica reaction in alkali-activated slag mortars. Cem Concr Res n.d. https://doi.org/S0008884618302047.

[30] Provis JL, Palomo A, Shi C. Advances in understanding alkali-activated materials. Cem Concr Res 2015. https://doi.org/10.1016/j.cemconres.2015.04.013.

[31] Fernández-Jiménez A. Durability of alkali-activated fly ash cementitious materials. J Mater Sci 2007;42:3055–65. https://doi.org/10.1007/s10853-006-0584-8.

[32] Palomo A, Grutzeck MW, Blanco MT. Alkali-activated fly ashes: A cement for the future. Cem Concr Res 1999;29. https://doi.org/10.1016/S0008-8846(98)00243-9.

[33] Reig L, Tashima MM, Borrachero M V., Monzó J, Cheeseman CR, Payá J. Properties and microstructure of alkali-activated red clay brick waste. Constr Build Mater 2013;43:98–106. https://doi.org/10.1016/j.conbuildmat.2013.01.031.

[34] Allahverdi A, Najafi Kani E, Hossain KMA, Lachemi M. Methods to control efflorescence in alkali-activated cement-based materials. Handbook of Alkali-Activated Cements, Mortars and Concretes, 2014. https://doi.org/10.1533/9781782422884.3.463.

[35] Wianglor K, Sinthupinyo S, Piyaworapaiboon M, Chaipanich A. Effect of alkali-activated metakaolin cement on compressive strength of mortars. Appl Clay Sci 2017;141:272–9. https://doi.org/10.1016/j.clay.2017.01.025.

[36] Choi S, Choi J, Song J, Yeon B. Rheological and mechanical properties of fiber-reinforced alkali-activated composite 2015;96:112–8.

[37] Ding Y, Dai JG, Shi CJ. Mechanical properties of alkali-activated concrete: A state-of-the-art review. Constr Build Mater 2016. https://doi.org/10.1016/j.conbuildmat.2016.09.121.

[38] Aydın S, Baradan B. The effect of fiber properties on high performance alkali-activated slag/silica fume mortars. Compos B Eng 2013;45:63–9. https://doi.org/10.1016/j.compositesb.2012.09.080.

[39] Allahverdi A, Kani EN. Use of construction and demolition waste (CDW) for alkali-activated or geopolymer cements. Handbook of Recycled Concrete and Demolition Waste, 2013. https://doi.org/10.1533/9780857096906.3.439.

[40] Asaad MA, Huseien GF, Memon RP, Ghoshal SK, Mohammadhosseini H, Alyousef R. Enduring performance of alkali-activated mortars with metakaolin as granulated blast furnace slag replacement. Case Studies in Construction Materials 2022;16:e00845. https://doi.org/10.1016/J.CSCM.2021.E00845.

[41] Rovnaník P, Kusák I, Bayer P, Schmid P, Fiala L. Electrical and Self-Sensing Properties of Alkali-Activated Slag Composite with Graphite Filler. Materials 2019. https://doi.org/10.3390/ma12101616.

[42] Funke H, Gelbrich S, Kroll L. The Durability and Performance of Short Fibers for a Newly Developed Alkali-Activated Binder. Fibers 2016;4:11. https://doi.org/10.3390/fib4010011.

[43] Pavel K, Oleg P, Hryhorii V, Serhii L. The Development of Alkali-activated Cement Mixtures for Fast Rehabilitation and Strengthening of Concrete Structures. Procedia Eng 2017;195:142–6. https://doi.org/10.1016/j.proeng.2017.04.536.

[44] Sedira N, Castro-Gomes J, Magrinho M. Red clay brick and tungsten mining waste-based alkali-activated binder: Microstructural and mechanical properties. Constr Build Mater 2018;190:1034–48. https://doi.org/10.1016/j.conbuildmat.2018.09.153.

[45] He P, Zhang B, Lu J-X, Poon CS. A ternary optimization of alkali-activated cement mortars incorporating glass powder, slag and calcium aluminate cement. Constr Build Mater 2020;240:117983. https://doi.org/10.1016/j.conbuildmat.2019.117983.

[46] Li C, Sun H, Li L. A review: The comparison between alkali-activated slag (Si + Ca) and metakaolin (Si + Al) cements. Cem Concr Res 2010. https://doi.org/10.1016/j.cemconres.2010.03.020.

[47] Kusak I, Lunak M. On the effect of addition of carbon nanotubes on the electric conductivity of alkali-activated slag mortars. IOP Conf Ser Mater Sci Eng 2017;246. https://doi.org/10.1088/1757-899X/246/1/012044.

[48] Provis JL, Bernal SA. Geopolymers and related alkali-activated materials. Annu Rev Mater Res 2014;44. https://doi.org/10.1146/annurev-matsci-070813-113515.

[49] Duxson P, Fernández-Jiménez A, Provis JL, Lukey GC, Palomo A, Deventer JSJ van. Geopolymer technology: the current state of the art. J Mater Sci 2007;42:2917–33. https://doi.org/10.1007/s10853-006-0637-z.

[50] Lahoti M, Tan KH, Yang E-H. A critical review of geopolymer properties for structural fire-resistance applications. Constr Build Mater 2019;221:514–26. https://doi.org/10.1016/J.CONBUILDMAT.2019.06.076.

[51] Jiang C, Wang A, Bao X, Ni T, Ling J. A review on geopolymer in potential coating application: Materials, preparation and basic properties. Journal of Building Engineering 2020;32. https://doi.org/10.1016/j.jobe.2020.101734.

[52] Moutinho S, Costa C, Andrejkovičová S, Mariz L, Sequeira C, Terroso D, et al. Assessment of properties of metakaolin-based geopolymers applied in the conservation of tile facades. Constr Build Mater 2020;259:119759. https://doi.org/10.1016/J.CONBUILDMAT.2020.119759.

[53] Panizza M, Natali M, Garbin E, Tamburini S, Secco M. Assessment of geopolymers with Construction and Demolition Waste (CDW) aggregates as a building material. Constr Build Mater 2018;181:119–33. https://doi.org/10.1016/J.CONBUILDMAT.2018.06.018.

[54] Panda B, Paul SC, Hui LJ, Tay YWD, Tan MJ. Additive manufacturing of geopolymer for sustainable built environment. J Clean Prod 2017;167. https://doi.org/10.1016/j.jclepro.2017.08.165.

[55] Liu J, Lv C. Properties of 3D-Printed Polymer Fiber-Reinforced Mortars: A Review. Polymers (Basel) 2022;14. https://doi.org/10.3390/polym14071315.

[56] Abulencia AB, Villoria MBD, Libre RGD, Quiatchon PRJ, Dollente IJR, Guades EJ, et al. Geopolymers as sustainable material for strengthening and restoring unreinforced masonry structures: A review. Buildings 2021;11. https://doi.org/10.3390/buildings11110532.

[57] Bazant Z, Kaplan M. Concrete for high temperatures: Material properties and mathematical models 1996.

[58] R. RN, Beaucour a.-L, Hebert R, Noumowé a., Ledésert B, Bodet R. Thermal stability of different siliceous and calcareous aggregates subjected to high temperature. MATEC Web of Conferences 2013;6:07001. https://doi.org/10.1051/matecconf/20130607001.

[59] Guo Z, Shi X. Experiment and Calculation of Reinforced Concrete at Elevated Temperatures. Elsevier; 2011. https://doi.org/10.1016/C2010-0-65988-8.

[60] Mehta PK (Povindar K, Monteiro PJM. Concrete : microstructure, properties, and materials. 2006. https://doi.org/10.1036/0071462899.

[61] Mohd Ali AZ, Sanjayan J, Guerrieri M. Specimens size, aggregate size, and aggregate type effect on spalling of concrete in fire. Fire Mater 2017:1–10. https://doi.org/10.1002/fam.2457.

[62] Vickers L, Riessen A Van, Rickard WD a. Fire-Resistant Geopolymers Role of Fibres and Fillers to Enhance Thermal Properties. 2015.

[63] Hager I. Behaviour of cement concrete at high temperature. Bulletin of the Polish Academy of Sciences: Technical Sciences 2013;61:145–54. https://doi.org/10.2478/bpasts-2013-0013.

[64] Novák J, Kohoutková A. Fibre reinforced concrete exposed to elevated temperature. IOP Conf Ser Mater Sci Eng 2017;246. https://doi.org/10.1088/1757-899X/246/1/012045.

[65] Ezziane M, Kadri T, Molez L, Jauberthie R, Belhacen A. High temperature behaviour of polypropylene fibres reinforced mortars. Fire Saf J 2015;71:324–31. https://doi.org/10.1016/j.firesaf.2014.11.022.

[66] Ding Y, Azevedo C, Aguiar JB, Jalali S. Study on residual behaviour and flexural toughness of fibre cocktail reinforced self compacting high performance concrete after exposure to high temperature. Constr Build Mater 2012;26:21–31. https://doi.org/10.1016/j.conbuildmat.2011.04.058.

[67] Kong DLY, Sanjayan JG, Sagoe-Crentsil K. Factors affecting the performance of metakaolin geopolymers exposed to elevated temperatures. J Mater Sci 2008;43:824–31. https://doi.org/10.1007/s10853-007-2205-6.

[68] Abdel-Ghani NT, Elsayed HA, AbdelMoied S. Geopolymer synthesis by the alkali-activation of blast furnace steel slag and its fire-resistance. HBRC Journal 2016. https://doi.org/10.1016/j.hbrcj.2016.06.001.

[69] Zhang Z, Provis JL, Reid A, Wang H. Mechanical, thermal insulation, thermal resistance and acoustic absorption properties of geopolymer foam concrete. Cem Concr Compos 2015;62:97–105. https://doi.org/10.1016/J.CEMCONCOMP.2015.03.013.

[70] Kong DLY, Sanjayan JG. Effect of elevated temperatures on geopolymer paste, mortar and concrete. Cem Concr Res 2010;40:334–9. https://doi.org/10.1016/J.CEMCONRES.2009.10.017.

[71] Li T, Zhang Y, Dai JG. Flexural behavior and microstructure of hybrid basalt textile and steel fiber reinforced alkali-activated slag panels exposed to elevated temperatures. Constr Build Mater 2017;152:651–60. https://doi.org/10.1016/j.conbuildmat.2017.07.059.

[72] Carabba L, Manzi S, Rambaldi E, Ridolfi G, Bignozzi MC. High-temperature behaviour of alkali-activated composites based on fly ash and recycled refractory particles. Journal of Ceramic Science and Technology 2017. https://doi.org/10.4416/JCST2017-00047.

[73] Huseien GF, Sam ARM, Mirza J, Tahir MM, Asaad MA, Ismail M, et al. Waste ceramic powder incorporated alkali activated mortars exposed to elevated Temperatures: Performance evaluation. Constr Build Mater 2018;187:307–17. https://doi.org/10.1016/j.conbuildmat.2018.07.226.

[74] Çelikten S, Sarıdemir M, Özgür Deneme İ. Mechanical and microstructural properties of alkali-activated slag and slag + fly ash mortars exposed to high temperature. Constr Build Mater 2019;217:50–61. https://doi.org/10.1016/j.conbuildmat.2019.05.055.

[75] Siqueira JEL. Utilização de fibras naturais e sintéticas em argamassas de revestimento de alvenaria. Florianópolis, SC, 2006.

[76] Bentur A, Mindess S. Fibre Reinforced Cementitious Composites. Second. Taylor & Francis; 2007.

[77] Peled A, Bentur A, Mobasher B. Textile Reinforced Concrete. CRC Press - Taylor & Francis Group; 2017.

[78] American Concrete Institute. ACI 440R-96: Report on Fiber Reinforced Plastic (FRP) Reinforcement for Concrete Structures (Reaproved 2002) 2002;96:1–68.

[79] Kunz P. 3-Co 2010. http://www.3-co.com/Pro/Engineers/Special.Concrete/snfrc.htm.

[80] Felekoğlu B, Tosun K, Baradan B. Effects of fibre type and matrix structure on the mechanical performance of self-compacting micro-concrete composites. Cem Concr Res 2009;39:1023–32. https://doi.org/10.1016/j.cemconres.2009.07.007.

[81] Kamenny Vek Advanced Basalt Fiber n.d. http://basfiber.com/ (accessed August 10, 2018).

[82] Satyanarayana KG, Arizaga GGC, Wypych F. Biodegradable composites based on lignocellulosic fibers-An overview. Progress in Polymer Science (Oxford) 2009;34:982–1021. https://doi.org/10.1016/j.progpolymsci.2008.12.002.

[83] Onuaguluchi O, Banthia N. Plant-based natural fibre reinforced cement composites: A review. Cem Concr Compos 2016;68:96–108. https://doi.org/10.1016/j.cemconcomp.2016.02.014.

[84] Di Bella G, Fiore V, Galtieri G, Borsellino C, Valenza A. Effects of natural fibres reinforcement in lime plasters (kenaf and sisal vs. Polypropylene). Constr Build Mater 2014;58:159–65. https://doi.org/10.1016/j.conbuildmat.2014.02.026.

[85] Al-Oqla FM, Salit MS. Materials Selection for Natural Fiber Composites. Elsevier Science, 2017; 2017.

[86] Toledo Filho RD, Ghavami K, England GL, Scrivener K. Development of vegetable fibre-mortar composites of improved durability. Cem Concr Compos 2003;25:185–96. https://doi.org/10.1016/S0958-9465(02)00018-5.

[87] Illampas R, Oliveira D V., Lourenço PB. Design of Strain-Hardening Natural TRM Composites: Current Challenges and Future Research Paths. Materials 2023;16. https://doi.org/10.3390/ma16134558.

[88] Ferreira SR, Lima PRL, Silva FA, Toledo Filho RD. Effect of sisal fiber hornification on the fiber-matrix bonding characteristcs and bending behavior of cement based composites. Key Eng Mater 2014;600:421–32. https://doi.org/10.4028/www.scientific.net/KEM.600.421.

[89] Ferreira SR, Silva F de A, Lima PRL, Toledo Filho RD. Effect of hornification on the structure, tensile behavior and fiber matrix bond of sisal, jute and curauá fiber cement based composite systems. Constr Build Mater 2017;139:551–61. https://doi.org/10.1016/j.conbuildmat.2016.10.004.

[90] Ballesteros JEM, dos Santos V, Mármol G, Frías M, Fiorelli J. Potential of the hornification treatment on eucalyptus and pine fibers for fiber-cement applications. Cellulose 2017;24:2275–86. https://doi.org/10.1007/s10570-017-1253-6.

[91] Faruk O, Bledzki AK, Fink HP, Sain M. Biocomposites reinforced with natural fibers: 2000-2010. Prog Polym Sci 2012;37:1552–96. https://doi.org/10.1016/j.progpolymsci.2012.04.003.

[92] Ferreira SR, Silva FDA, Lima PRL, Toledo Filho RD. Effect of fiber treatments on the sisal fiber properties and fiber-matrix bond in cement based systems. Constr Build Mater 2015;101:730–40. https://doi.org/10.1016/j.conbuildmat.2015.10.120.

[93] Cao M, Xu L, Zhang C. Rheology, fiber distribution and mechanical properties of calcium carbonate (CaCO3) whisker reinforced cement mortar. Compos Part A Appl Sci Manuf 2016;90:662–9. https://doi.org/10.1016/j.compositesa.2016.08.033.

[94] Cai J, Pan J. Using Calcium Carbonate Whisker in Engineered Cementitious Composites. Proceedings of the 9th International Conference on Fracture Mechanics of Concrete and Concrete Structures, IA-FraMCoS; 2016, p. 1–11. https://doi.org/10.21012/FC9.031.

[95] Cao M, Zhang C, Li Y, Wei J. Using Calcium Carbonate Whisker in Hybrid Fiber-Reinforced Cementitious Composites. Journal of Materials in Civil Engineering 2015;27. https://doi.org/10.1061/(ASCE)MT.1943-5533.0001041.

[96] Low NMP, Beaudoin J. Mechanical Properties of High Performance Cement Binders Reinforced With Wollastonite Micro-Fibres. Cem Concr Res 1992;22:981–9. https://doi.org/10.1016/0008-8846(92)90122-c.

[97] Kwon S, Nishiwaki T, Choi H, Mihashi H. Effect of Wollastonite Microfiber on Ultra-High-Performance Fiber-Reinforced Cement-Based Composites Based on Application of Multi-Scale Fiber-Reinforcement System. Journal of Advanced Concrete Technology 2015;13:332–44. https://doi.org/10.3151/jact.13.332.

[98] Silva FJ, Thaumaturgo C. Fibre reinforcement and fracture response in geopolymeric mortars. Fatigue Fract Eng Mater Struct 2003;26:167–72. https://doi.org/10.1046/j.1460-2695.2003.00625.x.

[99] Carozzi FG, Bellini A, D'Antino T, de Felice G, Focacci F, Hojdys Ł, et al. Experimental investigation of tensile and bond properties of Carbon-FRCM composites for strengthening masonry elements. Compos B Eng 2017;128:100–19. https://doi.org/10.1016/J.COMPOSITESB.2017.06.018.

[100] Wang X, Lam CC, Iu VP. Comparison of different types of TRM composites for strengthening masonry panels. Constr Build Mater 2019;219:184–94. https://doi.org/10.1016/J.CONBUILDMAT.2019.05.179.

[101] Jiang J, Jiang C, Li B, Feng P. Bond behavior of basalt textile meshes in ultra-high ductility cementitious composites. Compos B Eng 2019;174:107022. https://doi.org/10.1016/J.COMPOSITESB.2019.107022.

[102] Ghiassi B. Mechanics and durability of textile reinforced mortars: A review of recent advances and open issues. RILEM Technical Letters 2019;4. https://doi.org/10.21809/rilemtechlett.2019.99.

[103] CEN. EN 1015-12:2000 Methods of test for mortar for masonry - Part 12: Determination of adhesive strength of hardened mortar. Comité Européen de Normalisation 2000.

[104] Cardani G, Valluzzi MR, Panizza M, Girardello P, Binda L. Influence of salt crystallization on composites-to-masonry bond evaluated on site by pull-off tests. Key Eng Mater, vol. 624, 2015. https://doi.org/10.4028/www.scientific.net/KEM.624.338.

[105] Shrestha KC, Ebead U, Younis A. EFFECT OF SURFACE ROUGHENING ON CONCRETE/TRM BOND. Proceedings of International Structural Engineering and Construction, vol. 4, 2017. https://doi.org/10.14455/ISEC.res.2017.161.

[106] Sueki S, Soranakom C, Mobasher B, Peled A. Pullout-Slip Response of Fabrics Embedded in a Cement Paste Matrix. Journal of Materials in Civil Engineering 2007;19. https://doi.org/10.1061/(asce)0899-1561(2007)19:9(718).

[107] Dalalbashi A, Ghiassi B, Oliveira D V., Freitas A. Effect of test setup on the fiber-to-mortar pull-out response in TRM composites: Experimental and analytical modeling. Compos B Eng 2018;143:250–68. https://doi.org/10.1016/j.compositesb.2018.02.010.

[108] Dalalbashi A, De Santis S, Ghiassi B, Oliveira D V. Slip rate effects and cyclic behaviour of textile-to-matrix bond in textile reinforced mortar composites. Mater Struct 2021;54:108. https://doi.org/10.1617/s11527-021-01706-w.

[109] De Santis S, Carozzi FG, de Felice G, Poggi C. Test methods for Textile Reinforced Mortar systems. Compos B Eng 2017;127:121–32. https://doi.org/10.1016/j.compositesb.2017.03.016.

[110] Dalalbashi A, Ghiassi B, Oliveira D V. A multi-level investigation on the mechanical response of TRM-strengthened masonry. Mater Struct 2021;54:224. https://doi.org/10.1617/s11527-021-01817-4.

[111] RILEM TC 232-TDT. Recommendation of RILEM TC 232-TDT: test methods and design of textile reinforced concrete. Mater Struct 2016;49:4923–7. https://doi.org/10.1617/s11527-016-0839-z.

[112] Consiglio Superiore dei Lavori Pubblici. Linea Guida per la identificazione, la qualificazione ed il controllo di accettazione di compositi fibrorinforzati a matrice inorganica (FRCM) da utilizzarsi per il consolidamento strutturale di costruzioni esistenti. 2018.

[113] Gunes ME, Pekmezci BY, Girgin ZC. Durability of natural hydraulic lime (NHL) based TRM composites through hot water immersion method. Materials and Structures/Materiaux et Constructions 2021;54. https://doi.org/10.1617/s11527-020-01608-3.

[114] Zhang Q, Yang QC, Li WJ, Gu XL, Dai HH. Study on model of flexure response of carbon fiber textile reinforced concrete (CTRC) sheets with short AR-glass fibers. Case Studies in Construction Materials 2023;18:e01791. https://doi.org/10.1016/J.CSCM.2022.E01791.

[115] Donnini J, Chiappini G, Lancioni G, Corinaldesi V. Tensile behaviour of glass FRCM systems with fabrics' overlap: Experimental results and numerical modeling. Compos Struct 2019;212:398–411. https://doi.org/10.1016/J.COMPSTRUCT.2019.01.053.

[116] Estevan L, Varona FB, Baeza FJ, Torres B, Bru D. Textile Reinforced Mortars (TRM) tensile behavior after high temperature exposure. Constr Build Mater 2022;328:127116. https://doi.org/10.1016/j.conbuildmat.2022.127116.

[117] Bertolesi E, Fagone M, Rotunno T, Grande E, Milani G. Experimental characterization of the textile-to-mortar bond through distributed optical sensors. Constr Build Mater 2022;326:126640. https://doi.org/10.1016/j.conbuildmat.2022.126640.

[118] Al-Lami K, D'antino T, Colombi P. Durability of Fabric-Reinforced Cementitious Matrix (FRCM) Composites: A Review n.d. https://doi.org/10.3390/app10051714.

[119] Donnini J. Durability of glass FRCM systems: Effects of different environments on mechanical properties. Compos B Eng 2019. https://doi.org/10.1016/j.compositesb.2019.107047.

[120] Ceroni F, Bonati A, Galimberti V, Occhiuzzi A. Effects of Environmental Conditioning on the Bond Behavior of FRP and FRCM Systems Applied to Concrete Elements. J Eng Mech 2018;144. https://doi.org/10.1061/(asce)em.1943-7889.0001375.

[121] Dalalbashi A, Ghiassi B, Oliveira D V. Aging of lime-based TRM composites under natural environmental conditions. Constr Build Mater 2021;270. https://doi.org/10.1016/j.conbuildmat.2020.121853.

[122] Dalalbashi A, Ghiassi B, Oliveira D V. Influence of freeze–thaw cycles on the pull-out response of lime-based TRM composites. Constr Build Mater 2021;313. https://doi.org/10.1016/j.conbuildmat.2021.125473.

[123] AC434. Acceptance criteria for concrete and masonry strengthening using fabric-reinforced cementitious matrix (FRCM) composite Systems. ICC Evaluation Service, Whittier, CA 2018.

[124] RILEM. 290-IMC : Durability of Inorganic Matrix Composites used for Strengthening of Masonry Constructions n.d. https://www.rilem.net/groupe/290-imc-durability-of-inorganic-matrix-composites-used-for-strengthening-of-masonry-constructions-384 (accessed September 21, 2023).

[125] Santis S De, Casadei P, Canio G De, Felice G De, Malena M, Mongelli M, et al. Seismic performance of masonry walls retrofitted with steel reinforced grout. Earthquake Engng Struct Dyn 2016;45:229–51. https://doi.org/10.1002/eqe.2625.

[126] Maddaloni G, Di Ludovico M, Balsamo A, Maddaloni G, Prota A. Dynamic assessment of innovative retrofit techniques for masonry buildings. Compos B Eng 2018;147. https://doi.org/10.1016/j.compositesb.2018.04.038.

[127] Akhoundi F, Vasconcelos G, Lourenço P, Silva LM, Cunha F, Fangueiro R. In-plane behavior of cavity masonry infills and strengthening with textile reinforced mortar. Eng Struct 2018;156:145–60. https://doi.org/10.1016/j.engstruct.2017.11.002.

[128] Dong Z, Deng M, Dai J, Ma P. Diagonal compressive behavior of unreinforced masonry walls strengthened with textile reinforced mortar added with short PVA fibers. Eng Struct 2021;246. https://doi.org/10.1016/J.ENGSTRUCT.2021.113034.

[129] Bertolesi E, Milani G. Diagonal Compressive Tests on Double Wythe Brick Ancient Masonry Panels Unreinforced and Reinforced with Innovative Cement Based Materials: Advanced FE Simulations. RILEM Bookseries 2019;18:1000–8. https://doi.org/10.1007/978-3-319-99441-3_108.

[130] Bustos-García A, Moreno-Fernández E, Zavalis R, Valivonis J. Diagonal compression tests on masonry wallets coated with mortars reinforced with glass fibers. Materials and Structures/Materiaux et Constructions 2019;52. https://doi.org/10.1617/s11527-019-1360-y.

[131] Lucchini SS, Facconi L, Minelli F, Plizzari G. Retrofitting unreinforced masonry by steel fiber reinforced mortar coating: uniaxial and diagonal compression tests. Materials and Structures/Materiaux et Constructions 2020;53:1–22. https://doi.org/10.1617/S11527-020-01574-W/FIGURES/12.

[132] Mezrea PE, Ispir M, Balci IA, Bal IE, Ilki A. Diagonal tensile tests on historical brick masonry wallets strengthened with fabric reinforced cementitious mortar. Structures 2021;33:935–46. https://doi.org/10.1016/J.ISTRUC.2021.04.076.

[133] Gattesco N, Boem I, Dudine A. Diagonal compression tests on masonry walls strengthened with a GFRP mesh reinforced mortar coating. Bulletin of Earthquake Engineering 2014:1–24. https://doi.org/10.1007/s10518-014-9684-z.

[134] Borri A, Castori G, Corradi M, Speranzini E. Shear behavior of unreinforced and reinforced masonry panels subjected to in situ diagonal compression tests. Constr Build Mater 2011;25:4403–14. https://doi.org/10.1016/j.conbuildmat.2011.01.009.

[135] Ferrara G, Caggegi C, Martinelli E, Gabor A. Shear capacity of masonry walls externally strengthened using Flax-TRM composite systems: experimental tests and comparative assessment. Constr Build Mater 2020;261. https://doi.org/10.1016/J.CONBUILDMAT.2020.120490.

[136] Pinho FFS, Lúcio VJG, Baião MFC. Rubble stone masonry walls in Portugal strengthened with reinforced micro-concrete layers. Bulletin of Earthquake Engineering 2011;10:161–80. https://doi.org/10.1007/s10518-011-9280-4.

[137] Papanicolaou CG, Triantafillou TC, Karlos K, Papathanasiou M. Textile-reinforced mortar (TRM) versus FRP as strengthening material of URM walls : in-plane cyclic loading. Mater Struct 2007;40:1081–97. https://doi.org/10.1617/s11527-006-9207-8.

[138] Garcia-Ramonda L, Pelà L, Roca P, Camata G. Experimental and numerical insights on the in-plane behaviour of unreinforced and TRM/SRG retrofitted brick masonry walls by diagonal compression and shear-compression testing. Constr Build Mater 2023;402:132997. https://doi.org/10.1016/J.CONBUILDMAT.2023.132997.

[139] Meriggi P, Caggegi C, Gabor A, de Felice G. Shear-compression tests on stone masonry walls strengthened with basalt textile reinforced mortar (TRM). Constr Build Mater 2022;316:125804. https://doi.org/10.1016/J.CONBUILDMAT.2021.125804.

[140] Ponte M, Penna A, Bento R. In-plane cyclic tests of strengthened rubble stone masonry. Materials and Structures/Materiaux et Constructions 2023;56:1–18. https://doi.org/10.1617/S11527-023-02126-8/TABLES/5.

[141] Silva B, Dalla Benetta M, da Porto F, Modena C. Experimental assessment of in-plane behaviour of three-leaf stone masonry walls. Constr Build Mater 2014;53:149–61. https://doi.org/10.1016/j.conbuildmat.2013.11.084.

[142] Milosevic J, Gago AS, Lopes M, Bento R. Experimental assessment of shear strength parameters on rubble stone masonry specimens. Constr Build Mater 2013;47:1372–80. https://doi.org/10.1016/j.conbuildmat.2013.06.036.

[143] Brignola A, Frumento S, Lagomarsino S, Podestà S. Identification of Shear Parameters of Masonry Panels Through the In-Situ Diagonal Compression Test. International Journal of Architectural Heritage 2008;3:52–73. https://doi.org/10.1080/15583050802138634.

[144] Dehghani A, Fischer G, Alahi F. Strengthening masonry infill panels using engineered cementitious composites. Mater Struct 2013. https://doi.org/10.1617/s11527-013-0176-4.

[145] Almeida J, Pereira E, Barros J. Performance assessment of overlay strengthened masonry under cyclic loading using the diagonal tensile test. 9th International Masonry Conference, July 7, 8, 9; Guimarães, Guimarães: 2014, p. 1–12.

[146] Dalalbashi A, Ghiassi B, Oliveira D V. In-Plane Behavior of Clay Brick Masonry Wallets Strengthened by TRM System. RILEM Bookseries, vol. 34, 2022, p. 143–51. https://doi.org/10.1007/978-3-030-76465-4_13.

[147] Angiolilli M, Gregori A, Cattari S. Performance of Fiber Reinforced Mortar coating for irregular stone masonry: Experimental and analytical investigations. Constr Build Mater 2021;294. https://doi.org/10.1016/J.CONBUILDMAT.2021.123508.

[148] Santa-Maria H, Duarte G, Garib A. Experimental Investigation of masonry panels externally strengthened with CFRPlaminates and fabric subjected to in-plane shear load. 13th World Conference on Earthquake Engineering, Vancouver, B.C., Canada: 2004.

[149] Gabor A, Bennani A, Jacquelin E, Lebon F. Modelling approaches of the in-plane shear behaviour of unreinforced and FRP strengthened masonry panels. Compos Struct 2006;74:277–88. https://doi.org/10.1016/j.compstruct.2005.04.012.

[150] Ozsayin B, Yilmaz E, Ispir M, Ozkaynak H, Yuksel E, Ilki A. Characteristics of CFRP retrofitted hollow brick infill walls of reinforced concrete frames. Constr Build Mater 2011;25:4017–24. https://doi.org/10.1016/j.conbuildmat.2011.04.036.

[151] Kadam SB, Singh Y, Li B. Strengthening of unreinforced masonry using welded wire mesh and micro-concrete – Behaviour under in-plane action. Constr Build Mater 2014;54:247–57. https://doi.org/10.1016/j.conbuildmat.2013.12.033.

[152] Borri A, Corradi M, Castori G, Molinari A. Stainless steel strip – A proposed shear reinforcement for masonry wall panels. Constr Build Mater 2019;211:594–604. https://doi.org/10.1016/J.CONBUILDMAT.2019.03.197.

[153] D'Antino T, Carozzi FG, Poggi C. Diagonal shear behavior of historic walls strengthened with composite reinforced mortar (CRM). Materials and Structures/Materiaux et Constructions 2019;52:1–15. https://doi.org/10.1617/S11527-019-1414-1/TABLES/5.

[154] Lin YW, Wotherspoon L, Scott A, Ingham JM. In-plane strengthening of clay brick unreinforced masonry wallettes using ECC shotcrete. Eng Struct 2014;66:57–65. https://doi.org/10.1016/j.engstruct.2014.01.043.

[155] Mustafaraj E, Yardim Y. In-plane Shear Strengthening of Unreinforced Masonry Walls Using GFRP Jacketing. Periodica Polytechnica Civil Engineering 2018;62:330–6. https://doi.org/10.3311/PPCI.11311.

[156] Vasconcelos G, Lourenço PB. Experimental characterization of stone masonry in shear and compression. Constr Build Mater 2009;23:3337–45. https://doi.org/10.1016/j.conbuildmat.2009.06.045.

[157] ACI Committee 549. ACI 549.4R-13: Guide to Design and Construction of Externally Bonded Fabric- Reinforced Cementitious Matrix (FRCM) Systems for Repair and Strengthening Concrete and Masonry Structures. Farmington Hills, Michigan: 2013.

[158] Li T, Galati N, Tumialan JG, Nanni A. Analysis of unreinforced masonry concrete walls strengthened with glass fiber-reinforced polymer bars. ACI Struct J 2005;102.

[159] Babaeidarabad S, Arboleda D, Loreto G, Nanni A. Shear strengthening of un-reinforced concrete masonry walls with fabric-reinforced-cementitious-matrix. Constr Build Mater 2014;65:243–53. https://doi.org/10.1016/j.conbuildmat.2014.04.116.

CHAPTER 4

SUMMARY OF APPENDED PAPERS

This chapter presents a summary of the papers that constitute this PhD thesis. The papers are presented in a sequence that reflects the contribution of the research developed to the projected objectives. In a first paper, ***PAPER I,*** *the focus of the study was the assessment of the use of synthetic polyacrylonitrile (PAN) fibres for the reinforcement of a natural hydraulic lime mortar to be implemented as part of overlay masonry strengthening.* ***PAPER II*** *focus on the need for materials that must have good mechanical performance after seismic and fire scenarios, and the development of and FRM that could integrate higher amounts of construction residues and recycled carbon fibres. This both papers make important contributions to investigate a new strengthening systems using FRM and to explore additional functionalities, such as the ability of the systems to withstand high temperatures.* ***PAPER III*** *assesses the mechanical behaviour of the interface between a strengthening layer and a substrate; this interface is critical when considering the development of masonry strengthening overlays. The paper present existing experimental set-up's and proposes direct shear tests in couplet specimens and investigates the peak and residual shear stresses and the failure modes obtained for several normal stress levels. The research presented in the paper had as objective the characterization and understanding of the bonding behaviour between the strengthening overlays and masonry substrates.* ***PAPER IV*** *and* ***PAPER V*** *are both dedicated to the characterization and assessment of overlay strengthening systems applied to infill masonry elements. First,* ***PAPER IV****, focus on the applicability of the diagonal tensile test to assess the cyclic response of strengthened masonry. Results included the evaluation of the load carrying capacity of masonry elements, damage evolution and stiffness degradation mechanisms. The main contribution to the predefined objectives is the investigation of experimental procedures to estimate the global efficiency of the strengthening*

systems applied to masonry elements. Finally, ***PAPER V*** *presents the research developed to carry the evaluation of the in-plane capacity of masonry elements, unreinforced, rendered and strengthened with the FRM developed in* ***PAPER II*** *and carbon meshes. The evaluation included uniaxial compressive tests and biaxial diagonal tensile test, under monotonic and cyclic actions. The biaxial diagonal tests were performed under exploratory set-up due to the absence of existing information. The contribution of* ***PAPER V*** *to the objectives of the thesis is mostly related with the development of additional testing procedures considering the different components under study and their importance for the overall mechanical and functional performance.*

4.1. PAPER I

- Almeida, J. A. P. P., Barros, J. A. O., & Pereira, E. N. B. (2024). **Toughness of Natural Hydraulic Lime Fibre-Reinforced Mortars for Masonry Strengthening Overlay Systems**. Applied Sciences, 14(05), 1947. https://doi.org/10.3390/APP14051947. Impact Factor: 2.7

Masonry structures are prone to damage and collapse when subjected to seismic actions. This deficient behaviour is a problem in a significant number of worldwide urban areas. In order to improve this well-known weakness of masonry behaviour, overlay strengthening systems composed by fibre reinforced mortars are currently under study, as part of solutions based on the application of reinforcement overlays on the surface of masonry elements.

In this study the use of synthetic polyacrylonitrile (PAN) fibres as reinforcement of a natural hydraulic lime mortar was assessed, as part of a solution to develop novel fibre reinforced mortars for overlay masonry strengthening. The influence on the fresh behaviour and on the mechanical properties were studied. Additionally, the contribution of the fibres for increasing ductility, toughness and fracture energy for different fibre fractions were assessed.

The fresh behaviour of the fibre reinforced mortar (FRM) was found to be adequate for the type of application for fibre volume fractions below 0.50%. The compressive and the flexural strengths were differently affected by the increase of the fibre volume fraction, with compressive strength showing a decrease while flexural strength substantially increased for increasing fibre volume fractions. The compressive and flexural toughness, related to the post-cracking responses, have both showed

increases for increasing fibre fractions. Even for fibre fractions as low as 0.25% an important increment of the capacity to dissipate energy was found.

4.2. PAPER II

- Almeida, J. A. P. P., Pereira, E. B., Barros, J. A. O. **Hybrid Fibre Reinforced Mortar for overlay masonry strengthening.**

This study presents the development of a sustainable hybrid fibre-reinforced mortar (FRM) for masonry overlay strengthening, combining natural hydraulic lime (NHL), geopolymer binders, recycled carbon fibres, and ceramic waste aggregates. Motivated by the need for durable, thermally stable materials compatible with historical masonry, the research investigates the mechanical performance and thermal behaviour of FRMs under varying NHL-geopolymer ratios (25%, 50%, 75%, 100%). Thermogravimetric analysis (TGA) revealed enhanced thermal stability in hybrid binders, with NHL-geopolymer mixtures exhibiting reduced mass loss compared to pure NHL after exposure to 600°C. Mechanical testing demonstrated that FRMs with ≥50% geopolymer content maintained adequate compressive and flexural strength, outperforming NHL-based mortars after temperature exposure. However, the 75% geopolymer mix showed anomalous underperformance, underscoring the need for further studies to fully understand the behaviour of these hybrid systems. The integration of recycled fibres and industrial by-products aligns with circular economy principles, reducing environmental impact while enhancing ductility. This work bridges a critical gap in overlay systems by demonstrating the feasibility of hybrid binders for fire-resistant masonry strengthening, offering a novel pathway to balance sustainability, mechanical performance, and substrate compatibility.

4.3. PAPER III

- Almeida, J. A. P. P., Bordigoni, D., Pereira, E. N. B., Barros, J. A. O., Aprile, A. **Assessment of the properties to characterize the interface between clay brick substrate and strengthening mortar.** Construction and Building Materials 2016; 103, 47-66. https://doi.org/10.1016/j.conbuildmat.2015.11.036. Impact factor: 7.693

The behaviour of masonry elements under in-plane and out-of-plane loads can be improved through the application of strengthening systems based on reinforcing overlays. After strengthening, the transition region between the original substrate and the strengthening layer is especially stressed, and premature failure of the strengthened masonry is reached if insufficient interfacial capacity is assured. Therefore, the assessment of the mechanical behaviour of the interface is critical to the development of the masonry strengthening system based on the application of strengthening overlays. In this research a method for the characterisation of the interface behaviour between two different materials, a polypropylene fibre reinforced mortar (PFRM) and a ceramic brick used for masonry construction is presented. Direct shear tests were carried out in couplet specimens. Due to the orthotropic nature of the bricks surface, the shear load was applied along three different directions in order to perform an overall estimation of the interface behaviour. The peak and residual shear stresses, as well as the failure modes, were obtained at different levels of the normal stress. Based on these experimental results constitutive laws were assessed for the simulation of the interface mechanical behaviour based on the Mohr and Mohr-Coulomb failure criteria.

4.4. PAPER IV

- Almeida, J. A. P. P., Pereira, E. B., Barros, J. A. O. **Assessment of overlay masonry strengthening system under in-plane monotonic and cyclic loading using the diagonal tensile test.** Construction and Building Materials 2015; 94, 851–865. http://dx.doi.org/10.1016/j.conbuildmat.2015.07.040. Impact factor: 7.693

The development of novel strengthening techniques to address the seismic vulnerability of masonry elements is gradually leading to simpler, faster and more effective strengthening strategies. In particular, the use of fabric reinforced cementitious matrix systems is considered of great potential, given the increase of ductility achieved with simple and economic strengthening procedures. To assess the effectiveness of these strengthening systems, and considering that the seismic action is involved, one important component of the structural behaviour is the in-plane cyclic response. In this work is discussed the applicability of the diagonal tensile test for the assessment of the cyclic response of strengthened masonry. The results obtained allowed to assess the contribution of the strengthening

system to the increase of the load carrying capacity of masonry elements, as well as to evaluate the damage evolution and the stiffness degradation mechanisms developing under cyclic loading.

4.5. PAPER V

- Almeida, J. A. P. P., Pereira, E. B., Barros, J. A. O. **Characterization of overlay strengthening of masonry by means of biaxial cyclic diagonal tensile tests**

The development of new methods to reduce the seismic vulnerability of masonry elements is leading to versatile and effective strategies. In this context, textile reinforced mortar systems are particularly promising due to their adaptability and cost-effectiveness compromise. For a continued development of more innovative systems targeting even better performances, it is of particular importance to develop the experimental procedures to assess the increasingly complex mechanical performance delivered by these systems. This work discusses the assessment of the in-plane capacity of masonry overlay strengthening systems through performing uniaxial compressive tests and biaxial diagonal tensile tests to assess monotonic and cyclic responses of plain and strengthened masonry. Particular attention was dedicated to the biaxial diagonal tests due to the lack of information on the use of this type of set-up, including the loading sequences and procedures to characterize the shear response. The results obtained show a detailed description of the development of the strengthening mechanisms throughout the different stages of the load-displacement responses, supporting the analysis of the compression and shear capacity increments associated to changes of crack patterns and failure modes.

CHAPTER 5

CONCLUSIONS AND FUTURE WORK

5.1. CONCLUSIONS

This thesis has explored the development and characterization of innovative strengthening systems for masonry structures, with a particular focus on the mechanical performance and functional properties of textile reinforced mortars (TRM) systems. Through a series of research papers, the study has systematically addressed key aspects of material selection, mechanical behaviour, and experimental methodologies to assess the efficiency of TRM.

The first stage of the research, presented in **PAPER I**, investigated the reinforcement potential of synthetic polyacrylonitrile (PAN) fibres in natural hydraulic lime mortars, aiming to enhance their application in overlay masonry strengthening. The findings highlighted the potential of this reinforcement approach in improving mechanical performance while maintaining compatibility with historical masonry. Expanding on this theme, **PAPER II** focused on the development of an FRM incorporating high amounts of construction residues and recycled carbon fibres. Given the need for materials that perform reliably under extreme conditions, this study also considered the behaviour of the system after fire scenarios. Together, these two papers contribute to the understanding of FRM as a viable strengthening solution, while also exploring additional functionalities such as high temperature resistance.

To further investigate the performance of these systems, **PAPER III** analysed the mechanical behaviour of the interface between the strengthening layer and the substrate. Since interface bonding plays a critical role in the effectiveness of masonry overlays, this study reviewed existing experimental

setups and introduced direct shear tests on couplet specimens. By evaluating peak and residual shear stresses and identifying failure modes under different normal stresses, the research provided valuable insights into the bonding mechanisms that govern the efficiency of these systems.

The final section of the thesis focused on the assessment of overlay strengthening systems applied to infill masonry elements. **PAPER IV** examined the applicability of the diagonal tensile test for evaluating the monotonic and cyclic response of strengthened masonry. Key findings included the assessment of load-carrying capacity, damage evolution, and stiffness degradation, contributing to the development of experimental procedures for estimating the global efficiency of the strengthening systems. **PAPER V** expanded on this by assessing biaxial diagonal tensile tests under both monotonic and cyclic actions, incorporating an exploratory testing setup due to the lack of established methodologies in the field. The contribution of this research lies in advancing testing procedures that although considering only the masonry element, implement loading procedures in both diagonal directions emulating the type of loads imposed by seismic actions.

Through these investigations, the thesis has provided a comprehensive framework for the development, characterization, and evaluation of FRM-based masonry strengthening systems. The findings contribute not only to advancing knowledge in the field of structural strengthening but also to supporting the implementation of sustainable and resilient solutions for masonry structures subjected to seismic and fire-related challenges.

A comprehensive program encompassing material innovation, interface characterization, structural testing, and methodological refinement has enabled several key contributions to the field. The primary achievements and outcomes are summarized below:

Material Development

- NHL-FRM with PAN Fibers: A natural hydraulic lime (NHL)-based FRM incorporating polyacrylonitrile (PAN) fibers demonstrated superior ductility and energy dissipation compared to cement-based FRMs. Mortars with 1.00% fibre content achieved flexural strengths of 5–7.5 MPa but required superplasticizers for workability. Lower fibre volumes (0.25–0.75%) still significantly improved toughness, making them viable for overlay applications.
- Hybrid Binders and Recycled Materials: Combining NHL with geopolymeric binders enhanced compressive strength (up to 104 MPa in pastes) and high-temperature resilience. Mortars with 50–75% geopolymer content retained 54–181% higher flexural strength after exposure

to 600°C compared to pure NHL systems. Recycled carbon fibres, ceramic aggregates and non-Portland cement binders further improved sustainability without compromising mechanical performance.

Interface Behaviour: direct shear tests revealed anisotropic behaviour at the brick-FRM interface depending on load orientation relative to surface ribs. Shear strength followed a hyperbolic Mohr criterion, with residual friction coefficients influenced by rib damage under perpendicular loading.

Structural Performance Enhancements

- Carbon fibre mesh with cementitious overlays, FRMCom, increased masonry shear strength by 2.3, though delamination occurred before fibres reached ultimate strain.
- FRM and COM strengthening systems, increased the compressive strength by 24 and 59 % when comparing with the rendered masonry elements
- FRM and COM strengthening systems, an increase of the shear strength of 23% for COM system and 18% for FRM system were observed

Methodological Advances

- Cyclic loading protocols enabled stiffness degradation analysis and validated ACI 549.4R-13 [157] models, conservative by a safety factor of 2.3.
- Biaxial cyclic diagonal tensile tests confirmed to be an effective set-up to evaluate the shear behaviour of masonry.
- Using DIC techniques in biaxial diagonal tests allowed to follow the evolution of the crack pattern and failure modes in a detailed manner.

5.2. FUTURE WORK

Building upon the experimental work conducted in this thesis, several immediate research directions emerge that warrant further investigation: developing a comprehensive understanding of the reinforcement system's tensile behaviour through standardized coupon-type testing; investigating the interfacial mechanics between the developed system and masonry substrates; and refining the biaxial diagonal test configuration for enhanced reliability and reproducibility.

Beyond these immediate priorities, several broader research directions could significantly advance TRM strengthening systems and deserve particular attention:

Material optimization: improvement of workability by incorporation of superplasticizers; use of alternative recycled fibres (e.g., glass fibres recovered from wind turbine blades); long-term durability studies on hybrid binders under freeze-thaw, moisture, and chemical exposure.

Interface and structural behaviour: evaluation of mechanical anchors or textile connectors to prevent overlay detachment; study of strain-hardening matrices to delay carbon mesh failure;

Testing and standardization: refinement of biaxial test set-up for vertical/horizontal stiffness; standardize cyclic protocols for stiffness degradation benchmarking; non-destructive evaluation by means of ultrasonic or acoustic emission techniques to monitor "*in-situ*" fibre and mesh rupture and interface damage.

Computational and analytical tools: use of finite element analysis (FEA) of anisotropic interface behaviour under combined stresses; development of constitutive models for cyclic and multidirectional loading, incorporating surface geometry and friction coefficients; training of machine learning models to predict TRM performance based on mix design, fibre type, mesh type, curing conditions and type of support surfaces.

Sustainability and scalability: lifecycle analysis (LCA) of NHL-geopolymer hybrids vs. conventional binder systems; scale of recycled ceramic aggregate production and assessment of supply chain viability.

Multifunctional systems: development of TRM's with additional functionalities as self-sensing, heating functions, insulation capabilities, etc.

PAPER I

TOUGHNESS OF NATURAL HYDRAULIC LIME FIBRE REINFORCED MORTARS FOR MASONRY STRENGTHENING OVERLAY SYSTEMS

REFERENCE: Almeida, J. A. P. P., Barros, J. A. O., & Pereira, E. N. B. (2024). Toughness of Natural Hydraulic Lime Fibre-Reinforced Mortars for Masonry Strengthening Overlay Systems. Applied Sciences, 14(05), 1947. https://doi.org/10.3390/APP14051947. Impact Factor: 2.7

ABSTRACT: Masonry structures are prone to damage and collapse when subjected to seismic actions. This deficient behaviour is a problem in a significant number of worldwide urban areas. To improve this well-known weakness of masonry behaviour, overlay strengthening systems composed by fibre reinforced mortars are currently under study, as part of solutions based on the application of reinforcement overlays on the surface of masonry elements.

In this study the use of synthetic polyacrylonitrile (PAN) fibres as reinforcement of a natural hydraulic lime mortar was assessed, as part of a solution to develop novel fibre reinforced mortars for overlay masonry strengthening. The influence on the fresh behaviour and on the mechanical properties were studied. Additionally, the contribution of the fibres for increasing ductility, toughness and fracture energy for different fibre fractions were assessed.

The fresh behaviour of the fibre reinforced mortar (FRM) was found to be adequate for the type of application for fibre volume fractions below 0.50%. The compressive and the flexural strengths were

differently affected by the increase of the fibre volume fraction, with compressive strength showing a decrease while flexural strength substantially increased for increasing fibre volume fractions. The compressive and flexural toughness, related to the post-cracking responses, have both showed increases for increasing fibre fractions. Even for fibre fractions as low as 0.25% an important increment of the capacity to dissipate energy was found.

KEYWORDS: Fibre reinforced mortar (FRM); Natural hydraulic lime (NHL); PAN fibres; Toughness; Experimental characterization; High ductility mortar.

1 INTRODUCTION

The effect of seismic actions on masonry structures is problematic in a significant number of worldwide urban areas. The devastating effects of these actions are highlighted by several authors for the cases of infill and structural masonry [1]–[3].

The development and characterization of masonry overlay strengthening systems based on the use of composite materials has been recently subject of intense research. Depending on the type of matrix, these composite materials can be divided into two main groups: cementitious [4]–[8] and polymeric [9]. Both show clear advantages when applied to infill and structural masonry elements that are vulnerable to seismic actions. Their main contributions are the increase of the load carrying capacity and energy dissipation ability, without altering significantly their original mass. Additionally, the strengthened elements develop a much higher ultimate deformation and residual strength [10]–[13]. Consequently, after reinforcement these become less susceptible to collapse during or after extreme events.

The improvement of the properties of mortars by means of the addition of natural fibres is well-known and has been employed empirically for centuries [14]. Recently, various fibre reinforced mortars (FRM) have been developed by adding natural [15]–[18] or man-made fibres, showing very attractive mechanical properties [19]–[21]. These FRM's can be used to upgrade the in-plane and the out-of-plane loading and deformation capacity of the original elements. Additionally, when used as external overlays these can help with protecting the reinforced walls from weathering agents. However, the FRM's developed in the recent past were frequently composed by Portland cement binder, which has been shown to lead to compatibility problems with historical masonry elements [22]. The use of natural

hydraulic lime (NHL) binders is believed to deliver mortars that are more compatible with masonry in terms of strength and hygroscopic behaviour [23]–[26]. Additionally, the choice for NHL mortars was found to be more sustainable when compared to the use of Portland cement (CEM) [27]. Flexural strength vs compressive strength of FRM´s developed recently are present in **Figure I.1** where mortars are composed by different types of binders and fibres. The mechanical performance of the mortars can be clearly divided into two groups. The first group, labelled as Geopolymer and CEM-FRM, is formed mainly by Portland cement mortars that show compressive and flexural strengths higher than 20 and 5 MPa respectively [28]–[33]. The second group integrates mainly fibre reinforced lime mortars (NHL-FRM), showing lower mechanical properties [34]–[41]. The area marked and identified as "target values" represents the desirable range of mechanical properties of FRM when applied as strengthening overlay.

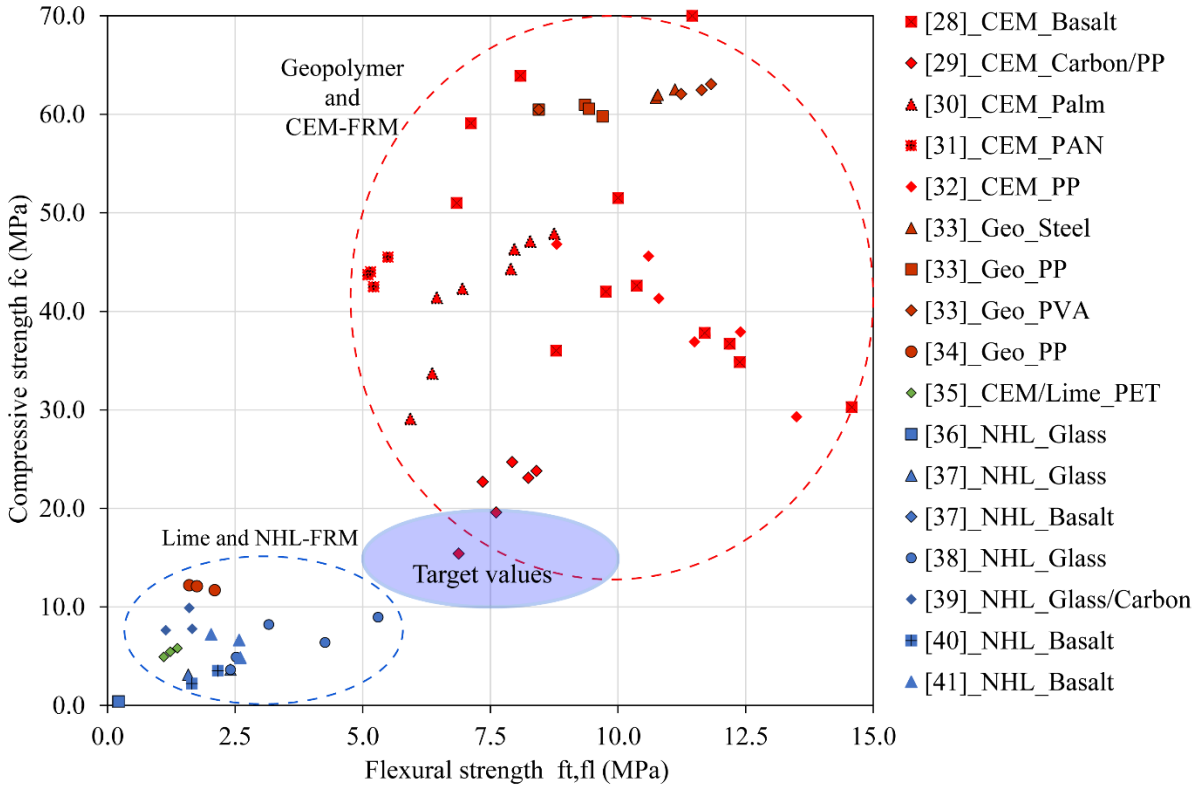


Figure I.1: Flexural and compressive strength of FRM´s developed by different authors.

2 RESEARCH SIGNIFICANCE

This study was aimed at the development of NHL based composite systems for masonry strengthening overlays. To maximise the post-cracking properties without compromising the cost or the durability,

the inclusion of synthetic polyacrylonitrile (PAN) fibres was studied. Several authors studied NHL-FRM´s [36]–[41], however these studies were mostly focussed on low compressive strength mortars (fc <10 MPa), used for the rehabilitation of heritage buildings. In contrast, this work targets higher compressive strength materials (10<fc<15 MPa), as part of a masonry strengthening overlay system. In order to achieve the required higher strength at early age, a small percentage of cement CEM 52.5 was included, 10% of the NHL in weight.

Considering the importance of the post-cracking behaviour on the overall strengthening efficiency, particular attention was dedicated to quantifying toughness and fracture energy for different fibre fractions. The fresh behaviour and the hardened mechanical properties of the developed NHL mortars were assessed in terms of ductility, toughness and fracture energy for different levels of fibre reinforcement, with a view on strengthening applications.

3 MATERIALS AND METHODS

The stiffening effect of PAN fibres on natural hydraulic lime (NHL) matrix was studied by adding different amounts of fibres to a matrix composed by NHL 5.0, white Portland cement in small dosages, and limestone aggregates. Fresh and hardened properties of the resulting FRM's were characterized for different fibre fractions, the details of this experimental program are given in the next section. In brief, while in the fresh state, workability was characterized using flow table tests, following the procedures indicated in EN1015-3 [42], the air content was obtained using the pressure method and the density was obtained by means of the fresh density method following EN1015-7 [43]. In the hardened state, the dry bulk density, the compression strength and elastic modulus, and the flexural strength were characterized according to EN 1015-10 [44], EN 12390 [45] and EN 1015-11 [46] respectively, at 28 days after mixing. Additionally, the evolution of the density and of the flexural strength were obtained at 7 and 90 days after mixing.

3.1. Materials

The materials used in this study are commercially available and were supplied directly by the producers. The natural hydraulic lime (NHL 5.0), see **Table I.1**, and the white Portland cement, CEM II/A-L 52.5 N (br.), composed by 80% to 94% of Portland clinker, 6 to 20% of limestone and 0 to 5% of other ingredients, were supplied by SECIL. The limestone crushed sand aggregate was supplied by

Eurocálcio and the grading curve is represented in **Figure I.2**. For comparison, the CEN Reference sand curve according to EN 196-1:2016 [47] is also shown.

Table I.1: Properties from the commercially available NHL5.0.

Physical Properties		
Fineness (>90um)	(%)	≤15.0
Fineness (>200um)	(%)	≤2.0
Setting time, start	(hour)	>1
Setting time, final	(hour)	≤15
Chemical Properties		
(Sulphate) SO_3	(%)	≤2
(Free Lime) $Ca(OH)_2$	(%)	≥15
(Andrite) $CaSO_4$	(%)	<1
Mechanical Properties		
Compressive strength at 7 days	(MPa)	≥2
Compressive strength at 28 days	(MPa)	≥5.0 and ≤15.0

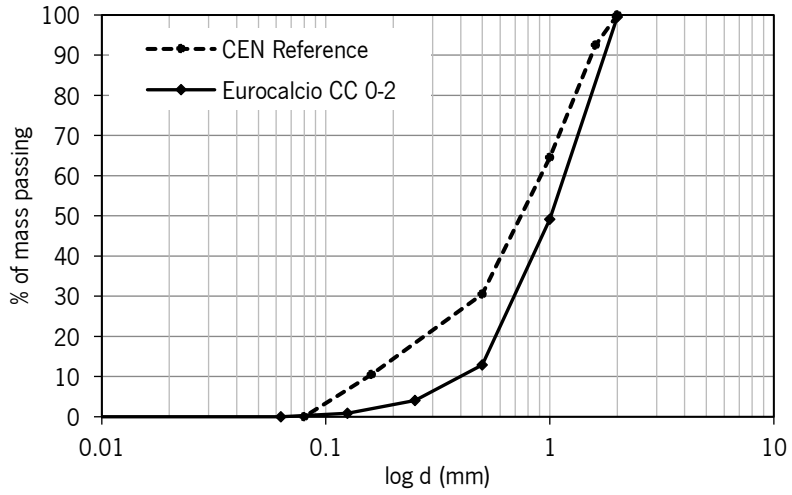


Figure I.2: Grading curve for the limestone sand and CEN Reference sand.

The PAN fibres were supplied by FISIPE and their properties are summarized in **Table I.2**. This type of PAN fibre is mainly used in dry mixed mortars, shotcrete and concrete, presenting a good chemical resistance, and according to the manufacturer it allows the exposure to temperatures not exceeding 220°C during short periods.

Table I.2: Properties of PAN fibres.

PAN fibres Binder+		
Density	(g/cm3)	1.17
Length	(mm)	6
Fineness	(dtex)	2.5
Fibres /g	(6mm length)	666700
Tensile strength	(MPa)	685
Elongation	(%)	14-16
Elastic Modulus	(GPa)	13.4

3.2. Fresh state

In a previous stage, the optimal water/binder and aggregate /binder ratios were obtained by changing the amount of water until a good workability for the application as strengthening overlay. The study mixtures were then designed by essentially maintaining the same water to binder and aggregate to binder ratios, 0.45 and 1.5 respectively, and by changing only the amount of fibres added, as shown in **Table I.3**. The mixing process followed the procedure presented in **Figure I.3**.

Table I.3: Composition of the mortars.

	Fract. by vol.	Weight of components (kg/m3)				
Mixture	Fibres	NHL5	CEM Br.	Sand	water	PAN fibres
R	0,00%	663,9	66,4	995,9	328,6	0,0
F_0.25	0,25%	662,2	66,2	993,3	327,8	2,9
F_0.50	0,50%	660,4	66,0	990,6	326,9	5,9
F_0.75	0,75%	658,7	65,9	988,0	326,0	8,8
F_1.00	1,00%	656,9	65,7	985,4	325,2	11,7

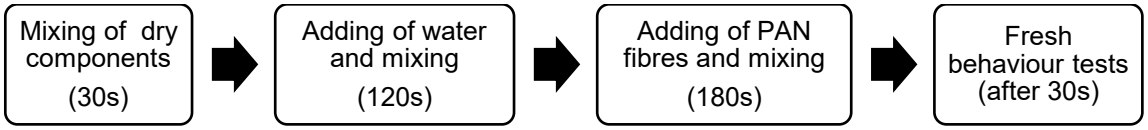


Figure I.3: Mixing procedure of the FRM.

The mini-slump flow test was carried out according to EN1015-3 [42] and the resulting value was obtained by averaging the diameter measured in two perpendicular directions of the spread sample of the fresh mortar, which has been placed on a table disc with the help of a mould with dimensions specified in EN1015-3 [42], see **Figure I.4a**. Then 15 vertical impacts were applied by raising the flow table and allowing it to fall freely through a given height.

The air content of the fresh mixtures was obtained following EN1015-7 [43]. According to this, a sample of each fresh mixture was placed inside the measuring container, see **Figure I.4b**. After closing the apparatus, water was introduced on the top of the mortar surface, and immediately after, air-pressure was applied by forcing the water into the mortar and displacing all the air from within pores. The change in the water level was measured as an indication of the volume of air displaced in the fresh mixture.



a) b)

Figure I.4: Equipment used to characterize the fresh behaviour of the mixtures: a) flow table; b) container to determine the air content of FRM.

3.3. Hardened state

The dry bulk density of the hardened mixtures was determined following EN 1015-10 [44] and expressed as the ratio between its mass in dried condition and the occupied volume.

The compressive behaviour of the hardened mixtures was evaluated by means of compressive and elastic modulus tests using cylinders with a diameter of 60 mm and a height of 120mm, following EN 12390 [45]. A servo-hydraulic actuator was used with 100 kN of maximum force, with feedback controller, and a load cell with 200 kN of maximum force, as shown in **Figure I.5a** and **b**. A monotonically increasing compressive displacement was imposed to the cylinder specimens at a rate of 0.01mm/s for failure tests. A cyclic load was imposed to the cylinders at a rate of 1.75kN/s for the elastic modulus characterization. Displacements were acquired by 3 LVDT's with 10 mm range.

The flexural behaviour of the mortars was studied following EN 1015-11 [46]. The three-point flexural tests were carried out on prismatic specimens with 40x40x160 mm^3 using a Lloyds Universal testing machine with a 50 kN actuator under displacement control. The tests were performed by applying a monotonically increasing displacement at mid-span at a rate of 0.01mm/s, see **Figure I.5c**.



a) b) c)

Figure I.5: Images showing the setup used for: a) elasticity modulus in compression; b) compressive strength; and c) flexural strength.

4 RESULTS

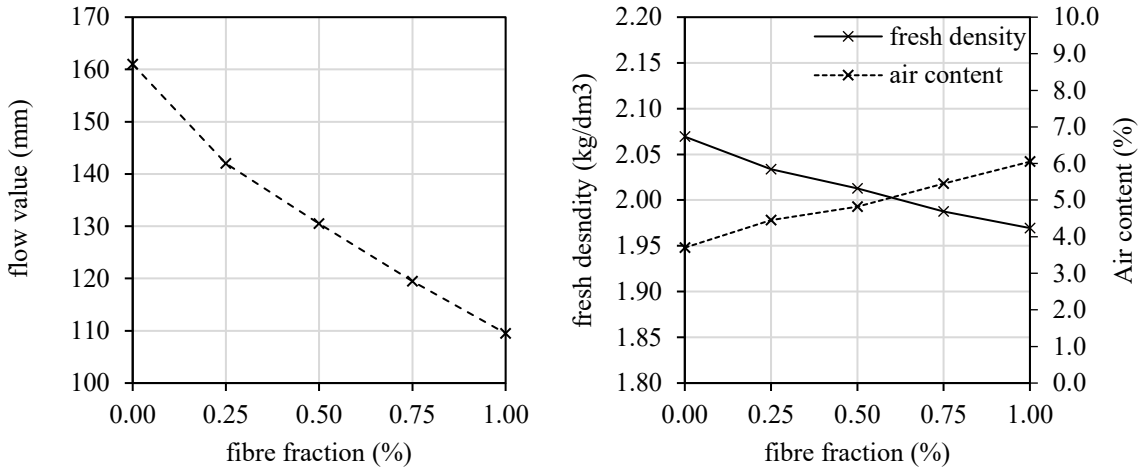
4.1. Fresh behaviour

The influence of the increasing fibre fraction on the workability of the mixtures is shown in **Figure I.6** and **Figure I.7a**, where the final diameter of the samples spread after imposing the 15 strokes is represented. Additionally, **Figure I.7b** represents the density obtained in the fresh state and the air content of each mixture against the fibre fraction. The main application envisaged for the mixtures developed, as strengthening overlay, makes workability a parameter of major concern. The mixture that showed the best fresh behaviour for that purpose was the mortar containing 0.25% of fibres in volume.



No fibres 0.25% 0.50% 0.75% 1.00%

Figure I.6: Flow table test results obtained for the different mixtures after 15 strokes.



a) b)

Figure I.7: a) Flow values obtained for different amounts of fibres; b) fresh density and air content values obtained for different fibre fractions.

4.2. Hardened behaviour

4.2.1. Compression testing

One group of specimens was cured for 28 days in a climatic chamber at 20°C and 60% relative humidity (RH). The compression test results obtained for these specimens are presented in **Table I.4**, where F_{max}, $\bar{F}_{max}$ and (CV) represents the maximum load the respective mean value and the coefficient of variation; $d_{F_{max}}$ and $\bar{d}_{F_{max}}$ represents the displacement for the maximum load and the respective mean value. Another group of specimens was cured at 20°C and 85% RH also for 28 days, and the results obtained are also presented in the **Table I.4**. As shown, the scatter of results obtained in each group of samples was in general low for the group cured at 85% RH, except for the values obtained for the reference mortar cured at a 60% RH.

Table I.4: Results from uniaxial compression tests to specimens cured in 60% RH and 85% RH.

	RH60_20_28				RH85_20_28			
	F_{max}	$\bar{F}_{max}$ (CV)	$d_{F_{max}}$	$\bar{d}_{F_{max}}$ (CV)	F_{max}	$\bar{F}_{max}$ (CV)	$d_{F_{max}}$	$\bar{d}_{F_{max}}$ (CV)
Specimen	(kN)	kN (%)	(mm)	mm (%)	(kN)	kN (%)	(mm)	mm (%)
R_01	16.3		0.28		36.1		0.61	
R_02	25.3		0.39		37.4		0.76	
R_03	23.6		0.27		33.0		0.57	
R_04	18.8	21.0 (20)	0.28	0.30 (19)	34.9	35.4 (5)	0.53	0.62 (16)
F0.25_01	26.3		0.33		38.5		0.55	
F0.25_02	26.0		0.28		37.8		0.56	
F0.25_03	24.3		0.36		39.9		0.48	
F0.25_04	22.9	24.9 (6)	0.31	0.32 (11)	35.4	37.9 (5)	0.58	0.54 (8)
F0.50_01	26.9		0.34		34.8		0.47	
F0.50_02	30.1		0.35		35.5		0.5	
F0.50_03	27.8		0.34		35.2		0.56	
F0.50_04	29.7	28.6 (5)	0.32	0.34 (3)	36.7	35.6 (2)	0.47	0.50 (9)
F0.75_01	24.5		0.46		31.9		0.59	
F0.75_02	30.3		0.48		34.0		0.53	
F0.75_03	29.9		0.49		31.8		0.55	
F0.75_04	31.3	29.0 (11)	0.44	0.47 (4)	30.6	32.1 (4)	0.73	0.60 (15)
F1.00_01	26.1		0.48		30.3		1.02	
F1.00_02	20.7		0.33		29.5		0.78	
F1.00_03	25.4		0.63		29.4		0.6	
F1.00_04	24.3	24.1 (10)	0.55	0.49 (26)	30.9	30.1 (2)	0.71	0.78 (23)

4.2.2. Flexural testing

One group of specimens for flexure tests was cured in a climatic room at 20°C and 85% RH conditions for 7, 28 and 90 days. The results obtained are shown in

Table I.5, **Table I.6** and

Table I.7, namely the tensile strength under flexure, $f_{ft,fl}$, the displacement obtained for the maximum load, $d_{f,max}$, the respective mean values, $\bar{f}_{ft,fl}$ and $\bar{d}_{f,max}$, and the coefficient of variation, (CV). Another group of specimens was cured at 20°C and 60% RH, and the results obtained at 28 and 90 days are presented in **Table I.6** and

Table I.7. The equivalent tensile strengths under flexure show in general a low coefficient of variation. However, in the case of the displacement obtained for the maximum load a higher scatter of results was observed, in some cases exceeding 15%. This result may reflect the fact that fibres contribute to distribute damage and originate multiple cracks, increasing deformability as well as the scatter of the post-cracking behaviour due to the brittle nature of the cracking process.

Table I.5: Flexure test results of specimens cured at 85% RH for 7 days.

	RH85_20_07			
	$f_{ft,fl}$	$\bar{f}_{ft,fl}$ (CV)	$d_{f,max}$	$\bar{d}_{f,max}$ (CV)
Specimen	(MPa)	MPa (%)	(mm)	mm (%)
R_01	2.02		0.16	
R_02	2.02		0.15	
R_03	2.57	2.2 (12)	0.18	0.16 (8)
F0.25_01	1.92		0.11	
F0.25_02	1.88		0.15	
F0.25_03	2.05	1.95 (4)	0.17	0.14 (16)
F0.50_01	3.26		0.42	
F0.50_02	2.92		0.44	
F0.50_03	2.63	2.94 (9)	0.37	0.41 (7)
F0.75_01	3.56		0.38	
F0.75_02	3.35		0.35	
F0.75_03	3.37	3.42 (3)	0.43	0.39 (9)
F1.00_01	3.75		0.51	
F1.00_02	3.47		0.53	
F1.00_03	3.36	3.53 (5)	0.46	0.5 (6)

Table I.6: Flexural test results of specimens cured at 85% RH and 60% RH for 28 days.

	RH85_20_28				RH60_20_28			
	$f_{ft,fl}$	$\bar{f}_{ft,fl}$ (CV)	$d_{f,max}$	$\bar{d}_{f,max}$ (CV)	$f_{ft,fl}$	$\bar{f}_{ft,fl}$ (CV)	$d_{f,max}$	$\bar{d}_{f,max}$ (CV)
Specimen	(MPa)	MPa (%)	(mm)	mm (%)	(MPa)	MPa (%)	(mm)	mm (%)
R_01	2.78		0.12		2.02		0.16	
R_02	3.18		0.19		2.02		0.15	
R_03	3.25	3.07 (7)	0.18	0.16 (19)	2.57	2.2 (12)	0.18	0.16 (8)
F0.25_01	4.14		0.21		1.92		0.11	
F0.25_02	3.88		0.14		1.88		0.15	
F0.25_03	4.10	4.04 (3)	0.15	0.17 (17)	2.05	1.95 (4)	0.17	0.14 (16)
F0.50_01	4.67		0.25		3.26		0.42	
F0.50_02	4.23		0.19		2.92		0.44	
F0.50_03	4.46	4.45 (4)	0.28	0.24 (17)	2.63	2.94 (9)	0.37	0.41 (7)
F0.75_01	6.06		0.32		3.56		0.38	
F0.75_02	5.41		0.36		3.35		0.35	
F0.75_03	5.41	5.63 (5)	0.34	0.34 (5)	3.37	3.42 (3)	0.43	0.39 (9)
F1.00_01	6.45		0.30		3.75		0.51	
F1.00_02	5.95		0.30		3.47		0.53	
F1.00_03	6.22	6.21 (3)	0.39	0.33 (12)	3.36	3.53 (5)	0.46	0.5 (6)

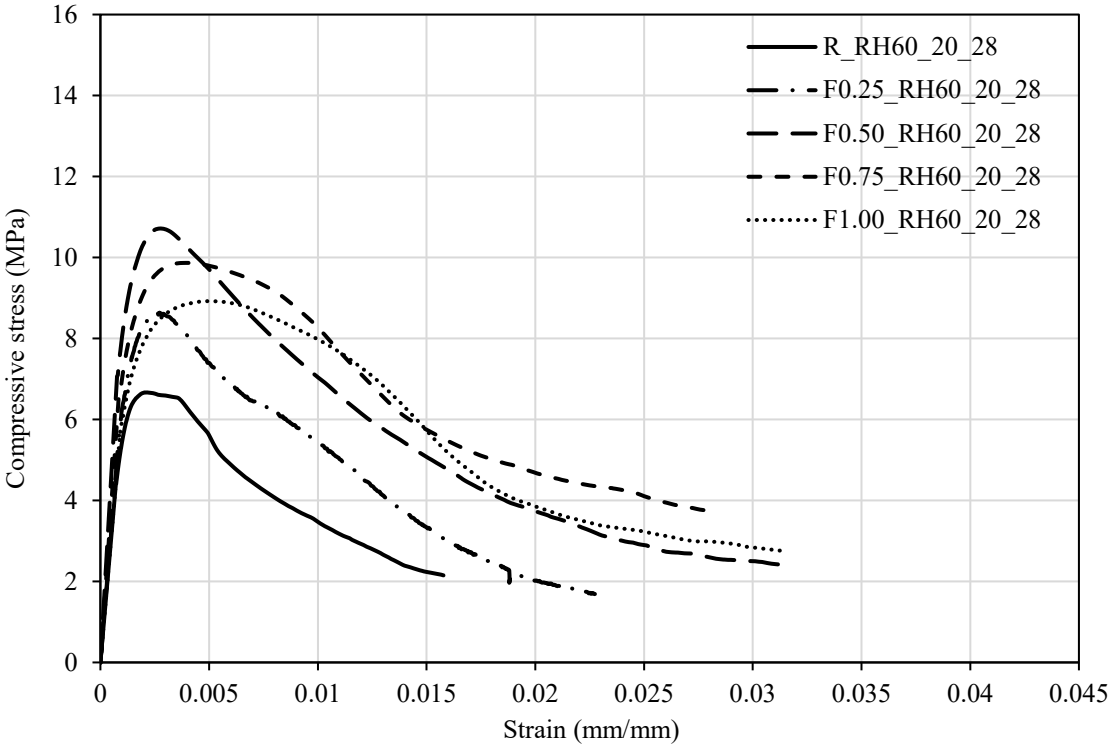
Table I.7: Flexural test results of specimens cured at 85% RH for 90 days.

	RH85_20_90				RH60_20_90			
Specimen	$f_{ft,fl}$ (MPa)	$\bar{f}_{ft,fl}$ (CV) MPa (%)	$d_{f,max}$ (mm)	$\bar{d}_{f,max}$ (CV) mm (%)	$f_{ft,fl}$ (MPa)	$\bar{f}_{ft,fl}$ (CV) MPa (%)	$d_{f,max}$ (mm)	$\bar{d}_{f,max}$ (CV) mm (%)
R_01	3.91		0.12		2.49		0.17	
R_02	4.19		0.13		2.21		0.12	
R_03	3.50	3.87 (7)	0.11	0.12 (7)	2.50	2.40 (6)	0.11	0.13 (17)
F0.25_01	4.40		0.15		2.97		0.12	
F0.25_02	4.75		0.16		3.16		0.14	
F0.25_03	3.95	4.37 (7)	0.14	0.15 (6)	3.71	3.28 (9)	0.16	0.14 (10)
F0.50_01	5.12		0.18		4.10		0.15	
F0.50_02	4.81		0.18		4.80		0.16	
F0.50_03	4.43	4.79 (6)	0.16	0.17 (8)	4.62	4.50 (7)	0.15	0.15 (4)
F0.75_01	5.87		0.29		5.00		0.16	
F0.75_02	5.37		0.28		5.45		0.28	
F0.75_03	6.05	5.77 (5)	0.30	0.29 (4)	4.93	5.13 (4)	0.17	0.20 (27)
F1.00_01	6.63		0.28		4.61		0.25	
F1.00_02	6.69		0.36		6.41		0.28	
F1.00_03	6.77	6.70 (1)	0.33	0.33 (10)	5.76	5.59 (13)	0.27	0.27 (6)

5 Discussion of results

5.1. Compressive behaviour

The compressive behaviour of representative specimens cured for 28 days in a climatic chamber at 20°C and 85% RH is shown in **Figure I.8**. The initial slope of the compressive stress – strain responses do not seem to be influenced by the addition of fibres, showing essentially similar slopes for different fibre fractions. However, the peak stress and the post-peak behaviour of the mixtures seem to be clearly influenced by the fibre content. As fibre fraction increases, the peak stress seems to decrease while the residual stresses increase. These changes suggest that the increase of fibre fraction led to the expected increase of ductility and the ability to dissipate energy after cracking, due to the contribution of the PAN fibres to restrain crack propagation.



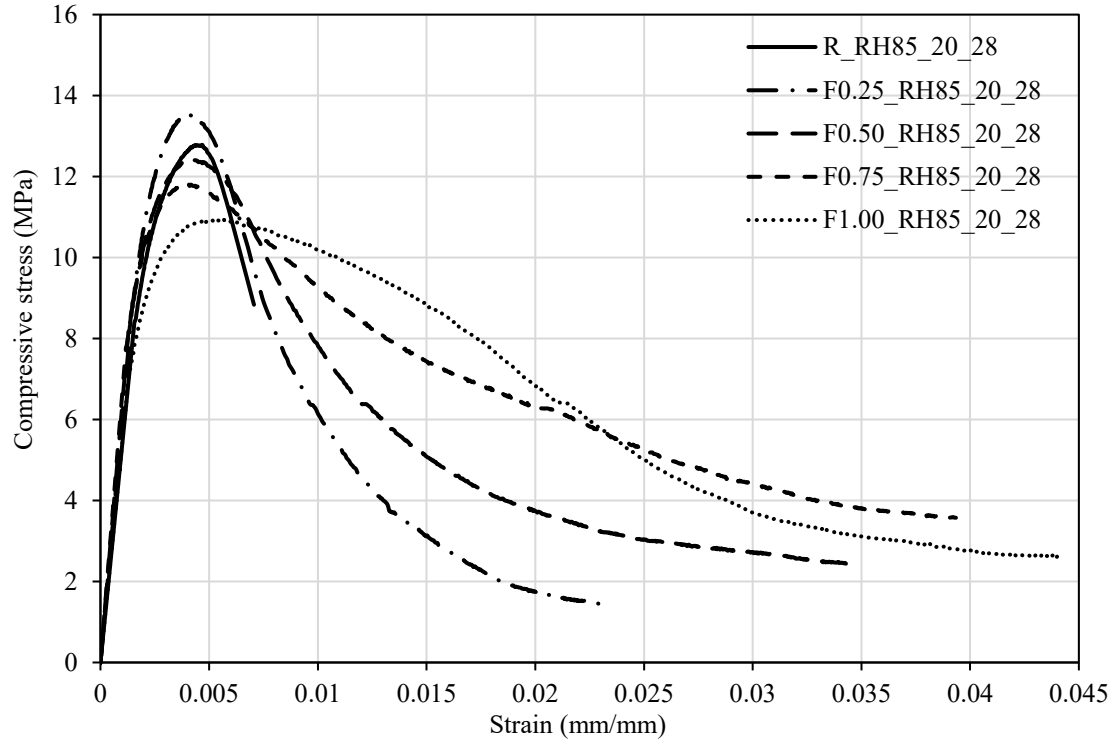


Figure I.8: Typical compressive stress-strain responses obtained for mortars with different fibre fractions and curing conditions.

Figure I.9 shows the main results obtained for the compressive strength at 28 days of curing after casting, for both curing environments. The specimens cured at 85% RH show, for all cases, higher

compressive strengths than the ones obtained for specimens cured at 60% RH, see **Figure I.9a**. The compressive strength shows a small variation with the increase of the fibre content for both curing conditions. In the case of 85% RH the maximum compressive strength was achieved for a fibre fraction of 0.25%, and at 60% RH the maximum compressive strength was achieved for a fibre fraction of 0.50%. The same behaviour can be observed for the elastic modulus, as shown in **Figure I.9b**. The values of the elastic modulus and compressive strength are in accordance to the ones expected for an NHL mortar.

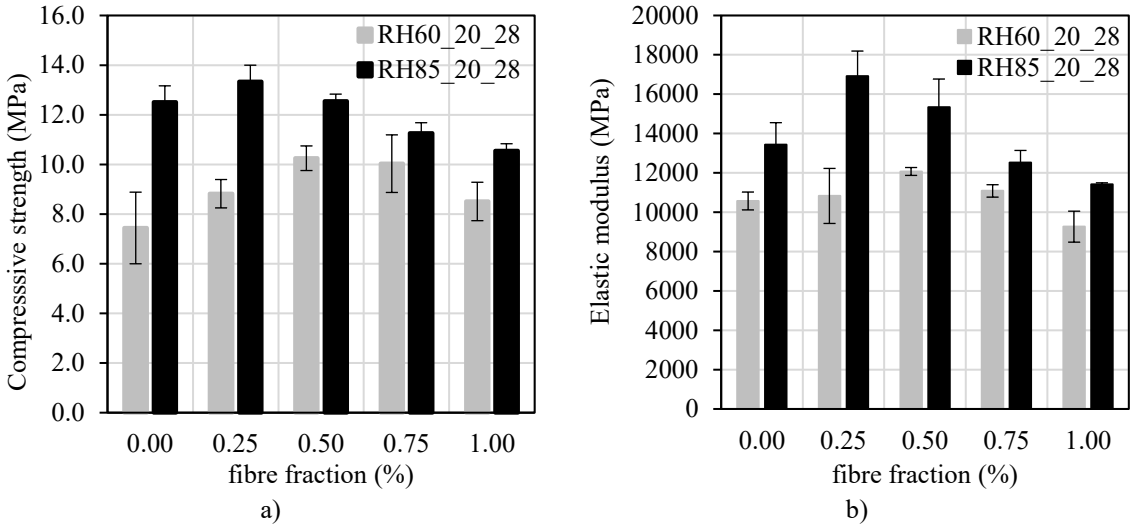


Figure I.9: Compressive behaviour of mixtures in two different curing environments: a) compressive strength; b) elastic modulus.

5.2. Flexural behaviour

The flexural responses obtained were adjusted to exclude the initial deformation for small loads due to the accommodation of the loading device and the supports. The approach used is schematically represented in **Figure I.10** and allowed to acquire more realistic values by disregarding the first non-linear part of the load vs. deflection curve [37], [48].

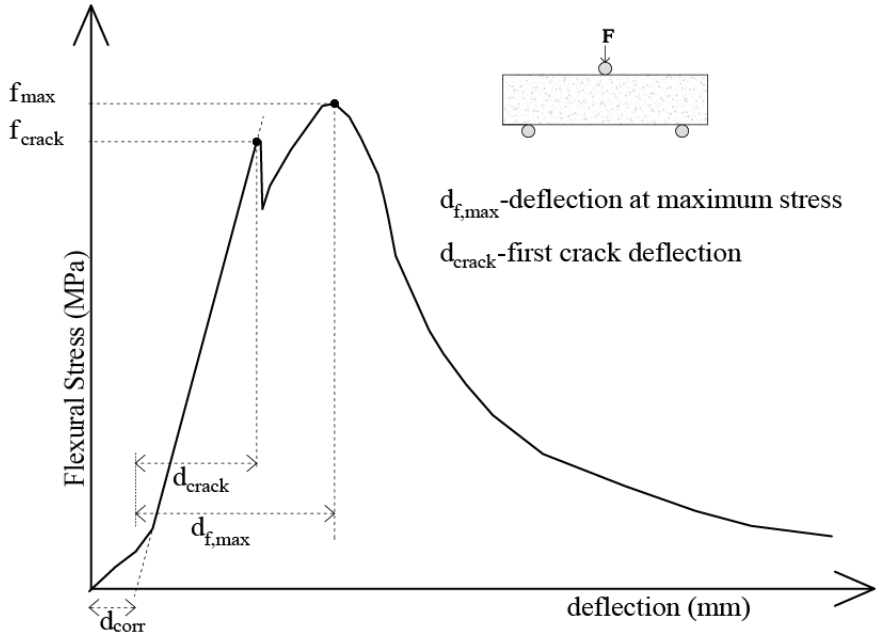


Figure I.10: Schematics of the flexural response and approach adopted to correct the experimental setup adjustments during loading [37].

After adjusting all flexural stress vs. deflection responses, representative curves for each fibre fraction were selected and plotted in **Figure I.11**. The effect of adding fibres to the matrix is clear, even for 0.25% of fibres. With the increase of the fibre fraction, it is possible to observe that the toughness of the material gradually increases, and the flexural response gradually shifts from a typically brittle fracture to a deflection-softening response for lower fibre fractions, and a deflection-hardening response for higher fibre volume fractions.

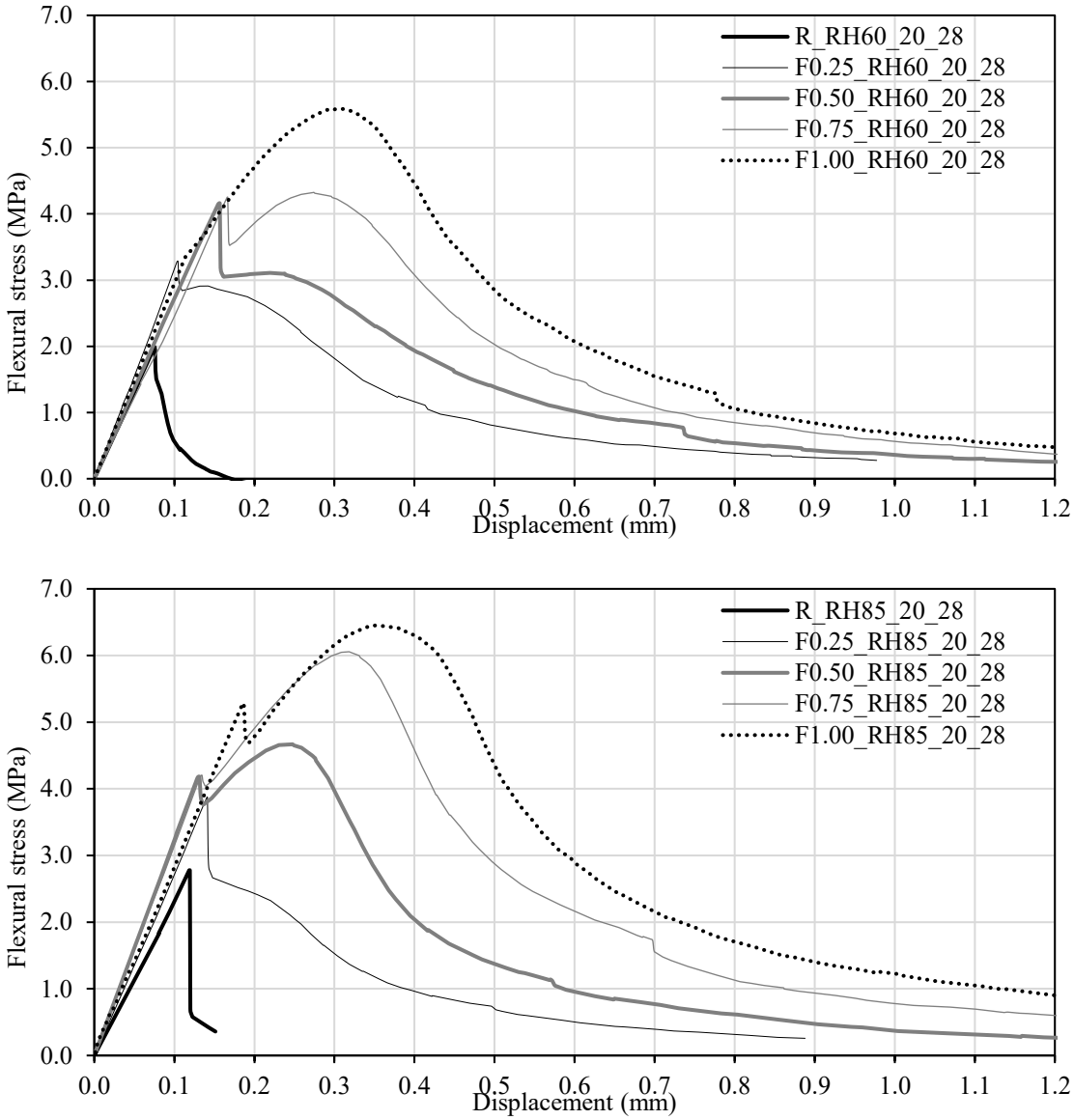


Figure I.11: Typical flexural stress vs displacement responses obtained from flexure tests for specimens cured at 60%RH and 80%RH.

The values of the modulus of rupture (MOR), see **Eq. (I.1)**, and limit of proportionality (LOP), see **Eq. (I.2)**, were computed and plotted against the fibre volume fraction in **Figure I.12a** and **b**, respectively. The MOR was obtained from the maximum load, F_{max}, and the LOP by finding the load at which the first non-linearity is observed, F_{crack}, see **Figure I.10**. These two values were obtained according to the RILEM Technical Committee 49 TFR [49]:

$$MOR = \frac{3F_{max}L}{2bd^2} \quad \textbf{(I.1)}$$

$$LOP = \frac{3F_{crack}L}{2bd^2} \quad \textbf{(I.2)}$$

The values of the MOR and LOP obtained for both curing environments show a clear increasing trend with the increase of the fibre volume fraction. The specimens cured at 85% RH show, for all fibre fractions, a higher MOR. Regarding the LOP, no clear trend was observed, and for the higher amounts of fibres, 0.75 and 1.00%, the LOP values obtained for 85% RH are lower or similar to the ones obtained for 60% RH.

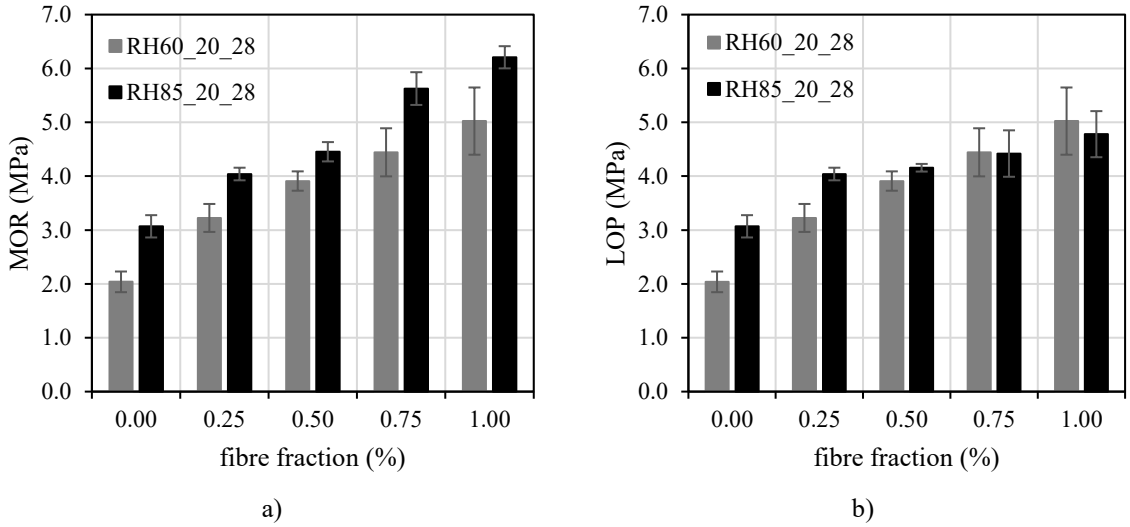


Figure I.12: RH 60 and 85% curing conditions: a) Modulus of rupture; b) Limit of proportionality

5.3. Toughness in compression

The energy dissipated during the fracture process in compression, also designated as work of fracture in compression [50],[51] can be obtained by dividing the area under the stress vs. displacement response into two parts, see **Figure I.13**. The area indicated as A_{pre} represents the energy dissipated in compression before the peak and A_{post} the energy dissipated after the peak. Since the post-cracking portion of the experimental response tends to extend over large deformations, it is important to define a reference residual stress, $\sigma_{0,}$ common to all specimens, up to which the energy dissipated during the fracture process in compression is computed. Therefore, the A_{post} value is limited by the ratio σ/σ_0, in this case assumed as 0.33.

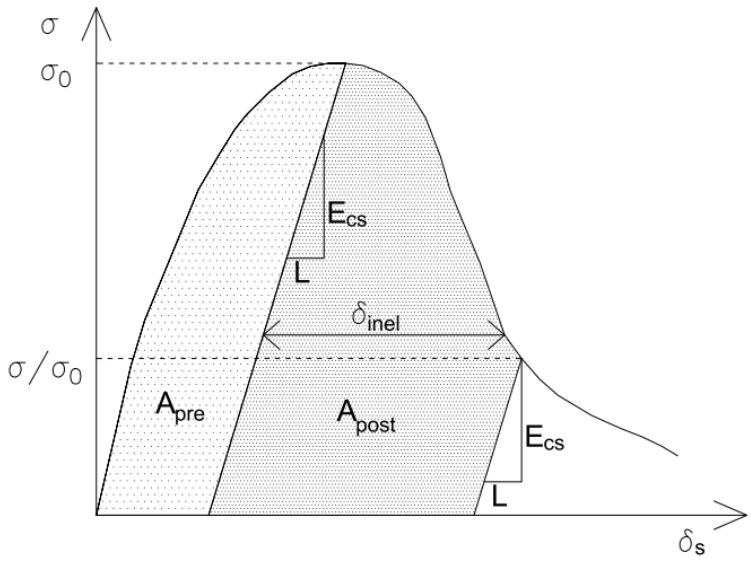


Figure I.13: Method to calculate the work of fracture in compression [50],[51].

The results obtained for both curing conditions are shown in **Figure I.14**. The increase of the fibre fraction resulted in the increase of the energy dissipated during the fracture process in compression. However, in the case of the specimens cured at 85% of RH, the value of the pre-peak energy dissipated remains approximately constant for mortars with different fibre content. Probably the higher RH curing environment favours the NHL based matrix curing, therefore leading to increased energy required to induce the same level of damage, as well as more consistent results between different specimens regardless of the fibre content.

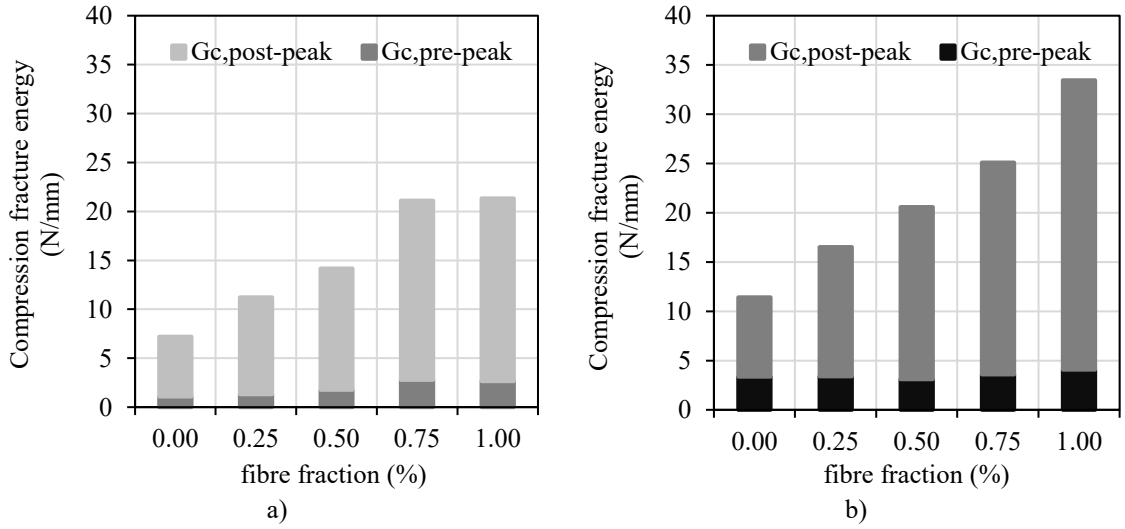


Figure I.14: Compression fracture energy for different curing conditions: a) RH 60 b) RH 85.

The toughness ratio in compression (TR_c) can be used to identify the capacity of the materials to absorb energy and plastically deform before failure. Considering that one of the main aims of this

study is to develop FRM´s that maximise the capacity of masonry elements to dissipate energy when used as overlay strengthening, this ratio was computed following the procedure adopted by other authors [48], [52], [53]. As described by **Eq. (I.3)** and represented in **Figure I.15**, TR_c represents the ratio between the area limited by the stress vs. strain response up to a predefined level of strain, and the area given by $f_c \times \varepsilon$, being f_c the compressive strength and ε the predefined level of strain, as shown in **Figure I.15**. The predefined strain values, ε, were assumed as 0.0105 and 0.0175, which represent three and five times the concrete ultimate strain ($TR_{c,3}$ and $TR_{c,5}$), assuming that this strain is 0.0035 according to EN1992-1-1:2010 (EC2), and following the methodology adopted in [48].

$$TRc = \frac{Area\ OABC}{f_c \times \varepsilon} \times 100 \qquad \textbf{(I.3)}$$

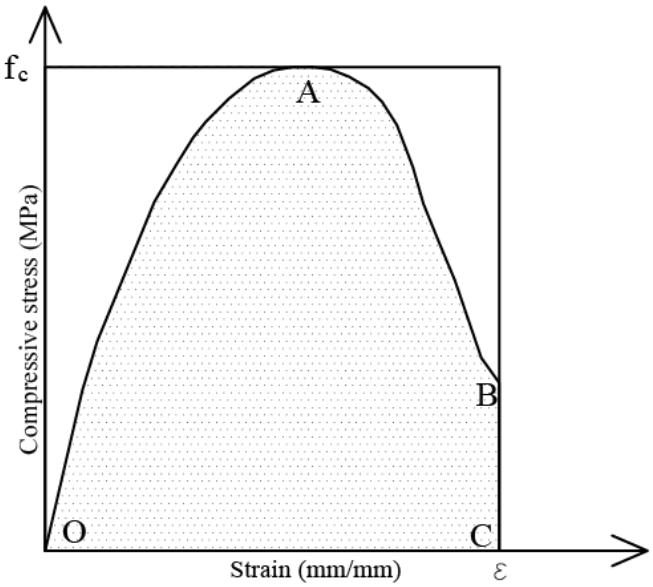


Figure I.15: Definition of compressive toughness ratio [52], [53].

The TR_c values obtained when considering lower predefined strains ε, $TR_{c,3}$, show an increase of around 25% when comparing the reference mixture without fibres, with the mixtures containing 0.75% and 1.00% of PAN fibres, see **Figure I.16a**. However, when higher values of the predefined strain ε are considered, $TR_{c,5}$ is considerably higher, reaching around 100% for the specimens cured in 85% RH, see **Figure I.16b**. This variation of the TR_c values reveals the significant contribution of the fibre reinforcement to the improvement of the post-peak behaviour of the mixtures while subjected to compression loading.

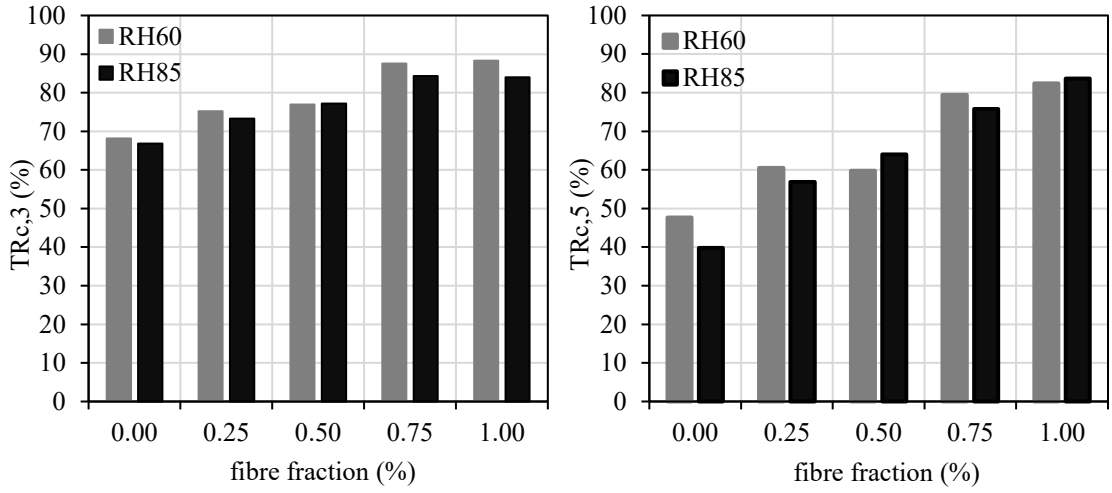


Figure I.16: Toughness ratio for RH 60 and 85 curing conditions: a) $TR_{c,3}$; b) $TR_{c,5}$.

The relation between compressive strength and toughness ratios for lower and higher deformation levels, $TR_{c,3}$ an $TR_{c,5}$, is shown in **Figure I.17** considering both curing conditions, RH60 and RH85. For RH60 when lower levels of deformation are used as a reference, lower variations of this ratio are obtained, changing from 60% to 85%, while more expressive increments, from 40% to 85%, are obtained when higher deformations are considered. For both cases the trend is similar, the specimens showing higher compressive strength tend to show lower toughness ratios because energy released during the matrix cracking tents to increase, which is more demanding to the fibre reinforcement.

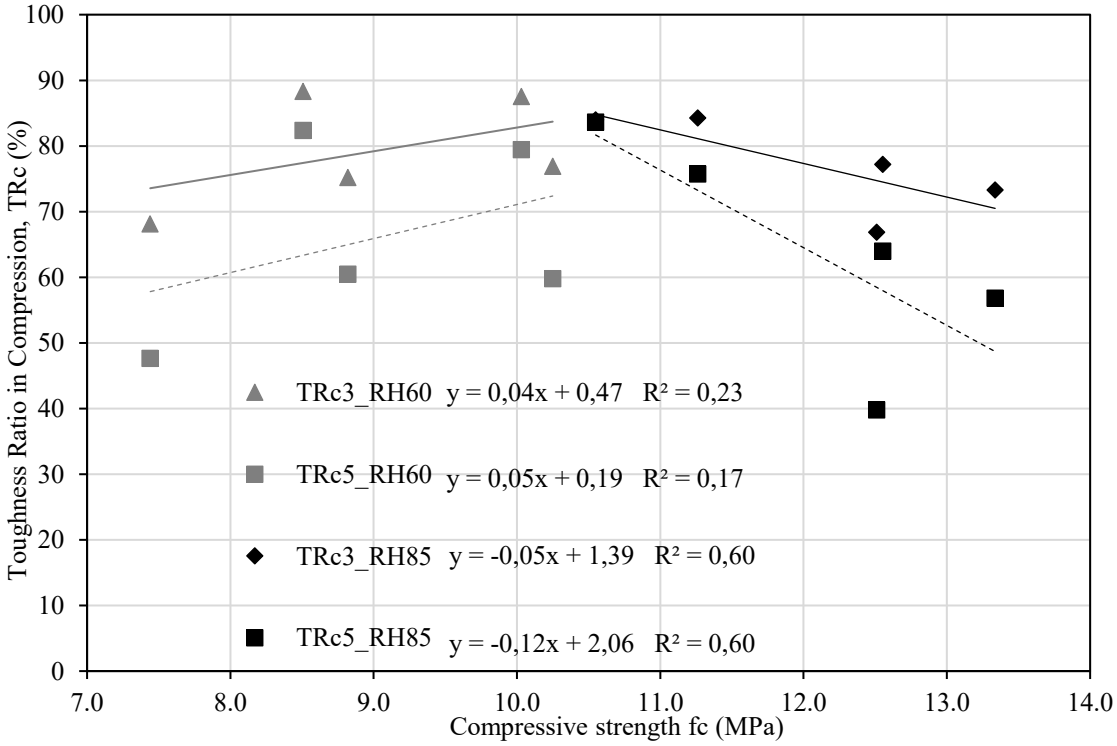


Figure I.17: Relation between compressive strength and toughness ratio, $TR_{c,3}$ and $TR_{c,5}$ for RH60 and RH85.

5.4. Toughness in flexure

The flexural toughness (T_b) was derived from the flexural load vs displacement responses previously shown and obtained from three-point loading tests, EN 1015-11 [46], adapted according to Jang et al. [41], see **Figure I.10**. The energy dissipated by the specimens during the fracture process in flexure is represented by the area under the load vs. deflection (F-d) curve. According to Iucolano et al. [37] the F-d response depends on: (i) the specimen size; (ii) the loading configuration (midpoint versus third-point loading); (iii) type of feedback control variable used during testing (load, load-point deflection, crosshead displacement, etc.); (iv) and loading rate. To minimize the effects of load configuration and specimen size, the normalization of the energy dissipation capacity is required. This can be achieved by using the normalised flexural toughness factor ratio, $Re_{(l/150)}$, presented in **Eq. (I.5)**, where for each specimen the flexural toughness factor (FT), see **Eq. (I.4)**, is normalized with respect to the MOR value [56] [57]. The deflection δ_{Tb}, adopted to calculate T_b and FT, was limited to $1/150$ of the distance between supports, see **Figure I.18**.

$$FT = \frac{T_b \times L}{\delta_{tb}.\times b.\times d^2} \quad \textbf{(I.4)}$$

$$Re(l\ /150)(\%) = \frac{FT}{MOR} \times 100 \quad \textbf{(I.5)}$$

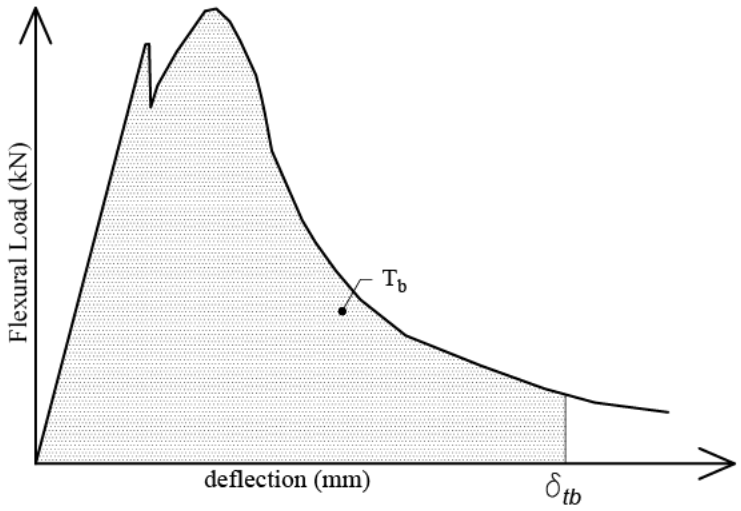


Figure I.18: Definition of flexural toughness ratio, [57].

The results obtained show that the fibre addition contributed to an increase of the FT value, see **Figure I.19**. For the reference mixture the FT value varied between 0.1 and 0.3 N/mm², for RH 60% and 85% respectively. These values increase about 10 and 16 times when 1.00% of fibres was added to both mixtures. The ratio Re(l/150) obtained for the fibre volume fraction of 1,00% show a variation between 4.9 and 6.8 times relatively to the reference mixture.

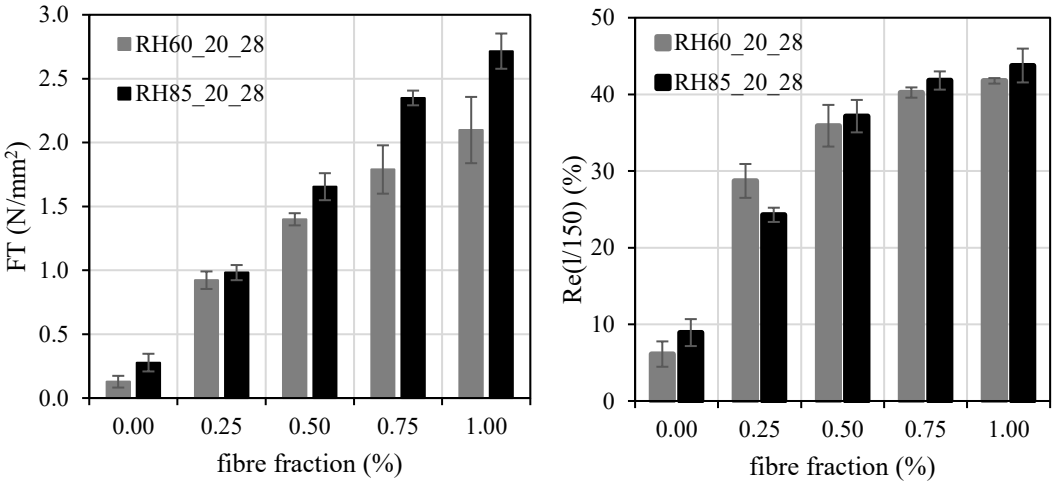


Figure I.19: Toughness values for RH 60% and 85% curing conditions: a) flexural toughness (FT); b) flexural toughness factor Re(l/150).

Figure I.20 shows the relation between the flexural strength and the toughness ratio in flexure obtained for L/150 deflection **Figure I.20:** . The results show an increase of the toughness ratio in flexure with the increase of the flexural strength. This strong correlation is indicative of higher ductility of NHL-FRM's with higher strength in flexure, in this case because the fibre reinforcement showed to contribute both to increase flexural strength and the residual stresses in flexure.

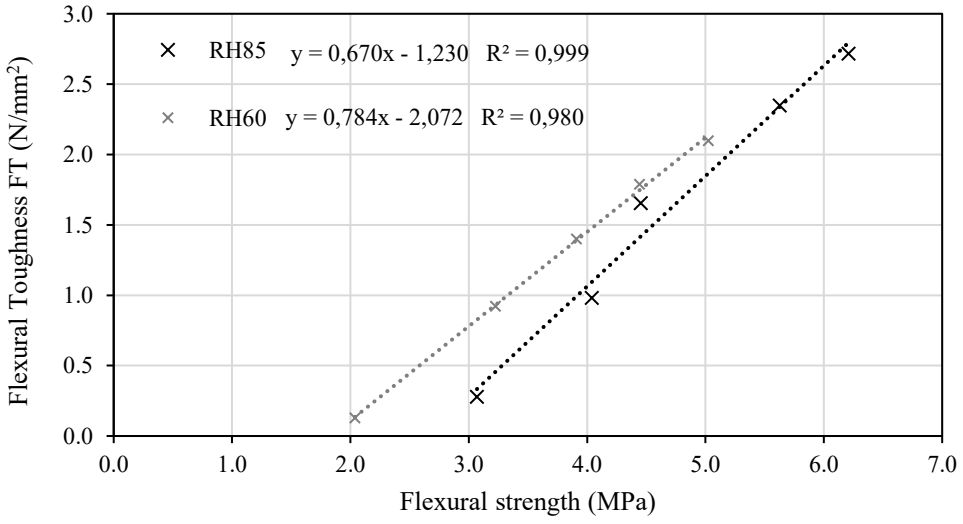


Figure I.20: Relation between flexural strength and toughness ratio.

5.5. Fibre reinforcement efficiency in flexure

5.5.1. Contribution for flexural strength

The fibre reinforcement efficiency of mortars developed in this work is analysed in **Figure I.21**, where data referred to mortars from different authors is also included. Mortars composed by different types of binders are presented, namely, CEM, NHL and geopolymeric. The type of fibres used by other authors vary from natural fibres to man-made fibres, Basalt, glass, PET, PVA and PAN. The influence of the amount of fibres on the flexure strength ratio of CEM-FRM is positive in most cases. In the NHL-FRM´s that influence present a high variation and can be negative, depending on the authors.

The use of PAN fibres up to 1.00 % in volume shows an efficiency level of NHL-FRM higher than the studies using basalt, glass or hemp fibres. The level of efficiency is justified by the good compatibility between the NHL matrix and the surface of the PAN fibre and by the tensile strength of the PAN fibres.

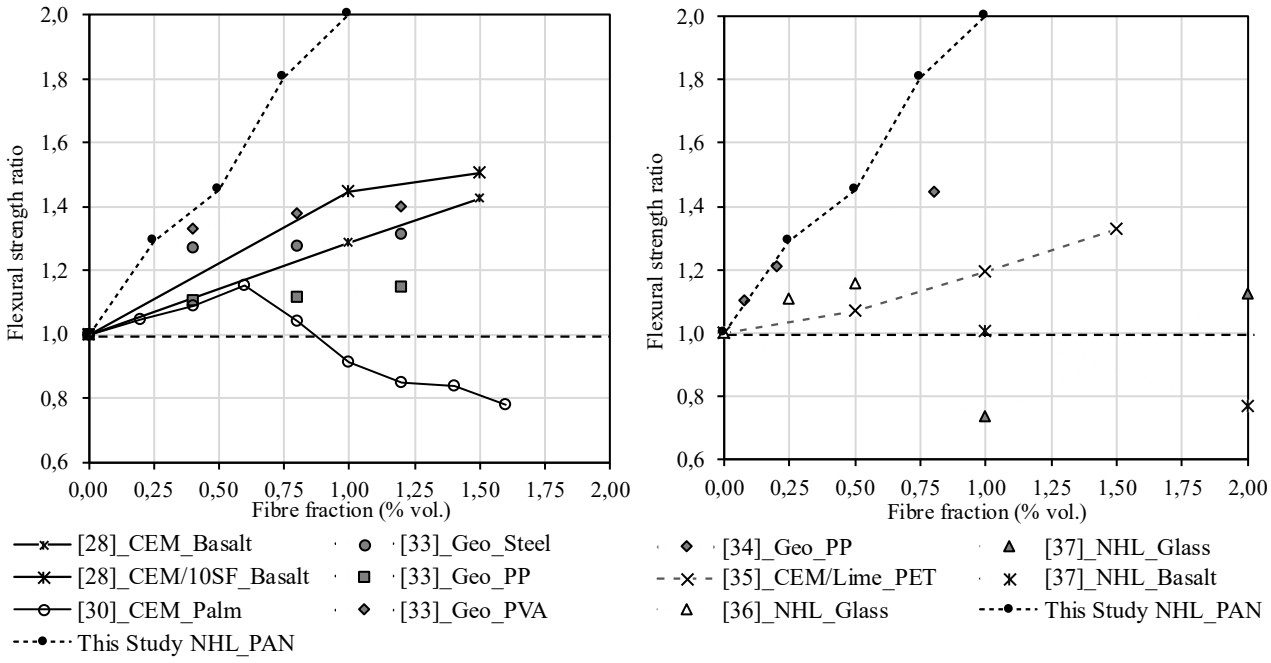


Figure I.21: Efficiency of fibre reinforcement on the normalized flexure strength.

5.5.2. Contribution for flexural toughness

The effect of the fibres on the ductility of mortars was evaluated by quantifying the flexural toughness ratios, see **Figure I.22**. Different procedures are suggested by the standards for the evaluation of the toughness in flexure [57]–[60]. In this study, a ratio between the flexural toughness from fibre

reinforced mortar and the plain mortar was used, allowing the comparison between values obtained from different sources.

Figure I.22 show that two groups of FRM can be identified, CEM-FRM and NHL-FRM. The first group independently of the type of fibre, for the same volume of fibres, always present a lower toughness ratio than the NHL-FRM group. This indicates a lower ductility of the CEM-FRM´s when compared to NHL-FRM´s. The NHL-FRM developed in this study presents a flexural toughness nine times higher, when considering 1.00% of fibres. Nonetheless for CEM-FRM´s the same ratio is around three. On the opposite there are NHL-FRM's presenting very high flexural toughness ratios [36], [38], showing higher efficiency for the same amount of fibre, see **Figure I.22**. Additionally, **Figure I.23** presents the flexural strength vs. flexural toughness ratio from FRM´s where is possible to identify that the mortar reinforced with glass fibres developed by Chan et al. [36], presents low mechanical performance. The mortar developed by Liguori et al [38] presents a high flexural strength and flexural toughness ratio. However, when considering the mechanical properties set as target for the overlay application, $10<f_c<15$ MPa and $5<f_{t,fl}<7$ MPa, these NHL-FRM clearly underperform in the compressive strength, see **Figure I.1**.

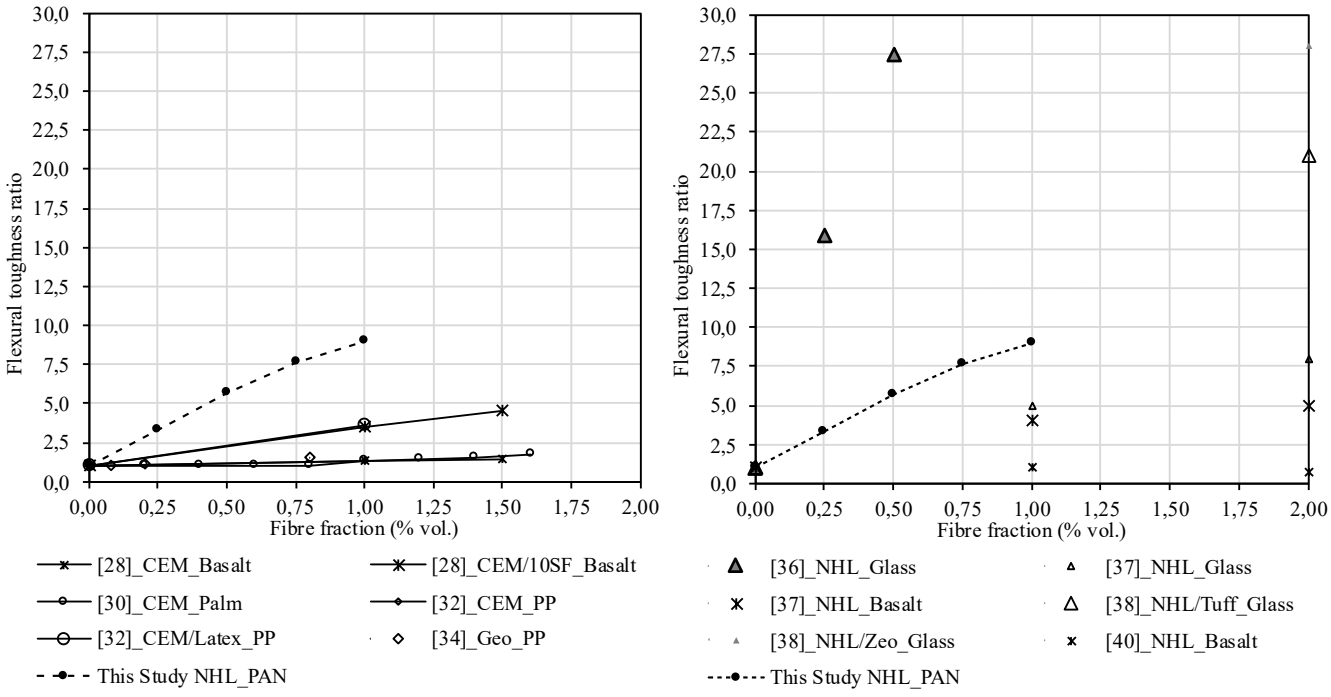


Figure I.22: Efficiency of fibre reinforcement on the flexural toughness ratio.

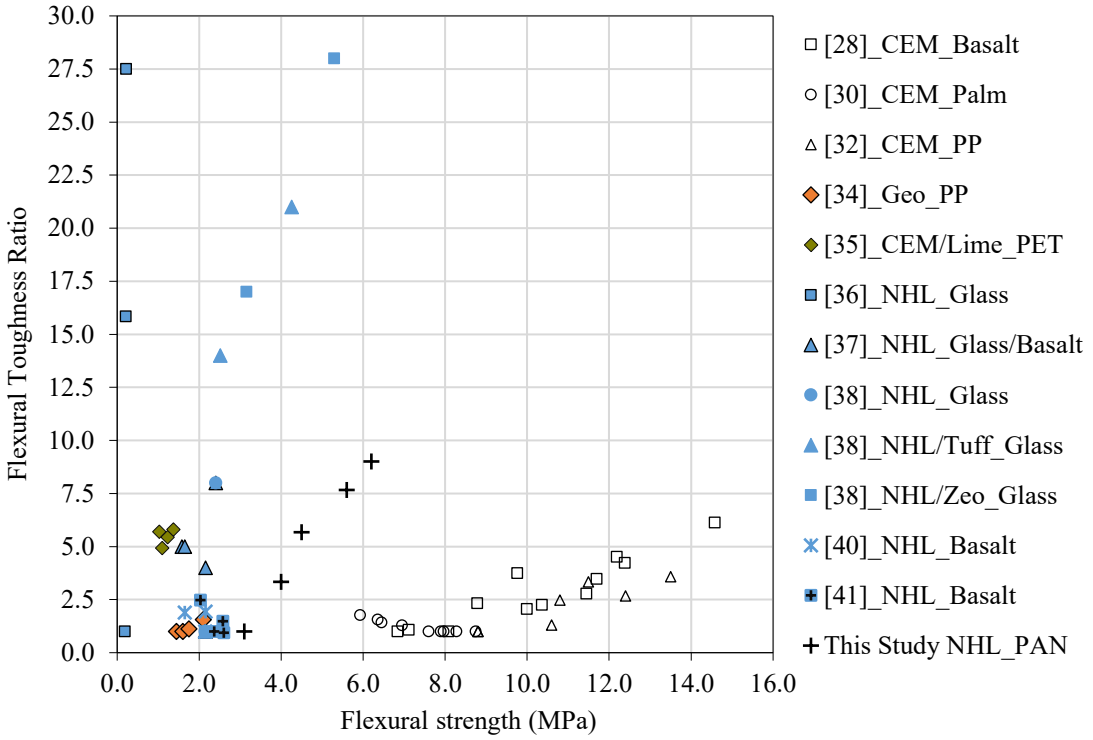


Figure I.23: Flexural strength vs. flexural toughness ratio from FRM.

6 Conclusions

The need to strengthen a vast number of existing masonry structures that are frequently under the effect of dynamic actions determine the importance of studying metrics that allow the performance evaluation of FRMs used as strengthening overlays. These metrics cannot be limited to maximum resistance or deformability, instead they must be oriented to improve and characterize materials with higher energy dissipation capacity.

In this work a new NHL-FRM material was developed to be used as an economically and environmentally sustainable strengthening overlay. The use of metrics geared towards the assessment of toughness and ductility lead to a material compatible with the application and meeting their requirements.

The main conclusions from the study are:

- The inclusion of PAN fibres in a NHL matrix changes the fresh and hardened behaviour of the mortar. The changes can be distinguished even for a low amount of fibre addition. The fresh behaviour of the FRM must be adequate for the type of application. In the case of this study

the mortar with 1.00% of fibre was presenting poor workability to be applied as overlay. A possible solution for this problem would be to use admixtures such as superplasticizers to improve the workability while maintaining the mechanical properties.

- The target values of compressive strength at 28 days, (10<fc<15 MPa), were achieved for F0.50_RH60 and F0.75_RH60 and for all mortars cured at RH85, the flexural strength target values (5<$f_{ft,fl}$<7.5 MPa) were achieved for F0.75_RH85, F1.00_RH65 and F1.00_RH85.
- The effectiveness of fibres on the flexural strength was maximized by using PAN fibres up to 1.00 % vol. with a NHL matrix. The compressive and flexural toughness of the FRM, related to the post-cracking behaviour, showed an increase with the increase of the fibre content. Additionally, even for lower amounts of fibres, 0.25%, there is an important variation on the capacity to dissipate energy. This capacity is maximized for mortars with 1.00% of fibres.
- The correlation between the mechanical properties in compression and flexure and the respective toughness ratios showed opposite trends. Meanwhile the toughness ratio in compression increase for lower compressive strength values the toughness ratio in flexure increase for higher flexural strength values.

The developed NHL-FRM with PAN fibres can be used as overlay strengthening of masonry elements, presenting a mechanical performance higher than other NHL FRM´s and ductility higher than CEM-FRMs.

7 REFERENCES

[1] D. Gautam and H. Chaulagain, "Structural performance and associated lessons to be learned from world earthquakes in Nepal after 25 April 2015 (MW 7.8) Gorkha earthquake," Eng Fail Anal, vol. 68, pp. 222–243, Oct. 2016, doi: http://dx.doi.org/10.1016/j.engfailanal.2016.06.002.

[2] F. Parisi and N. Augenti, "Earthquake damages to cultural heritage constructions and simplified assessment of artworks," Eng Fail Anal, vol. 34, pp. 735–760, Dec. 2013, doi: http://dx.doi.org/10.1016/j.engfailanal.2013.01.005.

[3] X. Romão et al., "Field observations and interpretation of the structural performance of constructions after the 11 May 2011 Lorca earthquake," Eng Fail Anal, vol. 34, pp. 670–692, Dec. 2013, doi: http://dx.doi.org/10.1016/j.engfailanal.2013.01.040.

[4] G. De Felice, S. De Santis, and L. Garmendia, "Mortar-based systems for externally bonded strengthening of masonry," Mater Struct, no. 47, pp. 2021–2037, 2014, doi: 10.1617/s11527-014-0360-1.

[5] D. García and J. Díez, "Stone masonry walls: Strengthening with TRM (I)," in Structural Analysis of Historic Construction, 2008, no. I, pp. 851–859.

[6] L. Garmendia, P. Larrinaga, D. García, and I. Marcos, "Textile-reinforced mortar as strengthening material for masonry arches," International Journal of Architectural Heritage, vol. 8, no. 5, pp. 627–648, 2014, doi: 10.1080/15583058.2012.704480.

[7] L. A. S. Kouris and T. C. Triantafillou, "State-of-the-art on strengthening of masonry structures with textile reinforced mortar (TRM)," Constr Build Mater, vol. 188, pp. 1221–1233, 2018, doi: 10.1016/j.conbuildmat.2018.08.039.

[8] G. de Felice et al., "Recommendation of RILEM Technical Committee 250-CSM: Test method for Textile Reinforced Mortar to substrate bond characterization," Materials and Structures/Materiaux et Constructions, vol. 51, no. 4, pp. 1–9, 2018, doi: 10.1617/s11527-018-1216-x.

[9] C. E. Bakis et al., "Fiber-Reinforced Polymer Composites for Construction—State-of-the-Art Review," Journal of Composites for Construction, 2002, doi: 10.1061/(ASCE)1090-0268(2002)6:2(73).

[10] C. Papanicolaou, T. C. Triantafillou, and M. Lekka, "Externally bonded grids as strengthening and seismic retrofitting materials of masonry panels," Constr Build Mater, vol. 25, no. 2, pp. 504–514, 2011, doi: 10.1016/j.conbuildmat.2010.07.018.

[11] J. A. P. P. Almeida, E. B. Pereira, and J. A. O. Barros, "Assessment of overlay masonry strengthening system under in-plane monotonic and cyclic loading using the diagonal tensile test," Constr Build Mater, vol. 94, pp. 851–865, Sep. 2015, doi: http://dx.doi.org/10.1016/j.conbuildmat.2015.07.040.

[12] M. A. Kyriakides and S. L. Billington, "Seismic Retrofit Of Masonry-Infilled Non-Ductile Reinforced Concrete Frames Using Sprayable Ductile Fiber-Reinforced Cementitious Composites," 2008.

[13] A. Dehghani, G. Fischer, and F. Nateghi Alahi, "Strengthening masonry infill panels using engineered cementitious composites," Mater Struct, pp. 1–20, 2013, doi: 10.1617/s11527-013-0176-4.

[14] M. Stefanidou, I. Papayianni, and V. Pachta, "Evaluation of inclusions in mortars of different historical periods from greek monuments," Archaeometry, vol. 54, no. 4, pp. 737–751, 2012, doi: 10.1111/j.1475-4754.2011.00645.x.

[15] M. A. Mansur and M. A. Aziz, "A study of jute fibre reinforced cement composites," International Journal of Cement Composites and Lightweight Concrete, vol. 4, no. 2, pp. 75–82, 1982, doi: 10.1016/0262-5075(82)90011-2.

[16] R. D. Toledo Filho, K. Scrivener, G. L. England, and K. Ghavami, "Durability of alkali-sensitive sisal and coconut fibres in cement mortar composites," Cem Concr Compos, vol. 22, pp. 127–143, 2000.

[17] J. Claramunt, M. Ardanuy, J. A. García-Hortal, and R. D. Toledo Filho, "The hornification of vegetable fibers to improve the durability of cement mortar composites," Cem Concr Compos, vol. 33, no. 5, pp. 586–595, 2011, doi: 10.1016/j.cemconcomp.2011.03.003.

[18] M. E. A. Fidelis, R. D. Toledo Filho, F. de A. Silva, V. Mechtcherine, M. Butler, and S. Hempel, "The effect of accelerated aging on the interface of jute textile reinforced concrete," Cem Concr Compos, vol. 74, pp. 7–15, 2016, doi: 10.1016/j.cemconcomp.2016.09.002.

[19] D. joo Kim, A. E. Naaman, and S. El-Tawil, "Comparative flexural behavior of four fiber reinforced cementitious composites," Cem Concr Compos, 2008, doi: 10.1016/j.cemconcomp.2008.08.002.

[20] R. Ralegaonkar, H. Gavali, P. Aswath, and S. Abolmaali, "Application of chopped basalt fibers in reinforced mortar: A review," Constr Build Mater, vol. 164, pp. 589–602, 2018, doi: 10.1016/j.conbuildmat.2017.12.245.

[21] B. N. Skourup and E. Erdogmus, "Characteristics of PVA fiber-reinforced mortars," in Proceedings of the 2009 Structures Congress - Don't Mess with Structural Engineers: Expanding Our Role, 2009, pp. 1622–1631.

[22] B. A. Silva, A. P. Ferreira Pinto, and A. Gomes, "Natural hydraulic lime versus cement for blended lime mortars for restoration works," Constr Build Mater, vol. 94, pp. 346–360, 2015, doi: 10.1016/j.conbuildmat.2015.06.058.

[23] S. Pavía and R. Hanley, "Flexural bond strength of natural hydraulic lime mortar and clay brick," Mater Struct, vol. 43, no. 7, pp. 913–922, 2010, doi: 10.1617/s11527-009-9555-2.

[24] J. S. Pozo-Antonio, "Evolution of mechanical properties and drying shrinkage in lime-based and lime cement-based mortars with pure limestone aggregate," Constr Build Mater, vol. 77, pp. 472–478, 2015, doi: 10.1016/j.conbuildmat.2014.12.115.

[25] A. Kalagri, I. Karatasios, and V. Kilikoglou, "The effect of aggregate size and type of binder on microstructure and mechanical properties of NHL mortars," Constr Build Mater, vol. 53, pp. 467–474, 2014, doi: 10.1016/j.conbuildmat.2013.11.111.

[26] D. Gulotta, S. Goidanich, C. Tedeschi, and L. Toniolo, "Commercial NHL-containing mortars for the preservation of historical architecture. Part 2: Durability to salt decay," Constr Build Mater, vol. 96, pp. 198–208, 2015, doi: 10.1016/j.conbuildmat.2015.08.006.

[27] M. Aly and S. Pavia, "Mechanical and hygric properties of natural hydraulic lime (NHL) mortars with pozzolans."

[28] A. Sadrmomtazi, B. Tahmouresi, and A. Saradar, "Effects of silica fume on mechanical strength and microstructure of basalt fiber reinforced cementitious composites (BFRCC)," Constr Build Mater, vol. 162, pp. 321–333, Feb. 2018, doi: 10.1016/J.CONBUILDMAT.2017.11.159.

[29] E. T. Dawood, Y. Z. Mohammad, W. A. Abbas, and M. A. Mannan, "Toughness, elasticity and physical properties for the evaluation of foamed concrete reinforced with hybrid fibers," Heliyon, 2018, doi: 10.1016/j.heliyon.2018.e01103.

[30] E. T. Dawood and M. Ramli, "High strength characteristics of cement mortar reinforced with hybrid fibres," Constr Build Mater, vol. 25, no. 5, pp. 2240–2247, May 2011, doi: 10.1016/j.conbuildmat.2010.11.008.

[31] Z.-C. Deng, H.-L. Deng, J.-H. Li, and G.-D. Liu, Flexural fatigue behavior and performance characteristics of polyacrylonitrile fiber reinforced concrete, vol. 302–303. 2006.

[32] F. Xu, M. Zhou, W. Shen, and B. Li, "Study on the toughness performance of polypropylene fiber and SBR polymer latex modified cement mortar," in Advanced Materials Research, 2009, vol. 79–82, pp. 1751–1754. doi: 10.4028/www.scientific.net/AMR.79-82.1751.

[33] M. M. Al-mashhadani, O. Canpolat, Y. Aygörmez, M. Uysal, and S. Erdem, "Mechanical and microstructural characterization of fiber reinforced fly ash based geopolymer composites," Constr Build Mater, vol. 167, pp. 505–513, Apr. 2018, doi: 10.1016/J.CONBUILDMAT.2018.02.061.

[34] M. Kheradmand, M. Mastali, Z. Abdollahnejad, and F. Pacheco-Torgal, "Experimental and numerical investigations on the flexural performance of geopolymers reinforced with short hybrid polymeric fibres," Compos B Eng, vol. 126, pp. 108–118, Oct. 2017, doi: 10.1016/J.COMPOSITESB.2017.06.001.

[35] L. a. Pereira de Oliveira and J. P. Castro-Gomes, "Physical and mechanical behaviour of recycled PET fibre reinforced mortar," Constr Build Mater, vol. 25, no. 4, pp. 1712–1717, Apr. 2011, doi: 10.1016/j.conbuildmat.2010.11.044.

[36] R. Chan and V. Bindiganavile, "Toughness of fibre reinforced hydraulic lime mortar. Part-1: Quasi-static response," Mater Struct, vol. 43, no. 10, pp. 1435–1444, Apr. 2010, doi: 10.1617/s11527-010-9598-4.

[37] F. Iucolano, B. Liguori, and C. Colella, "Fibre-reinforced lime-based mortars: A possible resource for ancient masonry restoration," Constr Build Mater, vol. 38, pp. 785–789, Jan. 2013, doi: 10.1016/j.conbuildmat.2012.09.050.

[38] B. Liguori, D. Caputo, and F. Iucolano, "Fiber-reinforced lime-based mortars : Effect of zeolite addition," Constr Build Mater, vol. 77, pp. 455–460, 2015, doi: 10.1016/j.conbuildmat.2014.12.067.

[39] B. S. Seker, F. Cakir, V. Acar, M. O. Seydibeyoglu, and H. Akbulut, "Combined effects of chopped carbon and glass fibres on mechanical properties of lime-based mortar," Advanced Composites Letters, vol. 26, no. 2, pp. 41–48, 2017, doi: 10.1177/096369351702600203.

[40] D. Asprone, E. Cadoni, F. Iucolano, and A. Prota, "Analysis of the strain-rate behavior of a basalt fiber reinforced natural hydraulic mortar," Cem Concr Compos, vol. 53, pp. 52–58, 2014, doi: 10.1016/j.cemconcomp.2014.06.009.

[41] M. L. Santarelli, F. Sbardella, M. Zuena, J. Tirillò, and F. Sarasini, "Basalt fiber reinforced natural hydraulic lime mortars: A potential bio-based material for restoration," Journal of Materials and Design, vol. 63, pp. 398–406, 2014, doi: 10.1016/j.matdes.2014.06.041.

[42] Comité Européen de Normalisation, "EN 1015-3:1999 - Methods of Test for Mortar for Masonry - Part 3: Determination of consistence of fresh mortar (by flow table)," p. 10, 2007.

[43] Comité Européen de Normalisation, "EN 1015-7:1999 - Methods of test for mortar for masonry - Part 7 : Determination of air content of fresh mortar," no. May, 2004.

[44] Comité Européen de Normalisation, "EN 1015-10:1999 - Methods of Test for Mortar for Masonry - Part 10: Determination of dry bulk density of hardened mortar," vol. 3, no. 1, 2006.

[45] Comité Européen de Normalisation, "EN 12390-13:2013 Testing hardened concrete. Part 13: Determination of secant modulus of elasticity in compression," vol. 44, no. 0, 2013.

[46] Comité Européen de Normalisation, "EN 1015-11:1999 Methods of test mortar for masonry – Part 11: Determination of flexural and compressive strength of hardened mortar." Brussels, 1999.

[47] Comité Européen de Normalisation, "EN 196-1:2005 Methods of testing cement - Part 1: Determination of strength." p. 36, 2005. doi: 10.1111/j.1748-720X.1990.tb01123.x.

[48] S. J. Jang and H. Do Yun, "Combined effects of steel fiber and coarse aggregate size on the compressive and flexural toughness of high-strength concrete," Compos Struct, vol. 185, pp. 203–211, 2018, doi: 10.1016/j.compstruct.2017.11.009.

[49] Rilem TC 49-TFR, "Test for the determination of modulus of rupture and limit of proportionality of thin fibre reinforced cement section," Mater Struct, vol. 17, no. No. 102, pp. 161–163, 1984.

[50] D. C. Jansen and S. P. Shah, "Effect of Length on Compressive Strain Softening of Concrete," J Eng Mech, vol. 123, no. 1, pp. 25–35, Jan. 1997, doi: 10.1061/(ASCE)0733-9399(1997)123:1(25).

[51] G. Vasconcelos, "Experimental investigations on the mechanics of stone masonry: Characterization of granites and behavior of ancient masonry shear walls," PhD dissertation, 2005.

[52] M. C. Nataraja, N. Dhang, and A. P. Gupta, "Stress–strain curves for steel-fiber reinforced concrete under compression," Cem Concr Compos, vol. 21, no. 5–6, pp. 383–390, Dec. 1999, doi: 10.1016/S0958-9465(99)00021-9.

[53] P. Bhargava, U. K. Sharma, and Surendra. K. Kaushik, "Compressive Stress-Strain Behavior of Small Scale Steel Fibre Reinforced High Strength Concrete Cylinders," Journal of Advanced Concrete Technology, vol. 4, no. 1, pp. 109–121, 2006, doi: 10.3151/jact.4.109.

[54] F. Fraternali, I. Farina, C. Polzone, E. Pagliuca, and L. Feo, "On the use of R-PET strips for the reinforcement of cement mortars," Compos B Eng, vol. 46, pp. 207–210, Mar. 2013, doi: 10.1016/J.COMPOSITESB.2012.09.070.

[55] M. del Zoppo, M. di Ludovico, A. Balsamo, and A. Prota, "Diagonal compression testing of masonry panels with irregular texture strengthened with inorganic composites," Materials and Structures/Materiaux et Constructions, vol. 53, no. 4, pp. 1–17, Aug. 2020, doi: 10.1617/S11527-020-01539-Z/TABLES/7.

[56] N. Banthia and S. Mindess, "Toughness Characterization of Fiber-Reinforced Concrete: Which Standard to Use," J Test Eval, vol. 32, no. 2, p. 11901, 2004, doi: 10.1520/JTE11901.

[57] JSCE, "JSCE-SF4 Method of tests for flexural strength and flexural toughness of steel fiber reinforced concrete," 1984.

[58] ASTM, "ASTM C1018-97 Standard Test Method for Flexural Toughness and First-Crack Strength of Fiber-Reinforced Concrete (Using Beam With Third-Point Loading)," ASTM Standard, vol. 04, no. October, p. 7, 1997, doi: 10.1520/C1018-97.

[59] American Society for Testing and Materials ASTM, "Standard Test Method for Flexural Performance of Fiber-Reinforced Concrete (Using Beam With Third-Point Loading)." pp. 1–9, 2012. doi: 10.1520/C1609.

[60] ASTM Committee, "C1399/C1399M Standard Test Method for Obtaining Average Residual-Strength of Fiber-Reinforced," ASTM standard C1399/C1399M, no. c, pp. 1–6, 2010, doi: 10.1520/C1399.

PAPER II

HYBRID FIBRE REINFORCED MORTAR FOR OVERLAY MASONRY STRENGTHENING

REFERENCE: Almeida, J. A. P. P., Pereira, E. B., Barros, J. A. O. Hybrid Fibre Reinforced Mortar for overlay masonry strengthening. *Under submission process.*

ABSTRACT: This study presents the development of a sustainable hybrid fibre-reinforced mortar (FRM) for masonry overlay strengthening, combining natural hydraulic lime (NHL), geopolymer binders, recycled carbon fibres, and ceramic waste aggregates. Motivated by the need for durable, thermally stable materials compatible with historical masonry, the research investigates the mechanical performance and thermal behaviour of FRMs under varying NHL-geopolymer ratios (25%, 50%, 75%, 100%). Thermogravimetric analysis (TGA) revealed enhanced thermal stability in hybrid binders, with NHL-geopolymer mixtures exhibiting reduced mass loss compared to pure NHL after exposure to 600°C. Mechanical testing demonstrated that FRMs with ≥50% geopolymer content maintained adequate compressive and flexural strength, outperforming NHL-based mortars after temperature exposure. However, the 75% geopolymer mix showed anomalous underperformance, underscoring the need for further studies to fully understand the behaviour of these hybrid systems. The integration of recycled fibres and industrial by-products aligns with circular economy principles, reducing environmental impact while enhancing ductility. This work bridges a critical gap in overlay systems by demonstrating the feasibility of hybrid binders for fire-resistant masonry strengthening,

offering a novel pathway to balance sustainability, mechanical performance, and substrate compatibility.

KEYWORDS: Fibre reinforced mortar; Natural hydraulic lime (NHL); Geopolymeric binder; Temperature exposure; High ductility; Toughness; Experimental characterization

1 INTRODUCTION

Nowadays it is common practice to apply reinforcing overlays to masonry substrates as part of strengthening solutions, and several commercial brands sell products that can be applied as a ready to use solution. To improve the tensile behaviour and ductility of the reinforced parts, the overlay typically comprises of a mortar, applied manually or with shotcrete equipment, and a mesh composed of steel, polymers, carbon, basalt or glass [1]–[6]. Bio-based meshes are also under research because of the environmental benefits and effectiveness, the most suitable are the flax, jute and sisal fibres [7]–[10].

The overlay strengthening has structural advantages including the increase of in-plane strength, the improvement of the out-of-plane stability, the uniform behaviour and the increase of the energy dissipation. Additionally, the durability and the low cost can also be underlined as positive aspects. On the other hand, there are some global drawbacks to highlight, as visual and architectural modifications, the high disruption during works and the increase of the dead weight of the strengthened elements [11]. At the local level the difference between the stiffness from the original element and the strengthening overlay can derive in high stresses at the interface leading to the delamination of the overlay [5]. This type of failure can be avoided by adjusting the properties of the strengthening layers to the ones from the substrates, and consequently using mortars with lower compressive strength, higher ductility and lower elastic modulus. This performance can be achieved with mortars that use alternative binders as hydraulic lime, alkali activated materials (AMM) or geopolymeric binders instead of Portland cement [12]–[20].

Geopolymeric and Alkali activation is a complex reaction taking place in alkaline solution with aluminosilicate materials. First the alkaline solution has the role of dissolving Si-O and Al-O bonding, later it promotes their incorporation in the geopolymer network by charge-balancing the alkali-metal cations. Alkali activator promotes the reaction, and for higher molar ratios of SiO_2/Al_2O_3 and Na_2O/Al_2O_3

higher mechanical strength and density are achieved [21], see in **Table II.1** the recommended molar ratios.

Table II.1: Recommended molar ratios for geopolymer [21].

Molar ratios	Range
SiO_2/Al_2O_3	3.50-4.50
Na_2O/Al_2O_3	0.80-1.20
H_2O/Na_2O	15-17.50
Na_2O/SiO_2	0.20-0.28

AAM's have gained attention in part due to their potential for reducing greenhouse gas emissions associated with traditional cement production and at the same time using as precursors, materials normally considered as by-products, [22], [23], see **Figure II.1** where the source materials as well as the cementitious materials composition are represented in a ternary diagram, [21], [24], [25]. The most used sources of aluminosilicate precursors for AAM and geopolymer formulation include, [22], [23]:

- fly ash, a by-product of coal combustion, rich in silica and alumina
- rice husk ash, a by-product from the combustion of rice milling residues, is a rich source of silica
- blast furnace slag, a by-product of the iron and steel industry, rich in silica, alumina, and calcium oxide
- metakaolin, thermally activated form of kaolin clay, is a high-purity source of alumina and silica with high reactivity
- natural pozzolans, such as volcanic ash and diatomaceous earth, rich in silica and alumina, have been used for centuries in traditional construction materials
- construction demolition waste (CDW), from concrete and mortars to ceramic bricks and tiles.

Overall, the use of these source materials provides a sustainable and environmentally friendly alternative to traditional cement production, and their use in AAM and geopolymer production is expected to continue to grow.

In recent years, studies on alternative binders as AAM had shown significant progress, with various applications, ranging from structural functions to coatings for fire protection or conservation and as

façade elements [26]–[30]. Moreover, there are studies on developing AMM to be used in additive manufacturing, with geopolymer mortar printed layer-by-layer directly from 3D computer-aided design (CAD) [31], [32]. However, according to Abulencia et al. [33], more studies should consider the development of geopolymers to be used as deep repointing, jacketing, and overlay strengthening of masonry elements, and additionally matching properties of the substrate mortars to prevent further damage to the structures.

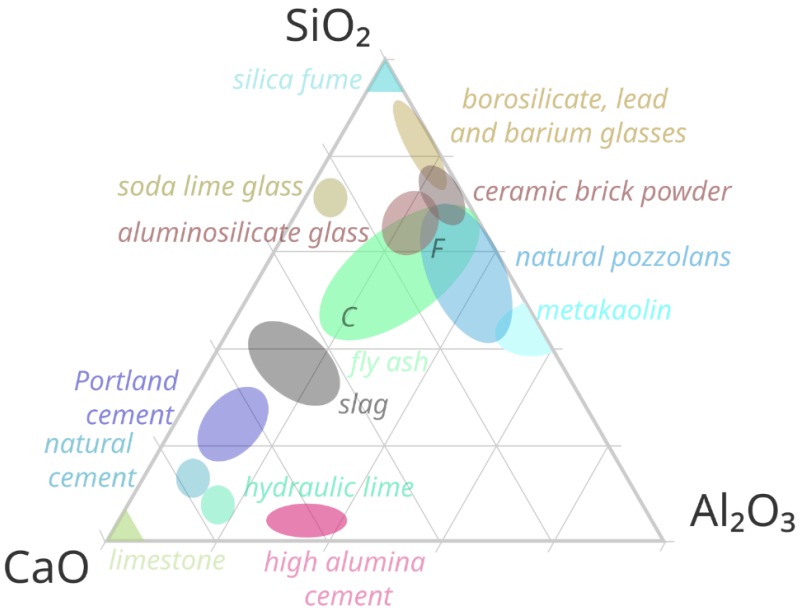


Figure II.1: Ternary diagram of the most common cementitious materials, adapted from [21], [24].

2 RESEARCH SIGNIFICANCE

This study focus was the development of a mortar to be used as overlay strengthening of masonry elements. The developed FRM incorporates a high amount of construction residues and recycled carbon fibres and polyacrylonitrile fibres.

The research on geopolymeric materials has increased in the last years, however the studies dedicated specifically on its use in strengthening overlays systems is reported to be missing [33]. Due to this need it was developed several compositions with and without geopolymeric binders and an experimental campaign was planned to evaluate the mechanical behaviour of the FRM. The development of the mortar also considered aspects of compatibility with substrates and behaviour of mortars after exposure to high temperatures. Due to these conditions, materials with greater thermal stability and resistances were prioritized in line with the application in masonry elements.

3 MATERIALS AND METHODS

3.1. Materials

Most of the materials used in this study are commercially available and were supplied directly by the producers or obtained in specialized warehouses. The only exceptions were the aggregate and brick dust, both processed from previously used bricks collected from masonry elements. The selection of the aggregates used in the development of the FRM's took in account the behaviour of mortars after exposure to high temperatures. Due to these conditions, materials with greater thermal stability were prioritized. The thermogravimetric behaviour of three aggregates was analysed, crushed brick, limestone and silica sand, the results from the thermogravimetry are presented in **Figure II.2**. In the temperature range from 650 and 870°C is possible to appreciate a clear difference between the behaviour of silica sand and crushed brick to the one from limestone sand. The loss of mass in limestone is associated to the thermal decomposition in quicklime and carbon dioxide. The crushed brick aggregates were select given the thermal stability and lower environmental impact.

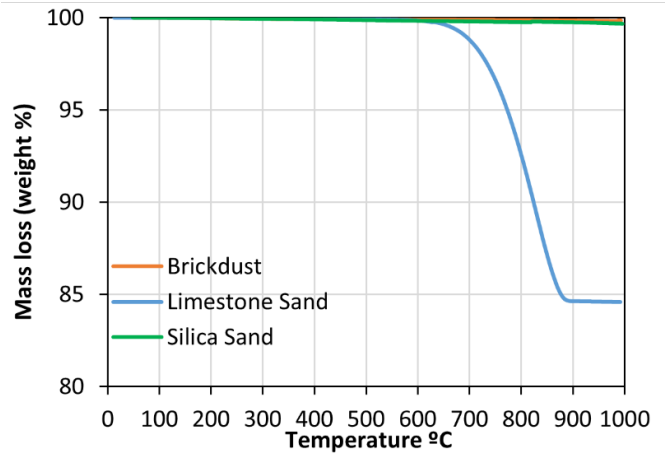


Figure II.2: Thermogravimetric curves of the different type of materials.

3.1.1. Processing of Recycled aggregates and brick dust

Red ceramic bricks were gathered from masonry elements and processed to obtain crushed brick aggregates (CBA) and fine red brick powder (RBP) to use as a geopolymer precursor. Multiple processing steps were taken to produce an aggregate with dimensions ranging from 0 to 2 mm. The bricks with initial dimensions of roughly 220x120x100 mm^3 were first crushed in a jaw crusher mill to produce a 0-15 mm aggregate, which was then sieved at 2 mm. The retained component was combined with twelve 450gr balls and placed in a Los Angeles drum mill in batches of 10kg, see **Figure II.3**. The aggregate was then reduced in size to 0-2 mm by running two 15-minute cycles.

Finally, the mixture was sieved in a 2 mm sieve once more, and the retained material was separated. The particle size distribution of the material after each step was obtained by sieving method according to EN 933-1 [34], and the curves are presented in **Figure II.5**.

a)  b)  c) 

Figure II.3: Phases of brick aggregate processing: a) original material collected from masonry elements; b) jaw crusher mill; c) drum mill with used milling material.

The processing of the fine red brick powder (RBP) started from the previously obtained 0-2mm aggregate, a vibratory disc mill RS 300 from RETSCH was used, see **Figure II.4a**. This equipment performs extremely quick cycles by setting the grinding jar into a 3-D motion, proven to be ideally suitable for applications in the building materials sector but also in geology, mineralogy and metallurgy. Before starting the milling process two experimental batches were run with a duration of 6 and 12 minutes to optimize the milling time. The difference in the particle size distribution can be seen in **Figure II.5b**, curve RBP6 and RBP12 for 6 and 12 minutes respectively. Giving the similar grading of the two samples it was decided to perform cycles with a duration of 6 minutes.

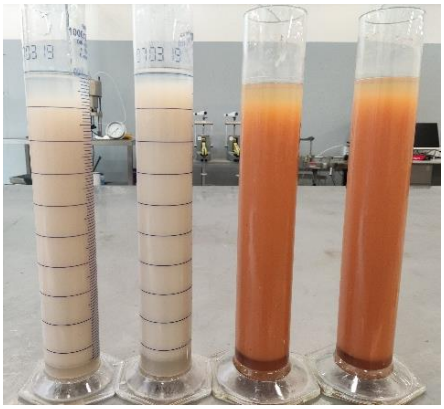
a)  b) 

Figure II.4: Red Brick Powder processing and analysis: a) Disc mill used; b) particle size distribution by sedimentation.

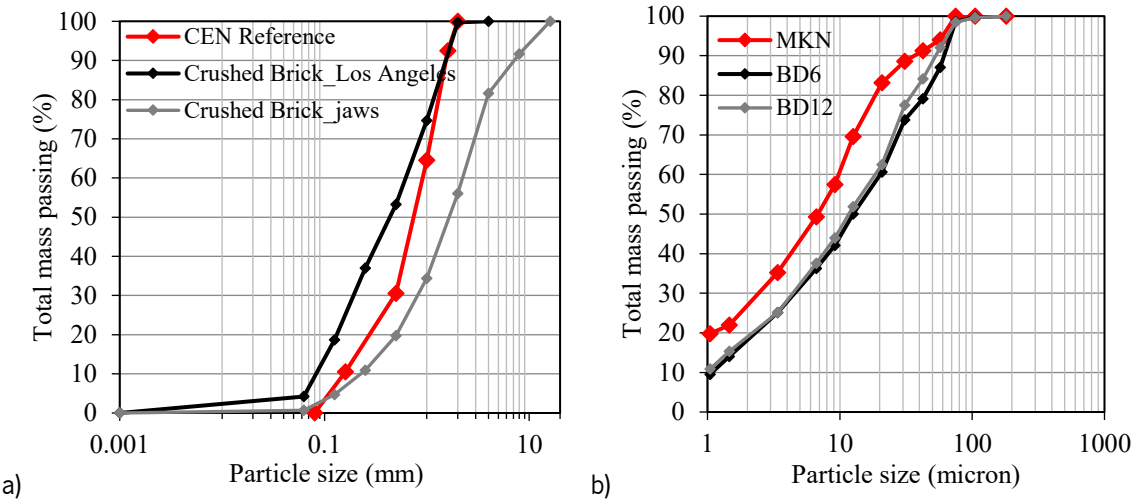


Figure II.5: Particle size distribution of materials: a) processed brick aggregate after each step and CEN reference curve; b) – Metakoalin and processed red brick powder after 6 and 12 minutes.

3.1.2. Binders

Two main types of binders were used in this study, a natural hydraulic lime (NHL 5.0) and a geopolymeric binder (GP). Natural hydraulic lime is a binder with an increasing usage in mortars applied in rehabilitation and strengthening of old masonry elements and in new construction, it presents properties from Portland cement and calcium hydroxide, because it has the contribution of hydration reactions for the early age strength and additional carbonation reactions contributing for the strength increase at long term [12], [35], [36]. The predominant hydraulic phase of NHL is the dicalcium silicate (C2S), in smaller amounts also other hydraulic phases as tricalcium silicate (C3S), tricalcium aluminate (C3A) and tetracalcium aluminoferrite (C4AF) can be found. On the other hand, the most important air hardening phase is the Portlandite $Ca(OH)_2$, the same phase present in air lime [37]. The physical, chemical and mechanical properties of the NHL provided by the supplier are presented in **Table II.2**.

The geopolymeric binder used in this work is composed by a mixture of sodium silicate (SS) solution (Na_2SiO_3) and sodium hydroxide (SH) solution (NaOH) in a mass proportion of 2:1 as activator. A mixture of metakaolin (MK) and red brick powder (RBP) with a proportion of 1:1 was used as precursor. The sodium silicate was provided as solution with a content of sodium oxide (Na2O) of 13% and a ratio (SiO_2/Na_2O) of 2.03. The sodium hydroxide was originally supplied in pearl form and after dissolved in water until a concentration of 10M was achieved. The chemical properties of the SS and SH are presented in **Table II.3)**.

Table II.2: Properties from the natural hydraulic lime, commercially available as Secil NHL5.0.

Physical Properties		
Fineness (>90um)	(%)	≤15.0
Fineness (>200um)	(%)	≤2.0
Chemical Properties		
(Sulphate) SO_3 (%)	(%)	≤2
(Free Lime) $Ca(OH)_2$	(%)	≥15
(Andrite) $CaSO_4$	(%)	<1
Mechanical Properties		
Compressive strength at 7 days	(MPa)	≥2
Compressive strength at 28 days	(MPa)	≥5.0 and ≤15.0

Table II.3: Properties of the activators used for the geopolymeric binder.

Property		**Sodium silicate (SS) CAS: 1344-09-8**	**Sodium hydroxide (SH) CAS: 1310-73-2**
Molar mass	(g/mol)	122.06	39.99
Specific gravity	(g/cm^3)	1.45	2.13
Appearance		Liquid, colorless	Solid, white
Melting point	(°C)	1088	323
pH		11-13	13-14

3.1.3. Fibres

Several types of fibres were considered in the development of the mortar namely, polyacrylonitrile (PAN), carbon (CF), polyvinyl-alcohol (PVA) and glass fibres (GF), their properties are summarized in **Table II.4**. The PAN fibres supplied by FISIPE are mainly used in dry mixed mortars, shotcrete and concrete, they present a good chemical resistance and permit temperature exposure up to 220°C during short periods. The recycled carbon fibres, supplied by ELGCarbon, present environmental benefits by reducing significantly the carbon footprint. The recycling process uses less than 10% of the energy required to produce virgin carbon fibre and at the same time it minimises the waste going to landfill and incineration. These recycled carbon fibres have similar mechanical properties to the original fibres resulting in 95% strength retention and 99% modulus retention. The PVA and the glass fibres were provided by Kuraray and Owens Corning respectively.

Table II.4: Properties of fibres.

Properties		PAN	Carbon	PVA	Glass
Density	(g/cm3)	1.17	1.80	1.30	2.68
Length	(mm)	6	3-10	8	6
Diameter	dtex(micron)	26	–	15(40)	14
Fineness	(dtex)	2.5	–	7	8.2
Tensile strength	(MPa)	685	3470	1600	1700
Elongation	(%)	14-16	–	6	–
Elastic Modulus	(GPa)	13.4	246	41	72

Sources: PVA - http://kuralon-frc.kuraray.com/product-application/for-mortar/recs

3.2. Composition of pastes and mortars

The composition was based on previous experience with geopolymeric and NHL FRM's [14], [38]. The mixtures were designed in a two steps process: first by mixing pastes with different percentage in weight of NHL and Geopolymeric binders; after fibres and aggregates were introduced by essentially maintaining the same amount of water for wetting the aggregates and aggregate/binder ratios in volume. The mixing process followed the procedure presented in **Figure II.6** and weights presented in **Table II.5**.

Table II.5: Composition of the mortars, weight of materials per m^3.

	Weight (kg)									
	Geopolymeric Paste				NHL Paste		Aggregates		Fibres	
	SS	SH	Mk	RBP	NHL 5.0	H2O for NHL	Dry	Wetting H2O	PAN	Carbon
Ref	0,00	0,00	0,00	0,00	610,10	244,04	762,30	162,62	5,90	9,00
25%Geo	60,25	30,13	67,95	66,08	457,57	183,03	762,30	162,62	5,90	9,00
50%Geo	120,49	60,27	135,90	132,17	305,05	122,02	762,30	162,62	5,90	9,00
75%Geo	180,74	90,40	203,84	198,25	152,52	61,01	762,30	162,62	5,90	9,00
100%Geo	240,98	120,53	271,79	264,33	0,00	0,00	762,30	162,62	5,90	9,00

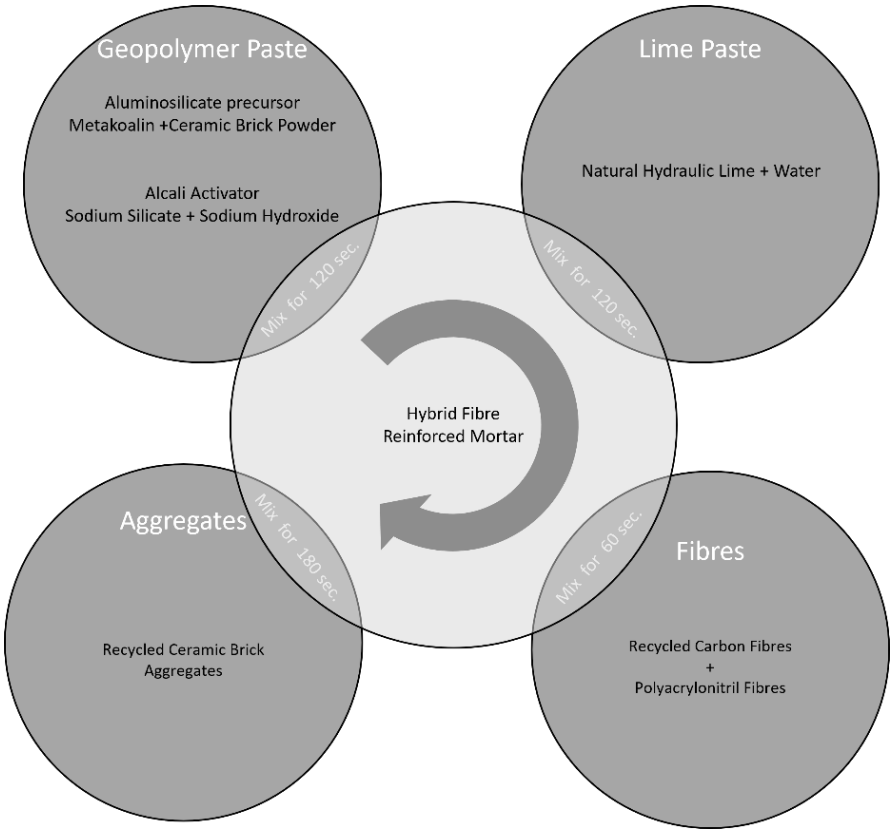


Figure II.6: Mixing procedure of the FRM.

3.3. Thermogravimetric analysis

The protocol adopted for the thermogravimetric analysis on the pastes was similar to the one described in literature [39], [40], with a temperature interval from 50 to 1000°C, and a heating rate of 10°C/min. The preparation of the samples was done after curing the pastes at 20°C inside a sealed plastic bag during the first 7 days and at 20°C and 60% RH until 90 days. First, a small amount of material was grinded in a ceramic mortar and dried at 50°C for 24h prior to the thermogravimetry, finally approximately 25 mg. of material was placed inside an alumina crucible. In additional to the thermogravimetry (TG) and differential thermogravimetry (DTG), also data from differential scanning calorimetry (DSC) was obtained, for that reason a second empty alumina crucible was also placed in the TA Q600 DSC equipment.

3.4. Fresh and hardened behaviour

The mini-slump flow value was measured by averaging the diameter measured in two perpendicular directions of the spread sample of the pastes and fresh mortar, which has been placed on a table disc

with the help of a mould with dimensions specified in EN1015-3 [41]. Then 15 vertical impacts were applied by raising the flow table and allowing it to fall freely through a given height [41].

The flexural and compressive behaviour of the mortars was studied by adopting the procedure described by the EN 1015-11 [42]. The three-point flexural tests were carried out on prismatic specimens with 40x40x160 mm^3 using a 50 kN actuator under displacement control, displacements were measured by one LVDT's with 10 mm range at the middle span. The tests were performed by applying a monotonically increasing displacement at mid-span at a rate of 0.01 mm/s. According to the procedure defined in EN 1015-11 [42] the compressive behaviour of the hardened mixtures was evaluated with the halves resulting from the flexural tests.

3.5. Residual Mechanical behaviour after temperature exposure

The residual mechanical characterization after temperature exposure was carried out by compressive tests in the pastes, in the case of FRM's flexural and compressive tests according to the EN1015-11 [42]. The residual compressive strength, $f^{T}_{(c,res)}$, and residual flexural strength, $f^{T}_{(c,res)}$, were computed together with the load vs displacement curves.

The specimens were kept in a curing chamber under 25°C and 65% relative humidity conditions and tested at 7 and 28 and 90 days for the pastes and at 28 days for the FRM specimens. After ageing, the specimens were exposed to high temperatures 24 hours prior to the mechanical tests. The procedure was similar to the one suggested by RILEM recommendation 129-MHT [43], starting with a heating cycle in the furnace at a constant heating rate of 4°C/min up to the maximum temperature. Subsequently, a plateau of 60 minutes at constant temperature was imposed followed by a natural cooling process until room temperature was reached.

4 RESULTS AND DISCUSSION

4.1. Characterization of Pastes

4.1.1. Thermogravimetric analysis of pastes

The results of the mass variation, differential mass variation and heat flow obtained from the thermogravimetric analysis to the pastes at 7 and 90 days can be seen in **Figure II.7**. The paste containing only NHL present three ranges of temperature where the mass variation is higher, these peaks are clearly identified in the **Figure II.7c** and **Figure II.7d** where the derivative of the mass vs

temperature is plotted. The first temperature range is between 50-200°C and is related to the dewatering of the adsorbed free water or evaporable water present on the porous and surface of the sample. The second rage is between 380 and 500°C and is related to the dihydroxylation, which is the process of decomposition of calcium hydroxide, $Ca(OH)_2$, and the portlandite dehydration [36]. Finally, in the range between the 550 and 800°C the carbonates decomposition takes place causing a major decline of the mass. On the opposite side the geopolymeric paste at 7 days, 100%Geo, present only one identifiable peak of mass variation, from 50 to 200°C, where the decline of mass is associated with the dewatering process and associated with the presence of NASH gel [44]. The evolution of the geopolymeric paste from 7 to 90 days is noticeable when comparing the 100%Geo derivative of the mass curve in **Figure II.7c** and **Figure II.7d** and the heat flow curve in **Figure II.7e** and **Figure II.7f**, where is possible to identify a first small peak at 100°C related to the dewatering process and a second peak at 180°C related with the presence of NASH gel.

The mass variation and heat flow, at 7 and 90 days, show a clear and steady evolution from the behaviour of the mixture containing only NHL as binder, Ref, to the mixture containing only geopolymeric binder, 100%Geo. However, is possible to identify a change in the derivative of the mass in the pastes with 25, 50 and 75% of geopolymeric binder between the range of 500 to 700°C. This effect is more obvious in the 50%Geo and 75%Geo pastes where at 90 days there is a clear inflection of the curve, see **Figure II.7d**.

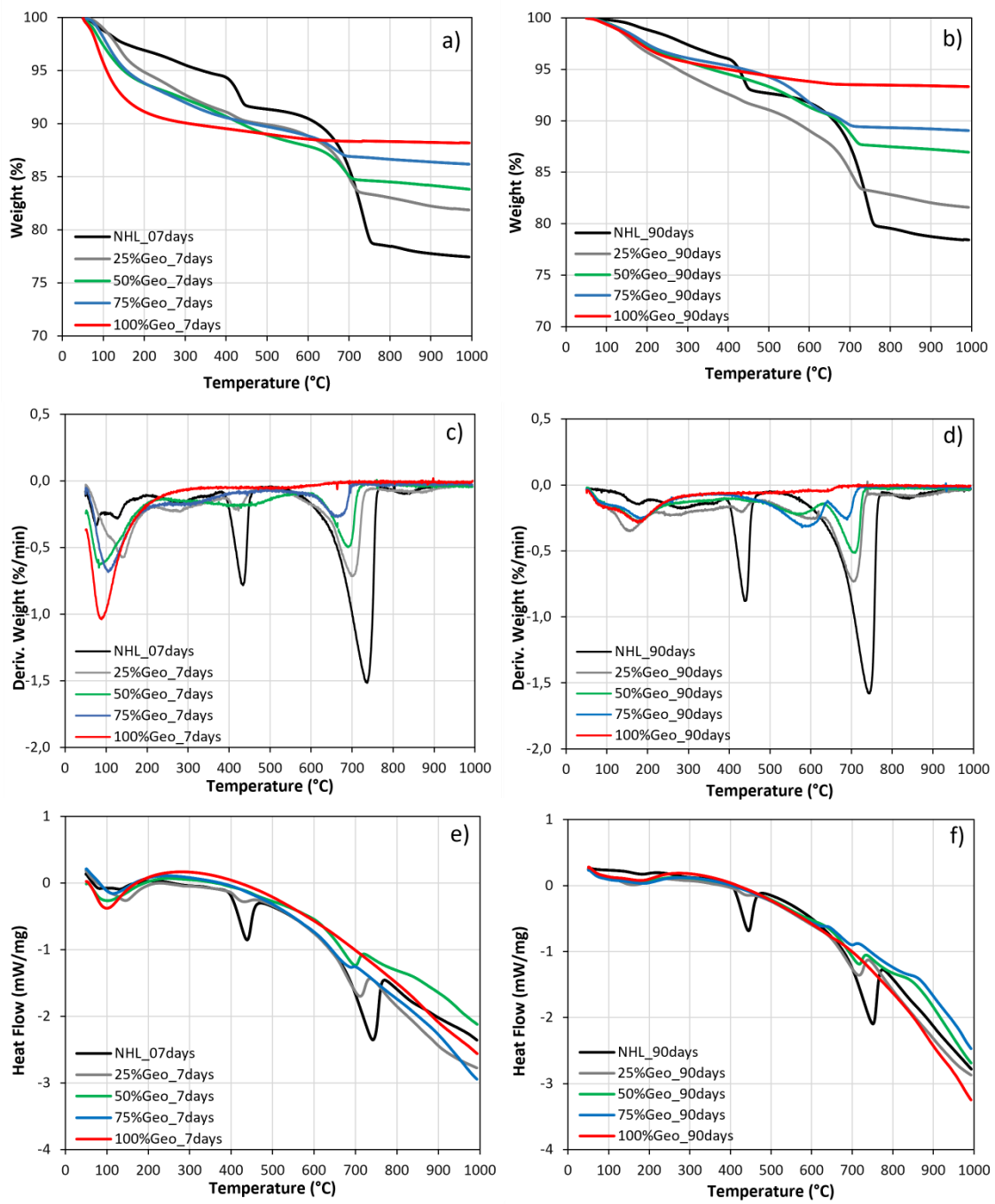


Figure II.7: Thermal analysis of pastes: thermogravimetry at a) 7 days and b) 90 days; differential thermogravimetry at c) 7 days and d) 90 days; heat flow at f) 7 days and e) 90 days.

4.1.2. Compressive strength of pastes

The compressive strength of the pastes was evaluated in cubic samples with 20mm side at ages of 7, 28 and 90 days for room temperature and after exposure to 600°C. The results obtained from the paste compressive tests are presented in **Figure II.8**. The compressive strength of pastes for all tested ages at room temperature steadily increased from the paste containing only NHL binder, NHL, to the paste containing only geopolymeric binder, 100%Geo, see **Figure II.8a**. This behaviour was

different for the pastes tested after exposure to 600°C, where there was an increase from pastes with NHL binder to pastes with geopolymeric binder, however the evolution with age was not verified, with strength at 90 days to be normally lower than 7 and 28 days. Additionally, the evolution of the normalized value of compressive strength between 20°C and 600°C is presented in **Figure II.8b** as ratio fc,T600/fcT20. The analysis of the ratio fc,T600/fcT20 at 7 28 and 90 days shows that for pastes with 50% and 75% of geopolymeric binder, the compressive strength always higher after exposure to 600°C with ratios between 1.01 and 1.70. This behaviour, obtained after exposure to 600°C are in line with the results observed in the thermogravimetry, see **Figure II.7d** where an inflection is observed in the same pastes in the range of temperatures between 500 and 700°C.

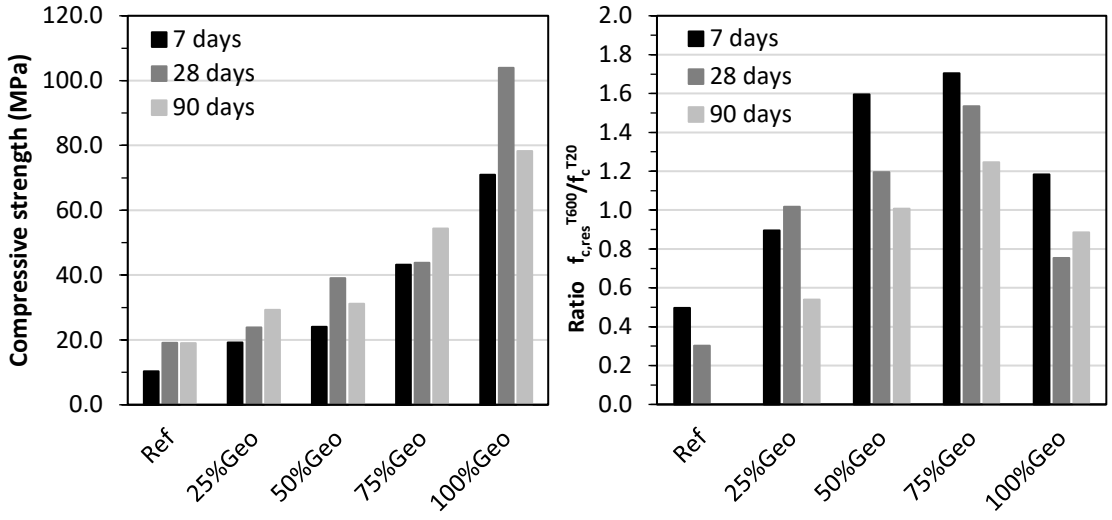


Figure II.8: Compressive behaviour of the pastes: a) compressive strength; b) ratio between the compressive strength at room temperature and residual compressive strength after 600°C

4.2. Characterization of Fibre Reinforced Mortars

4.2.1. Flexural Behaviour

The characterization of the FRM's in flexure was carried according to the procedure from EN1015-11 [42]. In additional to the standard set-up, the deflection was measured in the central part of the specimen during the flexural tests. The average and envelope of the load vs displacement (F-d) at mid-span responses from the flexural tests of the FRM's with different amounts of geopolymeric binder can be seen in **Figure II.9**. In all the FRM's is clear the influence from the exposure to temperature, with a strong degradation in the maximum load and lower displacement.

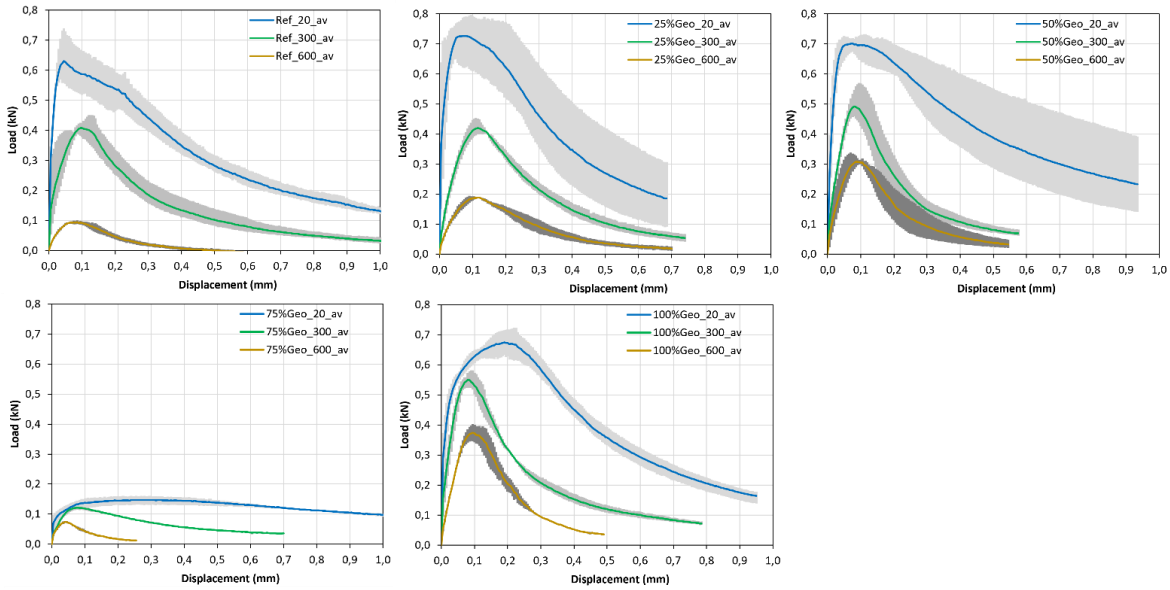


Figure II.9: Average load vs displacement at mid-span curves and envelope obtained from the flexural tests to FRM's.

The data collected from the tests was processed to quantify the flexural strength, f_{flex}., see **Eq. (II.1)**, and the displacement obtained at maximum load, df_{flex}, see **Table II.6**. The flexural strength at room temperature, f_{flex_20}, of FRM's with 25, 50 and 100% of geopolymeric binder increased 15, 8 and 6% when compared with NHL FRM. The same level of variation was verified for specimens tested after the exposure to 300°C. Furthermore, when the exposure temperature increased to 600°C the FRM´s with 25, 50 and 100% of geopolymeric binder flexural strength increased 54, 142, and 181%. The FRM with 75% of geopolymeric binder presented a significantly lower flexural strength than the reference, 100% NHL FRM, for all the tested temperatures.

The evaluation of the flexural toughness, Tb, for the different FRM's was carried by estimating the area under the (F-d) curve obtained from the flexural tests, [14]. However, to decrease the effect of the load configuration and different size of specimens, the energy dissipation capacity was normalized by using a flexural toughness factor ratio, Re2, see **Eq. (II.3)**, where for each specimen, the flexural toughness factor (FT), see **Eq. (II.2)**, is normalized with respect to the modulus of rupture, MOR, [45] [46]. The deflection, δ Tb, adopted to calculate Tb, and FT, was limited to $1/150$ of the distance between supports, b and d represent the with and height of the specimen.

$$f_{flex} = \frac{3 \times F \times L}{2 \times b \times d^2} \qquad \textbf{(II.1)}$$

$$FT = \frac{T_b \times L}{\delta_{tb} \times b \times d^2} \quad \textbf{(II.2)}$$

$$Re2\ (\%) = \frac{FT}{MOR} \times 100 \quad \textbf{(II.3)}$$

The flexural toughness factor (FT), obtained for the different FRM's and exposure temperatures can be seen in **Figure II.10a**. At room temperature an increase of the toughness is observed for all the FRM's when comparing to the NHL FRM, Ref, except for the 75%Geo.With the increase of the exposure temperature to 300 and 600°C there is a decrease of the flexural toughness factor for all FRM's, and for 600°C again there is a significant increase of toughness for all the FRM's except for 75%Geo. When considering the flexural toughness factor ratio, Re2, see **Figure II.10b**, the FRM containing 75% of geopolymeric binder present the higher value at room temperature and is in agreement with the other FRM's for exposure temperatures of 300 and 600°C. This is due to the of normalization of FT by the MOR value.

Table II.6: Results obtained from flexural and compressive tests of different FRM's at 28 days.

		$f_{flex.}$			df_{flex}			f_c			df_c		
		Av.	Std.	cv.	Av.	Std.	cv.	Av.	Std.	cv.	Av.	Std.	cv.
Age_temp	**name**	(MPa)	(MPa)	(%)	(mm)	(mm)	(%)	(MPa)	(MPa)	(%)	(mm)	(mm)	(%)
28 days_20°C	Ref	1,9	0,3	15	0,3	0,0	10	8,0	0,2	2	1,4	0,2	12
	25%Geo	2,2	0,3	13	0,5	0,1	16	11,9	0,4	3	1,3	0,1	8
	50%Geo	2,1	0,1	6	0,6	0,2	40	10,7	1,0	10	1,4	0,1	10
	75%Geo	0,5	0,0	7	0,5	0,0	8	1,3	0,1	10	1,0	0,3	30
	100%Geo	2,0	0,1	7	0,6	0,0	4	7,8	0,7	9	1,6	0,1	10
28 days_300°C	Ref	1,3	0,1	7	0,3	0,0	4	7,1	0,3	5	1,4	0,2	12
	25%Geo	1,3	0,1	7	0,5	0,1	11	9,1	0,4	5	1,3	0,1	7
	50%Geo	1,5	0,2	11	0,5	0,1	13	8,7	0,5	5	1,2	0,0	4
	75%Geo	0,4	0,0	3	0,4	0,0	4	1,6	0,1	5	0,7	0,1	8
	100%Geo	1,7	0,1	6	0,4	0,0	8	11,5	1,1	9	1,2	0,1	6
28 days_600°C	Ref	0,4	0,0	6	0,2	0,1	29	1,9	0,1	7	1,2	0,1	9
	25%Geo	0,6	0,0	3	0,4	0,1	22	4,3	0,4	10	1,1	0,2	16
	50%Geo	1,0	0,0	4	0,5	0,2	33	6,6	0,8	12	1,1	0,1	11
	75%Geo	0,3	0,0	4	0,3	0,0	6	1,1	0,1	12	0,5	0,0	8
	100%Geo	1,1	0,1	9	0,4	0,1	21	8,5	1,1	13	1,1	0,2	15

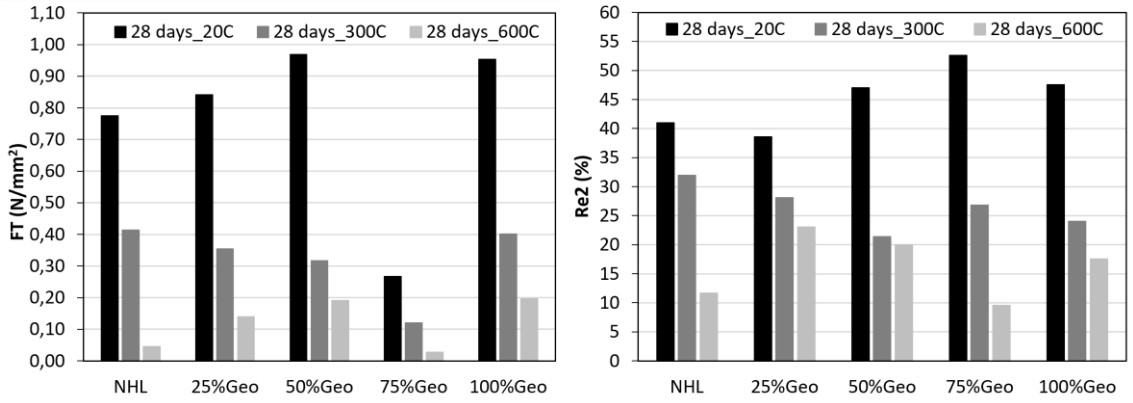


Figure II.10: Flexural toughness from FRM´s: a) flexural toughness factor, FT; b) flexural toughness factor ratio, Re_2.

4.2.2. Compressive Behaviour

The compressive strength, fc, of the FRM's was evaluated by testing the halves of the specimens previously tested in flexure, following the EN1015-11 [42]. The results obtained for 20°C and after exposure to 300 and 600°C can be consulted in **Table II.6** and **Figure II.11**. In addition, also the displacement at maximum stress is indicated in **Table II.6**. In general, for the same type of temperature exposure, the compressive strength of FRM's with geopolymeric binder was higher than for the NHL FRM. The only exception was the 75%Geo FRM that presented always smaller values of compressive strength. The increase of the compressive strength at room temperature was higher for the FRM 25%Geo and for 300°C and 600°C for the 100%Geo, with an increase of 50, 60 and 360% respect to the reference FRM, Ref.

Figure II.11b shows the compressive toughness ratio TRc,0.75Fmax of the FRM's for the several levels of temperature exposure. TRc,0.75Fmax was computed according to **Eq. (II.4)** and considering the F vs d response of the compressive test until a residual load of 75% of the maximum load, see **Figure II.11a**. The same strategy was used by other authors [47]–[49], nevertheless in this study the limit of the F vs d curve was imposed as a ratio of the maximum load instead of a value of displacement or strain. The results obtained for all the FRM's show a decrease of the fracture energy in compression with the increase of the exposure temperature, **Figure II.11a**. When considering the TRc,0.75Fmax there is an almost uniform behaviour among the different FRM's and different types of exposure.

$$\mathrm{TR_{c,0.75Fmax}}\ (\%) = \frac{Area\ under\ F\ vs.\ d\ curve}{Fmax\ \times d_{0.75Fmax}} \times 100 \qquad \textbf{(II.4)}$$

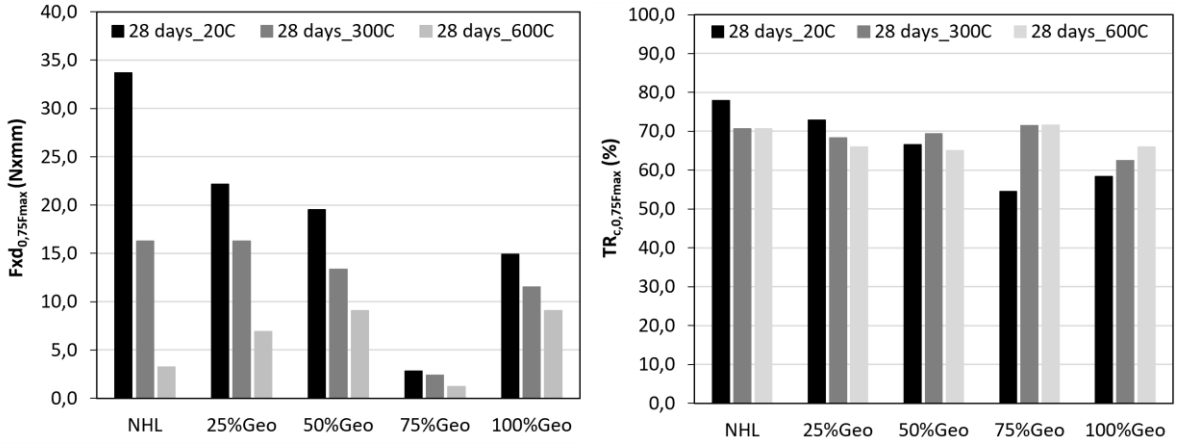


Figure II.11: Compressive behaviour of the FRM: a) fracture energy in compression; b) compressive toughness ratio $TR_{c0.75Fmax}$.

5 CONCLUSIONS

The aim of this study was the development of a fibre reinforced mortar to be used as overlay strengthening of masonry elements. The compatibility with substrates and behaviour of mortars after exposure to high temperatures lead to the use of recycled carbon fibres and polyacrylonitrile fibres and processed construction ceramic waste as aggregates. The main conclusions that can be drawn from the development of fibre reinforced mortars recurring to hybrid binders are as follows:

- The thermogravimetric analysis to NHL pastes shows three ranges with higher mass variation, from 50 and 200 °C related to the dewatering of the adsorbed free water, between 380 and 500 °C related to the decomposition of calcium hydroxide and the portlandite dehydration, and between 550 and 800 °C related to the carbonate's decomposition. For geopolymeric paste, 100%Geo, only one peak from 50 to 200 °C, related with the dewatering process and associated with the presence of NASH gel can be identified. Additionally, there is a clear evolution from the pastes containing only NHL to the mixture containing only geopolymeric binder.
- The compressive strength at 28 days progressively increased from the paste containing only NHL binder, 19 MPa, to the paste containing only geopolymeric binder, 104 MPa. After

temperature exposure, 600 °C, there was also an increase from pastes with NHL binder to pastes with geopolymeric binder, however the evolution with age was not verified, with strength at 90 days to be normally lower than 7 and 28 days.

- The ratio $f_{c,T600}/f_{c,T20}$ at 7, 28 and 90 days was higher for pastes with 50 and 75 % of geopolymeric binder, showing a better performance after temperature exposure.
- The flexural strength at room temperature, f_{flex_20}, of FRM's with 25, 50 and 100 % of geopolymeric binder increased 15, 8 and 6 % when compared with NHL FRM. After the exposure to 600 °C the increase was 54, 142, and 181 % when compared with NHL FRM at same temperature. The FRM with 75 % of geopolymeric binder presented a significantly lower flexural strength than the NHL FRM for all temperatures.
- The compressive strength of FRM's at same level of temperature exposure, was higher for FRM's with geopolymeric binder than for the NHL FRM. The only exception was the 75%Geo FRM that presented always inferior values.

The results obtained show the possible use of this type of hybrid binders in FRM's to strengthen masonry elements, with compressive and flexural strength values adequate with overlay strengthening systems. Nonetheless, additional studies on the durability of these hybrid binders should be carried to evaluate their potential.

REFERENCES

[1] S. B. Kadam, Y. Singh, and B. Li, "Strengthening of unreinforced masonry using welded wire mesh and micro-concrete – Behaviour under in-plane action," Constr Build Mater, vol. 54, pp. 247–257, 2014, doi: 10.1016/j.conbuildmat.2013.12.033.

[2] A. Figueiredo, H. Varum, A. Costa, D. Silveira, and C. Oliveira, "Seismic retrofitting solution of an adobe masonry wall," Mater Struct, vol. 46, no. 1–2, pp. 203–219, Jul. 2012, doi: 10.1617/s11527-012-9895-1.

[3] C. G. Papanicolaou, T. C. Triantafillou, K. Karlos, and M. Papathanasiou, "Textile-reinforced mortar (TRM) versus FRP as strengthening material of URM walls : in-plane cyclic loading," Mater Struct, vol. 40, pp. 1081–1097, 2007, doi: 10.1617/s11527-006-9207-8.

[4] M. Corradi, A. Borri, G. Castori, and R. Sisti, "Shear strengthening of wall panels through jacketing with cement mortar reinforced by GFRP grids," Compos B Eng, vol. 64, pp. 33–42, 2014, doi: 10.1016/j.compositesb.2014.03.022.

[5] J. A. P. P. Almeida, E. B. Pereira, and J. A. O. Barros, "Assessment of overlay masonry strengthening system under in-plane monotonic and cyclic loading using the diagonal tensile test," Constr Build Mater, vol. 94, pp. 851–865, Jul. 2015, doi: 10.1016/J.CONBUILDMAT.2015.07.040.

[6] G. P. Lignola et al., "Performance assessment of basalt FRCM for retrofit applications on masonry," Compos B Eng, 2017, doi: 10.1016/j.compositesb.2017.05.003.

[7] G. Ferrara, M. Pepe, R. D. T. Filho, and E. Martinelli, "Mechanical response and analysis of cracking process in hybrid TRM composites with flax textile and Curauá fibres," Polymers (Basel), vol. 13, no. 5, 2021, doi: 10.3390/polym13050715.

[8] N. Trochoutsou, M. di Benedetti, K. Pilakoutas, and M. Guadagnini, "Mechanical Characterisation of Flax and Jute Textile-Reinforced Mortars," Constr Build Mater, vol. 271, 2021, doi: 10.1016/j.conbuildmat.2020.121564.

[9] G. Di Bella, V. Fiore, G. Galtieri, C. Borsellino, and A. Valenza, "Effects of natural fibres reinforcement in lime plasters (kenaf and sisal vs. Polypropylene)," Constr Build Mater, vol. 58, pp. 159–165, 2014, doi: 10.1016/j.conbuildmat.2014.02.026.

[10] L. Yan, B. Kasal, and L. Huang, "A review of recent research on the use of cellulosic fibres, their fibre fabric reinforced cementitious, geo-polymer and polymer composites in civil engineering," Compos B Eng, vol. 92, pp. 94–132, May 2016, doi: 10.1016/J.COMPOSITESB.2016.02.002.

[11] M. Elgawady, P. Lestuzzi, and M. Badoux, "Dynamic versus static cyclic tests of masonry walls before and after retrofitting with GFRP," in Proc. 13th World Conference on Earthquake Engineering, Vancouver, B.C., Canada, 2004. Accessed: Jan. 22, 2014. [Online]. Available: http://www.iau-neyshabur.ac.ir/Tashakol/Omran/Maghale/Dynamic Versus static .pdf

[12] D. Gulotta, S. Goidanich, C. Tedeschi, T. G. Nijland, and L. Toniolo, "Commercial NHL-containing mortars for the preservation of historical architecture. Part 1: Compositional and mechanical characterisation," Constr Build Mater, vol. 38, 2013, doi: 10.1016/j.conbuildmat.2012.08.029.

[13] P. F. G. Banfill, E. M. Szadurski, and A. M. Forster, "Deterioration of natural hydraulic lime mortars, II: Effects of chemically accelerated leaching on physical and mechanical properties of carbonated materials," Constr Build Mater, vol. 111, pp. 182–190, 2016, doi: 10.1016/j.conbuildmat.2016.02.055.

[14] J. A. P. P. Almeida, J. A. O. Barros, and E. N. B. Pereira, "Toughness of Natural Hydraulic Lime Fibre-Reinforced Mortars for Masonry Strengthening Overlay Systems," Applied Sciences, vol. 14, no. 05, p. 1947, Feb. 2024, doi: 10.3390/APP14051947.

[15] F. Iucolano, B. Liguori, and C. Colella, "Fibre-reinforced lime-based mortars: A possible resource for ancient masonry restoration," Constr Build Mater, vol. 38, pp. 785–789, Jan. 2013, doi: 10.1016/j.conbuildmat.2012.09.050.

[16] M. L. Santarelli, F. Sbardella, M. Zuena, J. Tirillò, and F. Sarasini, "Basalt fiber reinforced natural hydraulic lime mortars: A potential bio-based material for restoration," Journal of Materials and Design, vol. 63, pp. 398–406, 2014, doi: 10.1016/j.matdes.2014.06.041.

[17] P. Michal and P. Kabele, "Mechanical Properties of Fiber Reinforced Lime-Based Mortar Evaluated from Four-Point Bending Test," 21st International Conference ENGINEERING MECHANICS 2015, vol. 821, pp. 242–243, 2015, doi: 10.4028/www.scientific.net/AMM.821.526.

[18] G. De Felice, S. De Santis, and L. Garmendia, "Mortar-based systems for externally bonded strengthening of masonry," Mater Struct, no. 47, pp. 2021–2037, 2014, doi: 10.1617/s11527-014-0360-1.

[19] D. Asprone, E. Cadoni, F. Iucolano, and A. Prota, "Analysis of the strain-rate behavior of a basalt fiber reinforced natural hydraulic mortar," Cem Concr Compos, vol. 53, pp. 52–58, 2014, doi: 10.1016/j.cemconcomp.2014.06.009.

[20] R. Chan and V. Bindiganavile, "Toughness of fibre reinforced hydraulic lime mortar. Part-1: Quasi-static response," Mater Struct, vol. 43, no. 10, pp. 1435–1444, Apr. 2010, doi: 10.1617/s11527-010-9598-4.

[21] M. Nodehi, & Vahid, and M. Taghvaee, "Alkali-Activated Materials and Geopolymer: a Review of Common Precursors and Activators Addressing Circular Economy," Circular Economy and Sustainability 2021 2:1, vol. 2, no. 1, pp. 165–196, Jun. 2021, doi: 10.1007/S43615-021-00029-W.

[22] J. L. Provis and S. A. Bernal, "Geopolymers and related alkali-activated materials," Annu Rev Mater Res, vol. 44, 2014, doi: 10.1146/annurev-matsci-070813-113515.

[23] A. Palomo, M. W. Grutzeck, and M. T. Blanco, "Alkali-activated fly ashes: A cement for the future," Cem Concr Res, vol. 29, no. 8, 1999, doi: 10.1016/S0008-8846(98)00243-9.

[24] M. Amran et al., "Fly ash-based eco-efficient concretes: A comprehensive review of the short-term properties," Materials, vol. 14, no. 15. 2021. doi: 10.3390/ma14154264.

[25] H. Du and K. H. Tan, "Properties of high volume glass powder concrete," Cem Concr Compos, vol. 75, 2017, doi: 10.1016/j.cemconcomp.2016.10.010.

[26] P. Duxson, A. Fernández-Jiménez, J. L. Provis, G. C. Lukey, A. Palomo, and J. S. J. van Deventer, "Geopolymer technology: the current state of the art," J Mater Sci, vol. 42, no. 4, pp. 2917–2933, 2007, doi: 10.1007/s10853-006-0637-z.

[27] M. Lahoti, K. H. Tan, and E.-H. Yang, "A critical review of geopolymer properties for structural fire-resistance applications," Constr Build Mater, vol. 221, pp. 514–526, Oct. 2019, doi: 10.1016/J.CONBUILDMAT.2019.06.076.

[28] C. Jiang, A. Wang, X. Bao, T. Ni, and J. Ling, "A review on geopolymer in potential coating application: Materials, preparation and basic properties," Journal of Building Engineering, vol. 32. 2020. doi: 10.1016/j.jobe.2020.101734.

[29] S. Moutinho et al., "Assessment of properties of metakaolin-based geopolymers applied in the conservation of tile facades," Constr Build Mater, vol. 259, p. 119759, Oct. 2020, doi: 10.1016/J.CONBUILDMAT.2020.119759.

[30] M. Panizza, M. Natali, E. Garbin, S. Tamburini, and M. Secco, "Assessment of geopolymers with Construction and Demolition Waste (CDW) aggregates as a building material," Constr Build Mater, vol. 181, pp. 119–133, Aug. 2018, doi: 10.1016/J.CONBUILDMAT.2018.06.018.

[31] B. Panda, S. C. Paul, L. J. Hui, Y. W. D. Tay, and M. J. Tan, "Additive manufacturing of geopolymer for sustainable built environment," J Clean Prod, vol. 167, 2017, doi: 10.1016/j.jclepro.2017.08.165.

[32] J. Liu and C. Lv, "Properties of 3D-Printed Polymer Fiber-Reinforced Mortars: A Review," Polymers, vol. 14, no. 7. 2022. doi: 10.3390/polym14071315.

[33] A. B. Abulencia et al., "Geopolymers as sustainable material for strengthening and restoring unreinforced masonry structures: A review," Buildings, vol. 11, no. 11. 2021. doi: 10.3390/buildings11110532.

[34] Comité Européen de Normalisation, NP EN 933-1 Tests for geometrical properties of aggregates - Part 1: Determination of particle size distribution - Sieving method. CEN members: CEN, 1997, p. 16.

[35] J. Lanas, J. L. P. Bernal, M. A. Bello, and J. I. A. Galindo, "Mechanical properties of natural hydraulic lime-based mortars," Cem Concr Res, vol. 34, no. 12, pp. 2191–2201, 2004, doi: 10.1016/j.cemconres.2004.02.005.

[36] J. Grilo, A. Santos Silva, P. Faria, A. Gameiro, R. Veiga, and A. Velosa, "Mechanical and mineralogical properties of natural hydraulic lime-metakaolin mortars in different curing conditions," Constr Build Mater, vol. 51, pp. 287–294, 2014, doi: 10.1016/j.conbuildmat.2013.10.045.

[37] S. Xu, J. Wang, and Y. Sun, "Effect of water binder ratio on the early hydration of natural hydraulic lime," Mater Struct, vol. 48, pp. 3431–3441, 2015, doi: 10.1617/s11527-014-0410-8.

[38] B. Ferreira et al., "Tensile strain hardening of a metakaolin-based fibre reinforced composite," in 7th International Conference on Safety and Durability of Structures - ICOSADOS 2016, Vila Real, Portugal, 2016.

[39] M. Ramesh, M. Azenha, and P. B. Lourenço, "Mechanical properties of lime–cement masonry mortars in their early ages," Materials and Structures/Materiaux et Constructions, 2019, doi: 10.1617/s11527-019-1319-z.

[40] K. Scrivener, R. Snellings, and B. (Eds.) Lothenbach, A Practical Guide to Microstructural Analysis of Cementitious Materials. CRC Press, 2016. doi: https://doi.org/10.1201/b19074.

[41] CEN, "EN 1015-3:1999 - Methods of Test for Mortar for Masonry - Part 3: Determination of consistence of fresh mortar (by flow table)," p. 10, 2007.

[42] Comité Européen de Normalisation, "EN 1015-11:1999 Methods of test mortar for masonry – Part 11: Determination of flexural and compressive strength of hardened mortar." Brussels, 1999.

[43] Rilem TC 129-MHT, "Compressive strength for service and accident conditions," Mater Struct, vol. 28, no. 4, pp. 410–414, May 1995, doi: 10.1007/BF02479330.

[44] C. A. Rosas-Casarez and S. P. Arredondo-Rea, "Experimental study of XRD, FTIR and TGA techniques in geopolymeric materials," Proceedings of the, 2014, doi: 10.1111/j.1440-1843.2008.01456.x.

[45] N. Banthia and S. Mindess, "Toughness Characterization of Fiber-Reinforced Concrete: Which Standard to Use," J Test Eval, vol. 32, no. 2, p. 11901, 2004, doi: 10.1520/JTE11901.

[46] JSCE, "JSCE-SF4 Method of tests for flexural strength and flexural toughness of steel fiber reinforced concrete," 1984.

[47] M. C. Nataraja, N. Dhang, and A. P. Gupta, "Stress–strain curves for steel-fiber reinforced concrete under compression," Cem Concr Compos, vol. 21, no. 5–6, pp. 383–390, Dec. 1999, doi: 10.1016/S0958-9465(99)00021-9.

[48] P. Bhargava, U. K. Sharma, and Surendra. K. Kaushik, "Compressive Stress-Strain Behavior of Small Scale Steel Fibre Reinforced High Strength Concrete Cylinders," Journal of Advanced Concrete Technology, vol. 4, no. 1, pp. 109–121, 2006, doi: 10.3151/jact.4.109.

[49] S. J. Jang and H. Do Yun, "Combined effects of steel fiber and coarse aggregate size on the compressive and flexural toughness of high-strength concrete," Compos Struct, vol. 185, pp. 203–211, 2018, doi: 10.1016/j.compstruct.2017.11.009.

PAPER III

ASSESSMENT OF THE PROPERTIES TO CHARACTERIZE THE INTERFACE BETWEEN CLAY BRICK SUBSTRATE AND STRENGTHENING MORTAR

REFERENCE: Almeida, J. A. P. P., Bordigoni, D., Pereira, E. N. B., Barros, J. A. O., Aprile, A. Assessment of the properties to characterize the interface between clay brick substrate and strengthening mortar. Construction and Building Materials 2016; 103, 47-66. http://dx.doi.org/10.1016/j.conbuildmat.2015.11.036.

ABSTRACT: The behaviour of masonry elements under in-plane and out-of-plane loads can be improved through the application of strengthening systems based on reinforcing overlays. After strengthening, the transition region between the original substrate and the strengthening layer is especially stressed, and premature failure of the strengthened masonry is reached if insufficient interfacial capacity is assured. Therefore, the assessment of the mechanical behaviour of the interface is critical to the development of the masonry strengthening system based on the application of strengthening overlays. In this research a method for the characterisation of the interface behaviour between two different materials, a polypropylene fibre reinforced mortar (PFRM) and a ceramic brick used for masonry construction is presented. Direct shear tests were carried out in couplet specimens. Due to the orthotropic nature of the bricks surface, the shear load was applied along three different

directions in order to perform an overall estimation of the interface behaviour. The peak and residual shear stresses, as well as the failure modes, were obtained at different levels of the normal stress. Based on these experimental results constitutive laws were assessed for the simulation of the interface mechanical behaviour based on the Mohr and Mohr-Coulomb failure criteria.

KEYWORDS: Direct shear test; Failure criteria; Interface behaviour; Masonry strengthening overlay; Shear response

Nomenclature:

FRCM fabric reinforced cementitious matrix

PFRM polypropylene fibre reinforced mortar used in the FRCM system

A_{eff} effective interface area between the two units

c cohesion

$c_{0,p}^{*}$ initial apparent cohesion

c_{p}^{*} peak apparent cohesion

$\emptyset_{0,p}$ initial friction angle

$\emptyset_{p}$ friction angle

μ tangent of friction angle

N vertical load

τ shear stress

τ_{p} peak tangential stress

τ_{r} residual tangential stress

$\tau_{crit,i}$ tangential values estimated by the criterion

$\tau_{exp,i}$ tangential experimental values

$\bar{\tau}_{exp}$ tangential mean value of the experimental results

T_p peak horizontal load

T_r residual horizontal load

σ normal stress

χ tensile strength

χ' residual tensile strength

1 INTRODUCTION

Masonry was one of the main techniques used in the construction of old structures and still is widely used in new buildings. Nevertheless, it is in the case of already existing buildings that masonry often plays a key role as a structural component. The evolution of the design codes has tended to impose more demanding requirements, especially in the case of the action in seismic regions. Consequently, due to this and other durability driven performance insufficiencies, techniques to retrofit existing masonry constructions have recently been developed, and their performance evaluated. These techniques aim to fulfil higher demands in terms of load bearing capacity and increase the ductility response of masonry elements.

A considerable number of strengthening techniques are nowadays based on the application of reinforcing overlays. These systems often show vulnerability at the level of the interface due to the sharp gradient of mechanical properties between the substrate and the reinforcing material [1]. This work presents an experimental program developed with the aim of characterizing the mechanical properties of the interface between a polypropylene fibre reinforced mortar (PFRM) strengthening overlay, which is part of a FRCM based masonry strengthening system, and a masonry substrate. The results obtained were used to derive the orthotropic constitutive laws of the interface based on both the hyperbolic Mohr and the Mohr-Coloumb failure criteria.

1.1. Overlay strengthening techniques

Additional strengthening overlays can be applied to existing masonry with the aim of improving its structural behaviour. This technique is of special importance in areas of high seismic activity, as a

means to comply with the current code requirements in terms of resistance to horizontal loading, in particular the seismic action. Typically, the strengthening overlay can be applied manually or mechanically and is composed by a cement mortar matrix and a reinforcing mesh. The tensile and ductility behaviour of the strengthening overlay is improved by using fibres and meshes made of steel, polymers, carbon or glass [2-8]. The application of these reinforced strengthening overlays improves both the in-plane and the out-of-plane load carrying capacity of the masonry [9]. Alternatively, the overlay strengthening system can be composed of materials showing tensile strain-hardening behaviour in the hardened state, avoiding the use of reinforcement meshes. These materials, typically designated as strain hardening cementitious composites (SHCC), reach tensile strengths higher than the stress at crack initiation, and ultimate tensile strains clearly exceeding 1%. These materials typically develop diffuse crack patterns while loaded in tension, and the maximum crack width remains controlled typically below a maximum of 0.1 mm in the hardening phase. SHCC materials can be applied using the shotcreting technique or manually [10-11]. SHCC based strengthening systems can lead to the increase of the shear capacity of the masonry, to the improvement of its deformability and to the enhancement of its energy dissipation capacity during cyclic loading [12].

Some of the advantages and disadvantages of the masonry strengthening techniques that are based on the addition of strengthening overlays to the original masonry element are presented by Elgaway et al. [2], [13]. The advantages identified include the low cost, the durability, the uniform behaviour, the increase of in-plane strength up to 3.6 times, the improvement of the out-of-plane stability, and the increase of the energy dissipation ability before failure. The increase of the dead weight of the strengthened elements, the requirement of surface treatments, the architectural changes of the structure, and the high disturbance during works are the main disadvantages identified [2], [13].

1.2. Experimental characterization of the interface behaviour

1.2.1. Test setups

The mechanical response of the interface between different materials subjected to shear loads is an important topic both in the design of new construction and in the rehabilitation of existing structures [14-16]. Regarding the interface properties of masonry substrates, several authors have conducted research on the assessment of the shear force-slip response of the interface between units [17-21]. The testing schemes used to perform the experiments are diverse, mainly regarding the specimen's geometry, boundary conditions and loading configurations adopted during testing. Some of the most

popular loading arrangements and specimen geometries are presented by Van Der Pluijm [22] and Montazerolghaem et al. [23]. Although distinct loading arrangements have been tried, introducing a pure shear stress distribution in a joint is nearly impossible, as well as to achieve a totally uniform shear and normal stress distribution along the interface [22].

The characterization of the shear behaviour of mortar joints according to the standard EN1052-3 [24] is carried out by performing the triplet tests. However, according to Hofmann et al. [25] and Montazerolghaem et al. [23], this test setup induces local stress concentrations, as shown in **Figure III.1**. The approximated normal and the shear stresses were obtained using linear finite element analysis. These stress concentrations directly disturb the evenness of stress distribution in both ends of the mortar joint. The failure modes show a clear trend for the occurrence of stepped crack, which can introduce unwelcomed rotations, as reported by Lourenço et al. [26].

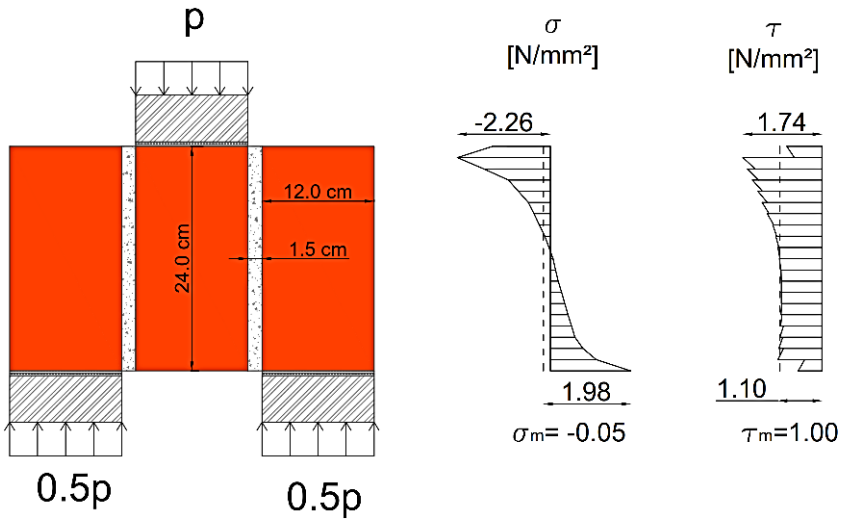


Figure III.1: Triplet test Shubert arrangement, adapted from [25].

The numerical evaluation performed by Hofmann et al. [25] shows that the couplet setup of Hofmann, presented in **Figure III.2** leads to a better approximation of a uniform shear stress distribution along the joint than other test setups. Nevertheless, the test setup is too complex to adopt as standard method. A simplified version of this test setup is presented by DIN, see **Figure III.3** leading to an almost uniform shear stress, even if an appreciable uneven normal stress distribution occurs at the joint.

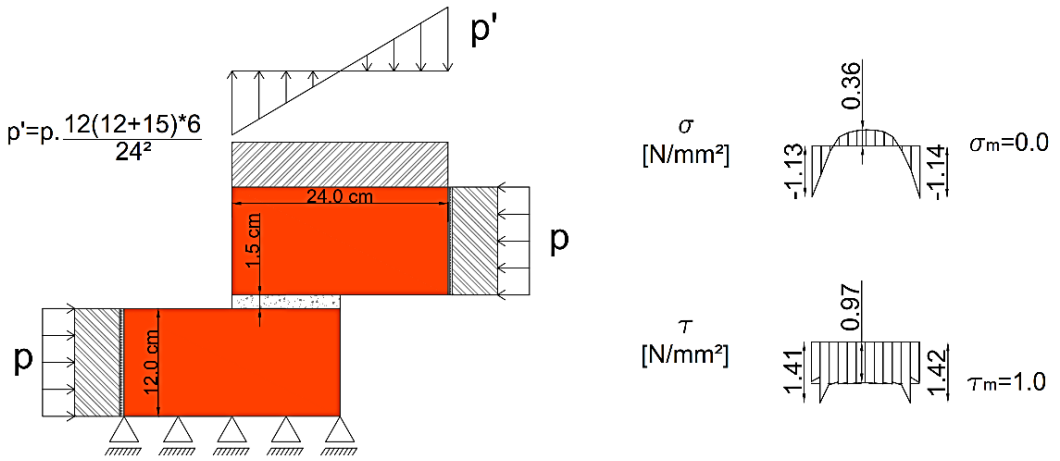


Figure III.2: Couplet test Hofmann arrangement, adapted from [25].

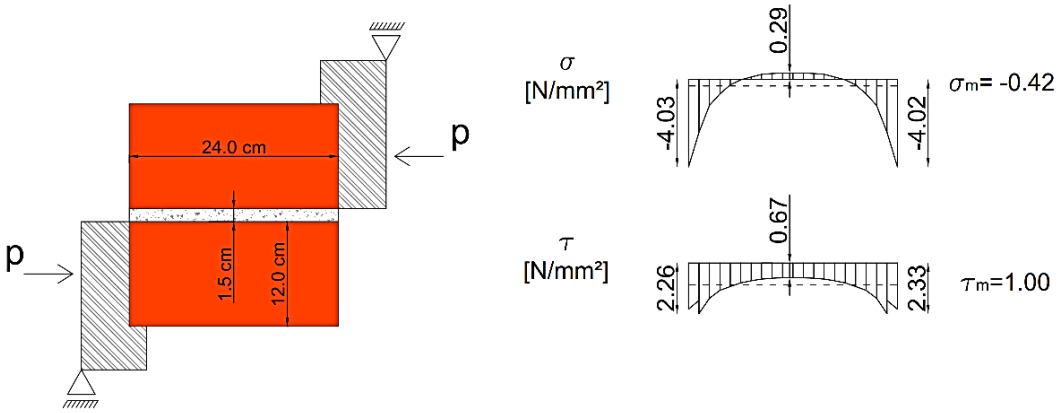


Figure III.3: Couplet test DIN arrangement, adapted from [25.

An alternative shear test setup proposed by Vasconcelos and Lourenço [18] also uses a specimen with two units, see **Figure III.4**. In this case the specimen is placed between two thick steel plates and attached to the steel plates by steel bolts, so that the shear force can be transmitted to the specimen. Thin steel sheets are attached to the steel plates to concentrate the shear load as close as possible to the bed joint, aiming to prevent bending moments and to provide a more uniform shear stress distribution. In addition, two thin sheets of Teflon are placed between the steel plates and the specimens to minimize bending effects due to friction.

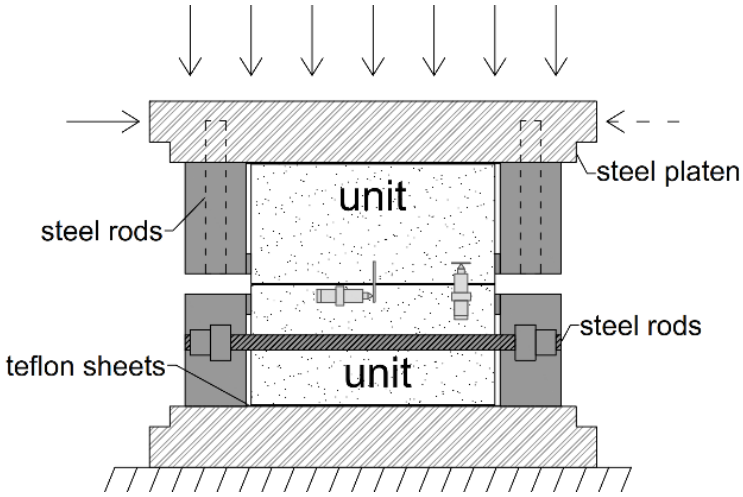


Figure III.4: Test setup used to perform cyclic direct shear tests, adapted from [18].

1.2.2. Data derived from the tests

The values of the two strength parameters, cohesion c or f_{v0} as described by EN 1052-3 [24], and the tangent of the friction angle $\mu = \tan \varphi$, for different types of interfaces obtained by triplet and couplet tests are presented in **Table III.1**.

Table III.1: Strength parameters for different types of interfaces.

Source	Type of test	Interface	c (f_{v0}) (N/mm²)	μ
Lourenço et al. [26]	Triplet	Concrete brick /Micro-concrete	1.39	1.03
Gabor et a. [27]	Triplet	Ceramic brick/Cement mortar	1.60	0.90
Alecci et al. [19]	Triplet	Ceramic brick/Cement mortar	0.53	–
Vasconcelos and Lourenço [28]	Couplet	Granite/Lime mortar	0.36	0.63
Abdou et al. [20]	Couplet	Ceramic brick/Cement mortar	1.61	1.05

1.3. Mohr and Mohr Coulomb failure criteria

The shear strength and shear force-slip response at the interface between the masonry substrate and the strengthening overlay is not unique, but dependent on the level of normal stress applied. In general, the material strength under a multiaxial stress state may be considered as a function of that stress state, and cannot be determined exclusively by either the tensile, the compressive or the shearing stresses independently of each other. A considerable number of failure criteria has been proposed, [29], assuming this consideration. The most commonly used in the case of isotropic materials is the Mohr criterion, which states that failure is governed by the following relation, see **Eq. (III.1**):

$$|\tau| = f(\sigma) \quad \textbf{(III.1)}$$

where the local shear strength, τ, considering a specific plane, is dependent only on the normal stress, σ, at the same plane.

The **Eq. (III.1**) represents the failure envelope of the corresponding Mohr circles considering all possible stress states. The envelope f(σ) can assume different shapes and can be determined experimentally. Considering the case of a hyperbolic shape, the simplest case is described by the **Eq. (III.2**) [30]:

$$f(\sigma) = \pm\sqrt{(c - \sigma \times tan\,\emptyset)^2 - (c + \chi \times tan\,\emptyset)^2} \quad \textbf{(III.2)}$$

where χ is the tensile strength, c the cohesion and $\emptyset$ the friction angle.

According to the Mohr's criterion, the material failure will occur at all states of stress for which the largest of Mohr's circles is tangent to the envelope.

An alternative and simpler shape of the Mohr envelope was proposed by Coulomb and is characterized by one straight line, as shown in **Figure III.5**, and represented by **Eq. (III.3**) [31].

$$f(\sigma) = c - \sigma \times tan\,\emptyset \quad \textbf{(III.3)}$$

The Mohr-Coulomb criterion is often preferred to describe the experimental results of mechanical tests on interfaces [20], [26], [28]. On the other hand, the use of Mohr hyperbolic criterion is not so common due to its additional complexity. Examples of its use on numerical modelling can be found in [32] and [33].

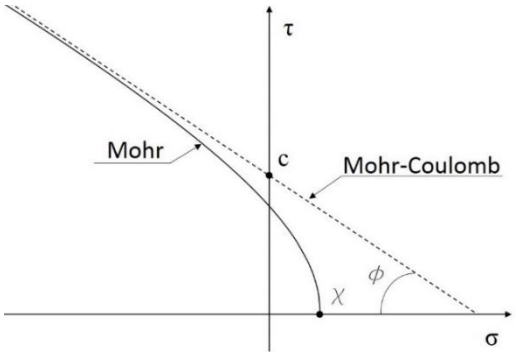


Figure III.5: Schematics of Mohr-Coulomb and Mohr failure criteria for positive tangential stresses.

2 OBJECTIVES AND RESEARCH SIGNIFICANCE

The determination of the mechanical properties of the interface between masonry substrates and PFRM strengthening overlays is regarded as essential for the optimisation of the performance of the FRCM strengthening system considered, since the interface is typically one of the weakest links in the system. Therefore, this research is dedicated to experimentally characterise the mechanical response of the interface between the masonry substrate and the strengthening overlay by performing direct shear tests. Therefore, this research is dedicated to the experimental characterisation of the mechanical response of the interface between the masonry substrate and the strengthening overlay by performing direct shear tests. In addition, the applicability of the analytical Mohr and the Mohr-Coloumb loading/failure criteria to approximate or predict the experimental results are discussed. These results may constitute an important step for the development of a constitutive model that represents the interface behaviour for general states of stress or deformation.

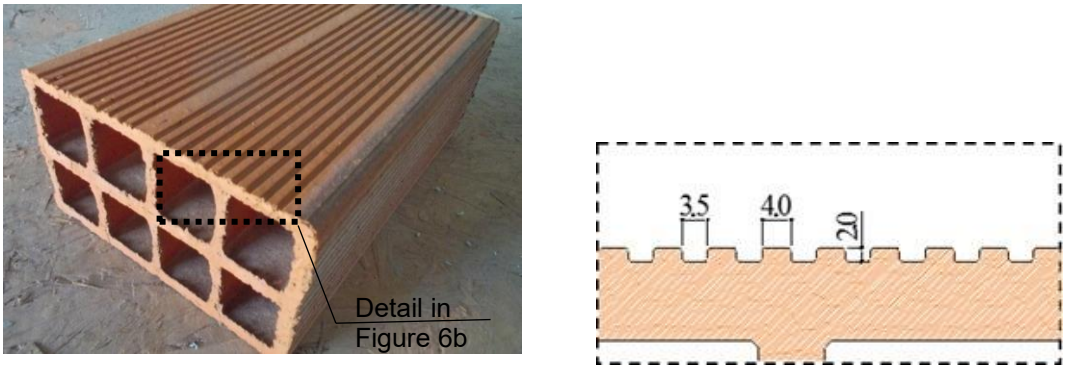
3 MATERIALS AND METHODS

3.1. Characterization of materials

The mechanical properties of the materials used to assemble the specimens tested in direct shear were characterized. The ceramic bricks were tested in compression, while PFRM specimens in the hardened state were tested in compression and flexure. The PFRM specimens were casted from the same mixtures used to produce the specimens for the direct shear tests. This procedure allowed to determine the properties of all mixtures used in the direct shear tests, since the curing conditions and the compositions were kept the same.

3.1.1. Characterization of ceramic brick

The type of ceramic brick selected, with 8 hollow cells, is regionally common, and is represented in **Figure III.6**. The dimensions are 30 × 20 × 11 cm3, respectively the length, width and thickness. The compressive strength of the ceramic brick was obtained by following the experimental procedure proposed by EN 772-1 [34]. The tests were carried out under load control, with the loading direction at perpendicular and parallel relatively to the holes longitudinal axis, with the application of a load rate of 1.10 and 1.65 kN/s, respectively. The average compressive strength and coefficient of variation obtained for 6 specimens in both cases were 2.21 (9 %) MPa, and 6.55 (8 %) MPa, where the value in round brackets is the coefficient of variation.



a) b)

Figure III.6: Ceramic brick used to mount the specimens: a) ceramic brick; b) detail of grooves, dimensions in mm.

3.1.2. Characterization of the PFRM in the hardened state

To characterize the evolution of the mechanical properties of the PFRM in the hardened state, three different curing ages were considered, 28, 56 and 84 days. For each curing age 12 specimens were tested in bending and 24 were tested in compression. All mixtures of PFRM were prepared using the same amount of water. The weight ratio of *water/dry material* was set to 0.14, considering that the dry material includes the binder, polymer fibres, aggregates and additives, as provided by the manufacturer of the pre-packed mixture.

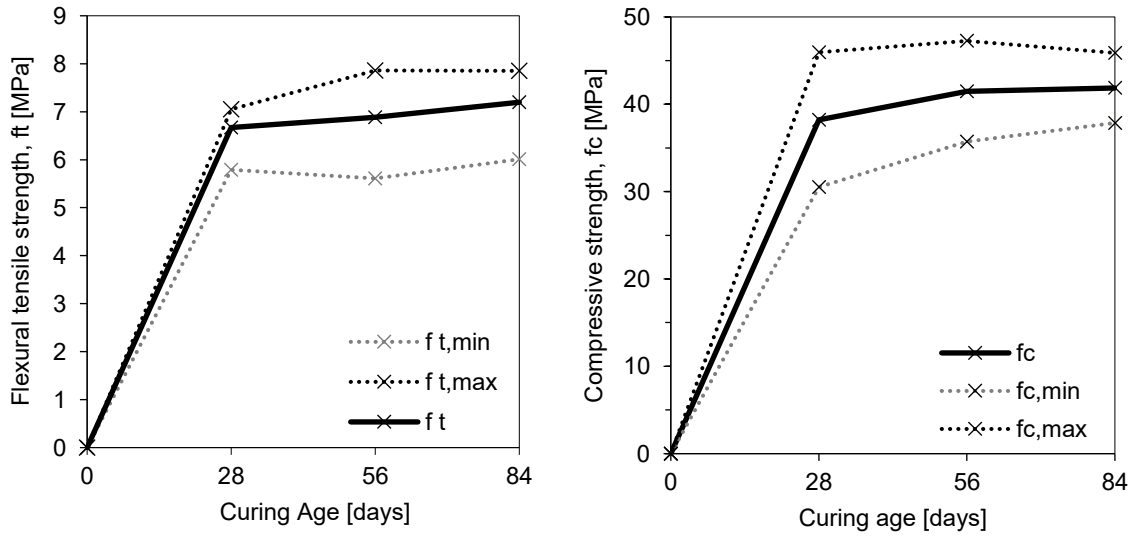
Specimens with dimensions of 160 x 40 x 40 mm3 were tested in bending by adopting the procedure described in EN 1015-11 [35] for three point bending tests (TPB). The tests were carried out under displacement control by applying a constant displacement rate at mid-span equal to 2.5 μm/s. The compressive tests of the PFRM followed the procedure proposed by EN 1015-11 [35] according to

which from each tested TPB specimen two specimens with dimensions of 40 x 40 x 70 mm2 were obtained. The 24 specimens were tested under load control, by imposing a loading rate equal to 0.4 kN/s. The maximum load obtained was registered to calculate the compressive strength.

The mean values of the compressive strength and of the equivalent tensile strength in flexure, f_c and f_{ft}, as well as the corresponding coefficients of variation, are presented in **Table III.2** for the different curing ages. The evolutions of the minimum, maximum and average values of the compressive strength and the equivalent tensile strength in flexure with respect to the curing age are shown in **Figure III.7**. The average tensile strength in flexure exceeded 6 MPa before 28 days, whereas the average compressive strength exceeded 40 MPa slightly before the 56 days. After 28 days of curing these properties seem do not alter significantly.

Table III.2: Summary of experimental results.

Curing age	Flexural Tensile Strength		Compressive Strength	
	f_t	CoV	f_c	CoV
(days)	(MPa)	(%)	(MPa)	(%)
28	6.59	6.5	38.22	16.1
56	6.93	10.8	41.49	11.1
84	6.95	8.6	41.87	4.8

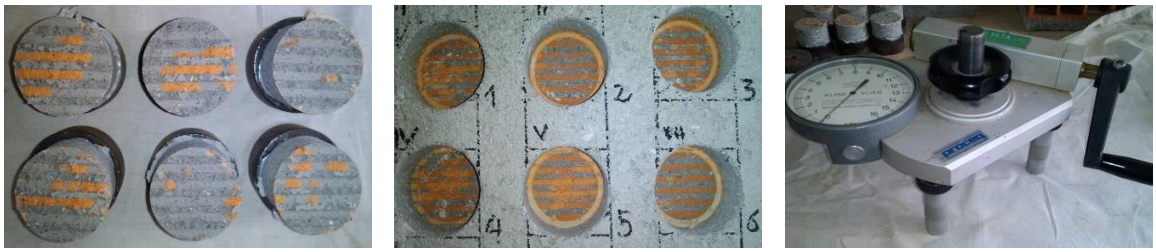


a) b)

Figure III.7: Evolution of the hardened state properties of the PFRM: a) equivalent tensile strength in flexure vs curing age; b) compressive strength vs curing age.

3.1.3. Pull-off of mortar patch from ceramic brick

The adhesion strength between the mortar and the ceramic brick was assessed by means of pull-off tests according the standard EN 1015-12, [36]. The specimens with 30 x 20 x 13.5 cm^3 were produced and cured at constant temperature and relative humidity of approximately 20 °C and 90 %, respectively. The preparation of the samples for testing started with the execution of a circular slot with 50 mm diameter, using a core drilling machine. After cleaning the surface, a metallic plate was bonded to the test area using an epoxy resin. The metallic plate was later attached to the pull-off machine, a Proceq- Z15, which has a maximum traction force of 16 kN, a free course of 3.5 mm and an accuracy greater than 98 %. The test procedure consisted of applying a traction force to the mortar surface through the circular plate. After the initial levelling of the equipment, the increasing traction force was applied at a constant loading rate of 40 N/s. The maximum force recorded corresponds to the adhesion force. The pull-off tests were carried out at 28 days after casting. The adhesive strength between the mortar and the ceramic brick was estimated using the contact area of each specimen, see **Figure III.8**. Based on the results of 16 tested specimens, an average adhesion strength of 0.6 MPa and a coefficient of variation equal to 14 % were obtained.



a) b) c)

Figure III.8: Pull-off test: a) detached PFRM layer; b) surface of the bricks after testing; c) pull-off device.

3.2. Preparation of the specimens for the direct shear tests

In order to consider the orthotropic characteristics of the brick surface, with a pattern composed of grooves in one direction, three shear loading orientations were investigated for assessing the interface shear behaviour and its relation to the loading direction with respect to the brick surface pattern (0 °, 45 ° and 90 °, see **Figure III.9**.

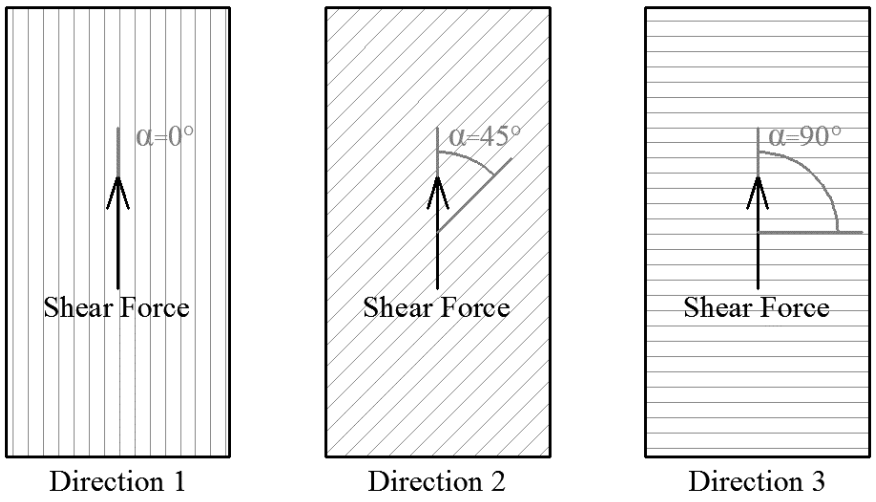


Figure III.9: Representation of the loading directions investigated.

In **Table III.3** the labels of all specimens for each batch of PFRM are shown, as well as the curing age when tested. The number of specimens tested for each of the three loading directions, 0 °, 45 ° and 90 °, was defined considering the need to identify the most appropriate failure criterion to describe the observed experimental responses.

Table III.3: Summary of the samples tested for each mortar batch.

Mix	Curing age	Samples
1	56 days	A1, A2, A4, B1, B3, D4
2	56 days	E1, E4, F1, F2, F3, F4, G2, G3, G4, H2, H3, I1, L1, L2, L3, L4, M1, M2, P1, P2, P3
3	28 days	N1, N2, Q1, Q2, R1, R2, R3, S2

The initiation and propagation of the shear crack along the interface plane was assured by means of two notches executed along the longer faces of the specimens. In this fashion, the effective contact area between the two units was decreased to 60 % of the initial area at this localization region. The sequence of steps carried out for the preparation of the specimens is detailed in **Figure III.10** and described subsequently:

- cutting of the bricks in two parts to obtain the surface for testing, **Figure III.10a)**;
- casting of the mould containing the brick part with the PFRM to create a compact and regular unit with a height of 80 mm, **Figure III.10b)**;
- removing of the framework after one week and turning the unit upside down, **Figure III.10c)**;

- pouring the PFRM fresh mortar on top of the existing unit, **Figure III.10d)**;
- cutting the specimens to obtain four or three specimens from each prism depending on the testing direction, **Figure III.10e)**;
- execution of two notches in both lateral longitudinal faces to impose the formation of the failure surface along the interface between the two materials **Figure III.10f)**;
- measurement of the effective dimensions of the specimens and labelling **Figure III.10f)**.

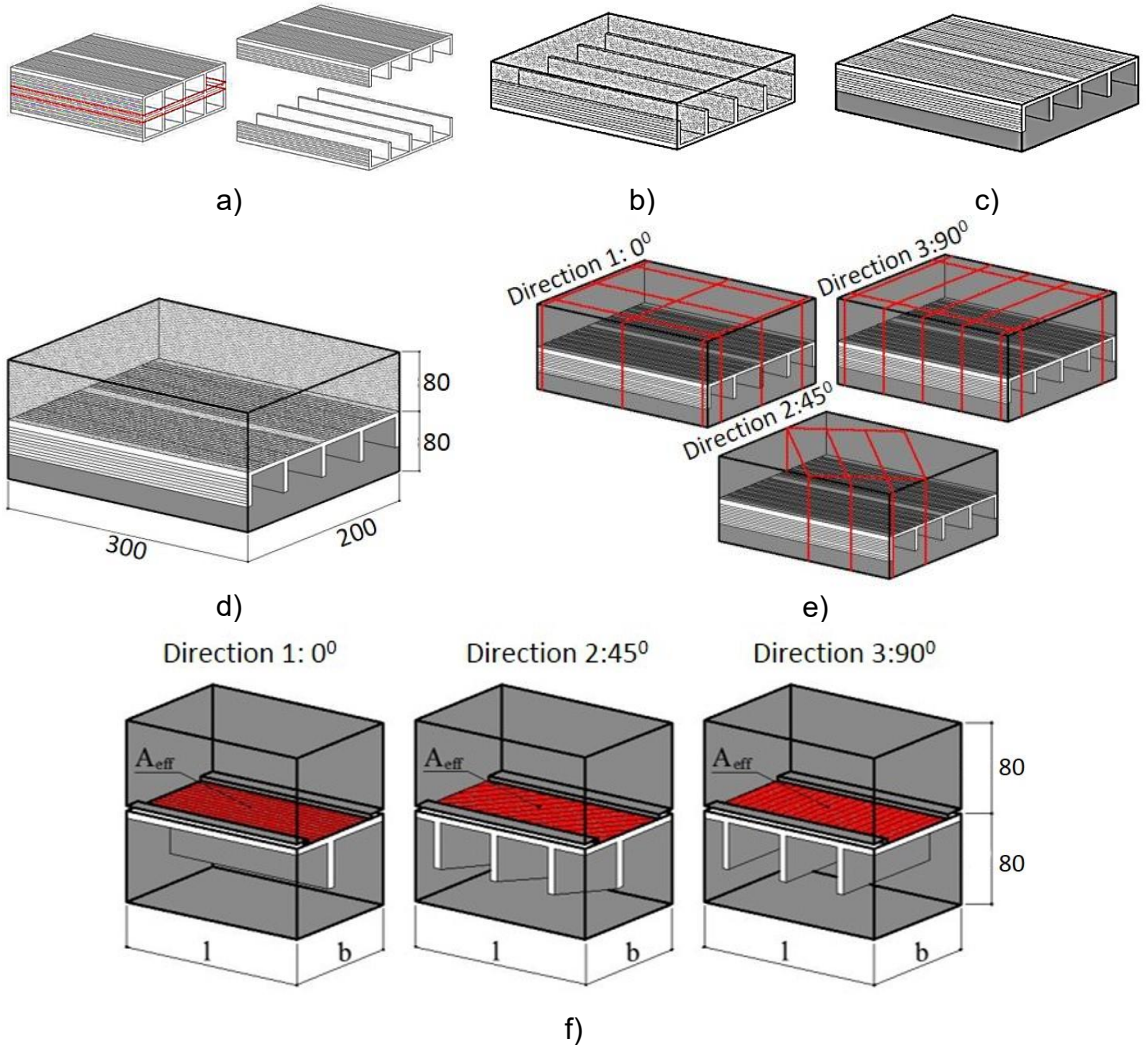


Figure III.10: Preparation of specimens: a) cutting the bricks; b) pouring mortar to create a compact and regular unit; c) demoulding and turning the unit upside down d) brick samples after casting; e) detailing of the cutting lines for obtaining the final specimens; f) final preparations on the specimens, including the execution of the lateral notches. Dimensions in mm.

3.3. Test setup and procedures

The stiffness of the reaction frame was checked before starting the tests. Shear tests are typically brittle, therefore the reaction frame must be stiff enough to allow the capturing of the softening part of the shear response in a controlled manner. Thus, one cycle of loading, up to 32 kN, and unloading was applied directly on the reaction system, since in preliminary tests was verified that the samples have reached peak shear forces in the interval 10 to 25 kN. The elastic response of the reaction frame revealed a maximum displacement, measured by two transducers and averaged, equal to 55 μm at a maximum load of 32 kN, corresponding to a constant stiffness of K=590 kN/mm.

The test setup is shown in **Figure III.11** and **Figure III.14**, where the A-unit represents the part of the specimen composed of the PFRM exclusively, whereas the B-unit represents the part of the specimen that contains the brick element. The horizontal displacement of the B-unit was constrained by means of a rigid support on the opposite side of the actuator in order to impose a relative sliding between the two units.

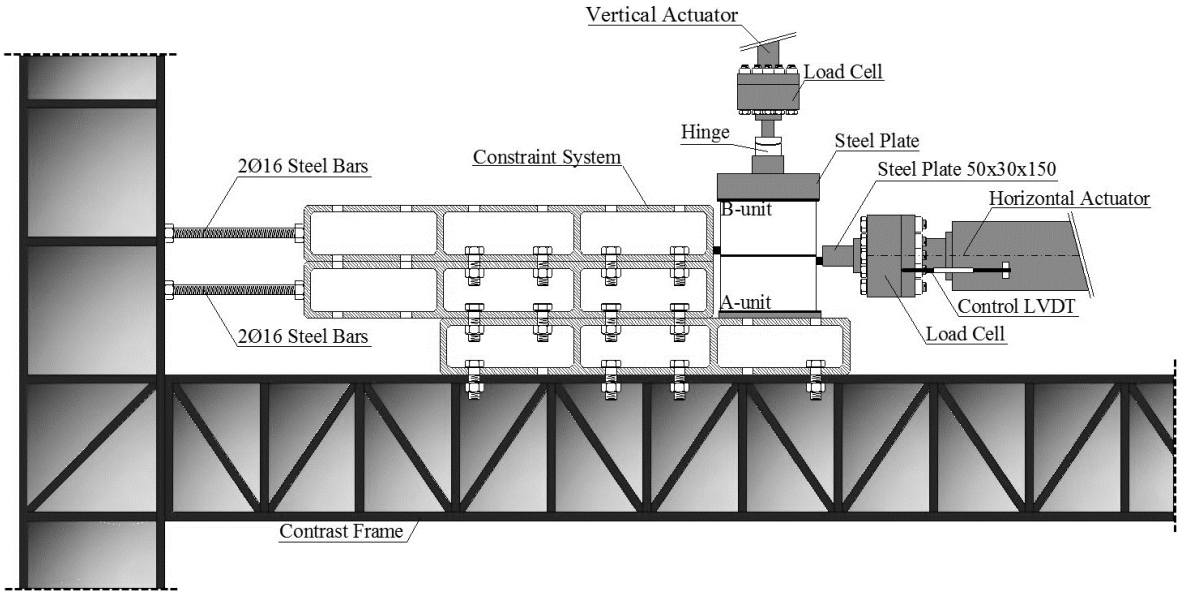


Figure III.11: Test setup global view.

To minimize the vertical distance between the load applied in the horizontal direction and the reciprocal reaction, and therefore minimize the moment causing the rotation of the specimen, a steel bar with the dimensions of 10 x 10 x 150 mm^3 was placed at the loaded surface of each unit, between the specimen and the actuator crosshead, and between the specimen and the reaction frame as well, see **Figure III.12**. By minimizing the distance between the imposed force and corresponding reaction, also the bending moment at the interface, which is responsible for modifying the normal

stress distribution, was minimized. Furthermore, two layers of thin aluminium plates, with a Teflon sheet in-between, were placed on the top and on the bottom of the specimen to minimize the tangential stresses on the external surfaces (**Figure III.12**).

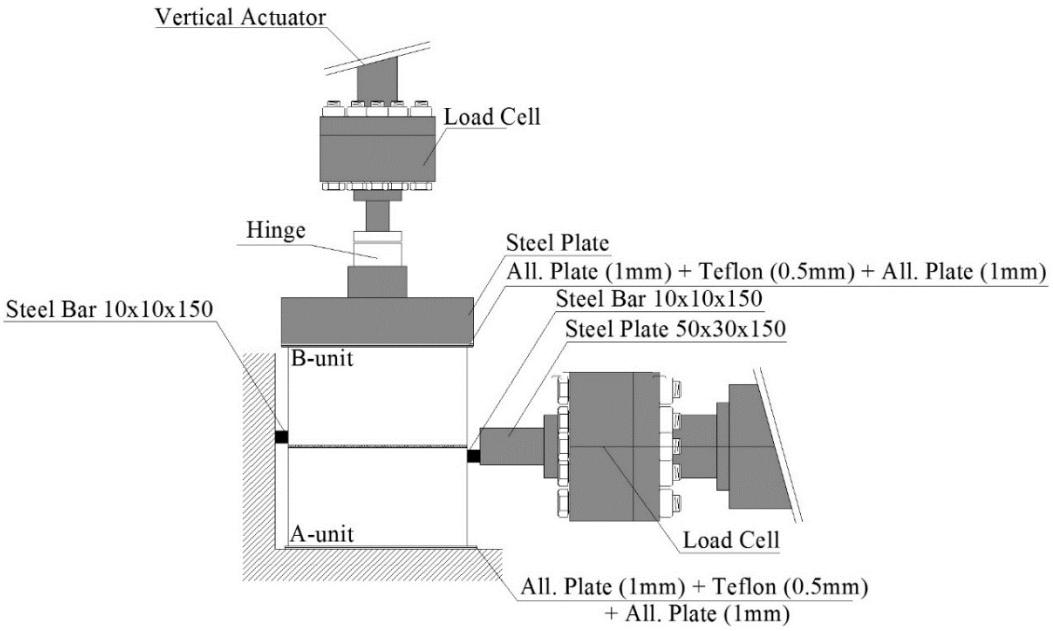
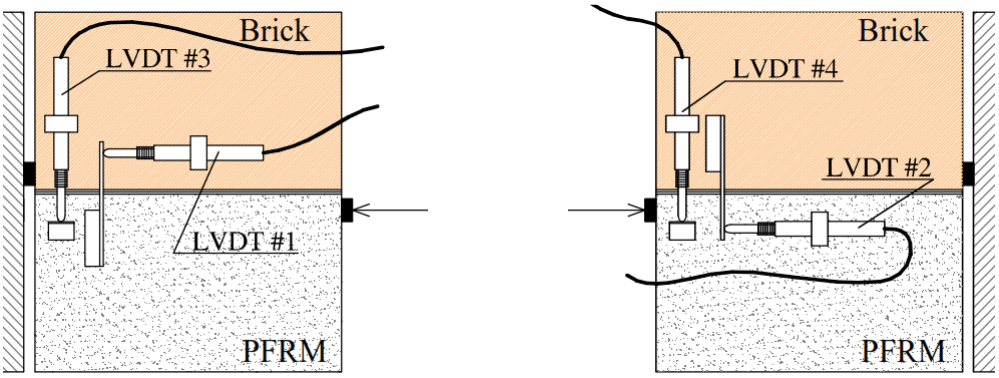


Figure III.12: Detail of the setup developed for the direct shear test.

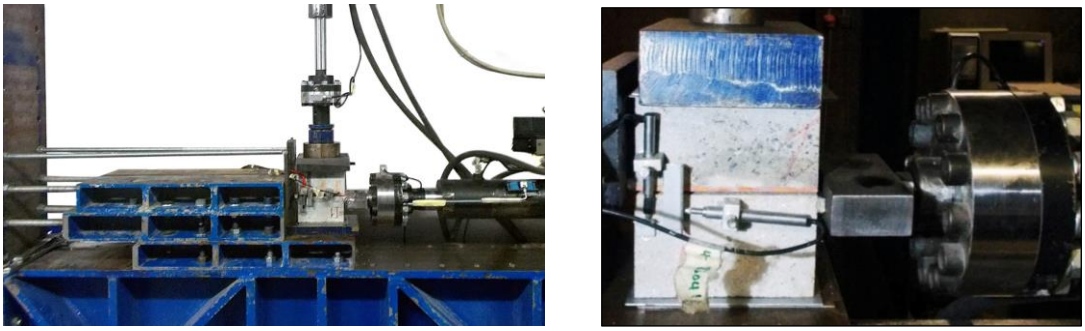
The testing procedure adopted consisted of imposing a controlled displacement in the horizontal direction at a constant load in the vertical direction. The horizontal displacement rate was 0.001 mm/s until reaching 0.6 mm, and subsequently 0.002 mm/s until the end of the test. The vertical actuator was used to apply the constant vertical load by means of a hinge and a rigid steel plate to distribute evenly the load on the top surface of the specimen.

Four linear variable displacement transducers (LVDT) were installed on both unloaded faces of the specimen (front and rear faces of the specimen) for monitoring the relative vertical displacement and the sliding between the two units. The transducers were positioned on the opposite corners of the samples, as shown in **Figure III.13**.



a) b)

Figure III.13: Position of LVDTs in the specimen: a) Front face, position of LVDT#1 and LVDT#3; b) Rear face, position of LVDT#2 and LVDT#4.



a) b)

Figure III.14: Setup of the direct shear test: a) general view; b) detail of the specimen during testing.

4 DIRECT SHEAR TEST RESULTS

4.1. Peak and residual shear stresses

The evaluation of the overall results was carried out in terms of the average values. The vertical stress, σ, the peak tangential stress, τ_p, and the residual tangential stress, τ_r, were calculated by means of the equations **Eq. (III.4**) to **Eq. (III.6**), respectively:

$$\sigma = \frac{N}{A_{eff}} \qquad \textbf{(III.4)}$$

$$\tau_p = \frac{T_p}{A_{eff}} \quad \textbf{(III.5)}$$

$$\tau_r = \frac{T_r}{A_{eff}} \quad \textbf{(III.6)}$$

where T_p and T_r are, respectively, the peak and the residual horizontal load measured by the load cell, N is the vertical load and A_{eff} is the effective area of contact between the two units.

The residual values of the tangential stress were considered equal to the tangential stress obtained when the slope of the tangential stress-slip response reached a minimum common value among all the specimens tested, as described subsequently. The experimental responses in terms of the tangential stress, τ, versus the slip, s, were linearized considering the slope for a constant slip increment equal to 0.01 mm, see **Eq. (III.7)**. In order to exclude the effect of the local scatter of the experimental results, the average slope, $\overline{K}t_{0.3mm}$, was evaluated by computing the central moving average for a slip of 0.3 mm considering $n = 30$, see **Eq. (III.8**). The maximum slope $\overline{K}t_{0.3mm}$ observed simultaneously in all the responses, -0.331 MPa/mm, was considered as the reference threshold for the evaluation of the residual tangential stress, τ_r.

$$Kt = \frac{\Delta\tau}{0.01\ mm} \quad \textbf{(III.7)}$$

$$\overline{K}t_{0.3mm} = \frac{\sum_{i=1}^{n} Kt_i}{n} \quad \textbf{(III.8)}$$

The results obtained for the different directions tested, 0 °, 45 ° and 90 ° orientation, are shown in **Table III.4**, where the PFRM mixtures used to cast the samples and the effective area, A_{eff}, are also indicated.

Table III.4: Experimental results.

Direction	Mix	Specimen	A_{eff} (mm^2)	σ (MPa)	τ_p (MPa)	τ_r (MPa)
1	1	A1	7342	0.23	3.35	0.48
		A2	5054	0.38	3.55	0.63
		A4	4847	0.45	3.89	0.73
		B1	6926	0.22	3.38	0.43
		B3	4992	0.46	4.16	0.78
		D4	5123	0.35	3.47	0.86
	2	E1	6028	0.36	3.82	1.04
		E4	5719	0.99	4.27	-
		F1	5764	2.04	5.52	3.13
		F2	4420	1.44	5.29	2.29
		F3	5940	1.50	5.19	2.17
		F4	5852	1.50	4.68	2.24
2	3	N1	5109	0.35	2.86	0.75
		N2	5016	0.26	2.94	0.40
	2	P1	4454	1.53	4.61	2.03
		P2	5412	0.15	2.50	0.80
		P3	4454	0.35	2.76	0.85
	3	Q1	4620	2.00	4.85	2.49
		Q2	4323	1.00	3.97	1.89
		R1	5320	0.35	3.05	0.80
		R2	5148	1.51	4.15	2.07
		R3	5280	0.25	2.74	1.01
		S2	4978	0.16	2.57	0.74
3	2	G2	5254	1.57	4.10	2.28
		G3	5720	0.35	2.76	1.06
		G4	5325	0.30	2.81	0.64
		H2	6580	0.97	3.69	1.89
		H3	5040	0.26	2.60	0.65
		I1	6248	0.25	2.47	0.85
		L1	4935	0.15	2.49	0.33
		L2	5076	0.16	2.39	-
		L3	4970	2.00	4.38	2.74
		L4	5396	1.50	4.40	2.66
		M1	4512	0.15	2.55	0.33
		M2	4230	0.36	2.91	0.41

In **Figure III.15**, **Figure III.16** and **Figure III.17** the tangential stress *versus* the average slip responses are shown for each level of the imposed vertical stress. The average slip was obtained by averaging the two horizontal transducers installed at the two opposite unloaded faces of the

specimens. The results obtained are divided into two groups, depending on the imposed normal stress during testing. The lower imposed normal stress results group include responses obtained for values below 0.5 MPa.

The $\tau - s$ responses obtained are essentially composed by three stages. The pre-peak stage is characterized by a linear rapid increase of the tangential stress for very low slip values, while the interface remains intact, and by a short non-linear branch immediately before the peak shear stress is reached. The second stage is composed by a post-peak branch that is characterized by a non-linear decrease of the load for an increasing value of the slip. The third stage is composed by the final softening branch that corresponds to a progressive reduction of the cohesion before the reaching of an approximately constant frictional resistance.

The results obtained showed that for higher normal stress the slip at peak increased and the overall response was more ductile. The dispersion of results obtained for direction 2 (45 º) was lower than the one registered for direction 1 (0 º).

The $\tau - s$ responses obtained for direction 3 (90º), see **Figure III.17**, reveal several local peaks in the softening branch. These results are explained by the fact that, for the 90° orientation series, the crack propagation along the interface was more progressive due to a sequential rupture of the brick ribs. A dispersion of results intermediate of the two previsous cases (0º and 45º) was obtained for the 90 º series.

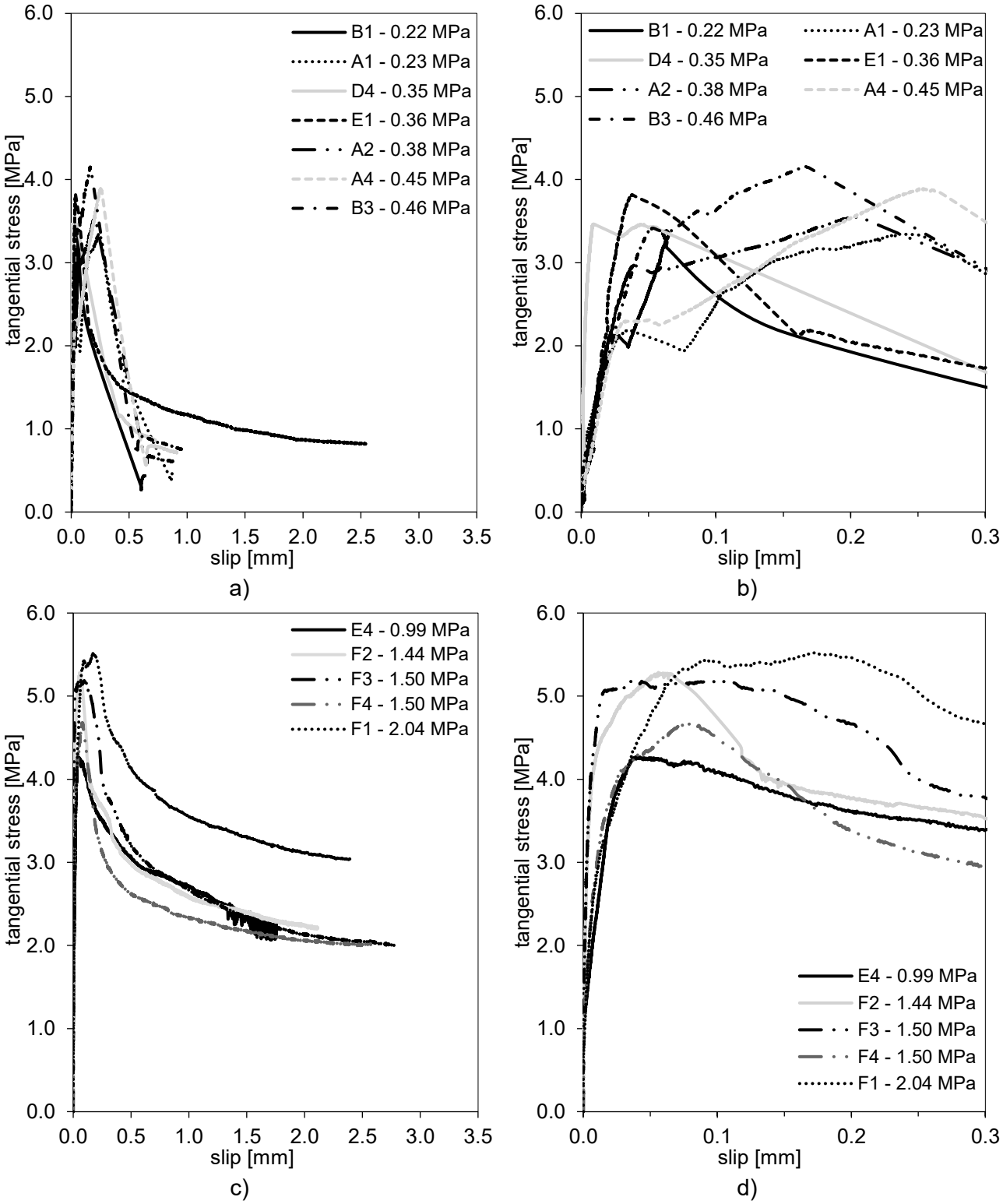


Figure III.15: τ-s responses for direction 1 (0 °): a) and b) responses for lower imposed normal stresses; c) and d) responses for higher imposed normal stresses; b) and d) detail of the initial stage up to an average slip of 0.3 mm.

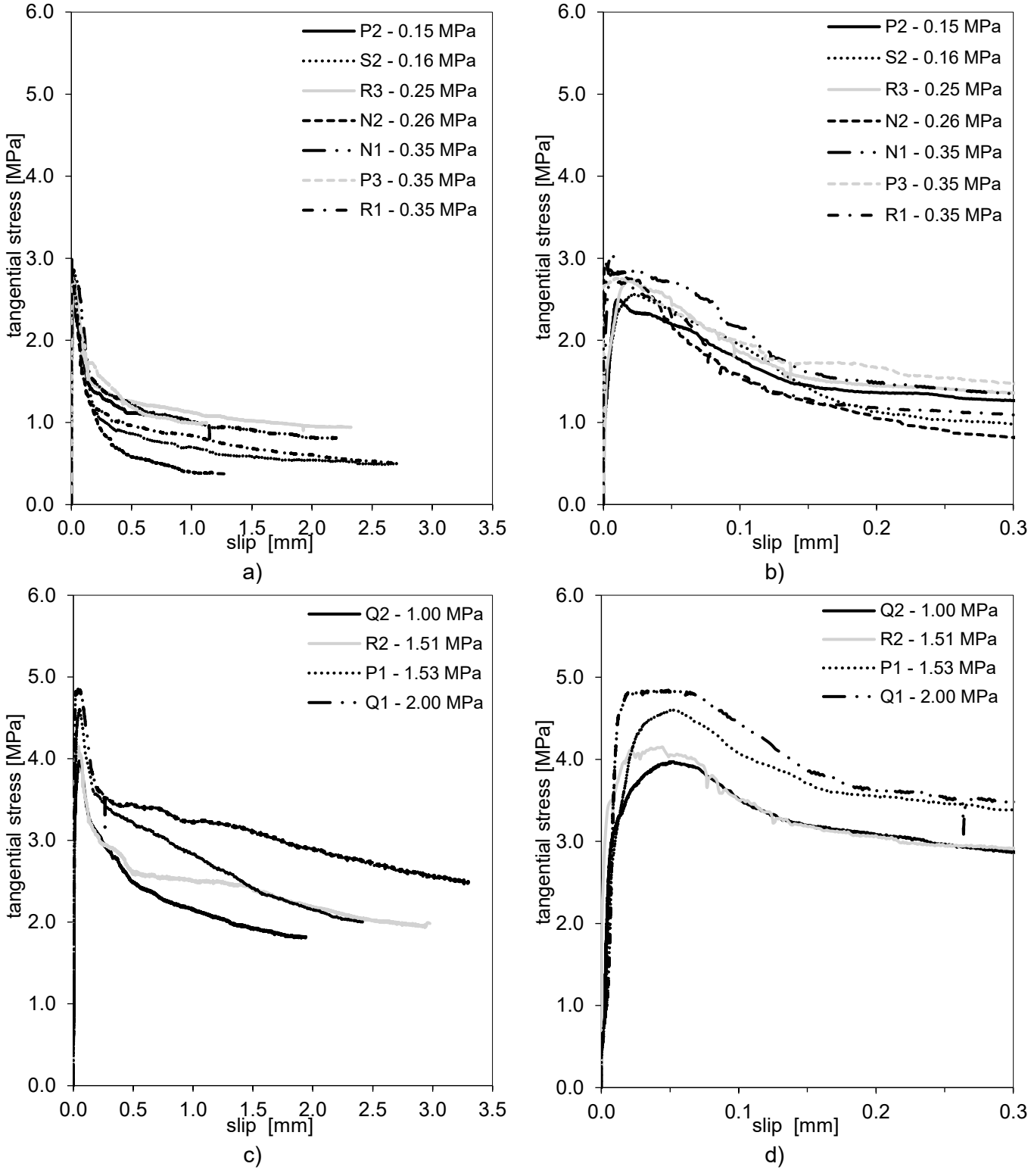


Figure III.16: τ-s responses for direction 2 (45 °): a) and b) responses for lower imposed normal stresses; c) and d) responses for higher imposed normal stresses; b) and d) detail of the initial stage up to an average slip of 0.3 mm.

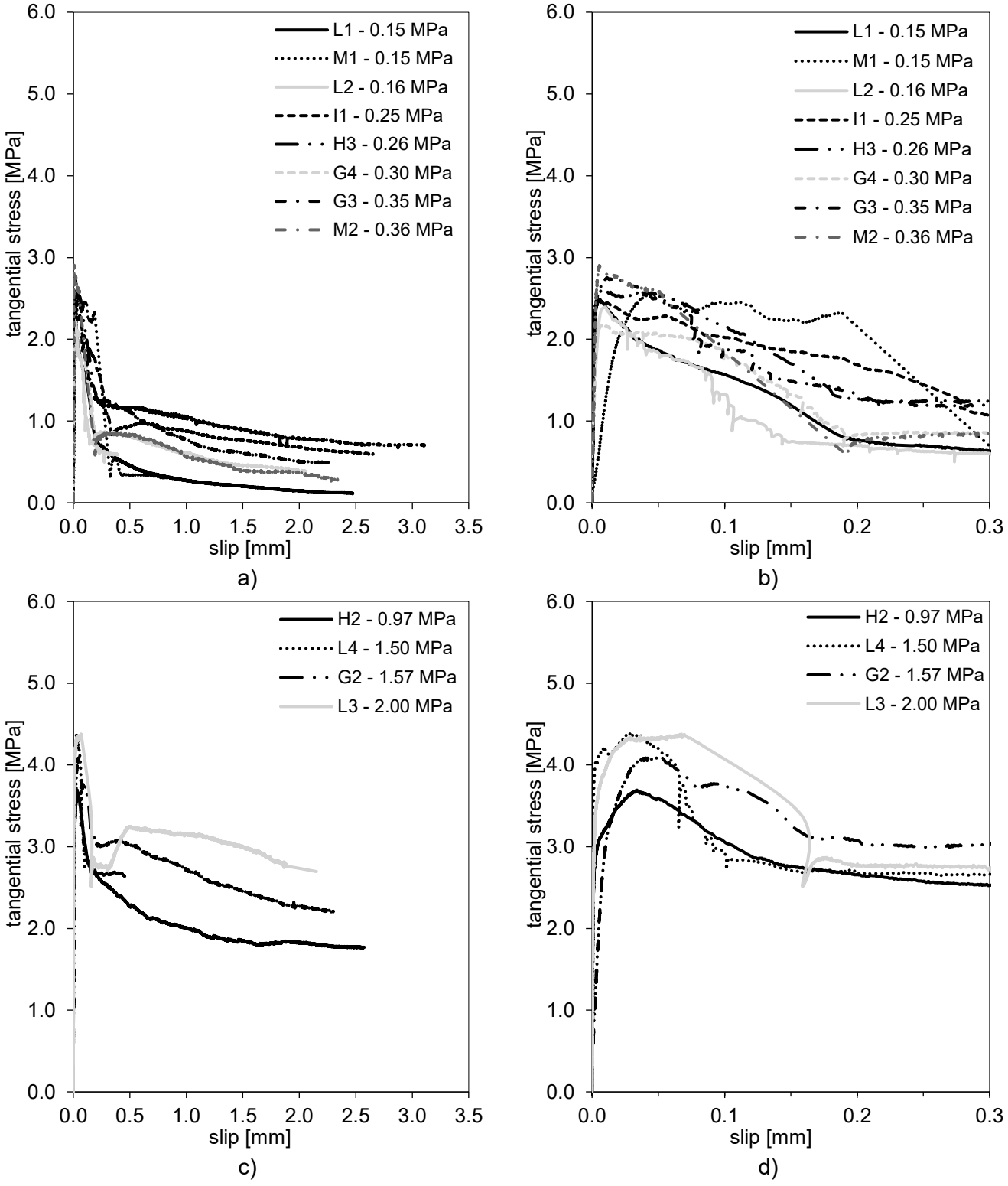


Figure III.17: τ-s responses for direction 3 (90 °): a) and b) responses for lower imposed normal stresses; c) and d) responses for higher imposed normal stresses; b) and d) detail of the initial stage up to an average slip of 0.3 mm.

4.2. Failure surfaces

For the specimens tested in direction 1 (0 °) the failure was governed by the simple sliding of the opposite material surfaces respective to each other, whereas for the specimens tested in direction 3 (90 °) the displacement perpendicular to the brick ribs led to the progressive failure of these ribs. For direction 2 (45 °) the specimens showed a mixed type of failure. **Figure III.18** and **Figure III.19** present a few examples of representative failure surfaces obtained after testing.



Direction 1 (0°) Direction 2 (45°) Direction 3 (90°)

Figure III.18: Front view of the ruptured specimens after testing.



Direction 1 (0 °) Direction 2 (45 °) Direction 3 (90 °)

Figure III.19: Opposite faces of the failure surfaces obtained after testing.

5 DISCUSSION OF RESULTS

5.1. Peak and residual shear stresses

Considering that the strengthening overlay in service conditions is typically subjected to low normal stresses, the characterization of the shear response of the interface was carried out initially considering normal stresses below 0.5 MPa. In **Figure III.20** to **Figure III.22**, the results obtained for the shear strength versus the normal stress are analysed (negative values are considered for compression). Based on the assumption that the peak tangential stress increases linearly with the normal stress, the linear regression of the results was carried out. The estimation of the friction angle based on the slope of the linear regression has resulted in a value of 70 °, 61 ° and 61 ° for directions 1, 2 and 3 respectively. These results are way beyond the values expected for the materials involved. As a result, it was decided to perform additional shear tests at higher values of the imposed normal stress, in order to better characterize the overall shape of the failure criterion. These additional tests were performed at normal stresses between -1 MPa and -2 MPa. Subsequently, the two different sets of data, i.e. for lower [-0.5 - 0] MPa and for higher [-2.0 - -1.0] MPa imposed normal stresses, were analysed separately, by performing individual linear regressions per each set. Identical analysis was performed for the residual shear stress values.

As shown in Figures **Figure III.20** to **Figure III.22** and in **Table III.5**, the slope of the linear regressions obtained varies considerably for all three tested directions, depending on whether lower or higher imposed normal stresses are considered. Considering the peak tangential stresses, the slope obtained for higher imposed normal stresses is always significantly lower than the slope obtained for lower imposed normal stresses. As a result, both the hyperbolic Mohr and the linear Mohr-Coulomb criteria were adopted to replicate the experimentally obtained behaviours. In the case of the residual tangential stresses, the analysis considering only the results obtained for lower normal stresses can be misleading if analysed isolated. The coefficients of determination obtained by linear regression for directions 0 °, 45 ° and 90 ° are low, especially in the case of the 45 ° loading direction. Consequently, the estimated values of the friction angle show some dispersion, especially in the case of the 45 ° loading direction. The analysis of results should therefore consider a wider range of results with both low and high confining stresses, preferably adopting a variable friction angle.

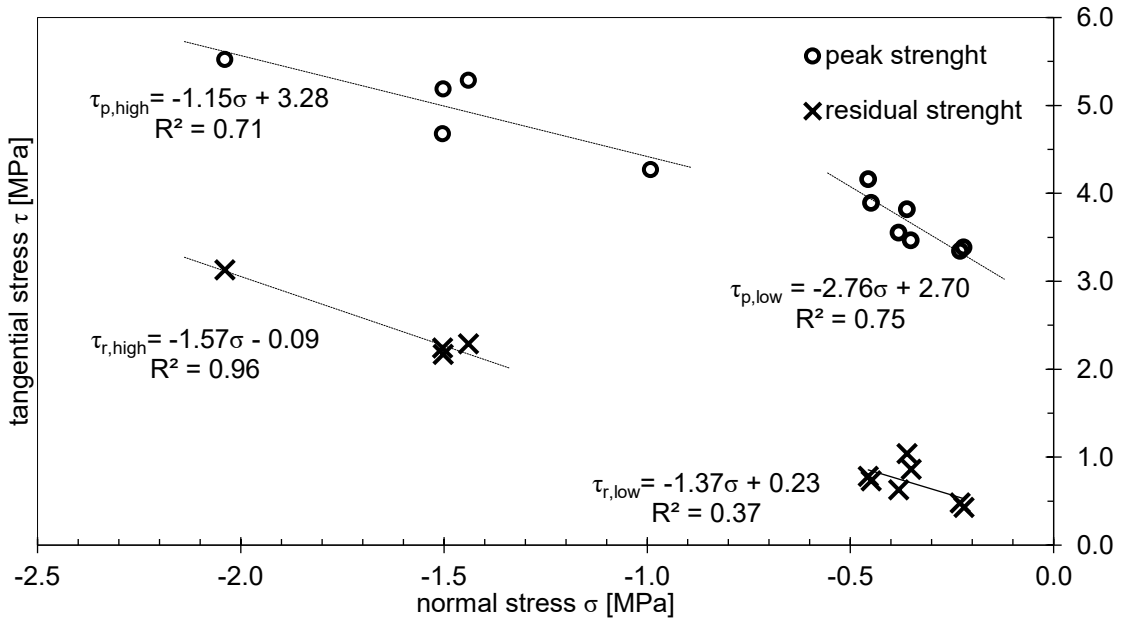


Figure III.20: Linear regressions for direction 1 (0 °) considering peak and residual shear stress values.

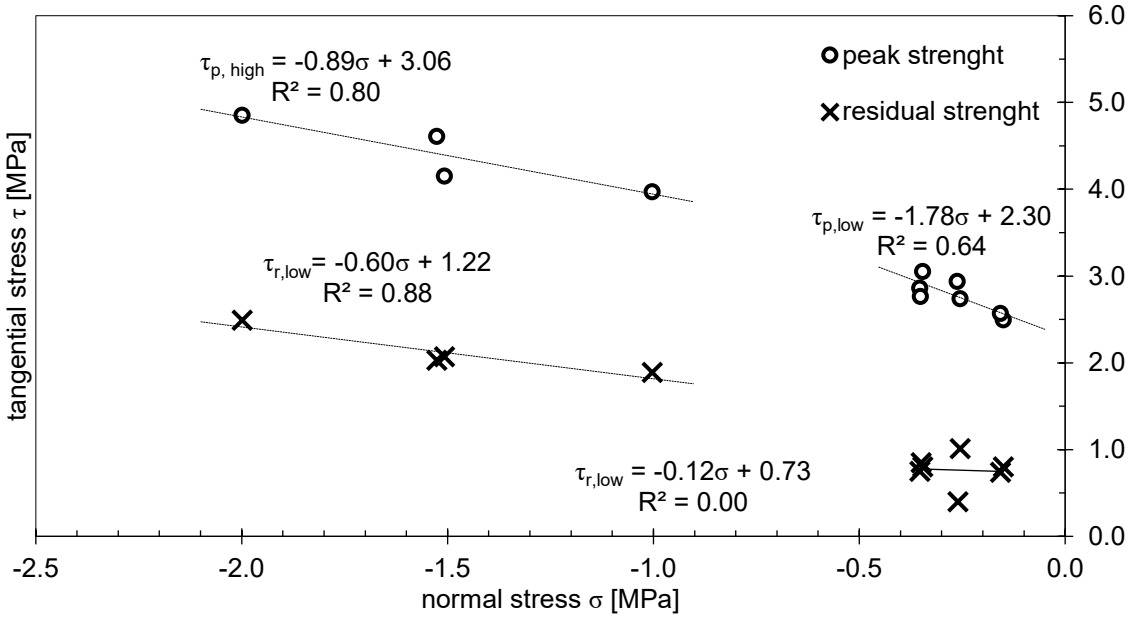


Figure III.21: Linear regressions for direction 2 (45 °) considering peak and residual shear stress values.

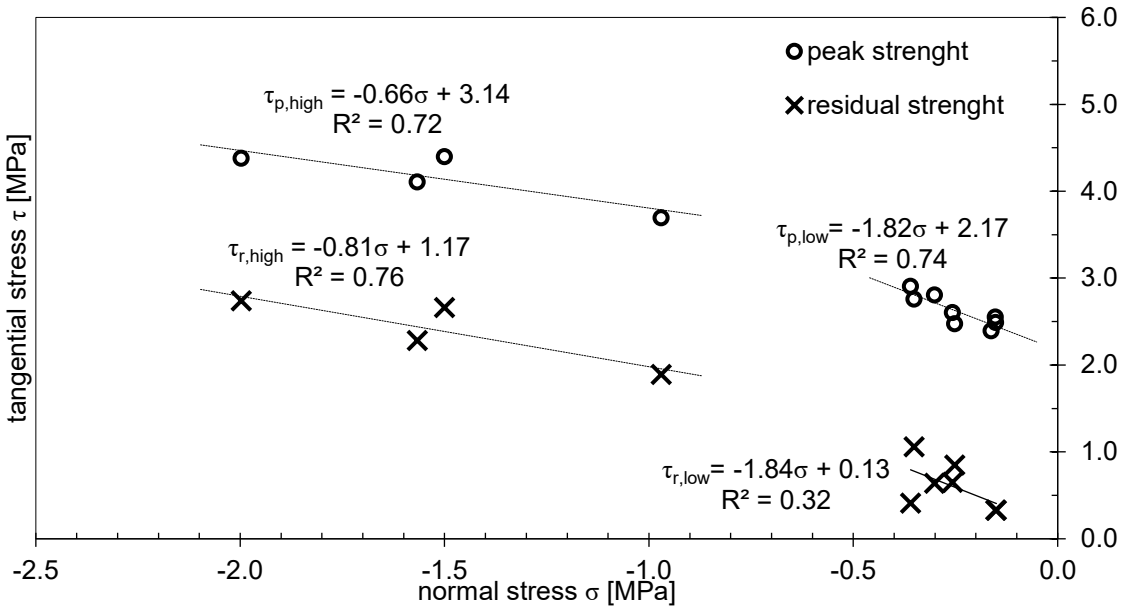


Figure III.22: Linear regressions for direction 3 (90 °) considering peak and residual shear stress values.

Table III.5: Estimation of the friction angle for lower and higher normal stresses based on the linear regressions.

	Peak tangential stress		Residual tangential stress	
	Lower	Higher	Lower	Higher
Direction 1: 0°	70	49	54	58
Direction 2: 45°	61	42	7	31
Direction 3: 90°	61	33	61	39

5.2. Mohr Criterion

Considering the observed differences between the response parameters obtained for higher and lower normal stresses, the hyperbolic Mohr failure criterion was selected for modelling the interaction between the normal and the shear stress components in the entire range of imposed normal stresses tested. Due to its hyperbolic shape, this criterion is expected to describe well the results obtained for both the lower and the higher normal stresses studied. The mathematical equation used to describe the Mohr failure criterion in terms of the peak values of the shear stress is presented in **Eq. (III.9**):

$$\tau = \pm\sqrt{\left(c_p^* - \sigma \times \tan \emptyset_p\right)^2 - \left(c_p^* + \chi \times \tan \emptyset_p\right)^2} \quad \textbf{(III.9)}$$

where τ is the tangential stress, σ is the normal stress, c_p^* is the apparent peak cohesion, $\emptyset_p$ is the peak friction angle and χ is the tensile strength.

The geometrical representation of the Mohr failure criterion is depicted in **Figure III.23**, where the compressive normal stress is considered as negative in the horizontal axis.

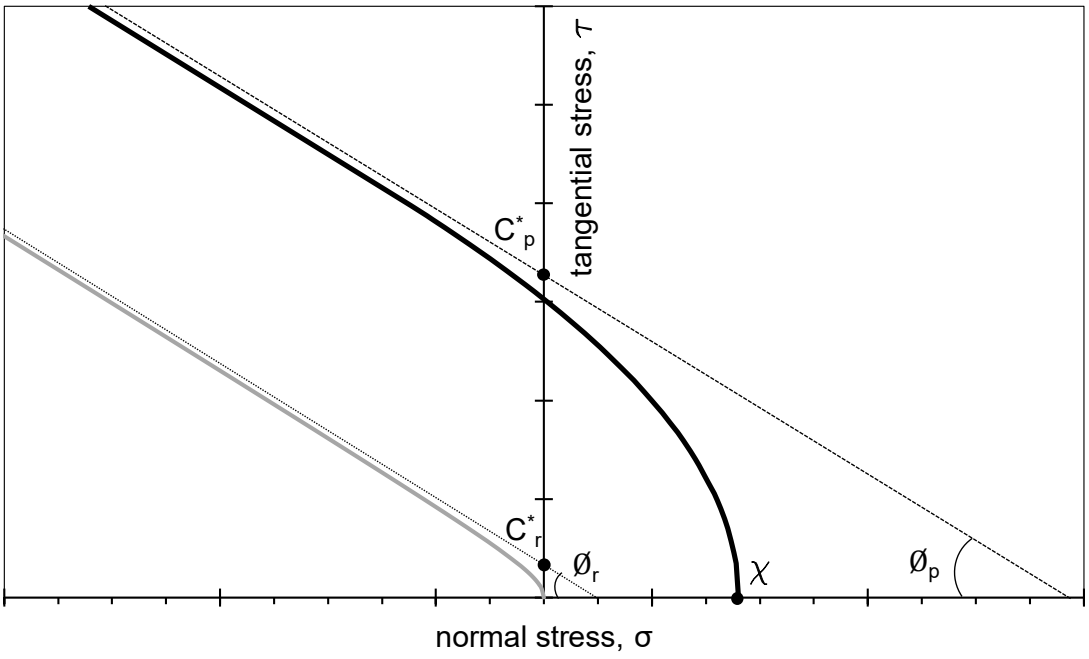


Figure III.23: Representation of the Mohr failure criterion when used to characterize the interaction between the normal stress and both the peak and residual values for positive tangential stresses. The subscript 'p' identifies the 'peak' failure surface parameters, and the subscript 'r' identifies the 'residual' parameters.

The equation describing the Mohr failure criterion may also be used to describe the interaction between the normal stress and the residual shear stress, as shown in **Eq. (III.10**) and represented in **Figure III.23**.

$$\tau = \pm\sqrt{(c_r^* - \sigma \times \tan \emptyset_r)^2 - (c_r^*)^2} \qquad \textbf{(III.10)}$$

where τ is the tangential stress, σ is the normal stress, c_r^* is the apparent residual cohesion and $\emptyset_r$ is the residual friction angle.

In this case the tensile strength parameter, χ, may be considered as zero due to the existence of a fully propagated crack along the interface, which implies the full separation of the two units forming the specimen if a tensile force is applied.

Regarding the peak results, the initial estimation of the friction angle, $\emptyset_{0,p}$, and initial apparent cohesion, $c^*_{0,p}$, was based on the previous linear regression analysis of the experimental data. The value for $\emptyset_{0,p}$ was estimated based on the linear regression of the higher imposed normal stress values (see **Figure III.20** to **Figure III.22**), while the value of $c^*_{0,p}$, was calibrated in order to satisfy, $\tau(\sigma = 0) = c$, where c is the real cohesion estimated using the linear regression of the lower imposed normal stress results. The estimation of the tensile strength parameter, χ, was based on the pull-off test results solely, since it is not expected to be influenced by the loading direction with respect to the orientation of the brick ribs.

The correlation degree reached while approximating the experimental results with the values obtained from the hyperbolic Mohr failure criterion, was evaluated by the coefficient of determination, R^2, as shown in **Eq. (III.11**):

$$R^2 = 1 - \frac{\sum_{i=1}^{n}(\tau_i - \tau_{Mohr,i})^2}{\sum_{i=1}^{n}(\tau_i - \bar{\tau})^2} \qquad \textbf{(III.11)}$$

Where n is the number of specimens, τ_i are the experimental data, $\bar{\tau}$ is the mean value of the experimental data, and $\tau_{Mohr,i}$ are the expected values estimated by **Eq. (III.9**) considering the parameters $\emptyset_p$, c^*_p, χ.

For each of the three loading orientations (0 °, 45 ° and 90 °) the initial parameters and the coefficients of determination obtained in each case are presented in **Table III.6**.

Table III.6: Estimated peak parameters for each loading direction.

	Estimated parameters		
	0°	45°	90°
$c^*_{0,p}$ (MPa)	6.2	5.5	6.6
$\emptyset_{0,p}$ (°)	49	42	33
χ (MPa)	0.6	0.6	0.6
R^2	0.57	0.89	0.94

Subsequently, using a nonlinear optimization algorithm [37] for maximising the R^2, the parameters that better adjust the Mohr curve to the experimental results were obtained. The limits of the search space were set by imposing $c_p^* \leq c_{0,p}^*$ and $\emptyset_p \geq \emptyset_{0,p}$. Additionally, considering that the adhesion strengths obtained by means of pull-off tests typically underestimate the tensile strength at the interface, and based on previous results published in the literature [38], the parameter χ was increased by 50% and the value of 0.9 MPa was adopted. The results obtained are presented in **Table III.7**.

Table III.7: Optimized peak values of Mohr criterion parameters for each loading direction.

	Optimized parameters		
	0°	45°	90°
c_p^* (MPa)	4.54	3.69	3.97
$\emptyset_p$ (°)	49.0	44.8	39.6
χ (MPa)	0.9	0.9	0.9
R^2	0.86	0.97	0.95

Regarding the residual results, the parameters c_r^* and $\emptyset_r$ were obtained by maximizing the coefficient of determination, R^2, with a nonlinear optimization algorithm. The values obtained for the parameters describing the Mohr criterion are presented in **Table III.8**. The correlation degree is higher than 0.92 for all directions. Nevertheless, in the case of the 45° loading direction, the apparent residual cohesion and residual friction angle do not lie between the respective ones obtained for the 0° and 90° loading directions. If this consideration is imposed as a condition, the values of c_r^*=0.41 and $\emptyset_r$=52.4° are obtained for a coefficient of determination R^2 =0.82.

The results obtained for both peak and residual Mohr criteria for each loading direction are represented in **Figure III.24** to **Figure III.26** and compared with the experimental results.

Table III.8: Optimized residual values of Mohr criterion parameters for each loading direction.

	Direction		
	0°	45°	90°
c_r^* (MPa)	0.28	1.66	0.53
$\emptyset_r$ (°)	53.7	33.7	51.1
R^2	0.98	0.92	0.94

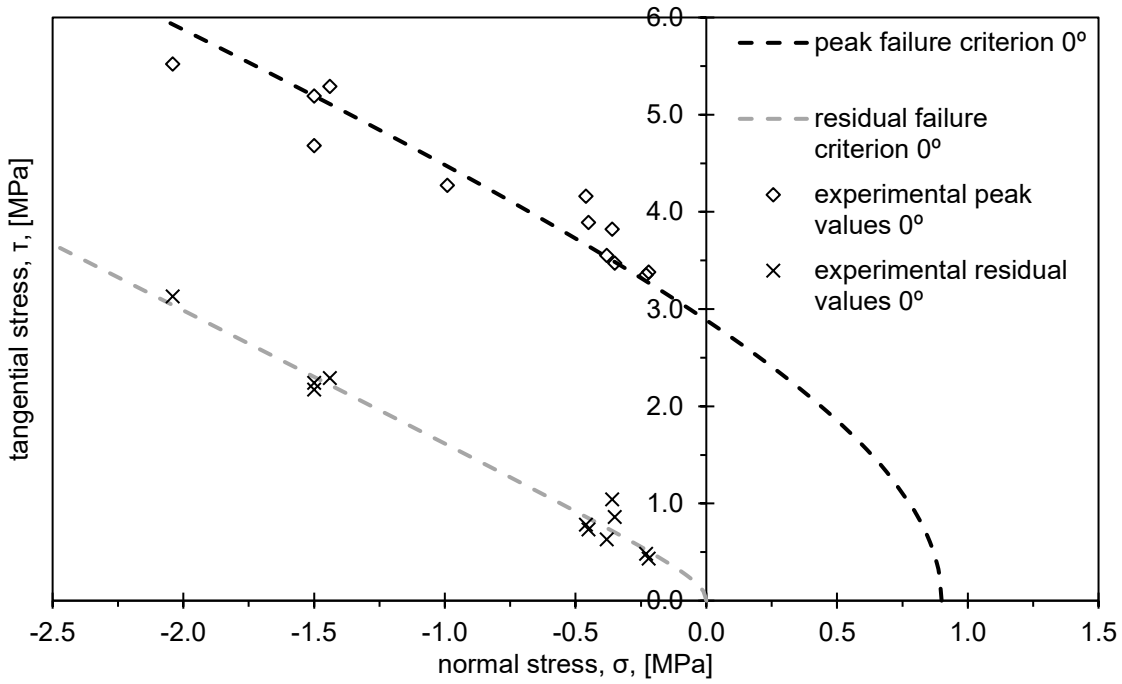


Figure III.24: Failure criteria for 0° loading direction.

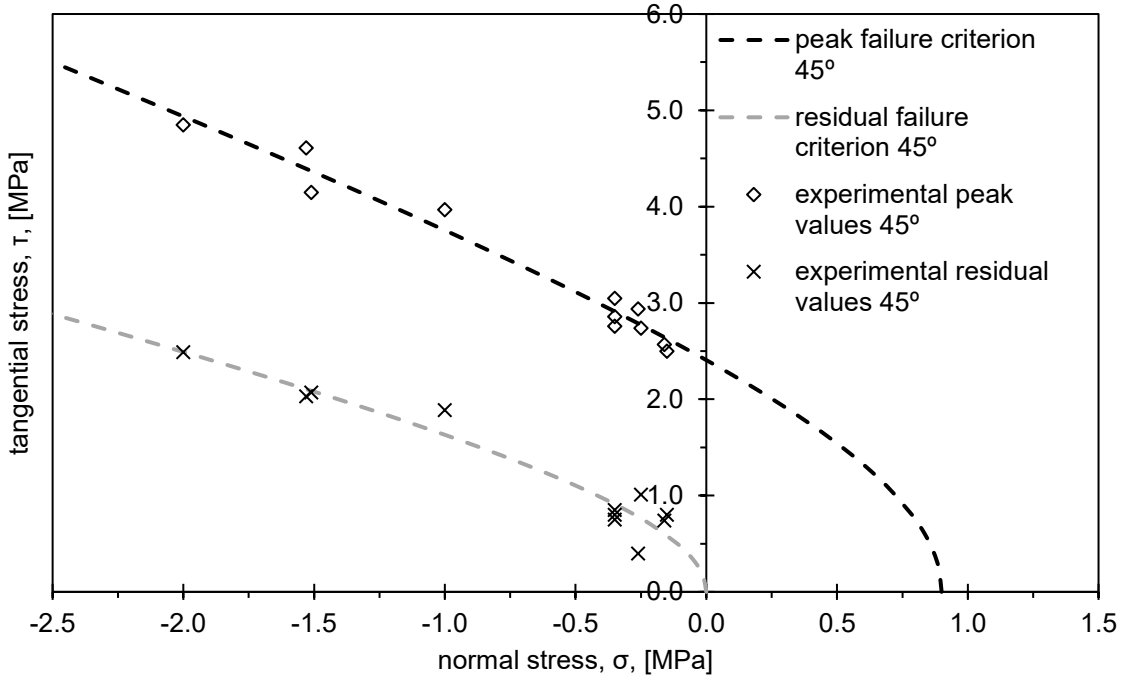


Figure III.25: Failure criteria for 45° loading direction.

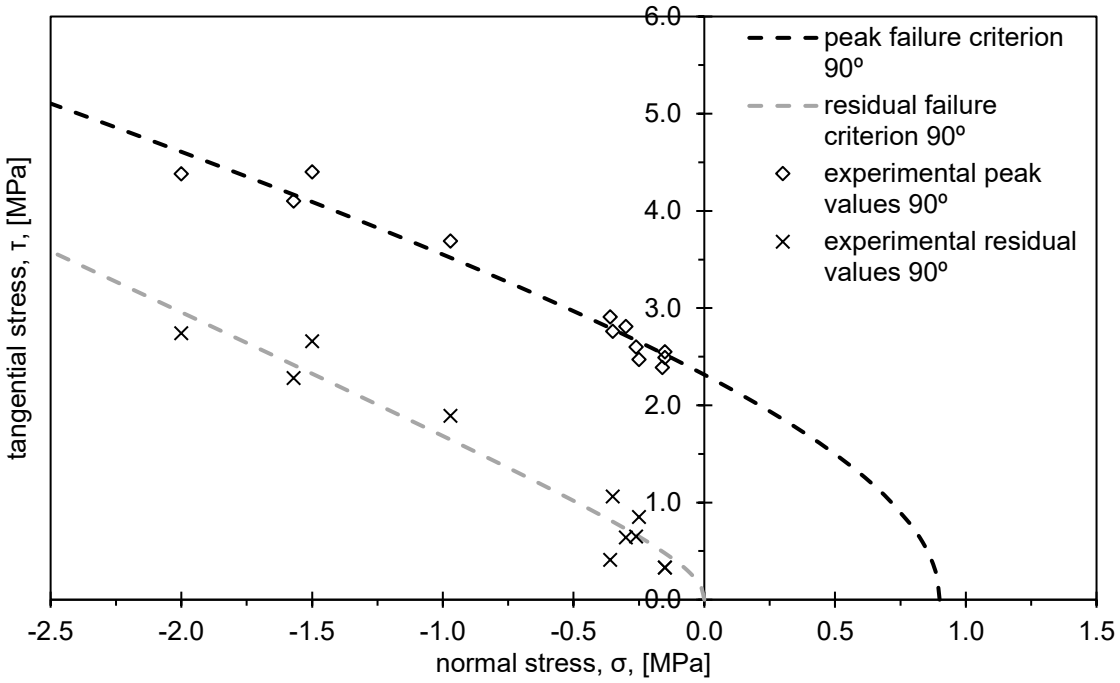


Figure III.26: Failure criteria for 90° loading direction.

5.3. Mohr-Coulomb criterion

The shape of the Mohr criterion proposed by Coulomb is simpler and consists of a line represented by **Eq. (III.12**). This criterion may be used to describe the interaction between the normal stresses and both the peak and the residual shear stresses obtained at the interface, as shown in **Figure III.27**. Considering the peak shear stress results, the adjusted equation becomes:

$$f(\sigma) = c_p \ - \sigma \times \tan \emptyset_p \qquad \textbf{(III.12)}$$

The parameters c_p and $\emptyset_p$ were evaluated by performing a linear regression of all the experimental results, as shown in **Figure III.28**.

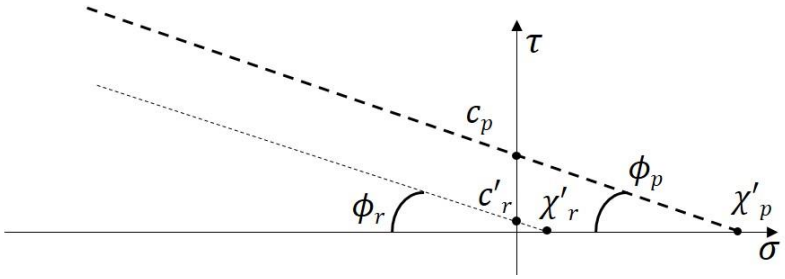


Figure III.27: Representation of the Mohr-Coulomb failure criteria for the peak and the residual shear stress results.

Considering the residual shear stress results, the formulation of the Mohr-Coulomb criterion must consider that the cohesion, c_r , should be approximately zero, as shown in **Figure III.27**. Therefore the Mohr-Coloumb criterion is described by **Eq. (III.13)**:

$$\tau = c'_r - \sigma \times \tan \emptyset_r \qquad \textbf{(III.13)}$$

where $\emptyset_r$ is the residual friction angle, and c'_r is the residual cohesion.

Considering the peak shear stress results, the linear regressions of the three sets of results obtained for the three loading directions show relatively high R^2 values, indicating that the linear approximation represents well the results obtained experimentally in the range of imposed normal stresses studied, see **Figure III.28**. Nevertheless, the values obtained for χ', see **Figure III.27** and **Table III.9**, are well above the tensile strengths obtained experimentally by means of the pull-off tests (0.57 MPa) or even the value adopted for the tensile strength, 0.9 MPa, that assures the maximum R^2 for the Mohr criterion (**Table III.7**). The clear difference between these values indicates that the linear approximation is not appropriate to describe the interface behaviour outside the range of the data experimentally observed, in particular in the tensile normal stress's quadrant.

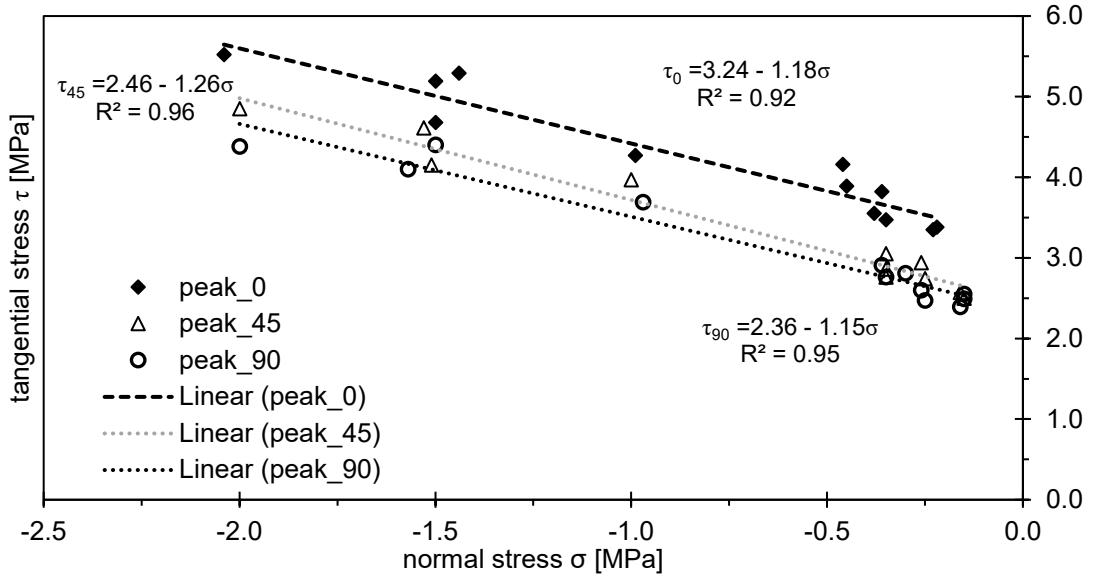


Figure III.28: Linear regression of the peak shear stress results for all orientations.

Table III.9: Estimated parameters considering the Mohr-Coulomb criterion and the peak shear stress results.

Direction	c_p (MPa)	$\emptyset_p$ (°)	R^2 --	χ' (MPa)
1 (0°)	3.24	50	0.92	2.74
2 (45°)	2.46	52	0.96	1.95
3 (90°)	2.36	49	0.95	2.05

Figure III.29 shows that the obtained residual shear stress results are in general quite similar, with a slight distinction in the case of the 45 ° orientation with respect to the loading direction. Nevertheless, the R^2 values are significantly high for all loading directions. The linear regression of the experimental results led to residual values for cohesion, c_r', between 0.22 and 0.52 MPa, although the expected result would be zero. In the case of the residual tensile strength, χ', the results obtained vary between 0.16 and 0.50, see **Table III.10**, which correspond to residual friction angles, $\emptyset_r$, varying between 46 ° and 54 °.

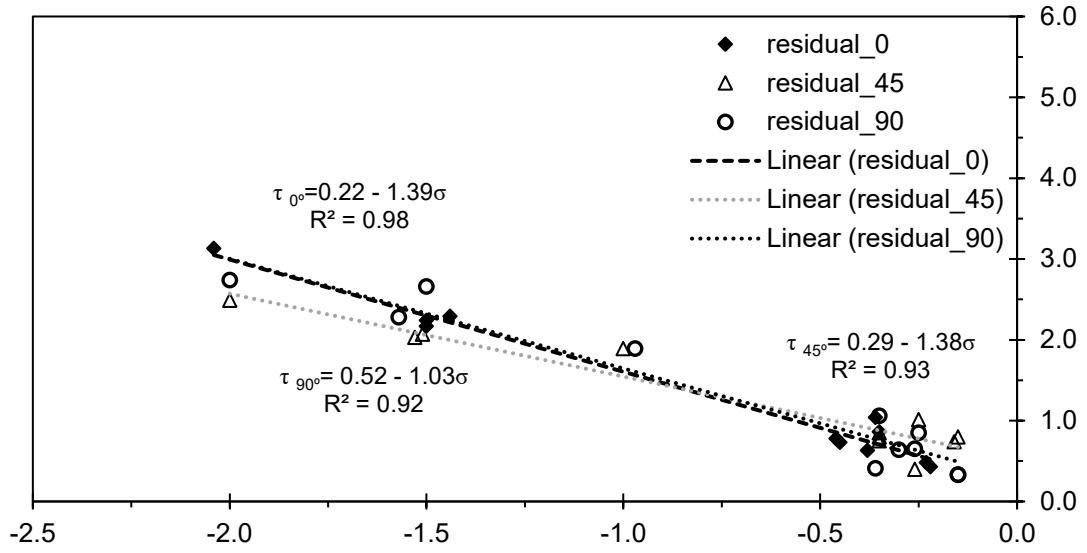


Figure III.29: Linear regression of the residual shear stress results for all orientations.

Table III.10: Estimated parameters considering the Mohr-Coulomb criterion for the residual shear stress results.

Direction	$\emptyset_r$ (°)	R^2 --	c_r'	χ' MPa
1 (0°)	54	0.98	0.22	0.16
2 (45°)	54	0.93	0.29	0.21
3 (90°)	46	0.92	0.52	0.50

5.4. Suitability of the criteria for describing the interface shear response

5.4.1. Comparison of Mohr and Mohr-Coulomb criteria

In order to compare the suitability of the Mohr-Coulomb linear criterion and the Mohr non-linear criterion for describing the experimental results, the experimental values of the shear stress, τ_{exp}, were compared with the estimated ones, $y(\tau_{exp}) = \tau_{crit}$. The two previously mentioned criteria were adopted to estimate the peak and the residual tangential stresses obtained in the experimental responses for the different levels of imposed normal stresses. The values used to compare the criteria are presented in **Table III.7** and **Table III.8** for the Mohr criterion, in the case of the Mohr-Coulomb criterion the values are presented in **Table III.9** and **Table III.10**.

The fitting quality of the criteria was assessed by computing the R^2 coefficient presented in **Eq. (III.14**).

$$R^2 = 1 - \frac{\sum_{i=1}^{n}(\tau_{crit,i} - \tau_{exp,i})^2}{\sum_{i=1}^{n}(\tau_{exp,i} - \bar{\tau}_{exp})^2} \quad \textbf{(III.14)}$$

where $\tau_{crit,i}$ are the values estimated by the criteria and $\tau_{exp,i}$ and $\bar{\tau}_{exp}$ are, respectively, the experimental values and the mean value of the experimental results.

The results estimated using the expressions of Mohr and Mohr-Coulomb criteria are compared with the corresponding experimental results in **Figure III.30** to **Figure III.32**. The fitting quality of the criteria was assessed by computing the R^2 values, as presented in **Table III.11**. As shown, for all three loading directions the non-linear Mohr criterion presents a better fitting to the residual experimental results. The Mohr-Coulomb criterion adjusts better to the peak experimental results. Nonetheless it is worth mentioning that both criteria present a good fitting to the experimental results.

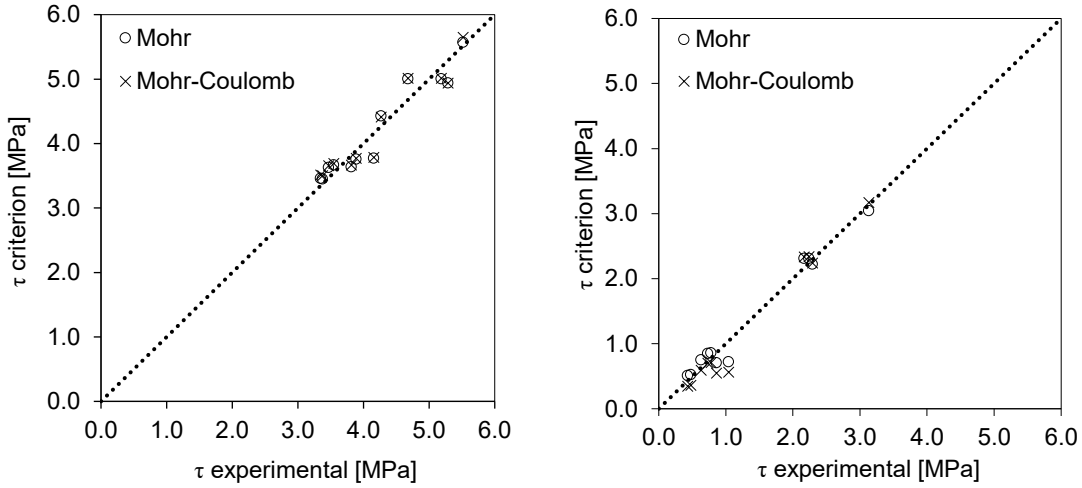


Figure III.30: Experimental versus criterion estimations for 0° loading direction: a) peak shear stresses; b) residual stresses.

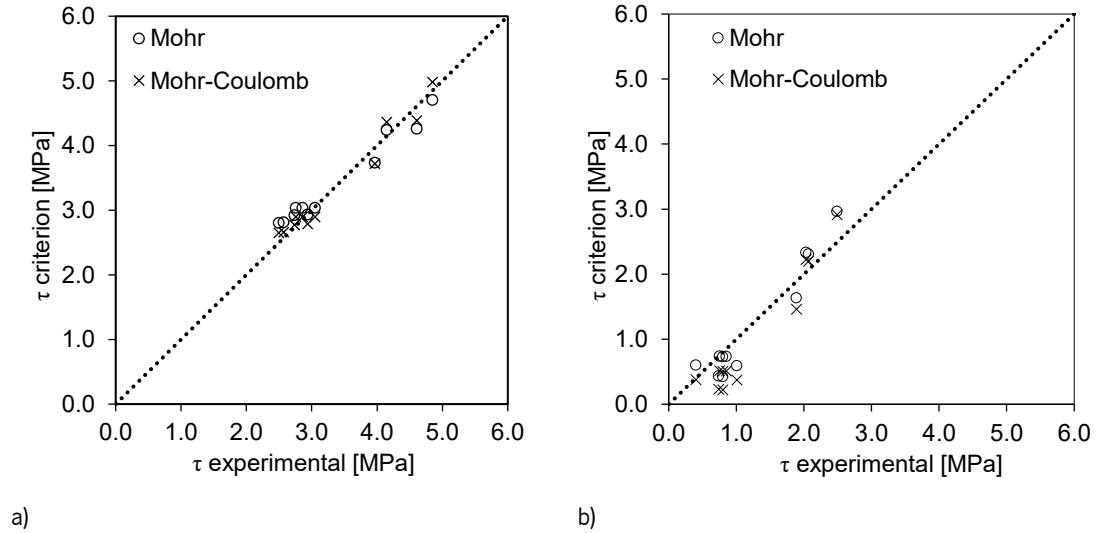


Figure III.31: Experimental versus criterion estimation for 45° loading direction: a) peak shear stresses; b) residual shear stresses.

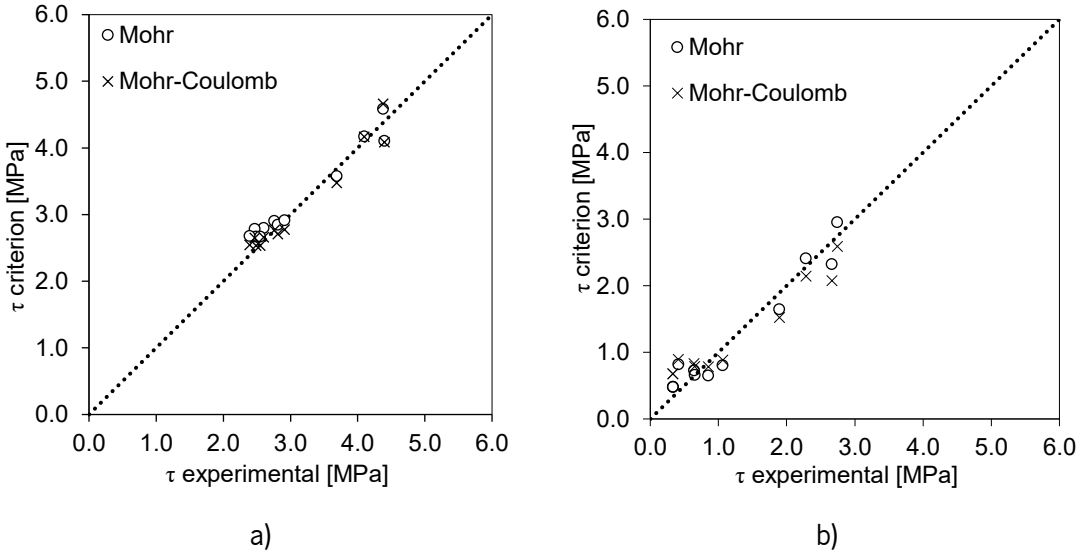


Figure III.32: Experimental versus criterion estimations for 90° loading direction: a) peak shear stresses; b) residual shear stresses.

Table III.11: Summary of the R^2 values obtained for each testing direction.

	Peak criteria		Residual criteria	
Direction	Mohr R^2	Mohr-Coulomb R^2	Mohr R^2	Mohr-Coulomb R^2
1 (0°)	0.90	0.97	0.98	0.98
2 (45°)	0.97	0.96	0.92	0.89
3 (90°)	0.96	0.95	0.94	0.80

5.4.2. Criterion for the interface behaviour

As discussed, the failure behaviour observed in all experiments was appropriately described by the two criteria. In general, both criteria present good correlation with the experimental results, although the Mohr criterion can better describe the behaviour of the interface also in the tensile region, as shown **Figure III.32**. Nonetheless, it became evident that the possibility to further characterize the interface shear stress-slip response in the tensile region would be beneficial for defining the optimal parameters in each case. However, the test setup would have to be adapted in order to allow combining shear and tensile loads during testing.

The failure criterion for peak shear stresses in the case of the loading direction 2 (45° orientation) assumed approximately an intermediate behaviour between the criteria deduced for 0° and 90° loading directions. In the case of the residual criterion this effect was not so clear, as shown in **Figure III.33**. The surface obtained by combining the failure criteria for all directions is represented in **Figure III.34**. The values for loading directions different from 0°, 45° and 90° were estimated based on a linear interpolation between the known values of the 0°, 45° and 90° curves.

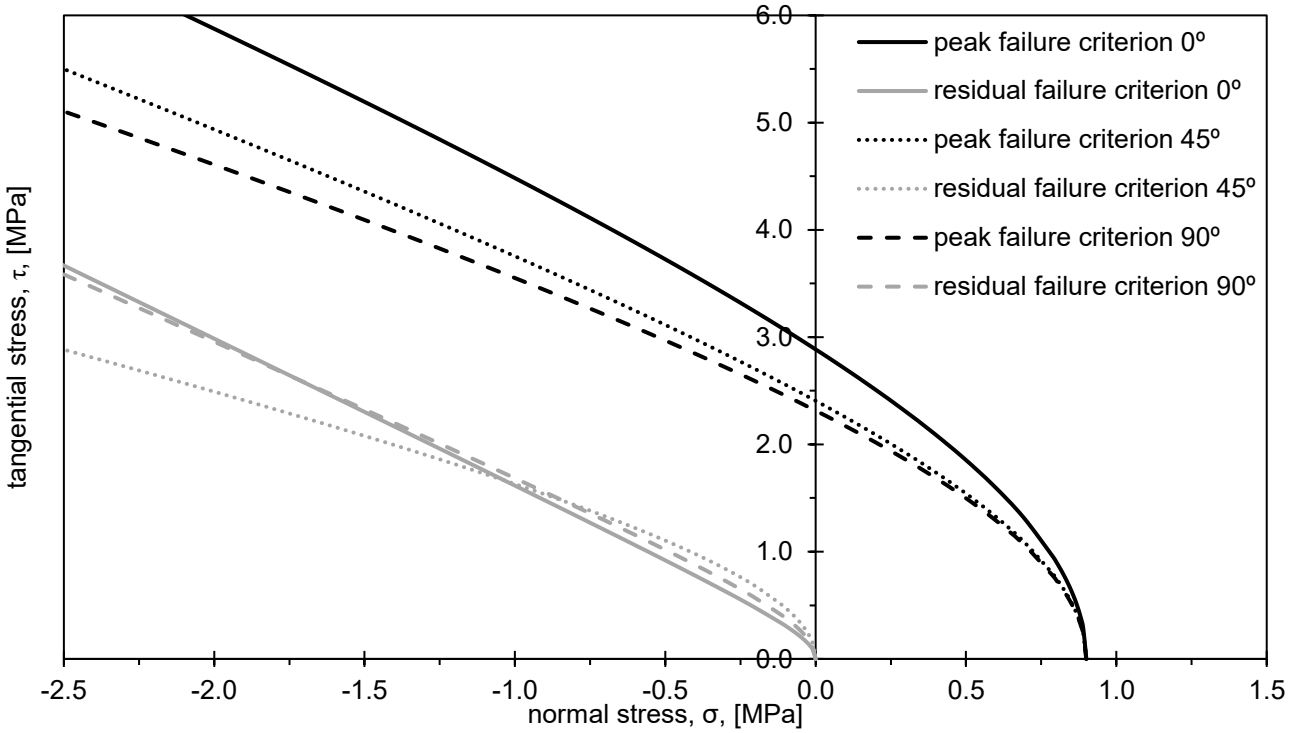
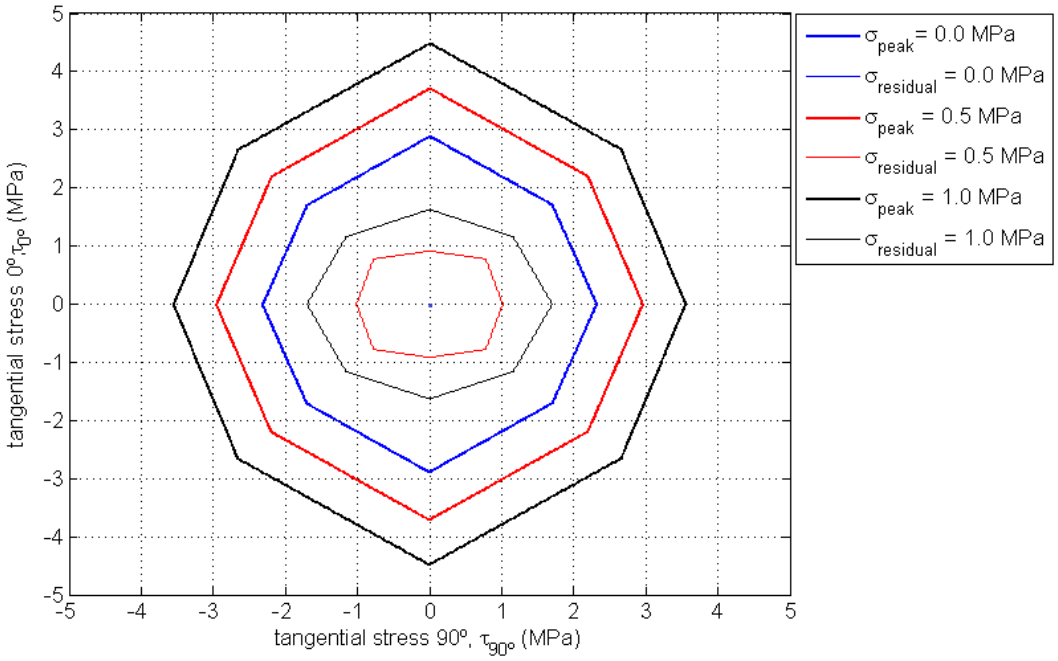
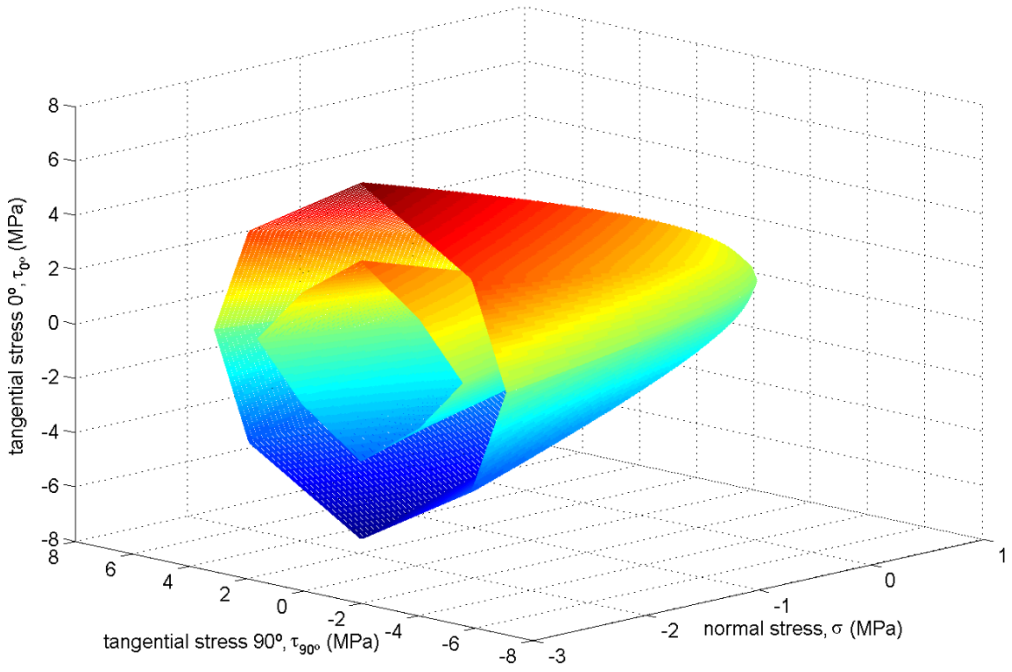


Figure III.33: Failure criteria for peak and residual shear stress.



a)



b)

Figure III.34: Combined failure criteria for all directions: a) representation of the peak and residual values for 0, 0.5 and 1.0 MPa normal stresses; b) 3D orthotropic representation of the peak and residual loading/failure criteria.

6 CONCLUSIONS

The test setup developed in this research aimed to assure a direct characterization of the interface behaviour between a ceramic brick substrate and the PFRM strengthening overlay. The results obtained showed the consistent development of a single failure surface for all specimens throughout the entire testing program, which is important for the objective characterization of the mechanical response of the interface. This feature is beneficial when compared with other test setups used in the characterization of the interface between two materials, for instance because there is no interaction between multiple failure surfaces or interfaces, which generally occurs when triplet test is used.

The brick surface type used was characterized by a principal direction of the surface ribs. A global overview on the anisotropic interface behaviour was obtained by applying the shear force along three different loading directions (*0 °, 45 °, 90 °*).

The experimental results showed in general a brittle post-peak behaviour and the achievement of a frictional residual strength related with the loading direction. When the shear load was parallel to the brick ribs (0 °), the failure surface was formed along the ribs together with the detachment of the two different materials and with negligible failure of the ribs on the brick surface and on the PFRM unit. A completely different failure characterized the 90 ° orientation series. The displacement imposed perpendicularly to the ribs caused a progressive cracking of the ribs on the brick surface. The intermediate orientation displayed a mixed behaviour.

The most suitable failure criterion to predict the experimental results is the hyperbolic approximation from the Mohr criterion, this criterion can predict the values in a wider range of data, including lower values of normal stress. For all tested directions, the correlation degree reached while approximating the experimental results, evaluated by the coefficient R^2, was higher than 0.90 for the peak shear stress and higher than 0.92 for the residual shear stress. In addition, it was found that the range of normal stresses considered to deduce the parameters of the loading/failure criterion had a significant impact on the results obtained. In particular, the value of the friction angle was very sensitive to the range of normal stresses considered to derive the Mohr-Coloumb loading/failure criterion parameters.

The testing procedure studied in this research could be further used to characterize the shear response for other loading orientations with respect to the brick ribs in order to have a complete overview on the orthotropic interface behaviour. Direct shear cyclic tests could also be performed to assess the influence of load inversion on the behaviour of the interface between the substrate and the reinforcing

layer. These results can in the future be used to extend the interface constitutive criteria for simulating cyclic loading conditions.

Acknowledgements

This research was carried in the framework of InoTec, Innovative material of ultra-high ductility for the rehabilitation of the built patrimony, funded by COMPETE/QREN/FEDER (NORTE-07-0202-FEDER-023024). InoTec project is promoted by CiviTest company and University of Minho. S&P Clever Reinforcement Ibérica is gratefully acknowledged for providing the materials used in the strengthening of the masonry specimens.

REFERENCES

[1] J. A. P. P. Almeida, E. B. Pereira, and J. A. O. Barros, "Assessment of overlay masonry strengthening system under in-plane monotonic and cyclic loading using the diagonal tensile test," Constr. Build. Mater., vol. 94, pp. 851–865, Sep. 2015.

[2] M. A. Elgawady, P. Lestuzzi, and M. Badoux, "A review of conventional seismic retrofitting techniques for URM," in 13th International Brick and Block Masonry Conference, 2004, pp. 1–10.

[3] H. Shakib, M. Mousavi, M. K. H. Rezaei, S. Dardaei, M. Ahmadizadeh, and M. Samadian, "Analytical and Experimental Seismic Evaluation of Unreinforced Masonry Walls Retrofitted by Shotcrete and CFRP Strips," in 12th Canadian Masonry Symposium, 2013, pp. 1–10.

[4] S. B. Kadam, Y. Singh, and B. Li, "Strengthening of unreinforced masonry using welded wire mesh and micro-concrete – Behaviour under in-plane action," Constr. Build. Mater., vol. 54, pp. 247–257, 2014.

[5] A. Figueiredo, H. Varum, A. Costa, D. Silveira, and C. Oliveira, "Seismic retrofitting solution of an adobe masonry wall," Mater. Struct., vol. 46, no. 1–2, pp. 203–219, Jul. 2012.

[6] C. G. Papanicolaou, T. C. Triantafillou, K. Karlos, and M. Papathanasiou, "Textile-reinforced mortar (TRM) versus FRP as strengthening material of URM walls : in-plane cyclic loading," Mater. Struct., vol. 40, pp. 1081–1097, 2007.

[7] E. Bernat-Maso, C. Escrig, C. A. Aranha, and L. Gil, "Experimental assessment of Textile Reinforced Sprayed Mortar strengthening system for brickwork wallettes," Constr. Build. Mater., vol. 50, pp. 226–236, 2014.

[8] M. Corradi, A. Borri, G. Castori, and R. Sisti, "Shear strengthening of wall panels through jacketing with cement mortar reinforced by GFRP grids," Compos. Part B Eng., vol. 64, pp. 33–42, 2014.

[9] Federal Emergency Management Agency, Techniques for the Seismic Rehabilitation of Existing Buildings - FEMA 547. Books Express Publishing, 2006, p. 572.

[10] Y. Kim, H. Kong, and V. C. Li, "Design of engineered cementitious composite suitable for wet-mixture shotcreting," ACI Mater. J., no. 100, 2003.

[11] E. Esmaeeli, E. Manning, and J. A. O. Barros, "Strain hardening fibre reinforced cement composites for the flexural strengthening of masonry elements of ancient structures," Constr. Build. Mater., vol. 38, pp. 1010–1021, Jan. 2013.

[12] A. Dehghani, G. Fischer, and F. Alahi, "Strengthening masonry infill panels using engineered cementitious composites," Mater. Struct., 2013.

[13] M. A. Elgawady, P. Lestuzzi, and M. Badoux, "Retrofitting of masonry walls using shotcrete," in NZSEE Conference, Yeni Zelanda, 2006, no. 45.

[14] M. R. Valluzzi, D. Tinazzi, and C. Modena, "Shear behavior of masonry panels strengthened by FRP laminates," Constr. Build. Mater., vol. 16, no. 7, pp. 409–416, Oct. 2002.

[15] S. S. Prakash and P. Alagusundaramoorthy, "Load resistance of masonry wallettes and shear triplets retrofitted with GFRP composites," Cem. Concr. Compos., vol. 30, no. 8, pp. 745–761, Sep. 2008.

[16] A. Bruedern, D. Abecasis, and V. Mechtcherine, "Development of Strain-Hardening Cement-based Composites for the strengthening of masonry," in Concrete Repair, Rehabilitation and Retrofitting II - Proceedings of the 2nd International Conference on Concrete Repair, Rehabilitation and Retrofitting, ICCRRR, 2009, pp. 887–894.

[17] B. V. Venkatarama Reddy and C. V. Uday Vyas, "Influence of shear bond strength on compressive strength and stress–strain characteristics of masonry," Mater. Struct., vol. 41, no. 10, pp. 1697–1712, Jan. 2008.

[18] G. F. M. Vasconcelos and P. B. Lourenço, "Experimental characterization of stone masonry in shear and compression," Constr. Build. Mater., vol. 23, no. 11, pp. 3337–3345, Nov. 2009.

[19] V. Alecci, M. Fagone, T. Rotunno, and M. De Stefano, "Shear strength of brick masonry walls assembled with different types of mortar," Constr. Build. Mater., vol. 40, pp. 1038–1045, Mar. 2013.

[20] L. Abdou, R. A. Saada, F. Meftah, and A. Mebarki, "Experimental investigations of the joint-mortar behaviour," Mech. Res. Commun., vol. 33, pp. 370–384, 2006.

[21] N. Augenti and F. Parisi, "Constitutive modelling of tuff masonry in direct shear," Constr. Build. Mater., vol. 25, no. 4, pp. 1612–1620, 2011.

[22] R. van der Pluijm, Out-of-Plane Bending of Masonry Behaviour and Strength. R. van der Pluijm, 1999, p. 259.

[23] M. Montazerolghaem and W. Jaeger, "A Comparative Numerical Evaluation of Masonry Initial Shear Test Methods and Modifications Proposed for EN 1052-3," in 9th International Masonry Conference, July 7, 8, 9; 2014; Guimarães, 2014, pp. 1–10.

[24] Comité Européen de Normalisation, "EN 1052-3:2002 Methods of test for mortar masonry - Part 3: Determination of inicial shear strength," vol. 3, no. c. Comité Européen de Normalisation, Brussels, p. 14, 2002.

[25] J. Hofmann, P.; Stöckl, S.; Mainz, "A comparative finite element evaluation of mortar joint shear tests," Mason. Int., vol. 3, no. 3, pp. 101–104, 1990.

[26] P. B. Lourenço, J. A. O. Barros, and J. T. Oliveira, "Shear testing of stack bonded masonry," Constr. Build. Mater., vol. 18, no. 2, pp. 125–132, Mar. 2004.

[27] A. Gabor, A. Bennani, E. Jacquelin, and F. Lebon, "Modelling approaches of the in-plane shear behaviour of unreinforced and FRP strengthened masonry panels," Compos. Struct., vol. 74, pp. 277–288, 2006.

[28] J. Milosevic, A. S. Gago, M. Lopes, and R. Bento, "Experimental assessment of shear strength parameters on rubble stone masonry specimens," Constr. Build. Mater., vol. 47, pp. 1372–1380, Oct. 2013.

[29] W.-F. Chen, Plasticity in reinforced concrete. J. Ross Publishing, 2007, p. 474.

[30] I. Carol and P. C. Prat, "Normal/shear cracking model: Application to discrete crack analysis," J. Eng. Mech., vol. 123, no. 8, p. 765, Aug. 1997.

[31] J. Heyman, Coulomb's Memoir on Statics: An Essay in the History of Civil Engineering. London: Imperial College Press, 1997.

[32] A. Caggiano, G. Etse, and E. Martinelli, "Zero-thickness interface model formulation for failure behavior of fiber-reinforced cementitious composites.," Comput. Struct., vol. 98–99, pp. 23–32, May 2012.

[33] C. M. López, I. Carol, and A. Aguado, "Meso-structural study of concrete fracture using interface elements . I : numerical model and tensile behavior," Mater. Struct., no. 41, pp. 583–599, 2008.

[34] Comité Européen de Normalisation, "EN 772-1:2000 Methods of test for masonry units. Determination of compressive strength." Comité Européen de Normalisation, Brussels, p. 14, 2000.

[35] Comité Européen de Normalisation, "EN 1015-11:1999 Methods of test mortar for masonry – Part 11: Determination of flexural and compressive strength of hardened mortar." Brussels, 1999.

[36] Comité Européen de Normalisation, "EN 1015-12:2000 Methods of test for mortar for masonry - Part 12: Determination of adhesive strength of hardened mortar." Brussels, 2000.

[37] I. Nenov and D. Fylstra, "Interval Methods for Accelerated Global Search in the Microsoft Excel Solver," Reliab. Comput., vol. 9, no. 2, pp. 143–159, 2003.

[38] L. Courard, B. Bissonnette, A. Garbacz, A. Vaysburd, K. Von Fay, G. Moczulski, and M. Morency, "Effect of Misalignment on Pull-off Test Results : Numerical and Experimental Assessments," ACI Mater. J., no. 111, pp. 153–162, 2014.

PAPER IV

ASSESSMENT OF OVERLAY MASONRY STRENGTHENING SYSTEM UNDER IN-PLANE MONOTONIC AND CYCLIC LOADING USING THE DIAGONAL TENSILE TEST

REFERENCE: Almeida, J. A. P. P., Pereira, E. B., Barros, J. A. O. Assessment of overlay masonry strengthening system under in-plane monotonic and cyclic loading using the diagonal tensile test. Construction and Building Materials 2015; 94, 851–865. http://dx.doi.org/10.1016/j.conbuildmat.2015.07.040.

ABSTRACT: The development of novel strengthening techniques to address the seismic vulnerability of masonry elements is gradually leading to simpler, faster and more effective strengthening strategies. In particular, the use of fabric reinforced cementitious matrix systems is considered of great potential, given the increase of ductility achieved with simple and economic strengthening procedures. To assess the effectiveness of these strengthening systems, and considering that the seismic action is involved, one important component of the structural behaviour is the in-plane cyclic response. In this work is discussed the applicability of the diagonal tensile test for the assessment of the cyclic response of strengthened masonry. The results obtained allowed to assess the contribution of the strengthening system to the increase of the load carrying capacity of masonry elements, as well as to evaluate the damage evolution and the stiffness degradation mechanisms developing under cyclic loading.

KEYWORDS: Infill masonry; High ductility; Strengthening system; Shear capacity; In-plane cyclic tests.

Nomenclature:

FRCM Fabric reinforced cementitious matrix

A_f Area of the mesh reinforcement by unit width

A_m Interface loading area between the steel shoe and the specimen

A_n Net area of the specimen cross section

$A_{n,r}$ Net area of the render cross section

$A_{n,PFRM}$ Net area of the PFRM cross section

E_f Tensile modulus of elasticity of the cracked FRCM specimen

f_{fv} Design tensile strength of FRCM reinforcement

$f_{fv,ult}$ Ultimate tensile strength of FRCM reinforcement

f'_m Compressive strength of the masonry

f'_t Tensile strength of the masonry

g Vertical gage length

G Modulus of stiffness in shear

h Height of the brick units

L Length of the wall in the direction of the shear force

n Number of fabric layers

n^* Percentage of the net area

P Applied load

S_s Shear stress

t Thickness of the specimen

V_{ref}^{exp} Shear capacity of the reference specimens obtained experimentally

V_{str}^{exp} Shear capacity of the strengthened specimens obtained experimentally

V_{ACI}^{an} Shear capacity of the specimen calculated following the ACI549.4R-13

$V_{ACI+PFRM}^{an}$ Shear capacity of the specimen calculated following ACI549.4R-13 plus the contribution of the PFRM layers

V_{Sup}^{an} Shear capacity of the specimen considering ultimate strain of the FRCM plus the contribution of the PFRM layers

V_{dt} Shear capacity due to diagonal tension failure

V_f Shear capacity of the FRCM system

V_m Shear capacity of the masonry specimen

V_{sf} Shear capacity due to shear friction failure

V_{ss} Shear capacity due to shear sliding failure

$V_{f,ult}$ Shear capacity of the FRCM system considering ultimate tensile strain

V_r Shear capacity of the render layer

V_{PFRM} Shear capacity of the PFRM layer

u_v Vertical shortening

u_h Horizontal elongation

w Length of brick units

γ Shearing strain

ε_{fv} Design value of the tensile strain of FRCM reinforcement

$\varepsilon_{fv,ult}$ Tensile strain ultimate value of FRCM reinforcement

μ_0 Coefficient of internal shear friction in mortar joint

μ_m Modified coefficient of internal shear friction in mortar joint

τ_0 Shear bond strength of the mortar joint

$\tau_{0,m}$ Modified shear bond strength of the mortar joint

θ Angle between horizontal and main diagonal of the wall

1 INTRODUCTION

Masonry constructions are composed of brittle or quasi-brittle materials, and generally have low resistance to seismic events. The current performance requirements prescribed by the design codes are frequently not accomplished by existing constructions, either because these requirements became more demanding, or because the negative effects of aging in the long-term behaviour of the materials resulted in a substantial decrease of the load carrying capacity of the masonry elements. Therefore,

the development of effective procedures to retrofit existing masonry constructions, in order to upgrade their load bearing capacity and increase their ductility response, is still of great importance.

This work presents the experimental program developed with the aim of characterizing and quantifying the contribution of a strengthening system based on fabric reinforced cementitious matrix (FRCM) to the increase of the load carrying capacity and deformability of masonry elements subjected to in-plane loading. In addition, this research investigates the adequacy and effectiveness of the application of the diagonal tensile test for the evaluation of the in-plane cyclic behaviour of strengthened masonry elements. The test procedure, which will be detailed in the following sections, was adapted to consider unidirectional cycles of loading and unloading.

1.1. Overlay strengthening techniques

The application of additional overlays to the existing masonry elements is a common strengthening technique, especially in areas of considerable seismic activity. Generally, the strengthening overlay consists of a mortar, applied manually or mechanically. These surface treatments, as designated by Elgawady et al. [1], typically incorporate different types of steel, polymers, carbon or glass fibres and fibres meshes used to enhance tensile behaviour and ductility of the strengthening overlay [2-6]. The application of these reinforced strengthening overlays improves both the in-plane and the out-of-plane load carrying capacity [7]. A different concept of overlay strengthening system was developed by using materials with tensile strain-hardening behaviour in the hardened state, avoiding the use of reinforcement meshes. These materials, with the designation of strain hardening cement composites (SHCC), have a tensile strength higher than the stress at crack initiation, and a tensile strain at tensile strength higher than 1%, with the capacity of developing diffuse crack patterns of a maximum crack width does not exceeding 0.1 mm in the hardening phase. The SHCC can be applied using the shotcreting technique or manually [8-9]. This technique can lead to the increase of the shear capacity of the masonry, to the improvement of its deformability and to the enhancement of its energy dissipation capacity during cyclic loading [10].

Some of the advantages and disadvantages of the masonry strengthening techniques based on the addition of strengthening overlays to the original masonry element are presented by Elgawady et al. [1], [11]. The advantages identified include the low cost, the durability, the uniform behaviour, the increase of in-plane strength up to 3.6 times, the improvement of the out-of-plane stability and the

increase of the energy dissipation ability before failure. The increase of the dead weight of the strengthened elements, the requirement of surface treatments, the architectural changes of the structure, and the high disturbance during works are the main disadvantages identified [1], [11]. The increase of the stiffness in shear walls due to the application of thick strengthening overlays may also lead to alterations of the structural behaviour. These alterations often result in substantial increments of the stresses at these elements, which in turn may lead to the increase of their strength requirements. In addition, the greater stiffness of the strengthening overlays, when compared to the original substrates, is especially demanding at the level of the interface, where high stresses are generated and the delamination of the overlay is promoted.

1.2. In-plane experimental characterization

The characterization of the structural behaviour of masonry elements is typically divided in two main different types, depending on the loading configuration: the in-plane and the out-of-plane behaviours [12], [13]. Concerning the in-plane characterization, the monotonic shear behaviour of elements is often assessed by means of the diagonal tensile tests, using masonry specimens built in the laboratory [14], [15], or in-situ [16], [17]. Different types of strengthening systems have already been evaluated using this type of test [10], [17-20]. As discussed in previous publications, Almeida et al. [21] the cyclic shear behaviour of masonry panels can be characterized by means of the diagonal tensile test. Brignola et al. [16] conducted force controlled cyclic tests, with a load gradient of 200 N/s, and the loading procedure was defined to obtain four or five cyclic load steps for each masonry panel. In the experimental campaign presented by Santa-Maria et al. [22], the test procedure started with the first diagonal loading and unloading, followed by the loading of the second diagonal and unloading. Two cycles were performed at each load level, the load increments at each level were of 25 kN.

The diagonal tensile test is regarded as a simple and expedite procedure for the in-plane behaviour characterization. However, it is important to stress that the capability of this type of test to disclose all the failure modes of masonry walls is limited. For example, the rocking/crushing mechanism cannot be evaluated [17]. For the evaluation of those mechanisms, other experimental procedures, such as the one used by Pinho et al. [23], or Vasconcelos et al. [24] must be carried out.

A summary of data available in literature referred to diagonal tensile tests on unreinforced clay brick masonry strengthened with additional overlays or composite materials is presented in **Table IV.1**.

Different types of masonry and strengthening systems are presented. It is possible to verify that most of the authors use a reduced amount of specimens for the characterization of a specific layout. However, whenever possible the coefficient of variation was calculated and the results obtained are in general quite low, especially for strengthened panels. Therefore, the use of a reduced number of specimens seems to lead to sufficiently representative experimental results.

Table IV.1: Summary of previous diagonal tensile test results on strengthened URM.

Reference	Type of masonry	Dimension of blockst (mm)	Dimension of the panel h	l (mm)	t	Nº of panels	Type of reinforcement	F_{max} (kN)	S_s (MPa)	CoV (%)	Capacity increment (%)
Santa-Maria et al. [22]	HCBM	290x140x112	1060	1100	140	5	--	132	--	15	--
						4	2 diagonal 150 mm-wide CFRP laminate	226	--	2	71
						5	2 diagonal CFRP fabric	196	--	4	48
						4	2 horizontal 150 mm-wide CFRP laminate	144	--	6	9
						5	2 horizontal CFRP fabric	182	--	8	38
Gabor et al. [25]	HCBM+CM	210x100x50	870	840	100	2	--	234	--	--	--
						1	unidirectional glass fibre, RFV	332	--	--	42
						1	unidirectional carbon fibre, RFC	361	--	--	54
						1	bidirectional glass fibre, RFW	384	--	--	64
Ozsayin et al. [26]	PCBM +CLM	87x84x56	350	350	70	2	--	--	0.95	--	--
						2	CFRP, strips	--	1.98	--	108
						2	CFRP, full surface	--	2.25	--	137
	PCBM +CM		500	500	70	2	--	--	0.92	--	--
						2	CFRP, strips	--	1.29	--	40
						2	CFRP, full surface	--	2.38	--	159
	PCBM +CLM					2	--	--	0.6	--	--
						2	CFRP, strips	--	1.39	--	132
						2	CFRP, full surface	--	1.16	--	93
Kadam et al. [2]	SCBM one-wythe thick+CM	230x110x70	700	700	110	3	--	25	--	2	--
					160	3	unidirectionally anchored welded wire mesh	164	--	7	561
						3	bidirectionally anchored welded wire mesh	174	--	13	602
	SCBM two-wythe thick+CM		750	750	230	3	--	46	--	7	--
					280	3	unidirectionally anchored welded wire mesh	236	--	8	413
						3	bidirectionally anchored welded wire mesh	223	--	15	385
Dehghani et al. [10]	SCBM+CM	225x105x40	450	450	105	2	--	51	--	--	
						8	ECC, (ft=3.8; fc=47 MPa), LT:10 and 15 mm	70-142	--	--	37-178

The test setup adopted for the diagonal tensile tests is represented in **Figure IV.1** and complies with the experimental procedure described by ASTM E519-02 [12]. The dimensions of the panels were set to 0.99 × 0.99 m considering equipment constrains, symmetry conditions and the dimensions adopted by other authors using similar brick dimensions and panel configurations. As discussed by Brignola et al. [16] and Calderini et al. [27], and evaluated by Frocht [28] the elastic solution considering homogeneous isotropic continuum providing the following stress state at the centre of the panel when only a diagonal compressive load is applied, $q = 0$; $\sigma_x = \sigma_y \cong -0.56P/A$; $\tau_{xy} = 1.05P/A$; $\sigma_I \cong 0.5P/A$; $\sigma_{II} \cong -1.62P/A$. Where A is the transversal area of the panel, P is assumed as positive and the loading direction angle always being 45°. The Mohr´s representation of the stress state in this region is depicted in **Figure IV.2**.

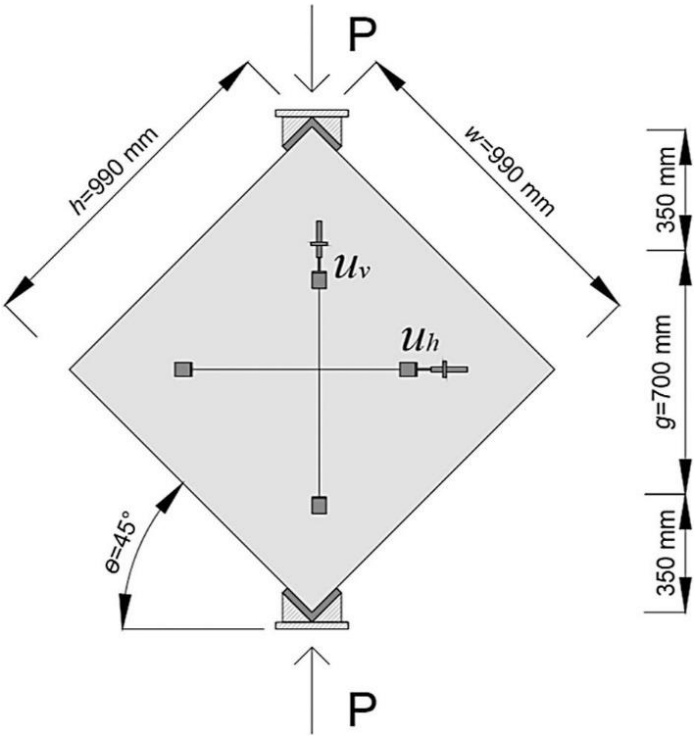


Figure IV.1: Diagonal tensile test, general set-up.

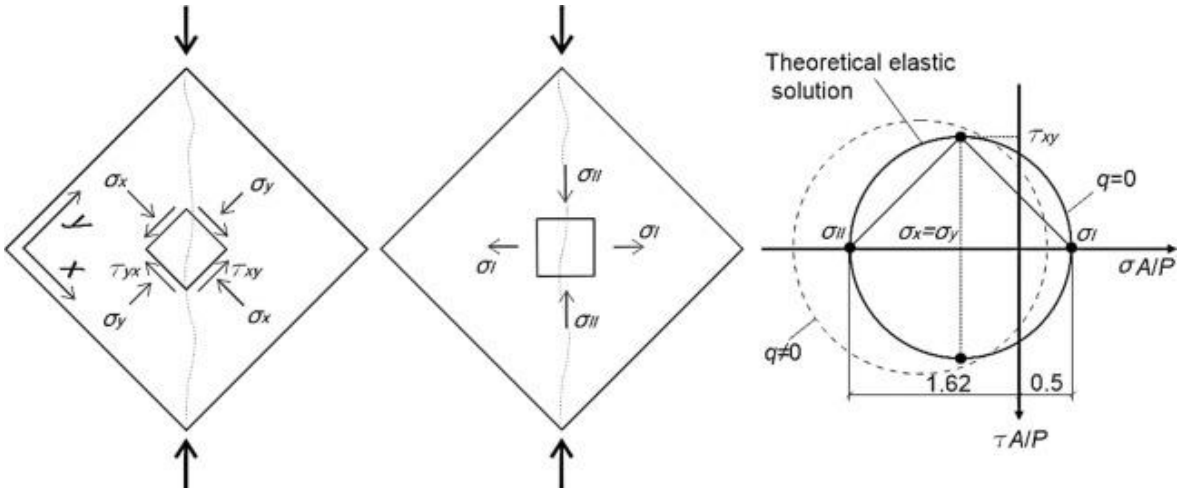


Figure IV.2: Mohr's representation of the stress state assumed in the central area of the specimen.

The values of the shear stress, shear strain and modulus of shear stiffness in the centre of the panel are also obtained according to the procedures indicated in ASTM E519-02 [12], in this case the stress state is characterized by a $\tau_{xy} = \sigma_I = \sigma_{II}$ [16]. The shear stress is obtained by the **Eq. (IV.1)**:

$$S_s = \frac{0.707 \times P}{A_n} \quad \textbf{(IV.1)}$$

where P is the applied load, A_n is the net area of the specimen's cross-section calculated according to **Eq. (IV.2)**:

$$A_n = \left(\frac{w+h}{2}\right) \times t \times n^* \quad \textbf{(IV.2)}$$

where w, h and t are, respectively, the width, the height, and the total thickness of the specimen, and n^* is the percentage of the gross area of the unit that is solid, expressed as a decimal.

The shear strain is computed as shown in **Eq. (IV.3)**:

$$\gamma = \frac{u_v + u_h}{g} \quad \textbf{(IV.3)}$$

where γ is the shearing strain, u_v is the vertical shortening, u_h is the horizontal elongation and g is the vertical gage length.

Finally, the modulus of stiffness in shear is calculated as shown in **(IV.4)**:

$$G = \frac{S_s}{\gamma} \quad \textbf{(IV.4)}$$

2 OBJECTIVES AND RESEARCH SIGNIFICANCE

This research discusses the relevance of diagonal tensile test for the characterization of the "in-plane" monotonic and cyclic behaviour of masonry specimens. An expeditious procedure is developed and applied to quantify the contribution of the reinforcement system to improve the masonry behaviour. The identification and interpretation of the damage mechanisms that develop during the diagonal tensile tests are presented, and an extrapolation of these to practical situations is discussed. Finally, a review of analytical calculation procedures to estimate the load carrying capacity and identify the mechanisms leading to rupture of strengthened masonry is carried out, and the results are presented and discussed.

3 MATERIALS AND METHODS

3.1. Materials used in the experiments

The materials used in the preparation of the masonry elements, representative of infill walls, and of the strengthening system were selected with the intention of representing regional real cases as much as possible. Although lime mortars are also frequently used in the structural rehabilitation of masonry walls, the system investigated was only based on Portland cement as binder. The masonry specimens were assembled using ceramic bricks (Length × Height × Thickness: 28.5 × 19.5 × 11.0 cm^3) and the following cement mortar for the joints: Portland cement 32.5 N, medium graded river sand and water, in a volume ratio of 1:5:2. After a layer of roughcast was applied: Portland cement 32.5 N, medium graded river sand and water, in a volume ratio of 1:4:2. Finally a render layer of a cementitious mortar with a thickness of 1.5 cm was added on both faces of the masonry specimen, same composition as the mortar used in the joints. The composition and workability of the mortars were initially optimized and then remained similar for all the assembled specimens. The main mechanical properties of the used materials were experimentally assessed, and the results obtained are summarized in **Table IV.2**.

Table IV.2: Properties of the masonry components.

Masonry components	
Compressive strength of units, parallel to hollows, EN 772-1 [29] ·,··	6.55 (8%) N/mm^2
Compressive strength of units, normal to hollows, EN 772-1 [29] ·,··	2.21 (9%) N/mm^2
Compressive strength, mortar joints and render, EN 1015-11 [30] ·	8.58 (7%) N/mm^2
Flexural strength, mortar joints and render, EN 1015-11 [30] ·	2.11 (3%) N/mm^2
Adhesion strength to render layer to brick, EN 1015-12 [31]·	0.51 (22%) N/mm^2

·The values in parenthesis represent the coefficient of variation.
··Values obtained experimentally in dry air condition state.

A commercially available system, herein designated FRMCom, was used for the strengthening of the masonry specimens. The FRMCom combines a carbon fibre mesh (CFM) with a cementitious mortar matrix reinforced with polypropylene fibres (PFRM). The polypropylene fibres have the main function of preventing cracking shrinkage of the mortar, while the CFM aims to assure strengthening attributes to the FRMCom system.

The experimental results obtained from the characterization of the main physical and mechanical properties of the PFRM in the hardened state are summarized in **Table IV.3**, and the corresponding followed standards are indicated. The mechanical tests were conducted in all cases 28 days after casting, in agreement with the EN 1015-11 [30]. The flexural strength was obtained by averaging the results obtained in 3 specimens and the compressive strength was obtained by averaging the results obtained in 6 specimens. All specimens were cured in laboratory ambient conditions, at an average temperature of 19 ± 2 °C and a relative humidity of about 55% ± 10%. The bending tests were performed by applying a constant load increment of 35 N/s and the compression tests were executed by applying an increasing force at a constant loading rate of 400 N/s until failure.

Table IV.3: Properties of the PFRM.

PFRM	
Density	2050 kg/m^3
Amount of water	14% by weight
Elasticity Modulus, [32]	40000 N/mm^2
Compressive strength*, EN 1015-11 [30]	44 (6%) N/mm^2
Flexural strength*, EN 1015-11 [30]	3.27 (6%) N/mm^2
Adhesion strength to render layer*, EN 1015-12 [31]	1.48 (20%) N/mm^2

* Values in parenthesis represent the coefficient of variation.

The adhesion strength was evaluated by means of pull-off tests conducted according the EN 1015-12 [31]. The specimens with 30 × 20 × 13.5 cm^3 were built following the same process used for the specimens of diagonal tensile tests and cured at constant temperature and relative humidity of 20 °C and 90%, respectively [31]. The preparation of the samples for testing implied the execution of a circular slot with a depth of 27 mm and a diameter of 50 mm, using a core drilling machine and water for easier cutting and for avoiding excessive vibrations. After cleaning the surface, a metallic plate was bonded to the test area. The metallic plate was later attached to the pull-off machine, after the initial levelling of the equipment, an increasing traction force was applied at a constant loading rate of

40 N/s. The maximum force recorded corresponds to the adhesion force that after has been divided by the area of the core providing the adhesion strength. The pull-off tests were carried out 28 days after casting.

In **Table IV.4** the properties of the CFM are presented, according to the data provided by the supplier [32].

Table IV.4: Properties of the CFM, [32].

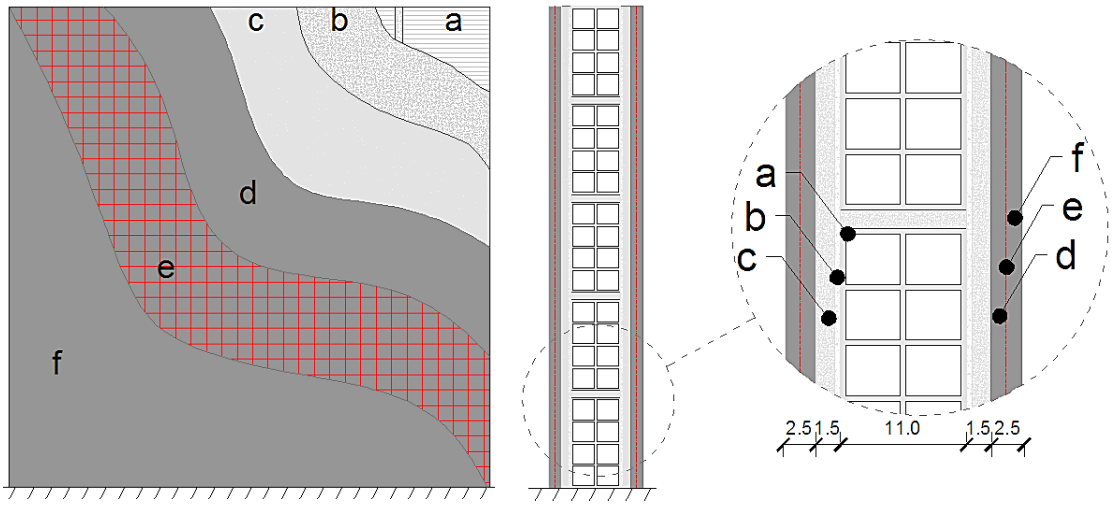
CFM	
Carbon fibres in both directions	50 threads/m
Elastic modulus	≥240 kN/mm²
Tensile strength	≥4300 N/mm²
Elongation at rupture	1.75 %
Ultimate tensile force	185 kN/m

3.2. Preparation of the specimens for the diagonal tensile tests

The procedure adopted in the production of the masonry walls involved the following steps: soaking of the bricks until saturation; placement of guides to keep a constant joint thickness of 1.5 cm; levelling of the bedding mortar; placement and levelling of a row of bricks; placement of vertical mortar joints with a thickness of 1.5 cm; verification of the thickness of the joints; check the plumb; repeat the previous steps until the wall was finished. Six walls were produced for the diagonal tensile tests, three for reference specimens and three for subsequent strengthening.

All masonry specimens (a) were sprinkled with a cement mortar (1:4:2) two days after (b), then a cement mortar layer with a thickness of 1.5 cm (volume ratio 1:5:2) was applied on both faces (c), as shown in **Figure IV.3a)** and **Figure IV.3b)**.

The specimens were strengthened using the FRMCom system, as shown in **Figure IV.3a)** and **Figure IV.3b)**, by carrying out the following steps: initial spraying of the wall with water; application of the first layer of PFRM with an approximate thickness of 1.2 cm (d); placement of the CFM on top of the PFRM layer (e); application of the second layer of PFRM with an approximate thickness of 1.2 cm (f); use of a ruler and a trowel to level and smoothen the mortar layer surfaces; spraying of the wall surfaces with water 15 min after finished, to avoid shrinkage. The strengthening operations were performed 14 days after the application of the render layer (c).

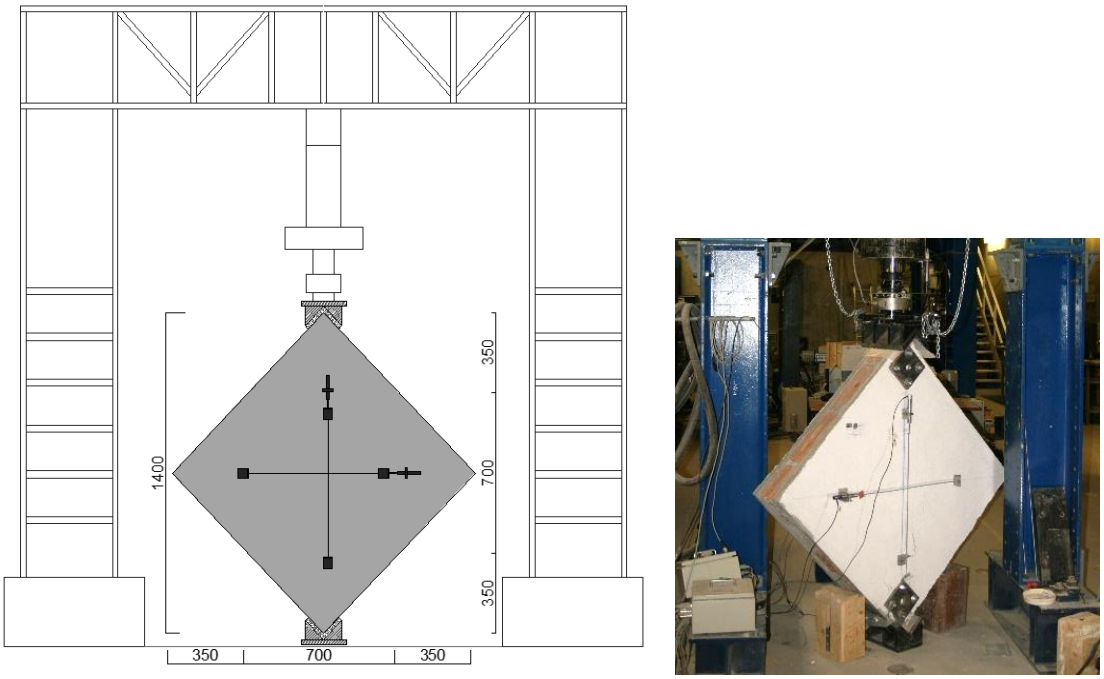


a) b)

Figure IV.3: General layout of specimens: a) Procedure adopted in the production of the specimens; b) Section of the specimens and detail of the FRMCom system. (Legend: a - masonry; b - roughcast mortar, mortar 1:4:2; c - render layer 1.5 cm thick, mortar 1:5:2; d - PFRM 1.2 cm; e - CFM; f - PFRM 1.2 cm. Dimensions in cm)

3.3. Set up used for the diagonal tensile tests

Diagonal tensile tests were performed to assess the contribution of the strengthening system for increasing the load carrying capacity, the deformability and the energy dissipation performance before failure of the masonry elements when subjected to a loading scheme that resembles the in-plane shear loading conditions. The specimens had a square geometry with approximately 990 mm side, as shown in **Figure IV.4**. The number of clay blocks used in the vertical and horizontal directions was 5 and 3.3, and the symmetry of blocks and joints both in the horizontal and in the vertical directions was guaranteed. The thickness of the reference specimens was 140 mm and the thickness of the strengthened specimens was 190 mm, as shown in **Figure IV.3**.



a) b)

Figure IV.4: Test set-up of the direct tensile test: a) Geometry of specimens and position of LVDTs (dimensions in mm); b) Detail of the positioning of the specimen and of the test set-up.

The set-up included a testing frame, an actuator with a 500 kN load cell, and a servo-hydraulic closed loop-controlled system, a data acquisition system and a monitoring system composed by 5 linear variable displacement transducers (LVDT's). The vertical and horizontal deformability of both specimen surfaces were determined in the central area, between 1/4 and 3/4 of the diagonal of the specimen, by using 2 LVDT's in each direction, as shown in **Figure IV.4a)**.

The dimensions of the steel shoes adopted a "V" shape with 152 mm in each side and 320 mm long, according to ASTM E-519-2 [12]. In the case of the strengthened specimens, the local crushing and splitting of the external strengthening layer at both loading edges were observed, as observed for specimen FRMCom_01 subsequently described. In order to avoid this premature local failure mechanism, in the subsequent specimens two steel plates were placed near the supports ($150 \times 150 \times 30$ mm^3) to provide additional confinement to the material in this region. These plates were transversely connected with 16 mm diameter steel rods crossing the specimen between the opposite faces in each support, as shown in **Figure IV.4b)**.

Each test was performed using displacement control of the actuator cross-head, by measuring the displacement of the cross-head with an external LVDT. The applied displacement rate was kept constant at 0.01 mm/s, for both monotonic and cyclic tests. In the case of the cyclic tests, the displacement amplitude was gradually increased until the last cycle was reached. The amplitude of the cycles was specified considering the displacement of the actuator cross-head at the peak of the monotonic test, the increase in each cycle was determined as 1/5 of that value. A maximum number of 7 cycles were imposed, and an additional final loading cycle was imposed by applying a monotonically increasing displacement until failure was reached (**Figure IV.5**). In the case of the strengthened specimens, the experimental procedure was interrupted after the 7th cycle, due to the loss of contact between the actuator and the loading shoe. The 8th cycle was started after correcting this residual vertical deformation, by lowering 5 mm the reference initial position of the actuator cross-head, as shown in **Figure IV.5**.

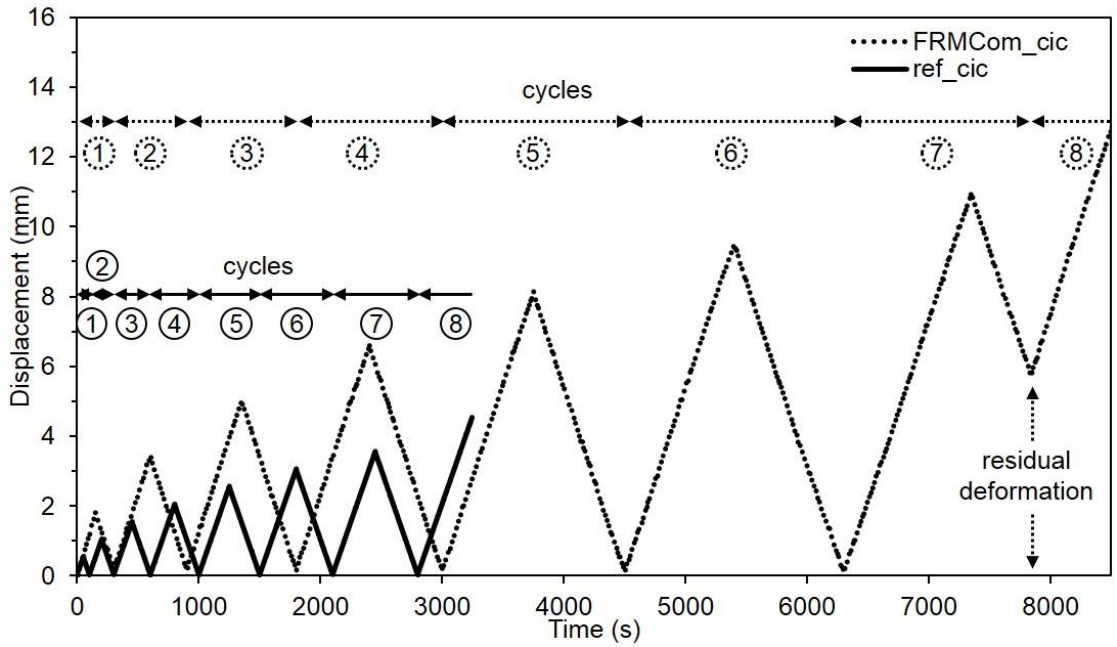


Figure IV.5: Displacement laws imposed during the cyclic tests.

4 DIAGONAL TENSILE TEST RESULTS

The main results obtained for the monotonic diagonal tensile tests, which include the peak load and the corresponding horizontal and vertical average displacements, are presented in **Table IV.5**. The results obtained for the cyclic tests are presented in **Table IV.6**. For each cycle the peak load and the corresponding displacements, horizontal and vertical, are indicated in this table. For the specimens

ref_03 and FRMCom_03 only the results up to the 6th and 7th cycles, respectively, are presented due to the occurrence of their premature failure at the referred cycles.

Table IV.5: Monotonic diagonal tensile test results.

ref_02			FRMCom_01		
Load (kN)	u_h (mm)	u_v (mm)	Load (kN)	u_h (mm)	u_v (mm)
97.34	0.12	-0.26	409.54	1.47	-0.68

Table IV.6: Cyclic diagonal compression test results.

	ref_01			ref_03			FRMCom_02			FRMCom_03		
Cycle	Load (kN)	u_h (mm)	u_v (mm)	Load (kN)	u_h (mm)	u_v (mm)	Load (kN)	u_h (mm)	u_v (mm)	Load (kN)	u_h (mm)	u_v (mm)
1st	14.51	0.00	-0.02	26.15	0.02	-0.04	115.68	0.02	-0.07	82.83	0.01	-0.05
2nd	42.50	0.01	-0.06	54.79	0.03	-0.09	219.93	0.06	-0.15	198.38	0.03	-0.12
3th	72.47	0.03	-0.11	84.66	0.05	-0.14	339.56	0.22	-0.29	310.40	0.11	-0.23
4th	100.48	0.04	-0.16	110.27	0.07	-0.18	401.35	0.78	-0.53	386.43	0.76	-0.44
5th	115.88	0.06	-0.19	136.54	0.10	-0.24	418.32	1.41	-0.66	430.81	1.37	-0.71
6th	98.44	0.13	-0.28	146.17	0.24	-0.32	383.04	1.90	-0.79	394.21	1.63	-0.74
7th	80.36	0.38	-0.32	–	–	–	312.35	2.59	-0.75	315.35	2.48	-0.46
8th	50.89	1.33	-0.42	–	–	–	298.16	3.07	-1.02	–	–	–

The load vs displacement responses of the reference and strengthened specimens in terms of the averaged vertical and horizontal LVDT measurements are shown in **Figure IV.6a)** and **Figure IV.6b)**. In general, the strengthened specimens have reached considerably higher strengths than the reference specimens. The post-peak behaviour of the reference specimens showed a smooth load decay, except for specimen ref_03_cic, which was supposed to undergo a cyclic loading sequence but failed suddenly after reaching a considerably higher peak load than the remaining reference specimens. The responses registered for the strengthened specimens were, in general, similar, showing a pre-peak stage of significant load carrying capacity increase, and the peak load was reached for substantially higher displacements than the ones observed for the reference specimens. After peak load the strengthened specimens presented a relatively smooth load decay with the increase of the horizontal deformation.

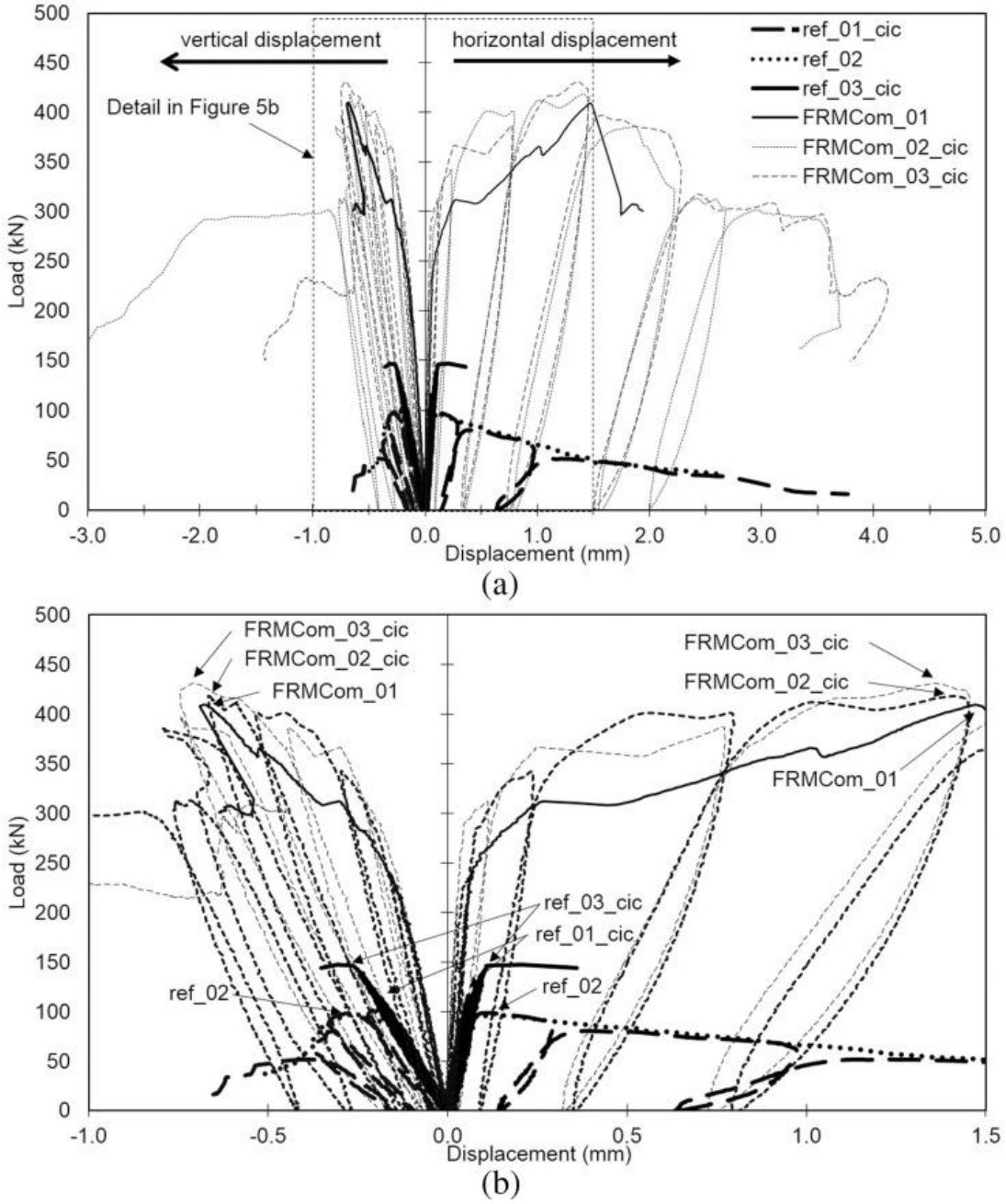


Figure IV.6: Load vs displacement responses of the strengthened specimens: (a) global response; (b) detail of the response until peak.

The typical crack patterns observed at the surface of the reference and strengthened specimens after testing are presented in **Figure IV.7a)** and **Figure IV.7b)**, respectively. The reference specimen presented a vertical crack that developed in a straight fashion from the lower to the upper support, very few and minor additional cracks presenting a very small tip opening developed after that main crack. The strengthened specimens presented, in a first phase, the same type of cracking as the reference specimens. However, at higher load levels multiple cracks developed, and the failure was reached when the strengthening overlay started to detach from the masonry substrate

(**Figure IV.7c)**). This detachment occurred at the interface between the render layer and the ceramic masonry brick surface, as shown in **Figure IV.7c)**.

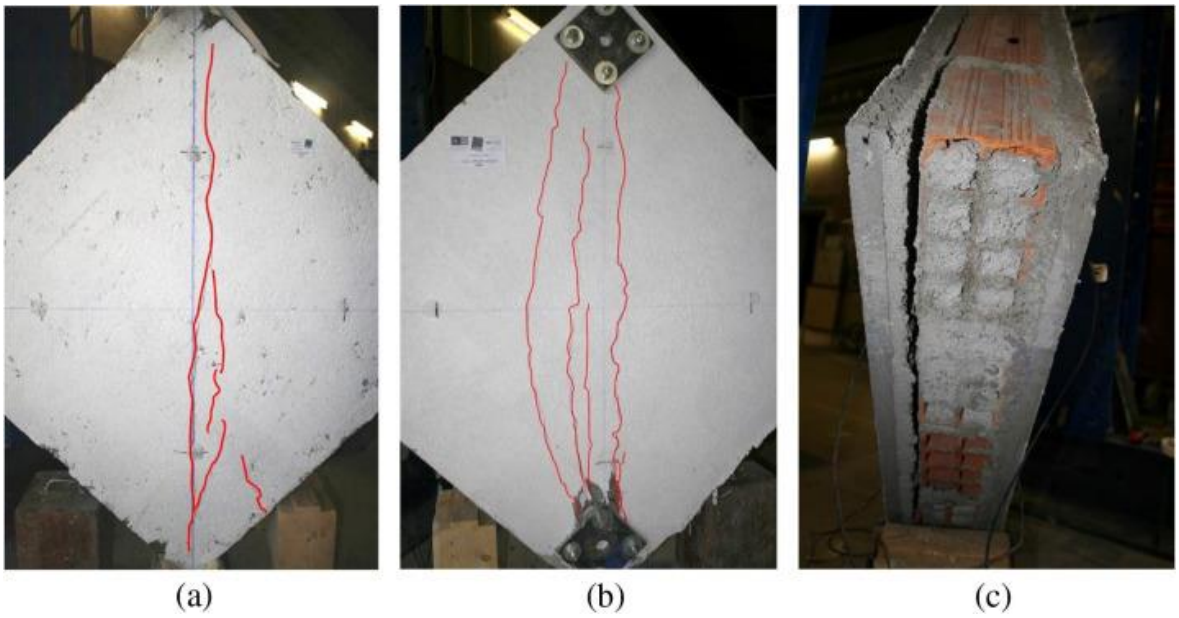


Figure IV.7: Image of the specimens after testing: (a) Crack pattern in reference specimen, ref-02 side B; (b) Crack pattern in strengthened specimen, FRMCom-03 side B; (c) Detachment between the strengthening overlay and substrate, FRMCom-03.

5 DISCUSSION OF RESULTS

5.1. Peak values and capacity ratios

The responses presented in **Figure IV.8** allow the clear distinguishing of the contribution of the strengthening system to the increase of the load carrying capacity of the tested masonry specimens. The shear stress and the shear strain were evaluated according to **Eq. (IV.1)** and Eq. **(IV.3)**, respectively, where for g a value of 700 mm was considered. The shear strength of strengthened specimens was approximately 2 times higher than that of the reference walls. Considering the shear strain values obtained, the scatter of the results registered in the case of the reference specimens was greater, essentially due to the absence of the effect provided by the strengthening system for stabilising the fracture process. However, the strengthened specimens also showed a considerable scatter of results in terms of ultimate shear strain, in this case probably due to the influence of brittle failure modes such as the formation of the typical diagonal tensile crack and the detachment of the PFRM layers.

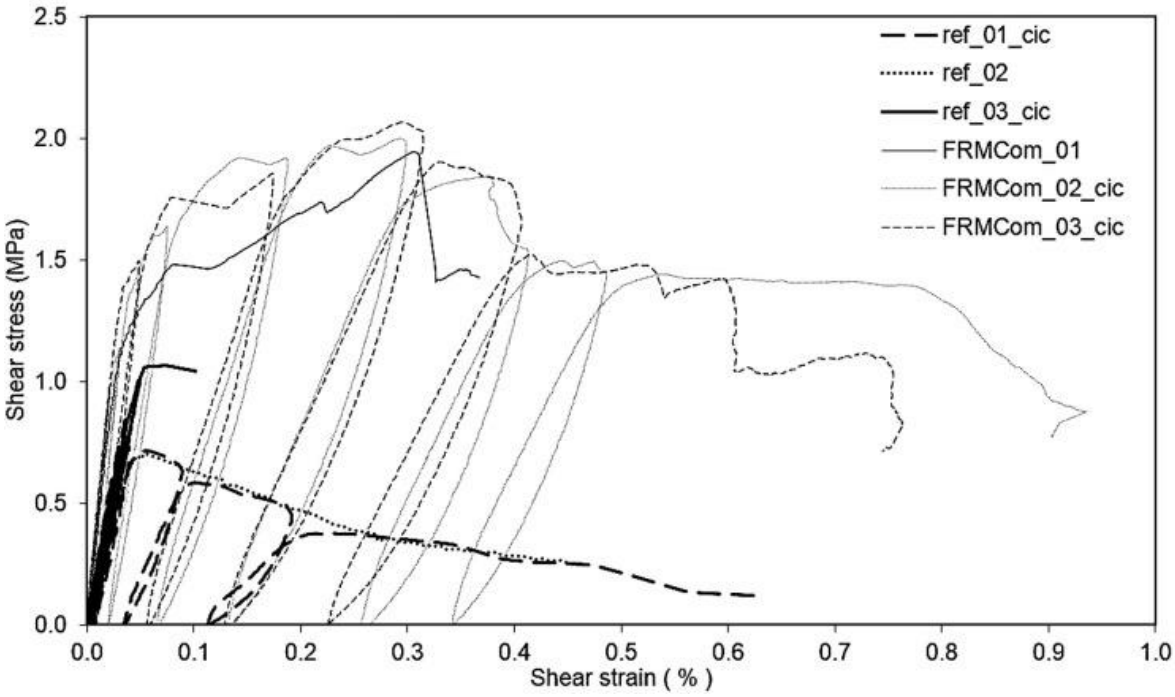


Figure IV.8: Shear stress vs shear strain response of the specimens.

The maximum shear stress values obtained for cyclic testing were slightly higher than the values obtained in monotonic tests. This is explained by the possible accommodation of the loading shoes during the initial loading/ unloading cycles, providing a more homogeneous diagonal load transmission to the specimen and therefore a slight increase of load capacity.

The collapse of the reference specimen ref_03_cic was reached shortly after the peak load was reached, as soon as the diagonal crack was formed. In contrast, the other two reference specimens have reached considerably higher deformation levels, and the collapse took place after a gradual load decay. In general, all reference specimens have shown elastic responses almost up to the peak load. In contrast, the strengthened specimens exhibited a substantially increased post-cracking load carrying capacity. The non-linear portions of the responses were much more significant than in the case of the reference specimens. The energy dissipation capacity was assessed for the monotonic tests by computing the area under the load vs displacement response, where the displacement represented the distance difference between the two opposite loaded edges of the specimen during testing (see **Figure IV.4**). When comparing reference and strengthened panels the increment of 1390% of the dissipated energy was obtained. Considering that the monotonic load–displacement responses approximate well the envelope of the cyclic tests, similar results of the dissipated energy increments are expected for the cyclic tests.

The average values of the shear stress, the shear strain and the shear modulus are computed in **Table IV.7** and **Table IV.8**. The ratios between the limit values of the shear stresses and the shear strains in the cases of the elastic and of the non-linear branches of the responses observed in the strengthened and in the reference specimens were computed as well. The elastic branch was considered to develop up to 33% of the peak load in the case of the specimens tested with monotonic loading, and up to the peak of the first cycle in the case of cyclic loading. These results show that the strengthening system has provided a shear strength increase of approximately 2.3.

Table IV.7: Average of the limit values of the shear stress, shearing strain and shear modulus obtained for the reference and the strengthened specimens.

Response range	Type of specimen	Shear Stress S_s (MPa)	Shearing Strain γ (%)	Modulus of shear stiffness G (MPa)
Elastic branch	Reference	0.185	0.007	2716.2
	Strengthened	0.532	0.012	4457.8
Peak	Reference	0.871	0.054	1696.1
	Strengthened	2.002	0.299	650.6

Table IV.8: Increase of capacity in terms of shear stress, shearing strain and increment of shear modulus obtained after strengthening.

Response range	Shear Stress S_s	Shearing Strain γ	Modulus of shear stiffness G
Elastic branch	2.1	1.1	1.6
Peak	2.3	5.5	0.4

The evolution of the damage due to the cyclic loading is shown in **Table IV.9**, where Gcycle represents the modulus of shear stiffness in each cycle, considering the linear part of the curve shear stress vs. shear strain during the loading sequence, and GE represents the modulus of shear stiffness in the elastic branch of the first cycle. The specimens strengthened with the FRMCom system presented similar ratios Gcycle/GE in the final cycles. In the case of the reference specimens the damage occurred suddenly in the case of the specimen ref_03, where the computed ratio was always 1.0 until failure. This result indicates that the specimen failed in a brittle manner. In the case of ref_01 the response obtained showed a gradual decay of the Gcycle/GE ratio, in a similar fashion to the observed in the case of the strengthened specimens.

Table IV.9: Variation of the Shear modulus during cyclic tests.

	ref_01		ref_03		FRMCom_02		FRMCom_03	
Cycle	G_{cycle} (MPa)	ratio G_{cycle}/G_E	G_{cycle} (MPa)	ratio G_{cycle}/G_E	G_{cycle} (MPa)	ratio G_{cycle}/G_E	G_{cycle} (MPa)	ratio G_{cycle}/G_E
Elastic	3326.6	–	2347.0	–	4427.2	–	4447.4	–
1st	3326.6	1.0	2347.0	1.0	4427.2	1.0	4447.4	1.0
2nd	2799.6	0.8	2297.7	1.0	4430.7	1.0	4467.3	1.0
3rd	2706.9	0.8	2358.8	1.0	4210.0	1.0	4513.1	1.0
4th	2526.8	0.8	2367.2	1.0	2627.8	0.6	3251.9	0.7
5th	2477.7	0.7	2436.7	1.0	1379.2	0.3	1325.5	0.3
6th	2083.7	0.6	2249.3	1.0	1044.5	0.2	975.7	0.2
7th	1036.0	0.3	–	–	913.9	0.2	847.3	0.2
8th	421.8	0.1	–	–	873.4	0.2	–	–

The effectiveness of different strengthening systems and the scatter of results obtained can be compared with the ones presented previously in **Table IV.1**. The mean values of the maximum load and coefficient of variation obtained in this research for reference specimens were 120 kN and 17%, which is expectable considering the brittle failure mechanism obtained. Meanwhile, for strengthened specimens the mean values of the maximum load and coefficient of variation obtained were 420 kN and 2%, representing an increase in the capacity of 250%. The number of specimens tested, although limited, agrees well with the number of specimens typically used by other authors for similar experimental characterizations and the coefficient of variation obtained is also comparable to the ones obtained by other researchers, as shown in **Table IV.1**.

5.1.1. Failure modes and crack patterns

During the diagonal tensile tests several types of mechanisms of structural degradation were observed (see **Figure IV.9**):

- Type A. Crushing of the masonry units next to the supports, toe crushing, development of horizontal cracks, (ref_01, FRMCom_01).
- Type B. Failure due to diagonal tensile stresses imposed during the tests, development of vertical cracks in the central area of the specimens (ref_01_cic, ref_02, ref_03_cic).
- Type C. Delamination of the render and strengthening overlay from the masonry, development of vertical cracks between the masonry and the rendering layers. Delamination starts in the two free corners of the specimen (FRMCom_01, FRMCom_02_cic, FRMCom_03_cic).
- Type D. Cracking and failure of webs and shells of the ceramic bricks (FRMCom_01, FRMCom_03_cic).

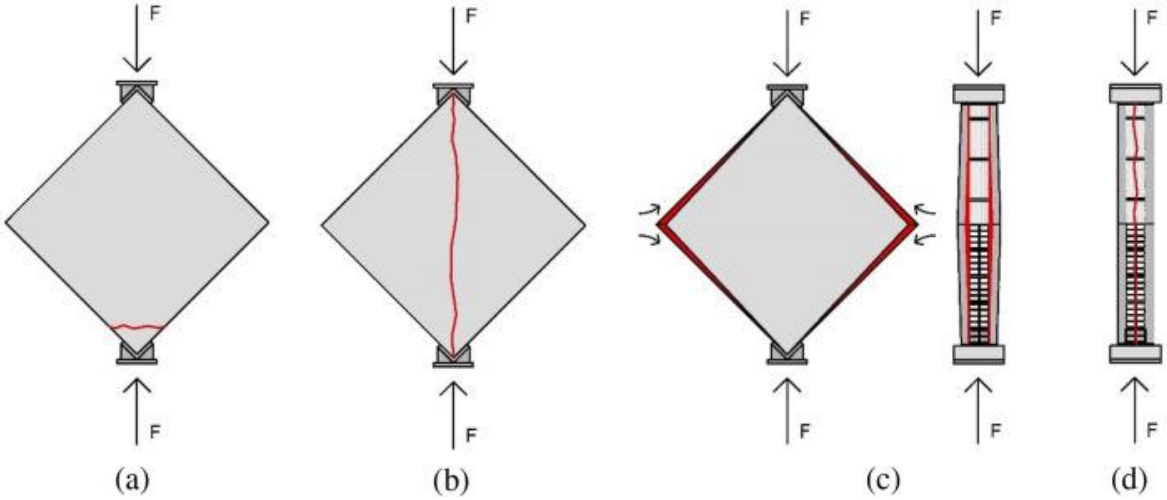


Figure IV.9: Schematics of the different mechanisms leading to structural degradation during the diagonal tensile tests: (a) Type A; (b) Type B; (c) Type C; (d) Type D.

The failure of the specimens was reached after the development of one or more of these mechanisms. In the case of the reference specimens the mechanisms developed were mainly of the types B and D. In the case of strengthened specimens, a sequence of the mechanisms type B, C and D occurred before failure. The mechanism type A occurred only when the first strengthened specimen, FRMCom_01, was tested. In the subsequent tests this failure mode did not occur, since the hollows of the brick in this zone were filled with a high compressive strength mortar, and metallic plates were applied to provide additional confinement to the loading areas.

The instant at which the different mechanisms were initiated can be identified in the **Figure IV.10**, where the letters identify the stage at which the respective type of mechanism tends to occur. For both types of specimens, it was possible to trace the degradation of the stiffness of the load vs displacement response. The stiffness of the load vs horizontal displacement response is represented by the slope of the loading–unloading branches Kd,h, while the stiffness of the load vs vertical displacement response is represented by the slope of the loading–unloading branches, Kd,v. After the limit of the elastic branch was reached (point b in **Figure IV.10**), both slopes, Kd,h and Kd,v, decrease faster for reference specimens, indicating that a higher degradation was obtained in each cycle. For the strengthened specimens the referred slopes show a lower variation per cycle, revealing that the contribution of the strengthening solution to the shear capacity of the specimens results in a reduction of the stiffness degradation. The variation of the stiffness of the load vs vertical displacement responses, Kd,h and Kd,v, and of the ratios between the stiffness of the first and of the consecutive cycles are presented in **Table IV.10**.

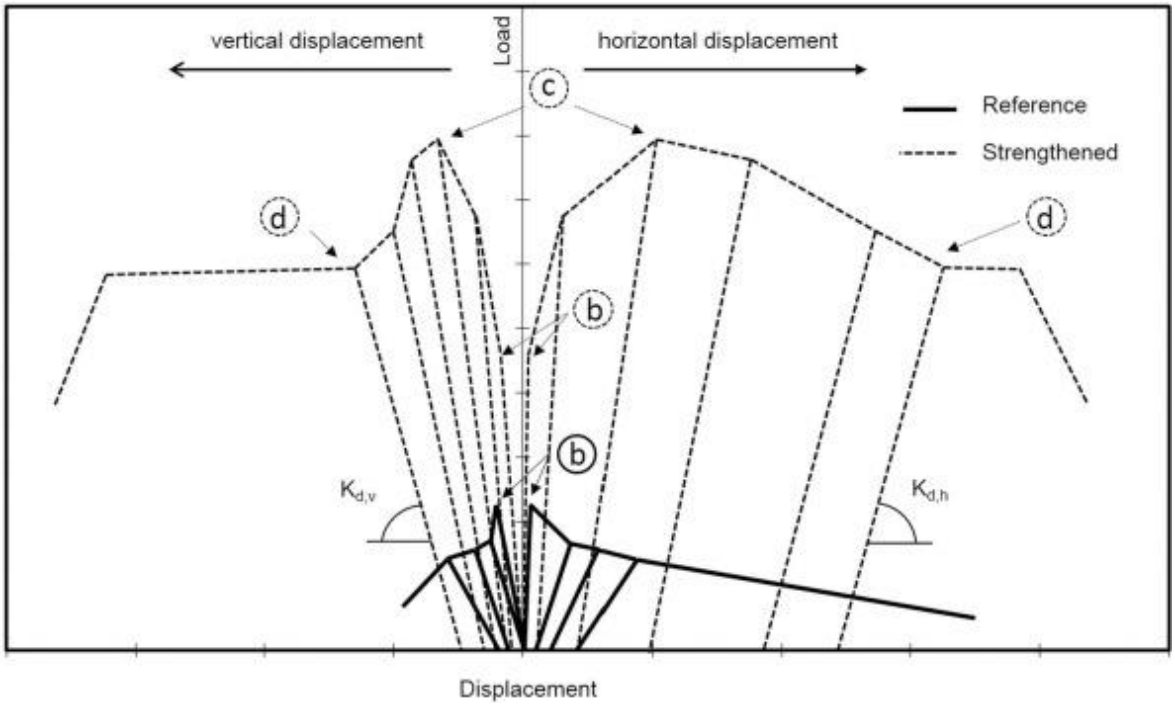


Figure IV.10: Identification of the onset of the different types of damage mechanisms.

Table IV.10: Evolution of the stiffness of the load vs horizontal displacement response from reference specimens under cyclic loading.

	ref_01				ref_03				FRMCom_02				FRMCom_03			
Cycle	K_{dv} (kN/mm)	ratio K_{dv}	K_{dh} (kN/mm)	ratio K_{dh}	K_{dv} (kN/mm)	ratio K_{dv}	K_{dh} (kN/mm)	ratio K_{dh}	K_{dv} (kN/mm)	ratio K_{dv}	K_{dh} (kN/mm)	ratio K_{dh}	K_{dv} (kN/mm)	ratio K_{dv}	K_{dh} (kN/mm)	ratio K_{dh}
1st	-672	1.00	4266	1.00	-704	1.00	1714	1.00	-1671	1.00	6211	1.00	-1815	1.00	13252	1.00
2nd	-669	1.00	3118	0.73	-641	0.91	1876	1.09	-1620	0.97	5819	0.94	-1694	0.93	8146	0.61
3rd	-660	0.98	2787	0.65	-617	0.88	1841	1.07	-1431	0.86	3674	0.59	-1686	0.93	7242	0.55
4th	-637	0.95	2254	0.53	-615	0.87	1736	1.01	-1096	0.66	1261	0.20	-1353	0.75	2309	0.17
5th	-618	0.92	2081	0.49	-609	0.86	1605	0.94	-683	0.41	422	0.07	-816	0.45	439	0.03
6th	-413	0.62	1480	0.35	-555	0.79	1318	0.77	-557	0.33	229	0.04	-517	0.28	254	0.02
7th	-241	0.36	234	0.05					-426	0.26	120	0.02	-632	0.35	124	0.01
8th	-114	0.17	32	0.01					-345	0.21	98	0.02				

The crack patterns observed after the diagonal tensile tests are shown in **Figure IV.11** and **Figure IV.12**. In general, the failure modes for the unreinforced masonry reference specimens were the typical ones expected for this type of test. In the case of the strengthened specimens the crack patterns observed, and failure mechanisms obtained, were influenced by the contribution of the strengthening system. The failure mode observed in this case was mostly characterized by a first

phase where diagonal tensile cracks were developing, followed by the delamination of the render layer plus strengthening mortar, and a final stage of failure determined by the internal crushing of the units. In the case of the FRMCom_02 and FRMCom_03 specimens several cracks were formed, particularly next to the supports of the specimen, as shown in **Figure IV.12**. The onset of the damage mechanism type D (**Figure IV.9**) is clearly revealed by the sudden increase of the vertical displacement when compared to the horizontal ones (**Figure IV.6**), as identified in **Figure IV.10** by the letter "d". The vertical displacement increments become, at this stage, much larger than the horizontal ones due to the crushing of the shells and webs of the ceramic bricks.

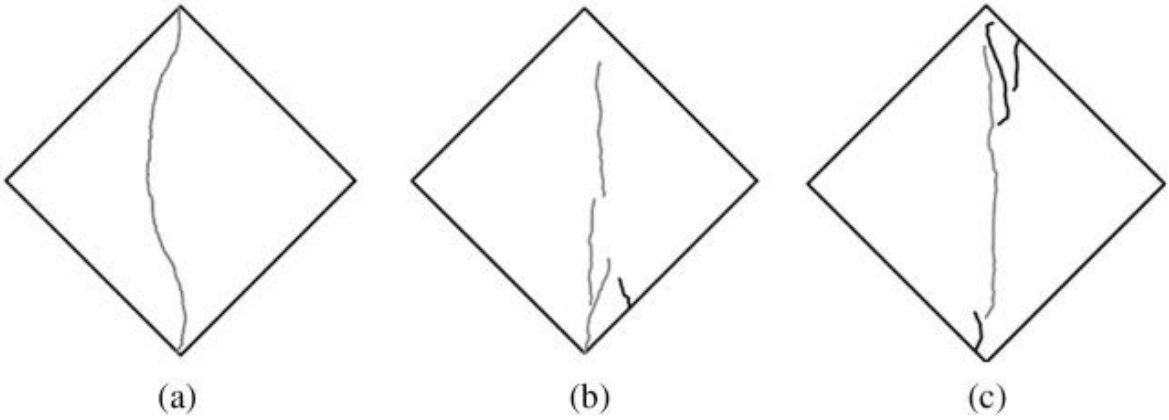


Figure IV.11: Crack patterns of reference specimens after testing: (a) ref_01_side A; (b) ref_02_side A; (c) ref_03_side A.

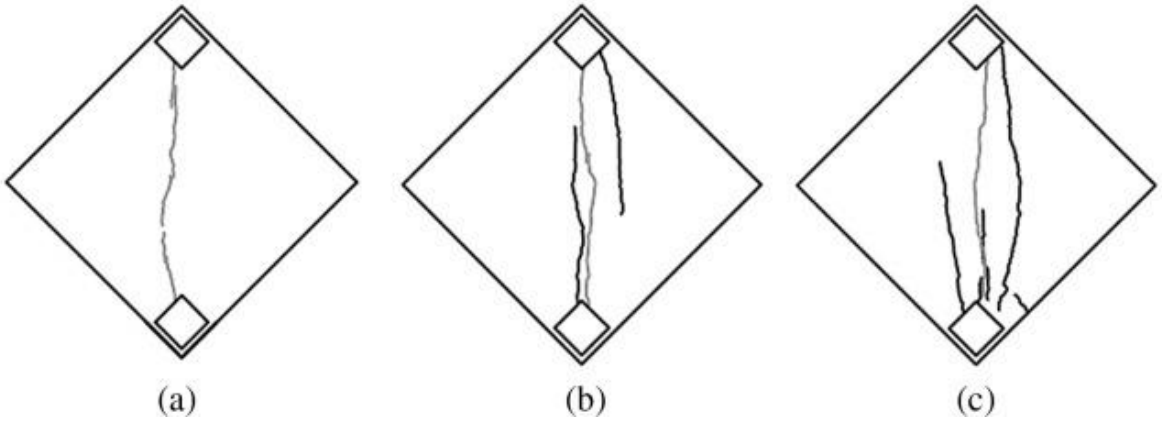


Figure IV.12: Crack patterns of strengthened specimens after testing: (a) FRMCom_01_side A; (b) FRMCom_02_side A; (c) FRMCom_03_side A.

5.2. Analytical description of the experimental results

According to the theory of elasticity, as previously discussed in the introductory section it can be assumed that during the diagonal tensile test the central area of a square masonry specimen is

approximately subjected to a stress state where $\sigma_x = \sigma_y \cong -0.56P/A$ (compression) and $\tau_{xy} = 1.05P/A$. The principal stresses in this case are $\sigma_I \cong 0.5P/A$ and $\sigma_{II} \cong -1.62P/A$. The contribution of FRCM systems to the in-plane shear capacity can be calculated following the analytical methodology presented in ACI 549.4R-13, [33]. According to this standard the nominal shear capacity, V_n, is computed as shown in Eq. **(IV.5)**:

$$V_n = V_m + V_f \quad \textbf{(IV.5)}$$

where V_m represents the contribution of the masonry wall, and V_f represents the contribution of the FRM system.

The contribution of the masonry wall can be obtained according to the methodology presented by Li et al. [34], and applied to diagonal tensile tests by Babaeidarabad et al. [35]. Four types of failure mechanisms can occur, and the shear capacity for each type can be computed through the following equations:

- Shear capacity due to shear sliding failure, V_{ss}, calculated according to **Eq. (IV.6)**:

$$V_{ss} = \frac{\tau_0}{1 - \mu_0 \times tan\,\theta} \times A_n \quad \textbf{(IV.6)}$$

where τ_0 is the shear bond strength of the mortar joint (MPa), μ_0 is the coefficient of internal shear friction in mortar joints, θ is the angle between horizontal and main diagonal of the wall (degrees), and A_n is the net area of the cross section of the masonry wall (mm²).

- Shear capacity due to shear friction failure, V_{sf}, calculated according to **Eq. (IV.7)**, **Eq. (IV.8)** and **Eq. (IV.9)**:

$$V_{sf} = \frac{\tau_{0,m}}{1 - \mu_m \times tan\,\theta} \times A_n \quad \textbf{(IV.7)}$$

$$\tau_{0,m} = \frac{\tau_0}{1 + 1.5 \times \mu_0 \times \frac{h}{w}} \quad \textbf{(IV.8)}$$

$$\mu_m = \frac{\mu_0}{1 + 1.5 \times \mu_0 \times \frac{h}{w}} \quad \textbf{(IV.9)}$$

where $\tau_{0,\mathrm{m}}$ is the modified shear bond strength in mortar joint (MPa), with h and w being the height and length of the bricks (mm), respectively, and μ_{m} is the modified coefficient of internal shear friction in mortar joint.

- Shear capacity due to the diagonal tension failure, V_{dt}, calculated according to **Eq. (IV.10)**:

$$V_{dt} = \frac{tan\,\theta + \sqrt{21.16 + tan\,\theta^2}}{10.58} \times f'_t \times A_n \quad \textbf{(IV.10)}$$

where f'_t is the tensile strength of masonry, $f'_t = 0.67 \times \sqrt[2]{f'_m}$,(MPa), with f'_m being the compressive strength of the masonry (MPa)

- Shear capacity due to toe crushing failure at the loading end, V_c, calculated according to **Eq. (IV.11)**:

$$V_c = \frac{2 \times w \times f'_m}{3 \times h + 2 \times w \times tan\,\theta} \times A_m \quad \textbf{(IV.11)}$$

where A_m (mm^2) is de interface loading area between the steel shoe and the wall.

Finally the shear capacity of the unreinforced or plain wall, V_m, is the minimum value of previous expressions, see Eq. **(IV.12)**:

$$V_m = min\{V_{ss}; V_{sf}; V_{dt}; V_c\} \quad \textbf{(IV.12)}$$

The behaviour of a near surface mounted FRP bars (NSM) based strengthening system is presented by Li et al. [34]. The developed theoretical formulation considers two different mechanisms, which are the debonding of the bar and the failure of the bar due to the tensile stresses. In contrast the FRMCom system uses a carbon mesh layer to resist the tensile stresses, and in this case only the failure of the fibres by tensile stresses is considered. The contribution of the FRM system for the shear capacity, V_f, is obtained according to **Eq. (IV.13)**:

$$V_f = 2 \times n \times A_f \times L \times f_{fv} \quad \textbf{(IV.13)}$$

where n is the number of fabric layers, A_f is the area of mesh reinforcement by unit width (mm²/mm), L is the length of the wall in the direction of the shear force (mm), f_{fv} is the design tensile strength of FRM shear reinforcement, $f_{fv} = E_f \times \varepsilon_{fv}$, (MPa), E_f is the tensile modulus of elasticity of the cracked FRM specimen, (MPa), and ε_{fv} is the design tensile strain of FRM shear reinforcement (mm/mm).

The shear capacity of the masonry specimens was calculated according to the analytical model presented previously using the values from **Table IV.11**. The compressive strength of the masonry was estimated according to EC6, since it was not possible to assess these parameters experimentally. However, previous studies conducted by Pereira et. al [36] indicate that these estimations, although slightly conservative, approximate well the experimental results. The characterization of the initial shear strength and the shear friction angle of mortar joints was carried by Capozucca [37], the values obtained are used in the analytical model as a lower bound value. The tensile behaviour of the FRCM composite system utilized was not experimentally characterized at this stage, since the failure is expected to be governed by the failure of the fibre mesh reinforcement. The mechanical characteristics of the FRCM system single components (matrix and fibre mesh) were previously presented in **Table IV.3** and **Table IV.4**.

Table IV.11: Values used in the analytical model to obtain the shear capacity of the specimens.

Description:	Value
Shear bond strength of the mortar joint, according to Capouzzuca [37]	$\tau_0 = 0.31$ MPa
Coefficient of internal shear friction in mortar joint according to Capouzzuca [37]	$\mu_0 = 0.60$
Angle between horizontal and main diagonal of the wall	$\theta = 45$ °
Net area of the masonry wall cross section	$A_n = 116600$ mm²
Height of the brick units	$h = 195$ mm
Length of brick units	$w = 285$ mm
Compressive strength of the masonry (according to EC6 [13])	$f'_m = 1.14$ MPa
Interface loading area between the steel shoe and the wall specimen	$A_m = 33440$mm²
Number of fabric layers	$n = 2$
Area of mesh reinforcement by unit width, CFM [32]	$A_f = 0.044$ mm²
Tensile modulus of elasticity of the cracked FRM specimen [32]	$E_f = 240000$ MPa
Design value of the tensile strain of FRM reinforcement (according to ACI 549.R-13 [33])	$\varepsilon_{fv} = 0.004$ mm/mm
Ultimate tensile strain of FRM reinforcement according to the supplier [32]	$\varepsilon_{fv,ult} = 0.0175$ mm/mm
Tensile strength of the render mortar	$f_{t,r} = 2.11$ MPa
Net area of the render cross section	$A_{n,r} = 31800$ mm²
Tensile strength of the PFRM	$f_{t,Ac} = 3.27$ MPa
Net area of the PFRM cross section	$A_{n,Ac} = 53000$ mm²

The contribution of the rendering and PFRM layers, considering diagonal tensile failure, V_r and V_{PFRM}, are obtained according to **Eq. (IV.10)** by using the net area of the cross section and the tensile strength of the respective materials.

Considering the equations **Eq. (IV.6)** to **Eq. (IV.12)** the result is a shear capacity of the unreinforced masonry wall, $V_m = 33.2\ kN$, and of the rendering layers, $V_r = 33.8\ kN$, which have to be summed in order to obtain the total capacity of the masonry specimen before strengthening, $V_{ref} = 67.0\ kN$.

With regards to the capacity of the strengthening system, according ACI 549.4R-13 the maximum allowable extension of the fibre reinforcement is 0.004 mm/mm. Considering this value and the **Eq. (IV.13)**, the maximum shear capacity of the strengthening system is $V_f = 118.3\ kN$. On the other hand, when considering the ultimate extension of the reinforcing fibres provided by the supplier, $\varepsilon_{fv,ult} = 0.0175$ mm/mm, [32], the maximum shear capacity is $V_{f,ult} = 517.5\ kN$. Finally, considering the diagonal tensile failure according to **Eq. (IV.10)**, the shear capacity of the PFRM layers is $V_{PFRM} = 87.3\ kN$.

The shear capacity values obtained experimentally are compared to the ones determined analytically in **Table IV.10**. Different experimental/analytical shear capacity ratios were computed, by following different sets of assumptions. For the reference case, the maximum shear capacity was estimated considering the contribution of the masonry, V_m, and rendering layer, V_r. For the "ACI" case, following ACI 549.4R-13, [33], the maximum shear capacity, V_{ACI}, was estimated considering the contribution of the masonry, V_m, of the rendering layer, V_r, and of the carbon strengthening mesh, V_f, by assuming 0.004 for the maximum allowable extension of the carbon fibres, as prescribed by ACI 549.4R-13, [33]. For the "ACI+PFRM" case, the maximum shear capacity, $V_{ACI+PFRM}$, was estimated considering the contribution of all previous factors and the additional contribution of the PFRM layers, V_{PFRM}. Finally, for the "Sup" case, V_{Sup}, it was considered the contribution of all the elements and the maximum allowable extension of the carbon fibres prescribed by the supplier, $V_{f,ult}$.

While comparing the results obtained analytically to the experimental ones, see **Table IV.12**, it is possible to confirm that the procedure proposed by ACI 549.4R-13, [33], leads to conservative results. This procedure leads to a safety factor of 2.3, which may be considered somewhat high considering the low scatter of the experimental results obtained. This value compares with a safety factor of 1.33 proposed by ACI 549.4R-13 [33] for similar types of strengthening systems. However, one may consider that the strengthening technique is still, to a certain extent, novel and therefore still encompasses significant uncertainties, most regarding durability and time dependent behaviour. When the contribution of the layers of the strengthening overlay is added to the analytical estimation, $V_{ACI+PFRM}$, the experimental vs analytical ratio decreases to 1.5. On the other hand, it is also possible to observe that, when considering the ultimate extension of the fibres, V_{Sup}^{an}, a ratio of 0.6 is obtained, meaning that the failure of the masonry model occurred before the ultimate extension in the fibres was reached. This was confirmed during the experimental program, since the failure was determined by the delamination of the strengthening system and crushing of the masonry, and not by the failure of the carbon mesh. Finally, if the contribution of the analytically estimated values of V_m and V_r is replaced by the experimentally obtained mean value of the diagonal tensile strength results in the reference specimens, the safety factors 1.8, 1.3 and 0.6 are obtained for V_{ACI}^{an}, $V_{ACI+PFRM}^{an}$ and V_{Sup}^{an}.

Table IV.12: Shear capacity obtained for reference and strengthened specimens.

		Reference	Strengthened		
Experimental (kN)		V_{ref}^{exp} 119.8	V_{str}^{exp} 419.5		
Analytical		V_{ref}^{an}	V_{ACI}^{an}	$V_{ACI+PFRM}^{an}$	V_{Sup}^{an}
(kN)	$V_m = 33.2$	+	+	+	+
	$V_r = 33.8$	+	+	+	+
	$V_f = 118.3$	–	+	+	–
	$V_{f,ult} = 517.5$	–	–	–	+
	$V_{PFRM} = 87.3$	–	–	+	+
		67.0	185.3	272.6	671.8
Ratio: Experimental/Analytical		1.8	2.3	1.5	0.6

6 CONCLUSIONS

The potentialities of a commercial system formed by a mortar reinforced with carbon fibre mesh (FRMCom system) for the strengthening of masonry walls were assessed in the present work by carrying out in-plane diagonal tensile tests. This strengthening system provided an increase of about 2.3 times of the shear strength of the reference specimens. The test procedure adopted allowed to evaluate the evolution of the damage in the specimens while subjected to cyclic loading, which was in general similar for all strengthened specimens. In the case of reference specimens, the damage developed in a more sudden manner.

In general, the failure modes of the reference specimens were the typical ones and expected for diagonal tensile testing. In contrast, the failure modes and crack patterns obtained for the strengthened specimens were characterized by a first phase at which the normal diagonal tensile cracks were developing gradually, followed by the delamination of the strengthening mortar immediately before failure. Additionally, in the case of the strengthened specimens several cracks were formed, particularly next to the supports of the specimen.

The adoption of a cyclic loading procedure on the diagonal tensile test, for the experimental characterization of the masonry, allowed the assessment of the stiffness degradation during each cycle, as well as the deterioration of the strengthening mechanisms. Additionally, it was possible to verify the adequacy of this test to assess the relevant in-plane failure mechanisms for typical masonry walls.

Although the experimental programme was limited the dispersion of the results allowed to assess and quantify the contribution by the strengthening system to the increase of the load carrying capacity with a reasonable accuracy. The FRMCom system strengthening technique provided a significant increment of strength and energy dissipation ability to this type of construction system, as well as higher shear strain combined with lower scatter of the obtained results. The delamination of the strengthening overlay may suggest that, in some cases, the adoption of transverse connecting systems between the masonry opposite faces may become essential to fully explore the contribution of the strengthening overlay to the load carrying capacity increment.

The analytical model described by ACI 549.4R-13 led to results that can be considered conservative, with a safety factor of 2.3. This is in part explained by the neglecting of the contribution of the layers of the strengthening mortar and by the limitation of the tensile strain of the carbon fibres to a value of 0.004 mm/mm. When the contribution of the strengthening mortar is considered, the safety factor decreases to 1.5. Finally, when the carbon fibres are allowed to reach the ultimate tensile strain of 0.0175 mm/mm, a safety factor of 0.6 is obtained indicating the premature failure of the strengthening system. This result was corroborated by the experimental results, where the premature failure of the strengthened specimens was observed before the ultimate tensile strain was reached on the carbon fibre reinforcement.

Acknowledgements

This research was carried in the framework of InoTec, Innovative material of ultra-high ductility for the rehabilitation of the built patrimony, funded by COMPETE/QREN/FEDER (NORTE-07-0202-FEDER-023024). InoTec project is promoted by CiviTest company and University of Minho. S&P Clever Reinforcement Ibérica is gratefully acknowledged for providing the materials used in the strengthening of the masonry specimens.

REFERENCES

[1] M. A. Elgawady, P. Lestuzzi, and M. Badoux, “A review of conventional seismic retrofitting techniques for URM,” in 13th International Brick and Block Masonry Conference, 2004, pp. 1–10.

[2] S. B. Kadam, Y. Singh, and B. Li, “Strengthening of unreinforced masonry using welded wire mesh and micro-concrete – Behaviour under in-plane action,” Constr. Build. Mater., vol. 54, pp. 247–257, 2014.

[3] A. Figueiredo, H. Varum, A. Costa, D. Silveira, and C. Oliveira, "Seismic retrofitting solution of an adobe masonry wall," Mater. Struct., vol. 46, no. 1–2, pp. 203–219, Jul. 2012.

[4] C. G. Papanicolaou, T. C. Triantafillou, K. Karlos, and M. Papathanasiou, "Textile-reinforced mortar (TRM) versus FRP as strengthening material of URM walls : in-plane cyclic loading," Mater. Struct., vol. 40, pp. 1081–1097, 2007.

[5] E. Bernat-Maso, C. Escrig, C. A. Aranha, and L. Gil, "Experimental assessment of Textile Reinforced Sprayed Mortar strengthening system for brickwork wallettes," Constr. Build. Mater., vol. 50, pp. 226–236, 2014.

[6] M. Corradi, A. Borri, G. Castori, and R. Sisti, "Shear strengthening of wall panels through jacketing with cement mortar reinforced by GFRP grids," Compos. Part B Eng., vol. 64, pp. 33–42, 2014.

[7] Federal Emergency Management Agency, Techniques for the Seismic Rehabilitation of Existing Buildings - FEMA 547. Books Express Publishing, 2006, p. 572.

[8] Y. Kim, H. Kong, and V. C. Li, "Design of engineered cementitious composite suitable for wet-mixture shotcreting," ACI Mater. J., no. 100, 2003.

[9] E. Esmaeeli, E. Manning, and J. A. O. Barros, "Strain hardening fibre reinforced cement composites for the flexural strengthening of masonry elements of ancient structures," Constr. Build. Mater., vol. 38, pp. 1010–1021, Jan. 2013.

[10] A. Dehghani, G. Fischer, and F. Alahi, "Strengthening masonry infill panels using engineered cementitious composites," Mater. Struct., 2013.

[11] M. A. Elgawady, P. Lestuzzi, and M. Badoux, "Retrofitting of masonry walls using shotcrete," in 2006 NZSEE Conference, Yeni Zelanda, 2006, no. 45.

[12] American Society for Testing and Materials, E 519-02 Standard test method for diagonal tension (shear) in masonry assemblages. 2002, pp. 1–5.

[13] Comité Européen de Normalisation, "EN 1996-1-1:1995 Eurocode 6 - Design of masonry structures - Part 1-1: General rules for reinforced and unreinforced masonry structures." Comité Européen de Normalisation, Brussels, CEN members, pp. 1–123, 2005.

[14] B. Silva, M. Dalla Benetta, F. da Porto, and C. Modena, "Experimental assessment of in-plane behaviour of three-leaf stone masonry walls," Constr. Build. Mater., vol. 53, pp. 149–161, Feb. 2014.

[15] J. Milosevic, A. S. Gago, M. Lopes, and R. Bento, "Experimental assessment of shear strength parameters on rubble stone masonry specimens," Constr. Build. Mater., vol. 47, pp. 1372–1380, Oct. 2013.

[16] A. Brignola, S. Frumento, S. Lagomarsino, and S. Podestà, "Identification of Shear Parameters of Masonry Panels Through the In-Situ Diagonal Compression Test," Int. J. Archit. Herit., vol. 3, no. 1, pp. 52–73, Dec. 2008.

[17] A. Borri, G. Castori, M. Corradi, and E. Speranzini, "Shear behavior of unreinforced and reinforced masonry panels subjected to in situ diagonal compression tests," Constr. Build. Mater., vol. 25, no. 12, pp. 4403–4414, Dec. 2011.

[18] F. Parisi, I. Iovinella, A. Balsamo, N. Augenti, and A. Prota, "In-plane behaviour of tuff masonry strengthened with inorganic matrix – grid composites," Compos. Part B, vol. 45, no. 1, pp. 1657–1666, 2013.

[19] N. Ismail, R. B. Petersen, M. J. Masia, and J. M. Ingham, "Diagonal shear behaviour of unreinforced masonry wallettes strengthened using twisted steel bars," Constr. Build. Mater., vol. 25, no. 12, pp. 4386–4393, Dec. 2011.

[20] A. Borri, G. Castori, and M. Corradi, "Shear behavior of masonry panels strengthened by high strength steel cords," Constr. Build. Mater., vol. 25, no. 2, pp. 494–503, Feb. 2011.

[21] J. A. P. P. de Almeida, E. N. B. Pereira, and J. A. O. Barros, "Performance assessment of overlay strengthened masonry under cyclic loading using the diagonal tensile test," in 9th International Masonry Conference, July 7, 8, 9; Guimarães, 2014.

[22] H. Santa-Maria, G. Duarte, and A. Garib, "Experimental Investigation of masonry panels externally strengthened with CFRPlaminates and fabric subjected to in-plane shear load," in 13th World Conference on Earthquake Engineering, 2004, no. 1627, pp. 1–10.

[23] F. F. S. Pinho, V. J. G. Lúcio, and M. F. C. Baião, "Rubble stone masonry walls in Portugal strengthened with reinforced micro-concrete layers," Bull. Earthq. Eng., vol. 10, no. 1, pp. 161–180, Apr. 2011.

[24] G. F. M. Vasconcelos and P. B. Lourenço, "Experimental characterization of stone masonry in shear and compression," Constr. Build. Mater., vol. 23, no. 11, pp. 3337–3345, Nov. 2009.

[25] A. Gabor, A. Bennani, E. Jacquelin, and F. Lebon, "Modelling approaches of the in-plane shear behaviour of unreinforced and FRP strengthened masonry panels," Compos. Struct., vol. 74, pp. 277–288, 2006.

[26] B. Ozsayin, E. Yilmaz, M. Ispir, H. Ozkaynak, E. Yuksel, and A. Ilki, "Characteristics of CFRP retrofitted hollow brick infill walls of reinforced concrete frames," Constr. Build. Mater., vol. 25, no. 10, pp. 4017–4024, 2011.

[27] C. Calderini, S. Cattari, and S. Lagomarsino, "The use of the diagonal compression test to identify the shear mechanical parameters of masonry," Constr. Build. Mater., vol. 24, no. 5, pp. 677–685, 2010.

[28] M. Frocht, "Recent advances in photoelasticity," ASME Trans, vol. 55, no. September–December, pp. 135–53, 1931.

[29] Comité Européen de Normalisation, "EN 772-1:2000 Methods of test for masonry units. Determination of compressive strength." Comité Européen de Normalisation, Brussels, p. 14, 2000.

[30] Comité Européen de Normalisation, "EN 1015-11:1999 Methods of test mortar for masonry – Part 11: Determination of flexural and compressive strength of hardened mortar." Brussels, 1999.

[31] Comité Européen de Normalisation, "EN 1015-12:2000 Methods of test for mortar for masonry - Part 12: Determination of adhesive strength of hardened mortar." Brussels, 2000.

[32] S&P Clever Reinforcement Company AG, "S&P ARMO-System FRCM Design Guidelines - Fiber Reinforced Cementitious Matrix (VER12.03.2013/IND)," Seween, 2013.

[33] American Concrete Institute (ACI), "ACI 549.4R-13 Guide to Design and Construction of Externally Bonded Fabric- Reinforced Cementitious Matrix (FRCM) Systems for Repair and Strengthening Concrete and Masonry Structures." Farmington Hills, Michigan, 2014.

[34] T. Li, N. Galati, J. G. Tumialan, and A. Nanni, "Analysis of unreinforced masonry concrete walls strengthened with glass fiber-reinforced polymer bars," ACI Struct. J., vol. 102, no. 4, 2005.

[35] S. Babaeidarabad, D. Arboleda, G. Loreto, and A. Nanni, "Shear strengthening of un-reinforced concrete masonry walls with fabric-reinforced-cementitious-matrix," Constr. Build. Mater., vol. 65, pp. 243–253, 2014.

[36] P. M. F. Pereira, J. B. Aguiar, A. Camões, and P. B. Lourenço, "The Portuguese masonry's mechanical characterization," in 8th International Masonry Conference 2010 in Dresden, 2010, pp. 611–622.

[37] R. Capozucca, "Shear Behaviour of Historic Masonry Made of Clay Bricks," Open Constr. Build. Technol. J., vol. 5, no. suppl 1M6, pp. 89–96, 2011.

PAPER V

CHARACTERIZATION OF OVERLAY STRENGTHENING OF MASONRY BY MEANS OF BIAXIAL CYCLIC DIAGONAL TENSILE TESTS

REFERENCE: Almeida, J. A. P. P., Pereira, E. N. B., Barros, J. A. O., Characterization of overlay strengthening of masonry by means of biaxial cyclic diagonal tensile tests. *Under submission process.*

ABSTRACT: The development of new methods to reduce the seismic vulnerability of masonry elements is leading to versatile and effective strategies. In this context, textile reinforced mortar systems are particularly promising due to their adaptability and cost-effectiveness compromise. For a continued development of more innovative systems targeting even better performances, it is of particular importance to develop the experimental procedures to assess the increasingly complex mechanical performance delivered by these systems. This work discusses the assessment of the in-plane capacity of masonry overlay strengthening systems through performing uniaxial compressive tests and biaxial diagonal tensile tests to assess monotonic and cyclic responses of plain and strengthened masonry. Particular attention was dedicated to the biaxial diagonal tests due to the lack of information on the use of this type of set-up, including the loading sequences and procedures to characterize the shear response. The results obtained show a detailed description of the development of the strengthening mechanisms throughout the different stages of the load-displacement responses,

supporting the analysis of the compression and shear capacity increments associated to changes of crack patterns and failure modes.

Keywords: Masonry strengthening; Textile reinforced mortar; In-plane experimental characterization; Uniaxial compressive tests; Biaxial diagonal tensile tests

1 INTRODUCTION

Textile reinforced mortar (TRM) is widely recognised as a successful system for enhancing the structural performance of masonry structures. Current studies indicate that TRM composites are generally successful at increasing the strength and flexibility of masonry walls, without significantly impacting their initial stiffness. However, given the broad array of TRM systems and masonry types available, more extensive studies are required to fully comprehend their performance. It's also worth noting that most of the results found in the literature are derived from static tests conducted on individual wall panels in laboratory environments. Natural seismic events involve dynamic actions, and studies involving shaking table tests on entire walls or even buildings are still scarce but essential for understanding how these structures react to earthquakes [1–3]. Set-ups for the dynamic characterisation are complex and expensive, therefore simpler procedures that provide an insight on the cyclic behaviour of innovative strengthening systems are very important in the innovation cycle, such as quasi-static cyclic tests [4]. The TRM in-plane strengthening efficiency of masonry can be assessed by performing uniaxial compressive tests [5,6], diagonal tensile tests also referred in literature as diagonal compression tests [7–14], and shear compression tests [15–19].

Regarding the shear capacity efficiency, see **Figure V.1**, it is often quantified by means of the diagonal tensile tests, using masonry specimens built in the laboratory [20,21], or in-situ [13,22]. Different types of strengthening systems have already been evaluated using cyclic diagonal tensile tests, [13,23–25]. As discussed in previous publications, Brignola et al [22] conducted force controlled cyclic tests, with a load gradient of 200 N/s in each cycle and the loading procedure defined to obtain four or five cyclic load steps for each masonry panel. An in-situ campaign developed by Angiolilli et al. [26] performed cyclic diagonal tensile tests on stone masonry specimens previously isolated from the original walls. Two reference panels and two TRM strengthened panels were tested. The TRM system was composed of a glass-fibre grid embedded in NHL-based mortar and carbon shear connectors. The tests were performed using force-control by applying 20 kN at each load cycle with a 0.1 kN/s

load rate, up to failure. An approach resembling biaxial tests was used in the experimental campaign presented by Santa-Maria et al [27]. The test procedure started with the first diagonal loading and unloading, followed by the loading of the second diagonal and unloading. Two cycles were performed at each load level, the load increments at each level were of 25 kN.

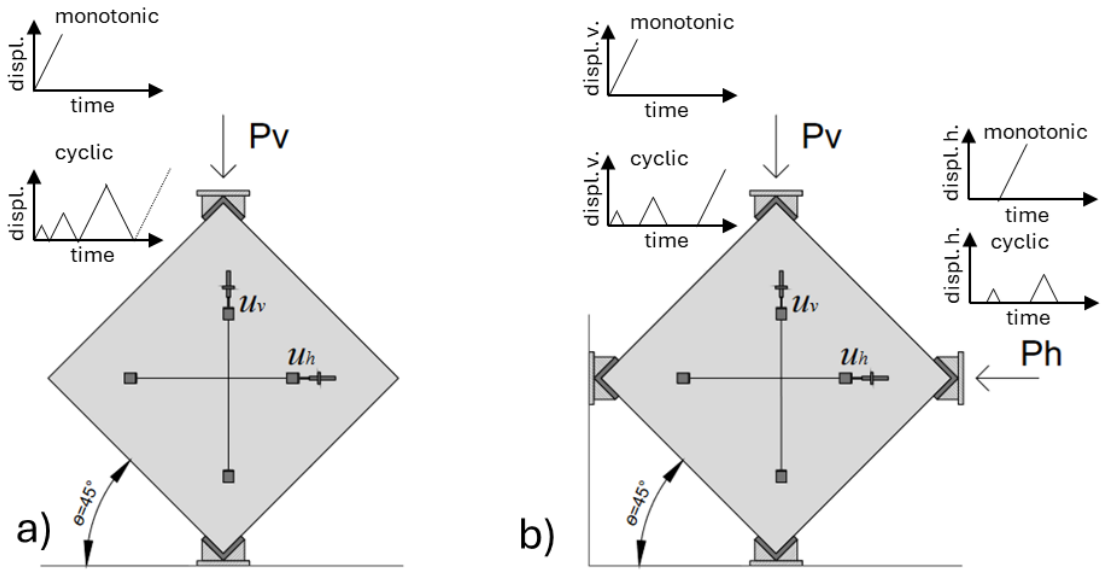


Figure V.1: Schematics of the experimental set-ups: a) diagonal tensile test; b) biaxial tensile test.

Diagonal tensile tests were also performed on unreinforced clay brick masonry strengthened with additional overlays or composite materials [28]. Different types of masonry and strengthening systems are discussed by the authors, and normally most of them use a reduced number of specimens for the characterization of a specific layout. However, the coefficient of variations obtained are in general quite low, especially for strengthened panels [28]. Therefore, the use of a reduced number of specimens seems to be sufficiently representative of the expected behaviour.

The diagonal tensile test is regarded as a simple and expedite procedure for the in-plane behaviour characterization. However, it is important to stress that the capability of this type of test to disclose all the failure modes of masonry walls is limited. For example, the rocking/crushing mechanisms cannot be evaluated, [13]. For the evaluation of those mechanisms, compression shear tests must be performed following experimental procedures that can consider the vertical load imposed to the masonry element and the effect of the horizontal displacements imposed by actuators [15,29].

Additionally to the in-plane failure mechanisms also the out-of-plane (OOP) mechanisms have an extreme importance and were studied by several authors, [30–37]. The OOP failure mechanisms are

primarily governed by the wall's geometry, support conditions, and the nature of connections to surrounding structural elements as RC frame elements, slabs or shear walls. The most common OOP mechanisms include flexural bending, where the wall acts as a vertical or horizontal beam and develops cracks perpendicular to the direction of loading, and rocking-sliding, where the wall pivots or slides at its base or along weak mortar joints. In two-way spanning panels, the wall undergoes biaxial bending, producing a complex pattern of vertical, horizontal, and diagonal cracks due to combined flexural and torsional stresses. The development and propagation of these cracks ultimately lead to local or global collapse, especially when the wall is slender or lacks sufficient edge restraints. The boundary conditions and the degree of connection to adjacent elements play a decisive role in the OOP behaviour. Walls with four-edge support or strong ties to slabs and frames exhibit higher resistance, as load is redistributed and arching action can develop, whereas walls with free or weakly connected edges are much more vulnerable to OOP collapse [35–38].

2 RESEARCH SIGNIFICANCE

The diagonal tensile tests are considered as a expedite to characterize the masonry behaviour under the type of actions to which elements are frequently subject. Most of the existing experimental work developed using diagonal tensile tests is focused on the characterization of masonry panels by imposing monotonic displacements or loads. Nonetheless in recent years also cyclic actions were included, with the goal of better resembling real case loading scenarios found in horizontal load cases such as seismic. In this work the authors aimed at accessing the possibility to adapt the experimental procedure and the test-setup of diagonal tensile tests to assess the influence of the alternated cyclic actions along both diagonals of the panels, as well as assess how the combined effect of the alternated cyclic imposed displacements affects the degradation of the stiffness and load bearing capacity of the masonry. Additionally, the study compares different masonry elements without strengthening and strengthened with two different overlay strengthening systems. Recurring to Image analysis techniques the authors analysed the evolution of the cracking process and failure modes, in relation to the evolution of stiffness and strength. Although some experimental procedures were found to require additional adaptation in future studies, the testing protocols showed promising features within the development cycle of innovative strengthening systems for masonry based on TRM and strengthening overlays.

3 MATERIALS AND METHODS

This section describes the properties of the materials used in the experimental tests, including the mortar used to mount the masonry specimens, the bricks, the fibre reinforced mortar and the carbon fibre mesh. The sequence of steps followed to mount the masonry specimens and apply the strengthening systems are also detailed. Finally, the set-up and procedures adopted for the uniaxial compressive and diagonal tensile tests are described, including the layout of the monitoring approach using LVDT´s and digital image correlation.

3.1 Materials

The unreinforced hollow brick masonry specimens were assembled with a commercial mortar, REN, from SECIL (Macieira, PT), and hollow ceramic bricks (Length x Height x Thickness: 285 x 195 x 110 mm^3) produced by A. Macedo (Vila Verde, PT). Five ceramic bricks units were tested according to EN 772-1 [39] in the direction normal to hollows, a compressive strength of 1.66 N/mm^2 was obtained, with coefficients of variation of 11%. In the direction parallel to hollows the compressive strength was 4.32 N/mm^2 and the coefficient of variation 8%. The same mortar was used for the screed and render layer, as well as for the masonry joints, REN, whose main mechanical properties are present in **Table V.1**.

Both strengthening systems were applied using the bidirectional carbon fibre mesh (CFM) produced by S&P (Amora, PT), with yarns spaced of 20 mm, a section of 44 mm2/m in both directions, an elongation at break between 1.8% and 2.1%, and a tensile strength of 189kN/m. The COM strengthening system was composed by the CFM and two 7.5 mm thick layers of a commercial mortar, *Mapei-Antique NHL Struturalle*. produced by Mapei (Italy). The FRM strengthening system was composed by the same type of CFM and two 7.5 mm layers of a fibre reinforced mortar developed previously by the authors [31]. The development of the mortar was driven by the need to reduce the environmental impact. For that reason, alternative binders and recycled ceramic brick as aggregate were used. The mortar was composed by a mix of natural hydraulic lime (NHL 5.0) from SECIL (Macieira, PT), and a geopolymeric binder (GP). The GP binder was a mix of sodium silicate solution (Na_2SiO_3) and sodium hydroxide solution (NaOH) in a mass proportion of 2:1 as activator, and the precursor was composed by a mixture of metakaolin and recycled red brick powder with a mass proportion of 1:1. Two types of fibres were considered for the formulation of the FRM mortar, polyacrylonitrile (PAN) supplied by FISIPE (Barreiro, PT) and recycled carbon fibre (CF) supplied by ELG Carbon (Bilston, UK). The recycled CF provide environmental benefits by reducing significantly

the carbon footprint and maintain 95 % strength retention and 99 % modulus retention compared to the original mechanical properties

Table V.1: Properties of mortars used to assemble, render and strengthen the masonry specimens.

	$f_{flex.}$			f_c			E		
	Av.	Std.	cv.	Av.	Std.	cv.	Av.	Std.	cv.
name	(MPa)	(MPa)	(%)	(MPa)	(MPa)	(%)	(GPa)	(GPa)	(%)
REN	1.3	0.6	5	7.4	0.9	12	7.3	0.3	5
M_FRM	3.1	0.1	6	10.7	1.0	10	10.9	0.7	6
M_COM	3.7	0.4	11	10.0	0.5	5	15.2	2.2	14

3.2 Specimens Preparation

Four different types of unreinforced ceramic masonry specimens were prepared for uniaxial compression tests and diagonal tensile tests. Each type was representing masonry elements before and after the strengthening process: unreinforced ceramic brick masonry, URM; unreinforced ceramic brick masonry with a rendering layer, URMR; unreinforced ceramic brick masonry with a rendering layer strengthened with a TRM commercial system, COM; unreinforced ceramic brick masonry with a rendering layer strengthened with a developed TRM system, FRM.

The unreinforced ceramic brick masonry specimens were manufactured according to the following steps: 1) soaking of the bricks in water; 2) placement of guides and levelling of the mortar; 3) placement and levelling of the bricks; 4) placement of the vertical mortar joints; 5) repetition of the previous steps until the specimen was concluded. A total of 12 specimens with 800 x 600 x 110 mm were mounted for uniaxial compressive characterization and 12 specimens with 1000 x 1000 x 110 mm were mounted for shear characterization by diagonal tensile tests. After mounting, the specimens were rough casted with M_Render mortar, see **Figure V.2a)**, and 24 hours later these were rendered with a M_Render mortar layer with thickness of 15 mm, applied on both faces, see **Figure V.2b and c)**.

The COM and FRM specimens were strengthened 14 days after the rendering of the masonry specimens. Both strengthening systems were applied according to the following procedure: 1) initial spraying of the render surface with water; 2) application of a 7.5 mm thick layer of strengthening mortar; 3) placement of the carbon fibre mesh over the mortar, see **Figure V.3a)**; 4) application of

the final 7.5 mm layer of strengthening mortar, see **Figure V.3a and b)**. The specimens were sprayed with water 15 min after finishing the process, and then a plastic film to wrap the entire specimens which remained in this condition until one day before testing to avoid shrinkage. The final thickness of the specimens was 110 mm for URM, 140 mm for URMR and 170 mm for the COM and FRM.

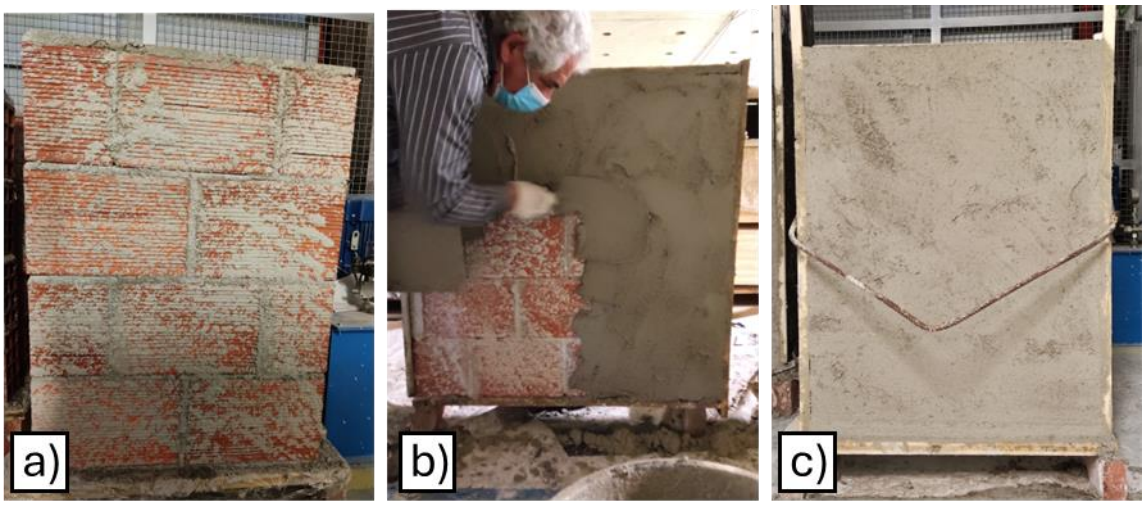


Figure V.2: Sequence of procedures during the preparation of the masonry elements: a) unreinforced ceramic brick specimen mounted, with one layer of screed mortar applied; b) rendering process; c) finish specimen of unreinforced ceramic brick masonry with render, corresponding to the URMR.

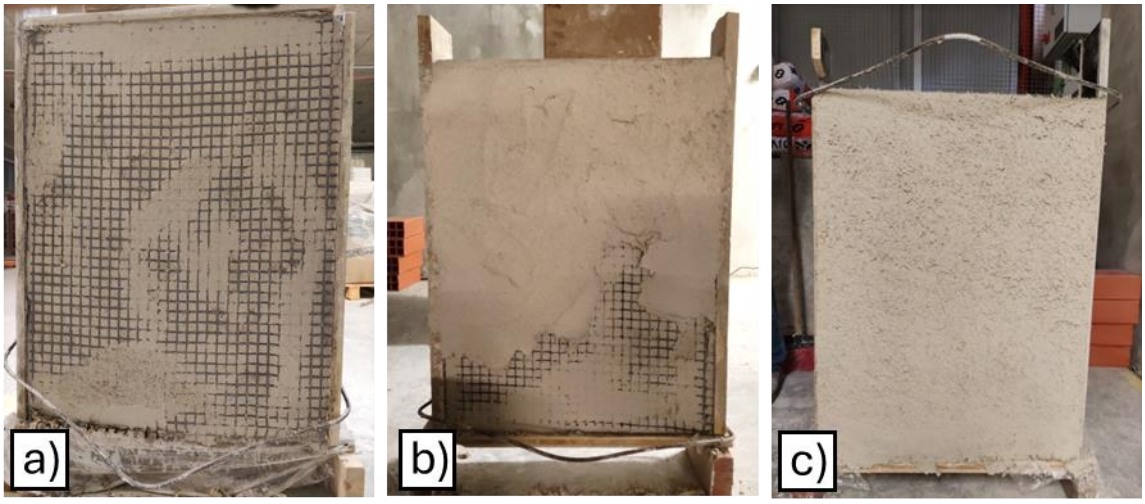


Figure V.3: Sequence of procedures during the strengthening of COM and FRM specimens: a) specimen with one small layer of strengthening mortar and overlayed carbon fibre mesh; b) covering of the carbon fibre mesh with the rendering layer; c) finished COM specimen.

3.3 Testing Set-Up and Procedures

3.3.1 Uniaxial compressive tests

The dimensions of the wallets assembled to perform the uniaxial compressive characterization of the reference masonry and both strengthening systems, COM and FRM, followed the specifications indicated in EN 1052-1 [41], with a final height and length of 800 and 600 mm respectively. The test set-up consisted of a testing frame, a 1000 kN capacity actuator connected to a servo-hydraulic closed loop-controlled system and a 1000 kN load cell. The vertical displacements were monitored using 2 LVDT's connected to a data acquisition system, as shown in **Figure V.4**. The tests were carried out under displacement control, measuring the displacement of the crosshead of the actuator with an external LVDT. For each set of specimens one monotonic and two cyclic uniaxial compressive tests were carried out by imposing the axial displacement at a rate of 0.01 mm/s. For cyclic tests, the displacement amplitude per cycle was increasing by 1.5 mm between cycles until failure or a maximum of 7 cycles were reached.

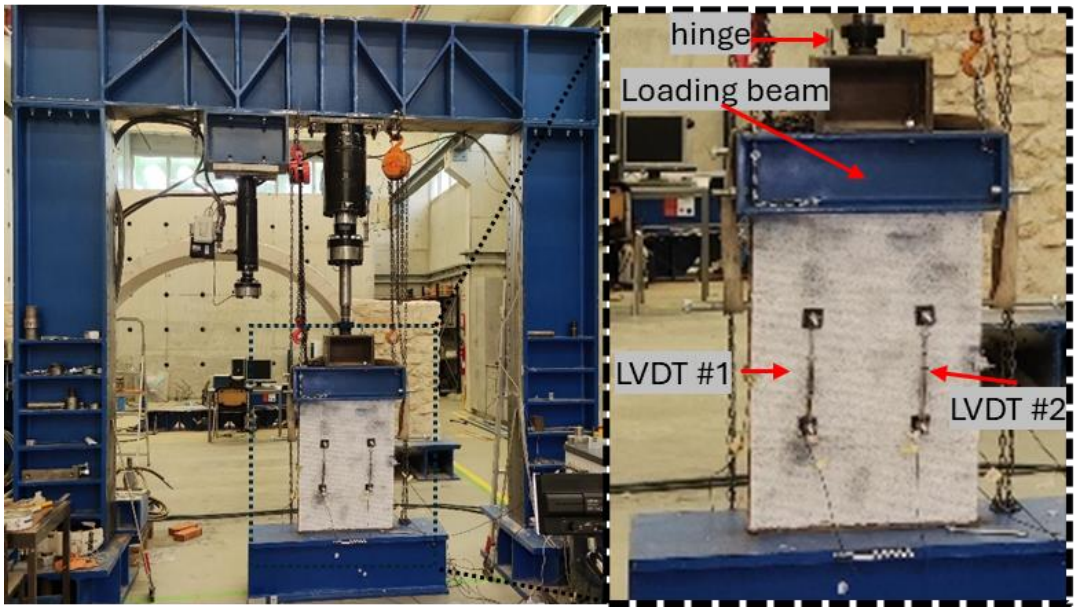


Figure V.4: Test set-up used for the uniaxial compression tests.

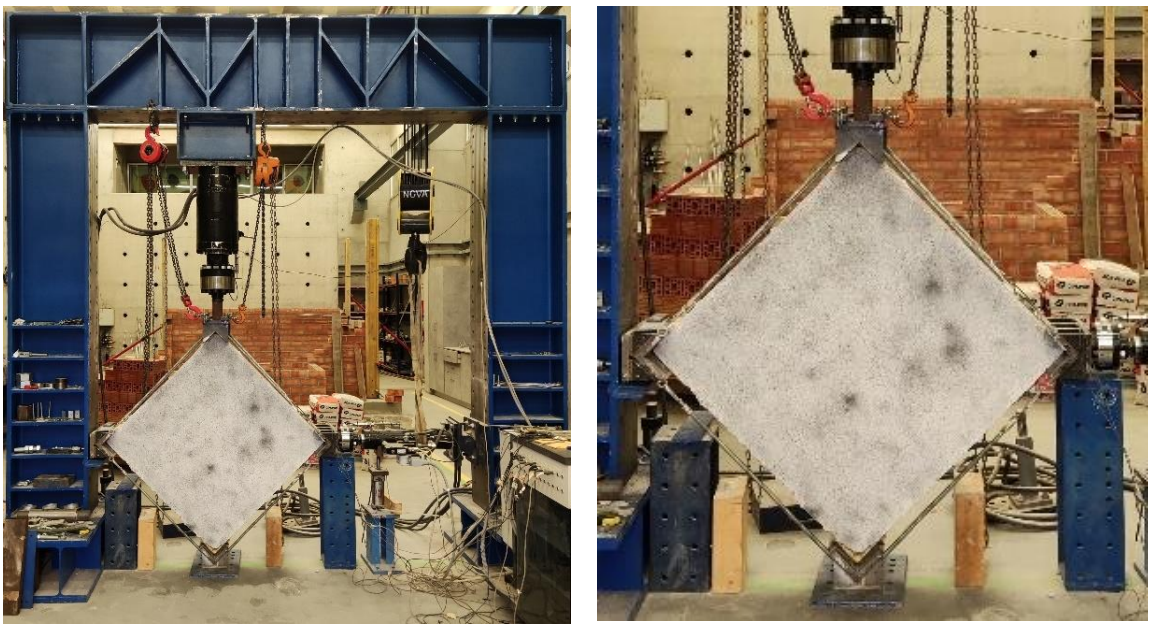
3.3.2 Biaxial diagonal tensile tests

The biaxial diagonal tensile tests were performed to assess the performance of the strengthening systems when alternate loading occurs in both orthogonal in-plane directions, somewhat resembling what occurs during seismic events with the inversion of the loading direction. The set-up included a testing frame, a 1000 kN vertical actuator with a 1000 kN load cell and a horizontal actuator with a

300 kN load cell, both connected to a servo-hydraulic closed loop-controlled system, see **Figure V.5**. The horizontal and vertical displacements were monitored using 2 LVDT's placed at approximately ¼ and ¾ of the diagonal length, connected to a data acquisition system recording data at a frequency of 4 hz .

The tests were conducted under displacement control of each actuator crosshead, by measuring the displacement of the crosshead with an external LVDT. The alternated vertical and horizontal displacements were imposed to the specimen at a rate of 0.01 mm/s, for both monotonic and cyclic tests. The actuator was adjusted to reach contact with the support shoe before the onset of each cycle, particularly for later cycles, due to the accumulated residual deformations. The loading procedure for cyclic tests was based on imposing the doubling of the displacement amplitude in each cycle, with a starting value of 0.25 mm, until a maximum number of 8 cycles (representing a peak displacement of 32 mm) or failure was reached.

The set-up was developed in agreement with the recommendations of ASTM E-519-2 [42]. Given the exploratory nature of the testing campaign some modifications were implemented, namely referring to the alternate loading sequence. Additionally, in the strengthened specimens FRM and COM, two steel plates with 150 x 150 x 30 mm^3 were placed in both faces of each corner and attached with one steel 16 mm rod to provide additional confinement to the material in the region of the supports and loads and following the procedures from previous work [28], see **Figure V.5**.



a) b)

Figure V.5: Test set-up adopted for bidirectional diagonal tensile tests: a) general view of the set-up; b) detail of one of the specimens.

3.4 Monitoring and Measurements Using Digital Image Correlation (Dic)

Digital Image Correlation (DIC) is a non-contact, image-based technique for measuring surface shape, deformation, and strain. Developed in the 1980s [43], DIC is based on recording digital images of a specimen under different loading conditions, and on correlation algorithms that allow to track the displacement of local regions between those images, achieving quantitative, full-field data on displacement and strain development. DIC systems can be classified as 2D-DIC or 3D-DIC depending on the use of one or multiple different perspectives are recorded simultaneously [44]. Both systems are very advantageous to control displacements and cracking patterns of masonry specimens under in-plane actions, such as in the case of the uniaxial compressive tests and the diagonal tensile tests. In addition, some DIC monitoring systems allow the measurement of deformations in masonry during the full test, offering the possibility to detect the crack initiation process even before becoming visible to the human eye [45].

Two image acquisition systems were used during the experimental campaign, a 3D-DIC and a 2D-DIC. The 3D-DIC system composed by two 2.0 Megapixels USB 3.0 cameras (Master and Slave) positioned in a linear support bar with 100 cm distance between each other and 300 cm perpendicular to the specimen. The acquisition was controlled by the ISTRA4D 4.4.7 software with frames obtained at 1 Hz frequency. In the case of the 2D-DIC, the tests were recorded with photographs taken with 10 seconds intervals using a high-resolution digital camera, Nikon D800E (Tokyo, Japan), with a pixel resolution of 4912 × 7360 and a TAMRON 24-70 MM F/2.8 lens (Saitama, Japan), to monitor the behaviour and deformations of the specimens using digital image analysis using the GOM software. A speckle pattern was applied to the surface of the specimens, with an average dot diameter of around 2 mm. **Figure V.6** shows an example of the speckle pattern applied on the surface of the specimens. In the case of the biaxial diagonal tensile tests the camera was rotated 45° to get the specimen framed at a smaller distance, see **Figure V.14**.

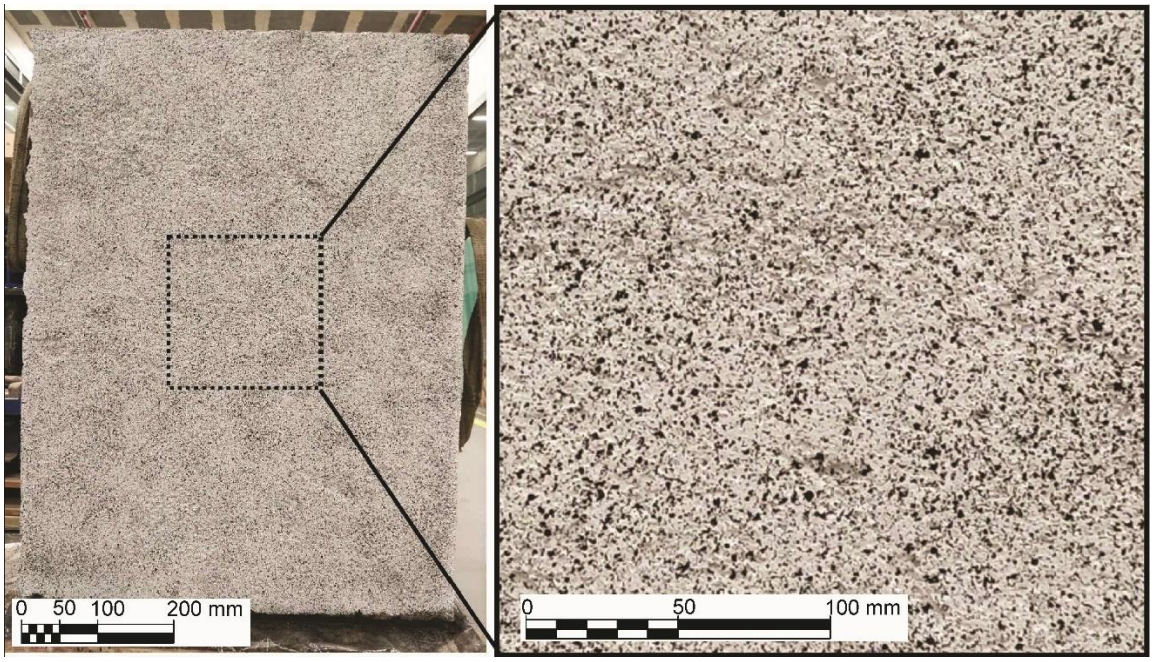


Figure V.6: Speckle pattern used for the DIC produced at the surface of the specimens used for the uniaxial compression tests.

4 RESULTS AND DISCUSSION

4.1 Uniaxial Compressive Tests

The compressive behaviour of masonry elements was assessed following the EN 1052-1 [41], according to which the strength of masonry in compression may be obtained following **Eq. (V.1)**, not considering the effects of loading restraint, slenderness or eccentricity of loading:

$$f_c = \frac{F_{i,max}}{A_i} \quad \textbf{(V.1)}$$

The values of compressive strength (fc) obtained for each type of specimen and elasticity modulus (E) are presented in **Table V.2**, along with the respective average values (Av.), the standard deviation (Std.) and the coefficient of variation (c.v.). The value of the elasticity modulus shown in **Table V.2** corresponds to the slope of tangent to the stress vs strain response in the range between 10% and 33 % of fmax, approximately obtained by linear regression.

Table V.2: Results from the uniaxial compressive tests.

	Area (mm^2)	F_{max} (kN)	f_c (MPa)	Av. (MPa)	Std. (MPa)	c.v. (%)	E (GPa)	Av. (GPa)	Std (GPa)	c.v. (%)
URM_01	64200	50.9	0.79				1.51			
URM_02	64200	78.8	1.23	0.98	0.18	19	--	1.78	0.26	15
URM_03	64200	59.0	0.92				2.04			
URMR_01	78650	142.4	1.81				5.31			
URMR_02	77350	153.0	1.98	1.92	0.08	4	7.52	6.42	1.10	17
URMR_03	78000	154.5	1.98				–			
COM_01	93775	199.4	2.13				18.34			
COM_02	93415	253.6	2.71	2.39	0.24	10	--	15.66	2.67	17
COM_03	93000	216.7	2.33				12.99			
FRM_01	93155	299.3	3.21				10.10			
FRM_02	93000	259.9	2.80	3.07	0.19	6	10.74	10.72	0.50	5
FRM_03	93775	298.7	3.19				11.33			

The uniaxial compressive tests results revealed that the application of a render layer has a great impact on the plain masonry mechanical properties, with the compressive strength increasing from 0.98 to 1.92 MPa. After strengthening the rendered masonry with both systems, COM and FRM, the same trend was verified, with an increase of the compressive strength to 2.39 and 3.07 MPa, respectively. In **Figure V.7** the ratios of the compressive strength and elasticity modulus are both related to the rendered masonry specimens, URMR. According to the results obtained it is possible to infer that, for the COM strengthening system, the increase of the elasticity modulus as a result of the strengthening procedure was not beneficial for the compressive strength capacity, when the results are compared with the ones obtained for the FRM system. This effect may be explained by the relatively high difference of rigidity between the masonry and the strengthening layer.

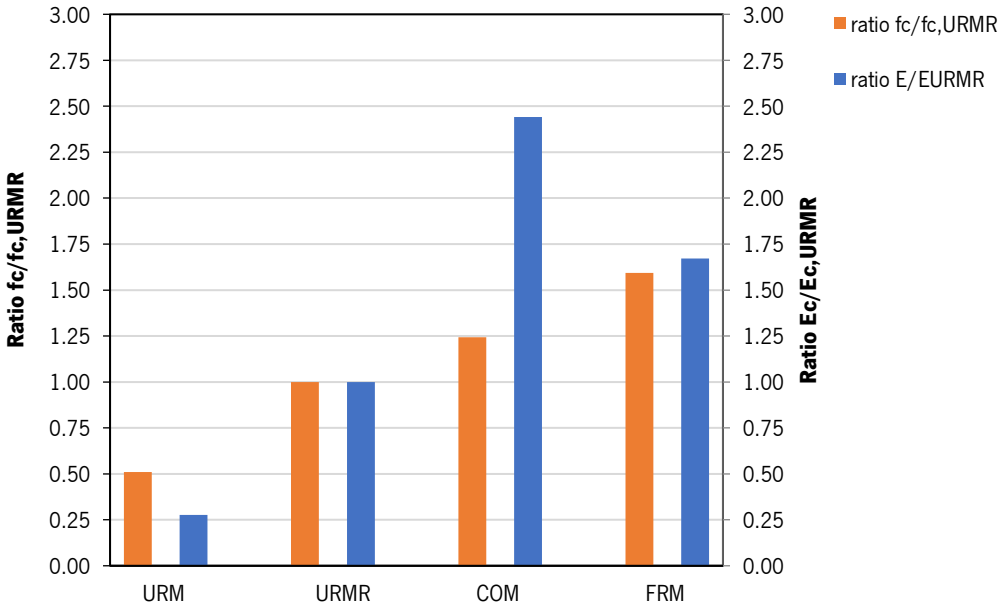
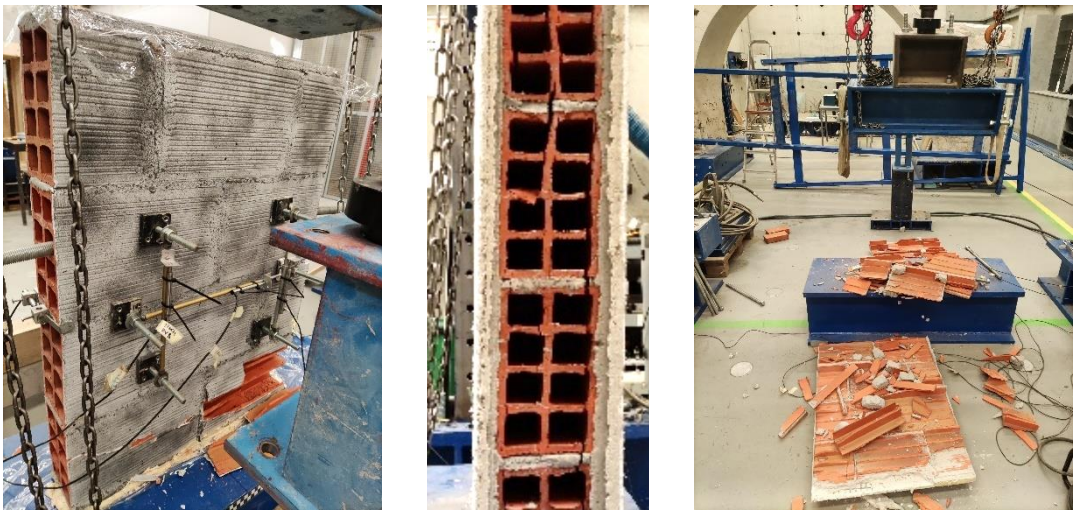


Figure V.7: Evolution of the ratios $f_c/f_{c,URMR}$ and E/E_{URMR} obtained for the uniaxial compressive tests.

4.1.1 Failure modes

The main failure modes obtained in the uniaxial compressive tests can be seen in **Figure V.8**. The URM and URMR specimens failed by crushing of the ceramic brick at the same horizontal level, as presented in **Figure V.8a)**. For the strengthened specimens, COM and FRM the failure occurred in two different phases, first the failure of the ceramic brick septs occurred, evolving in the vertical direction, as presented in **Figure V.8b)**. In a second phase a sudden rupture of the strengthening layers was observed, see **Figure V.8c)**. At this phase the strengthening layers were behaving as two separate elements without connection, leading to the abrupt failure of the specimens. This type of failure indicates the need to adopt connectors, particularly when TRM systems are applied in hollow ceramic brick masonry.



a) b) c)

Figure V.8: Failure modes obtained under compression: a) URM specimen, crushing of ceramic brick; b) failure of the ceramic brick septs in COM specimen; c) sudden failure of FRM specimen.

4.2 BIAXIAL DIAGONAL TENSILE TESTS

The failure due to diagonal cracking, linked with the tensile strength of masonry, can be evaluated by diagonal tensile tests following the procedures from ASTM E519-22 [42], according to which pure shear stress is induced at the centre of the specimen. The values of the shear stress at the centre of the panel can therefore be obtained by **Eq. (V.2)**.

$$SS = \frac{0.707 \times P}{A_n} \quad \textbf{(V.2)}$$

where P is the applied load, A_n is the net area of the specimen's cross-section calculated according to **Eq.(V.3)**:

$$A_n = \left(\frac{w + h}{2}\right) \times t \times n^* \quad \textbf{(V.3)}$$

where w, h and t are the width, the height, and the total thickness of the specimen, and n^* represents the percentage of the gross area of the unit that is solid, expressed as a decimal.

The values of the maximum load obtained throughout the biaxial diagonal tensile tests are presented in **Table V.3**. For specimens tested under cyclic procedure the peak load is indicated for each vertical, F_v, and horizontal cycle, F_h. additionally, also the maximum vertical and horizontal loads and shear stress according to **Eq. (V.2)** are indicated.

Table V.3: Results from the uniaxial compressive tests.

Cycle		1	2	3	4	5	6	7	8	Max	Shear Stress
Cycle displ. (mm)		0.25	0.50	1.00	2.00	4.00	8.00	16.00	32.00		(MPa)
URM_01	F_v (kN)	4.3	6.6	12.2	16.3	12.4	7.7			16.3	0.31
	F_h (kN)	1.1	2.1	4.5	5.8	8.1				8.1	0.15
URM_02	F_v (kN)	2.2	5.7	10.7	23.0	21.9	5.2	5.8		23.0	0.44
	F_h (kN)	0.9	2.0	6.8	13.1	3.0	9.0	11.7		13.1	0.25
URMR_01	F_v (kN)	5.2	10.2	25.8	68.6	88.3				88.3	0.93
	F_h (kN)	1.5	2.7	7.7	26.8	26.3	35.2			35.2	0.37
URMR_02	F_v (kN)	6.1	15.0	34.0	17.7	93.3				93.3	0.98
	F_h (kN)	2.0	2.9	7.4	17.7	3.7	36.3	52.4		52.4	0.55
URMR_03	F_v (kN)	6.7	14.9	33.3	78.2	96.0				96.0	1.01
	F_h (kN)	0.8	1.6	5.3	26.5	1.2	56.8	58.0		58.0	0.61
COM_01	F_v (kN)	139.7								139.7	1.04
	F_h (kN)	148.0								148.0	1.10
COM_02	F_v (kN)	0.6	7.3	30.8	67.3	154.8	183.8	165.7		183.8	1.36
	F_h (kN)	4.5	5.5	12.3	32.5	62.1	98.3	163.7	189.9	189.9	1.41
COM_03	F_v (kN)	6.7	8.1	19.2	48.6	110.9	159.4			159.4	1.18
	F_h (kN)	0.8	2.7	7.8	23.9	65.0				65.0	0.48
FRM_01	F_v (kN)	182.3								182.3	1.34
	F_h (kN)	152.2								152.2	1.12
FRM_02	F_v (kN)	4.1	6.7	12.8	24.2	63.7	124.3	161.7		161.7	1.19
	F_h (kN)	0.1	0.9	4.0	10.8	30.6	62.2	96.0	136.2	136.2	1.00
FRM_03	F_v (kN)	0.9	10.8	15.1	31.5	78.4	115.1	126.9		126.9	0.93
	F_h (kN)	1.0	1.7	6.4	20.8	54.2	79.8	64.4		79.8	0.59

Typical examples of the load vs displacement responses obtained during the experimental campaign are presented in **Figure V.9** and **Figure V.10**, in which the displacement represented is referred to the head of the vertical and horizontal actuators. In **Figure V.9** the response is referred to a diagonal biaxial tensile test performed according to a monotonic procedure. First, the vertical displacement was imposed, followed by the horizontal solicitation. **Figure V.10** represents the response of a specimen in which the experimental procedure was composed of a sequence of cyclic tests. The same sequence was used, first a vertical loading cycle was applied, followed by a horizontal cycle. Sequential vertical and horizontal cycles were imposed following the same procedure, until the rupture of the specimens was reached.

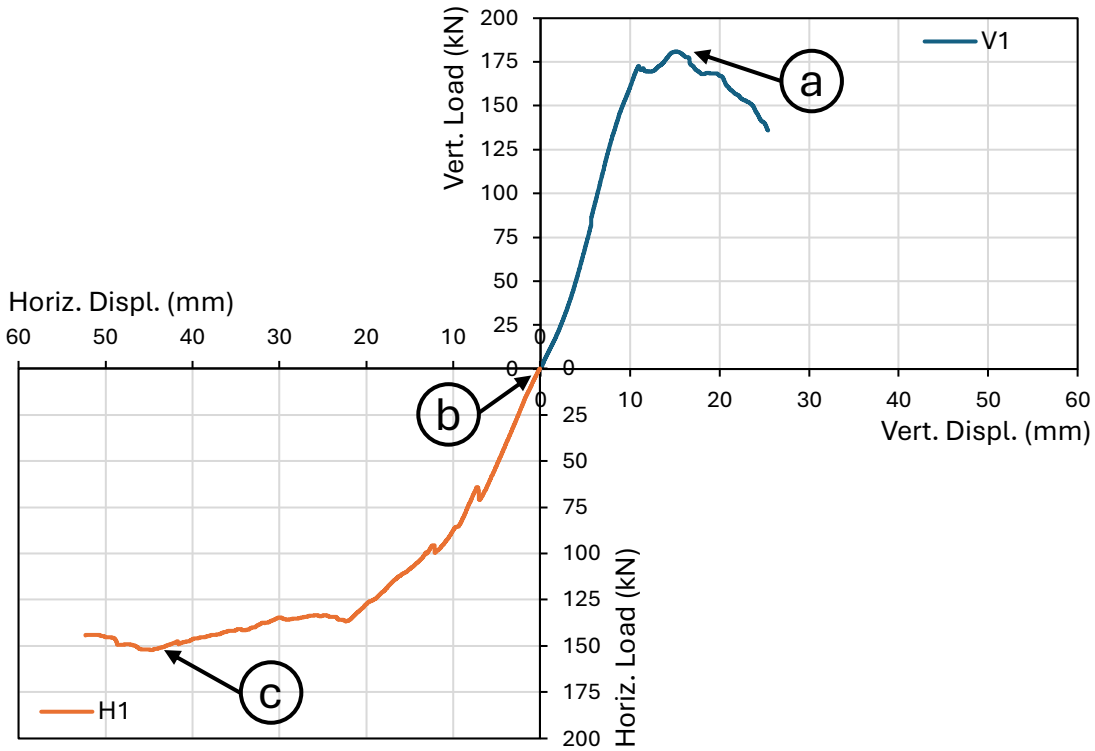


Figure V.9: Load vs displacement response obtained for FRM-01 under vertical and horizontal monotonic loading.

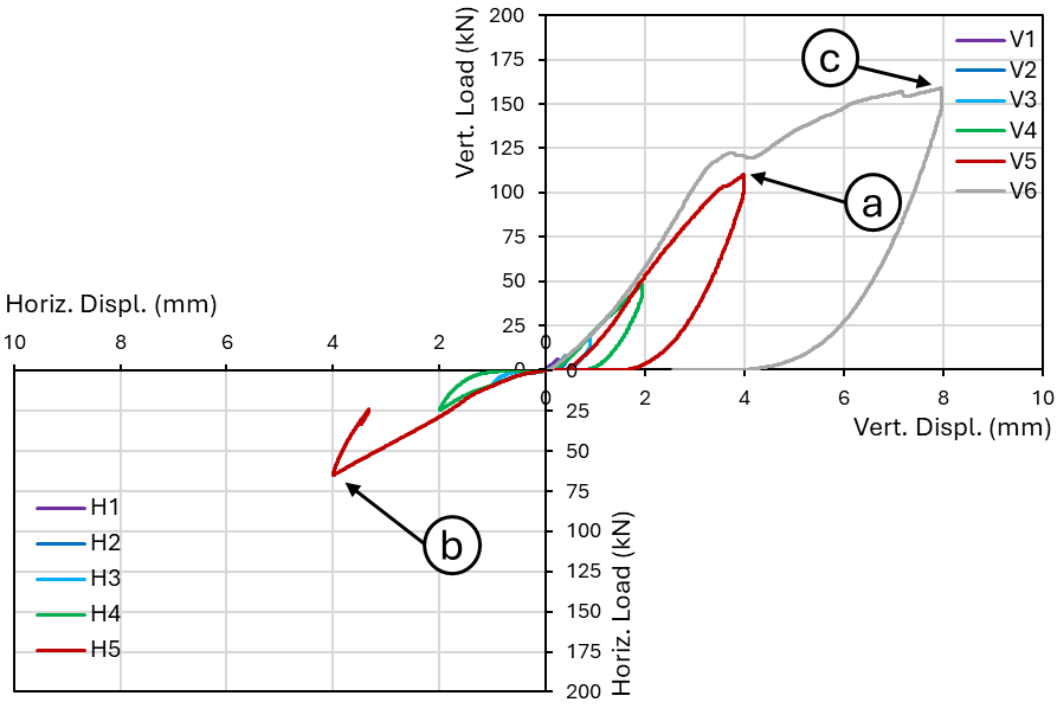


Figure V.10: Load vs displacement response obtained for COM-03 under vertical and horizontal cyclic loading.

In **Figure V.11** the maximum shear stress, Ss, values for vertical, SSv, and horizontal cycles, SSh, are presented with the standard deviation values and the respective ratio SSv/SSh. The shear stress value obtained in the vertical cycles, the first to be imposed according to the implemented procedure, was higher for all the tested typologies when compared to the maximum values obtained from the following horizontal cycles for each specimen. On the other hand, the ratio between SSv and SSh was higher for the plain masonry specimens and for the rendered masonry specimens, around 1.9 for URM and URMR, while close to 1.25 in the case of the strengthened specimens, COM and FRM. The observed decrease in this ratio signals the influence of the strengthening system. Even with damage imposed in the vertical direction, the specimens still show significant residual load bearing capacity in the horizontal direction. In contrast, in plain or rendered specimens, as soon as higher damage levels are reached in the vertical direction, the residual load bearing capacity of the specimen in the horizontal direction also decreases significantly.

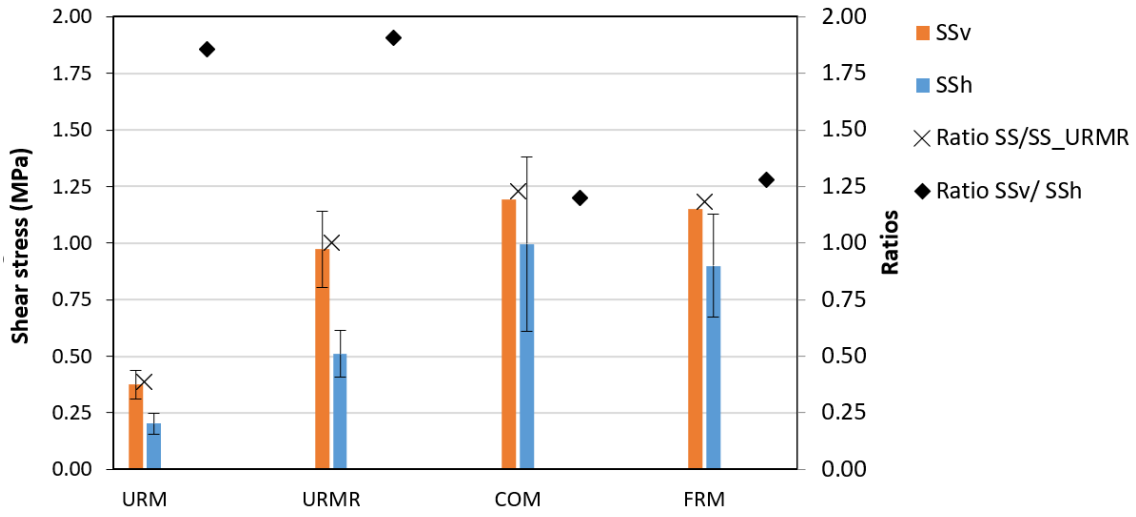


Figure V.11: Maximum shear stress obtained for vertical and horizontal loading cycles, and corresponding ratios.

Several representative examples of the stress vs strain responses obtained from 3D-DIC monitoring of the monotonic and cyclic biaxial diagonal tensile tests are presented. Nonetheless, data collection from the biaxial monotonic test to COM-01 was associated with several problems, so it was not possible to represent it. The biaxial monotonic response from FRM - 01, for the vertical solicitation, V1, and for the horizontal solicitation, H1, is presented in **Figure V.12**. The stress-strain responses,

show a clear change in the behaviour of the specimen, with much higher shear strain obtained for cycle H1 comparing to the first cycle V1. These can be explained by residual damage that is imposed in the horizontal direction when higher levels of deformation are imposed in the vertical direction.

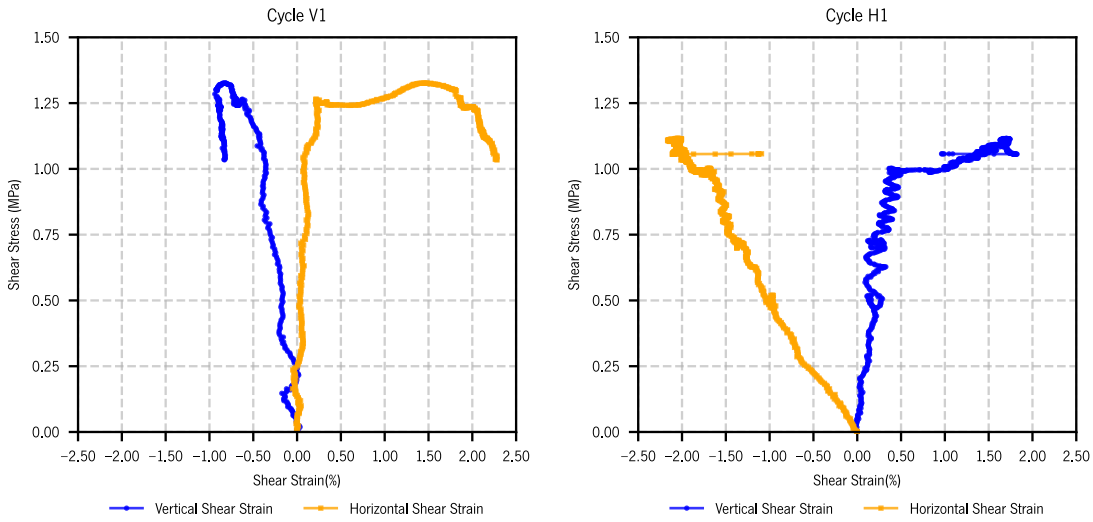
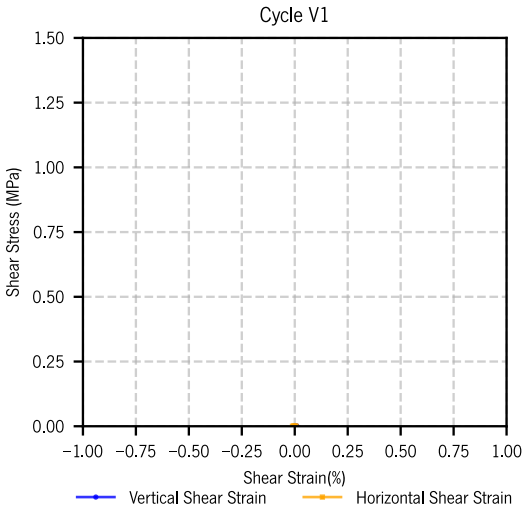
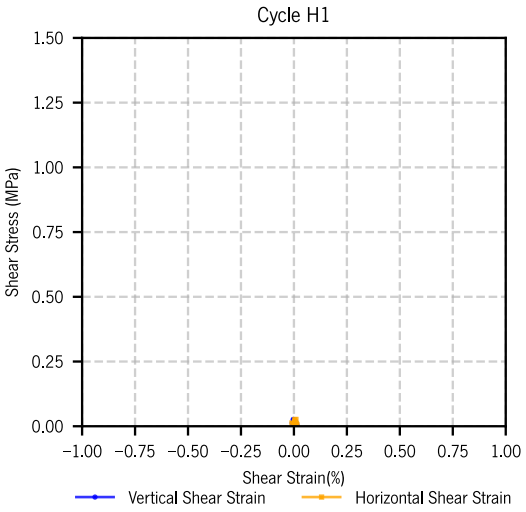
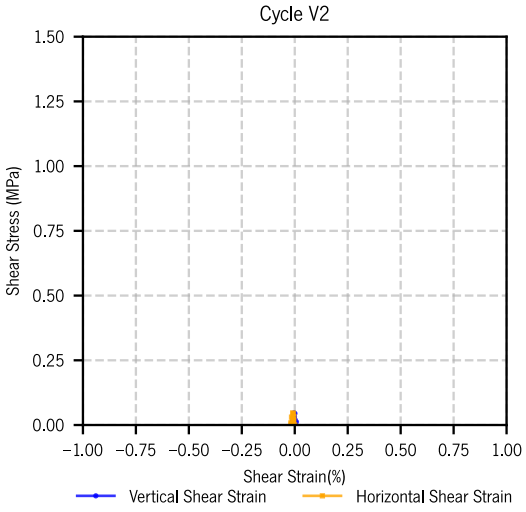


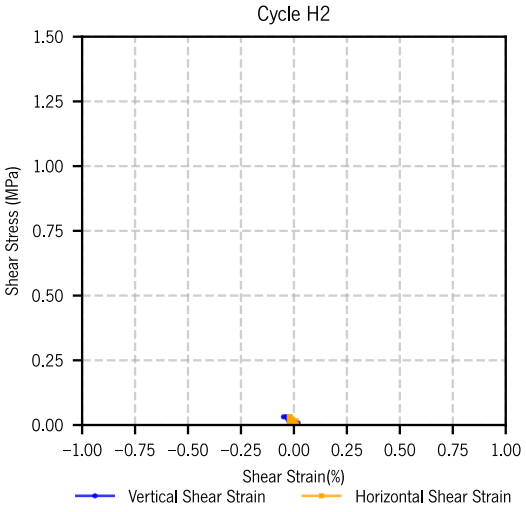
Figure V.12: Stress vs Strain curves obtained for the biaxial diagonal tests on specimen FRM - 01: vertical and horizontal strain for vertical and horizontal stages of the monotonic loading.

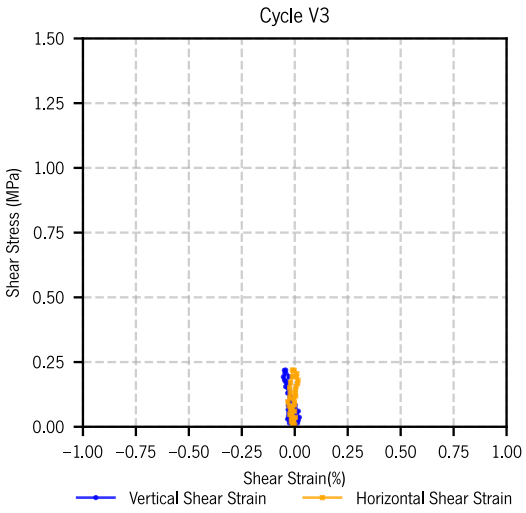
In **Figure V.13** and **Figure V.14** is presented the biaxial cyclic responses for COM-03 and FRM-03 respectively. The cyclic responses obtained for the initial cycles show small deformations and low shear stress, increasing the difficulty to assess the variation in stiffness. Nonetheless it is possible to evaluate the performance for each cycle to the COM and FRM strengthening systems. In both tests the strain measured in the direction of the applied load, associated with compressive stresses is bigger than the strain in the perpendicular direction, associated with tensile strains. When comparing the slope of the COM-03 and FRM-03 for Cycle V7 responses it is possible to infer that around the double strain is observed for COM-03, at the same level of shear stress.

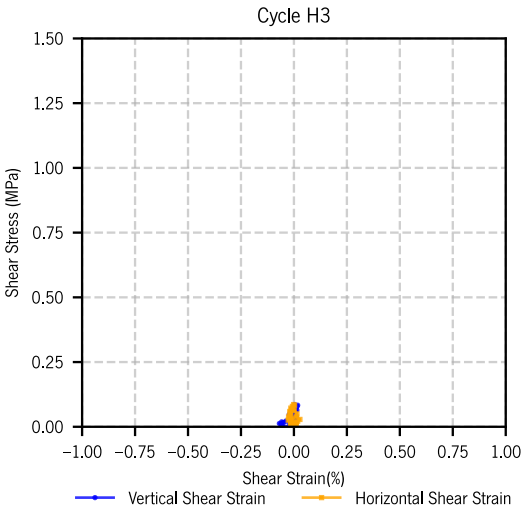

Cycle V1
Shear Stress (MPa)
Shear Strain(%)
Vertical Shear Strain
Horizontal Shear Strain

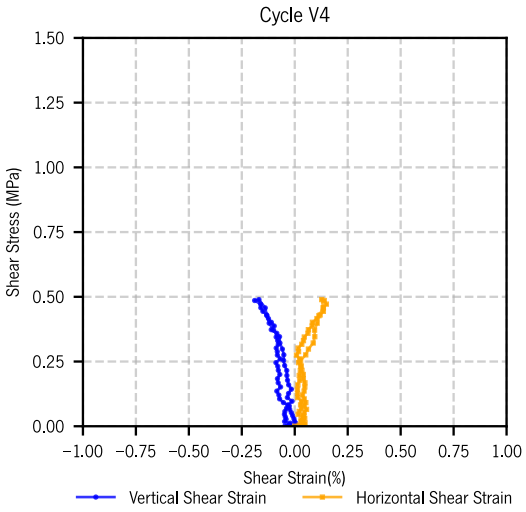

Cycle H1
Shear Stress (MPa)
Shear Strain(%)
Vertical Shear Strain
Horizontal Shear Strain

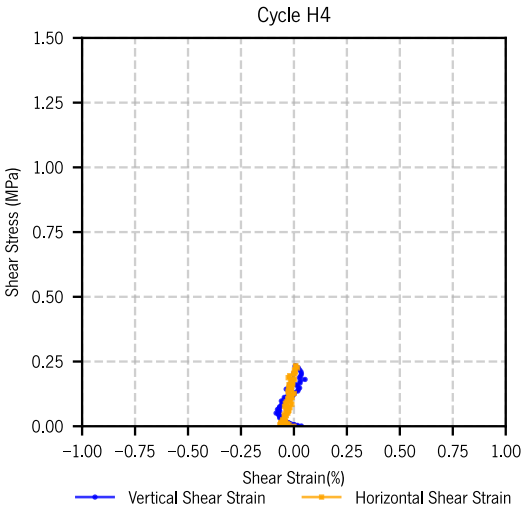

Cycle V2
Shear Stress (MPa)
Shear Strain(%)
Vertical Shear Strain
Horizontal Shear Strain

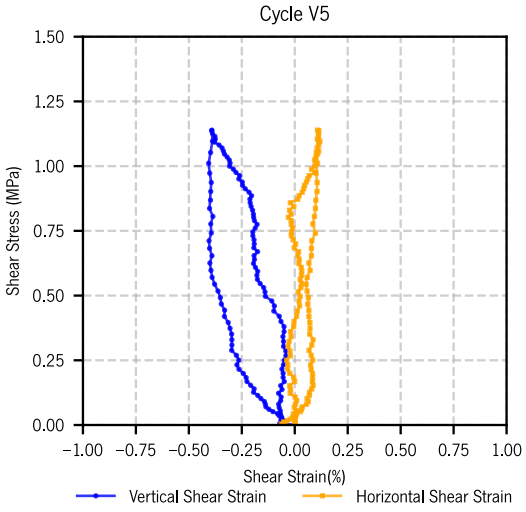

Cycle H2
Shear Stress (MPa)
Shear Strain(%)
Vertical Shear Strain
Horizontal Shear Strain

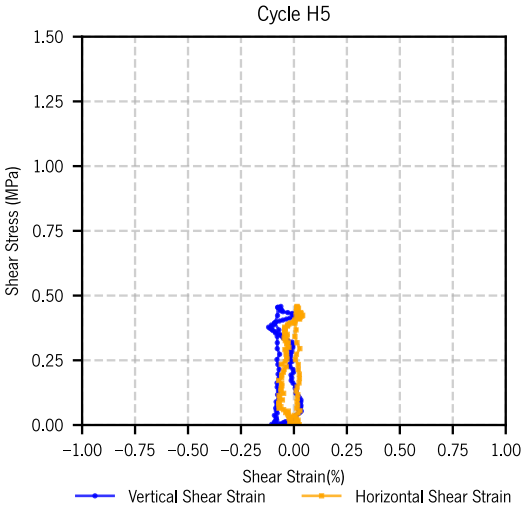

Cycle V3
Shear Stress (MPa)
Shear Strain(%)
Vertical Shear Strain
Horizontal Shear Strain

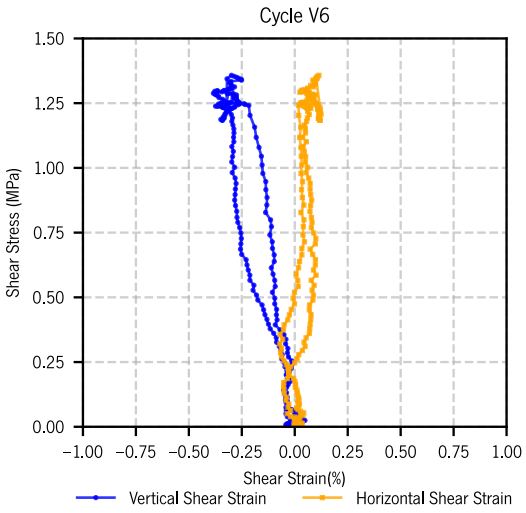

Cycle H3
Shear Stress (MPa)
Shear Strain(%)
Vertical Shear Strain
Horizontal Shear Strain

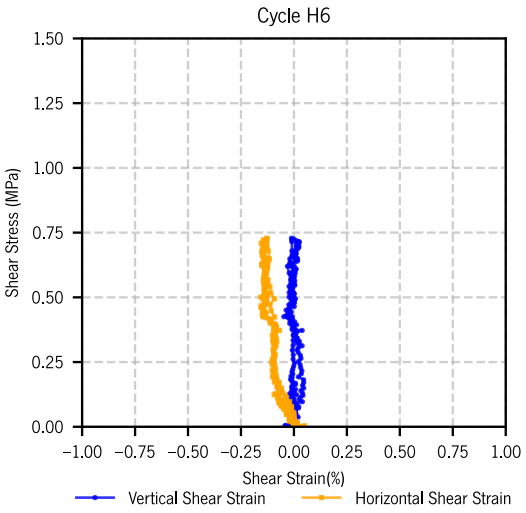

Cycle V4
Shear Stress (MPa)
Shear Strain(%)
Vertical Shear Strain
Horizontal Shear Strain


Cycle H4
Shear Stress (MPa)
Shear Strain(%)
Vertical Shear Strain
Horizontal Shear Strain


Cycle V5
Shear Stress (MPa)
Shear Strain(%)
Vertical Shear Strain
Horizontal Shear Strain


Cycle H5
Shear Stress (MPa)
Shear Strain(%)
Vertical Shear Strain
Horizontal Shear Strain


Cycle V6
Shear Stress (MPa)
Shear Strain(%)
Vertical Shear Strain
Horizontal Shear Strain


Cycle H6
Shear Stress (MPa)
Shear Strain(%)
Vertical Shear Strain
Horizontal Shear Strain

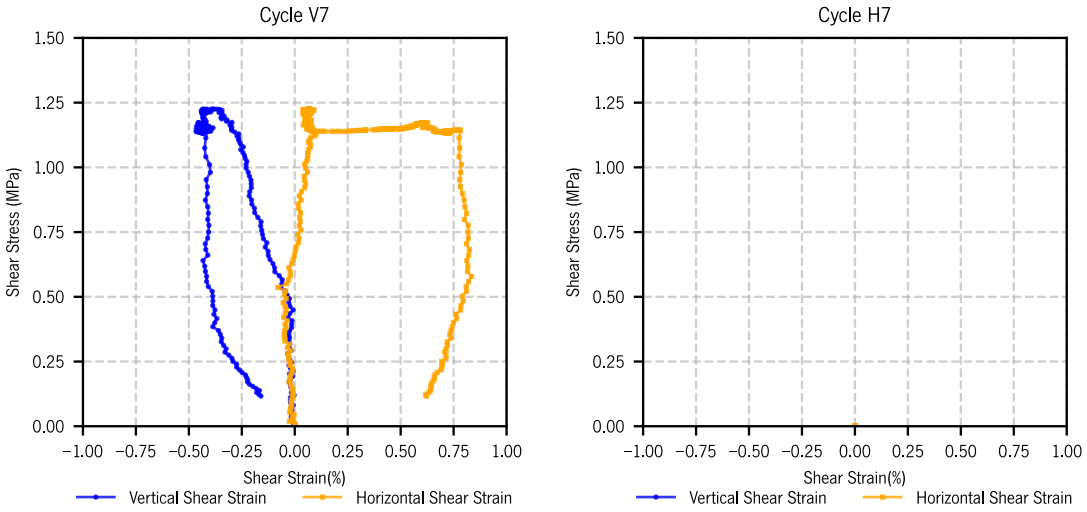
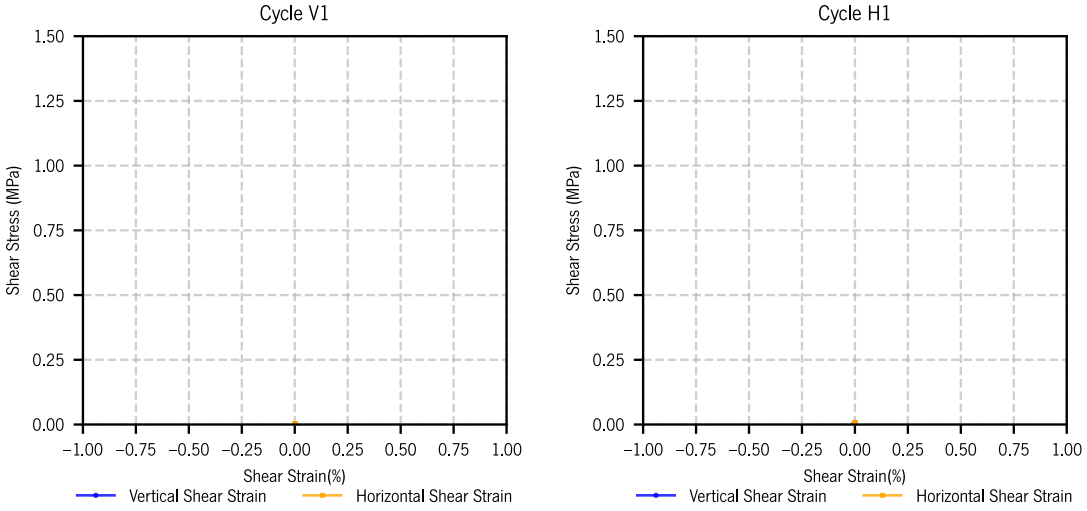
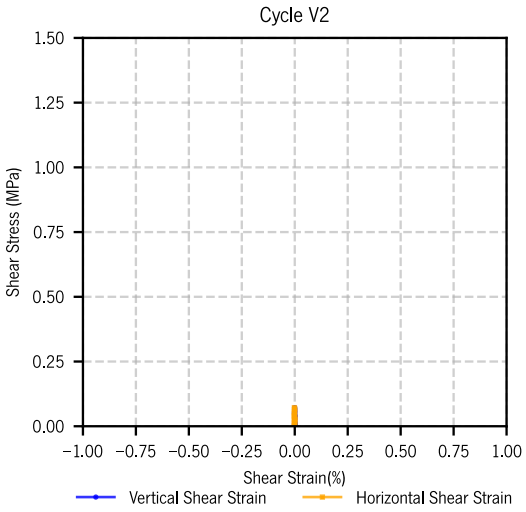
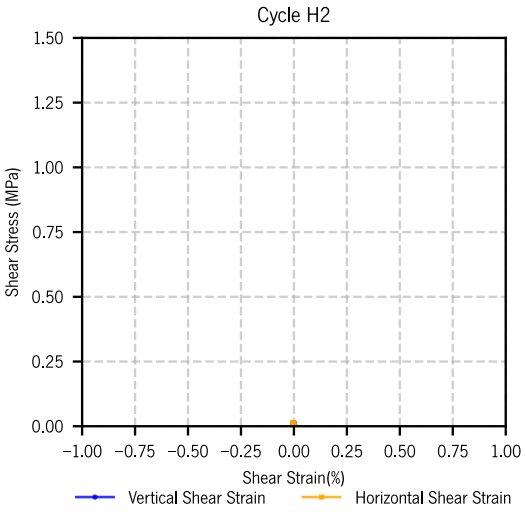
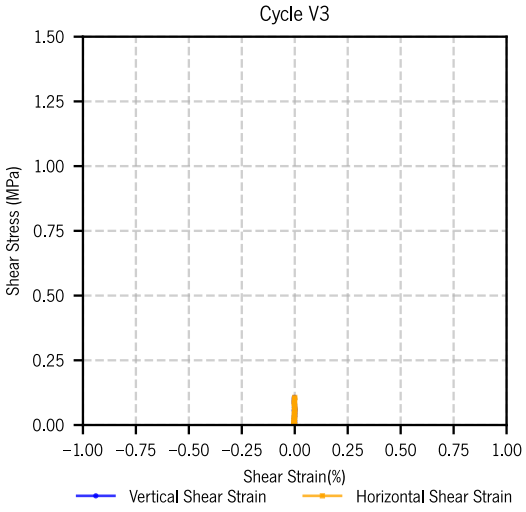


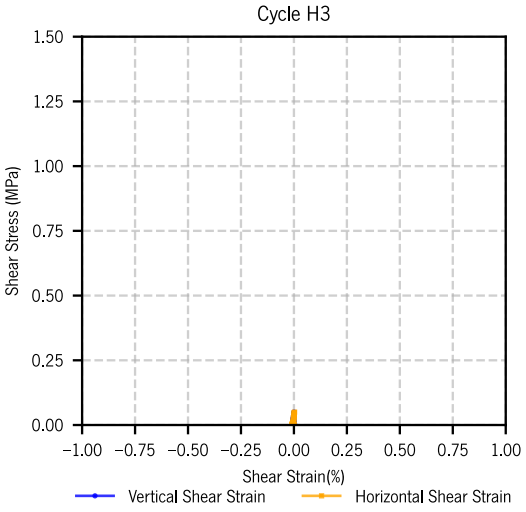
Figure V.13: Stress vs Strain curves obtained for the biaxial cyclic diagonal tests on specimen COM - 03: vertical and horizontal strain for each cycle.

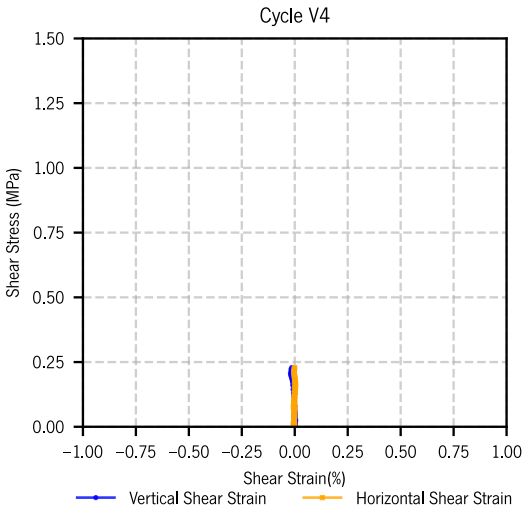


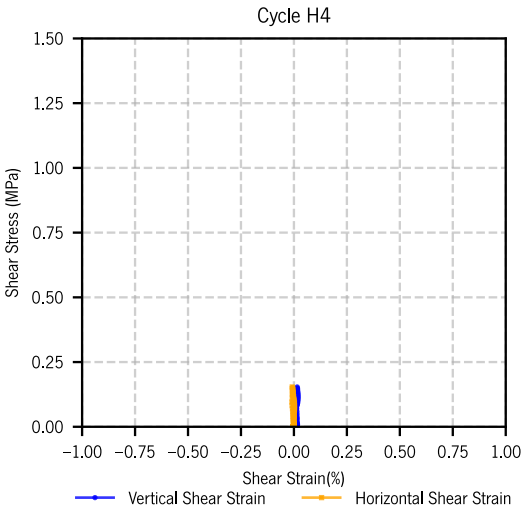

Cycle V2
Shear Stress (MPa)
Shear Strain(%)
Vertical Shear Strain
Horizontal Shear Strain

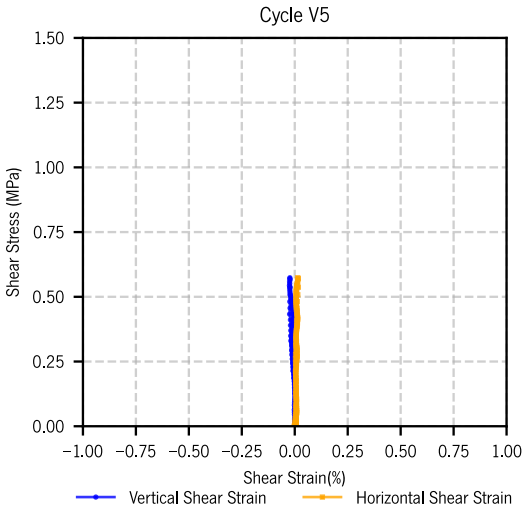

Cycle H2
Shear Stress (MPa)
Shear Strain(%)
Vertical Shear Strain
Horizontal Shear Strain

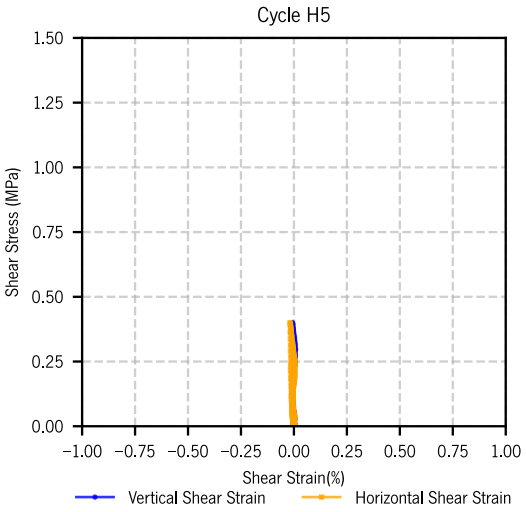

Cycle V3
Shear Stress (MPa)
Shear Strain(%)
Vertical Shear Strain
Horizontal Shear Strain

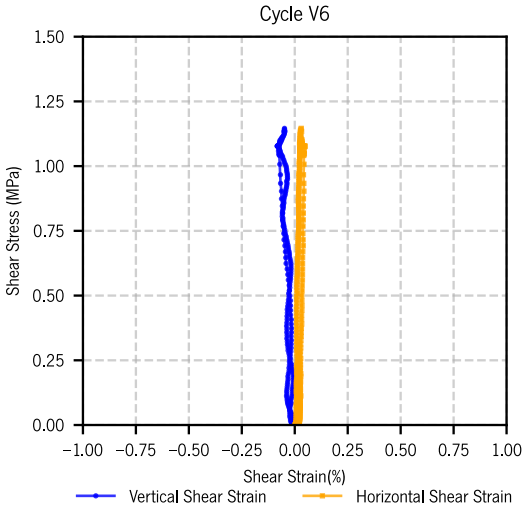

Cycle H3
Shear Stress (MPa)
Shear Strain(%)
Vertical Shear Strain
Horizontal Shear Strain

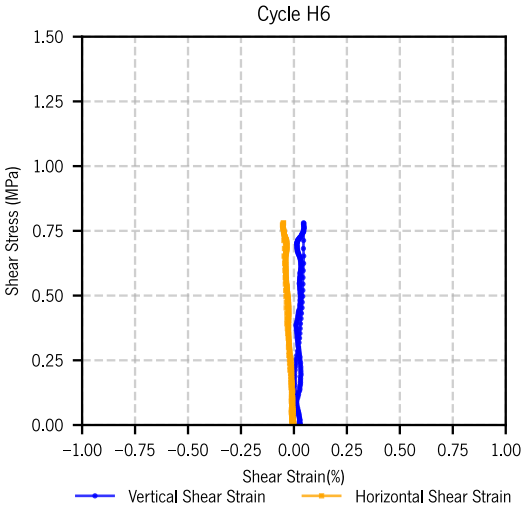

Cycle V4
Shear Stress (MPa)
Shear Strain(%)
Vertical Shear Strain
Horizontal Shear Strain

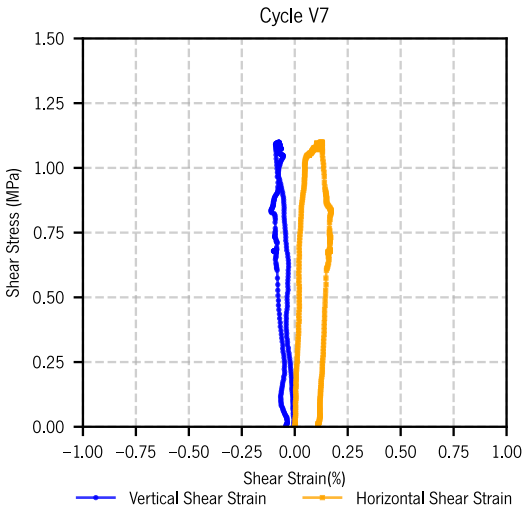

Cycle H4
Shear Stress (MPa)
Shear Strain(%)
Vertical Shear Strain
Horizontal Shear Strain


Cycle V5
Shear Stress (MPa)
Shear Strain(%)
Vertical Shear Strain
Horizontal Shear Strain


Cycle H5
Shear Stress (MPa)
Shear Strain(%)
Vertical Shear Strain
Horizontal Shear Strain


Cycle V6
Shear Stress (MPa)
Shear Strain(%)
Vertical Shear Strain
Horizontal Shear Strain


Cycle H6
Shear Stress (MPa)
Shear Strain(%)
Vertical Shear Strain
Horizontal Shear Strain


Cycle V7
Shear Stress (MPa)
Shear Strain(%)
Vertical Shear Strain
Horizontal Shear Strain

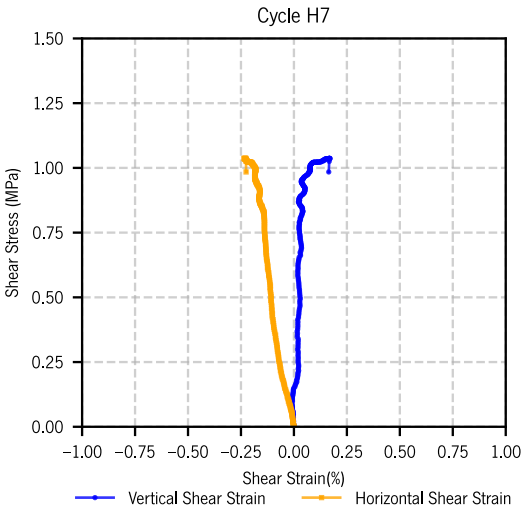

Cycle H7
Shear Stress (MPa)
Shear Strain(%)
Vertical Shear Strain
Horizontal Shear Strain

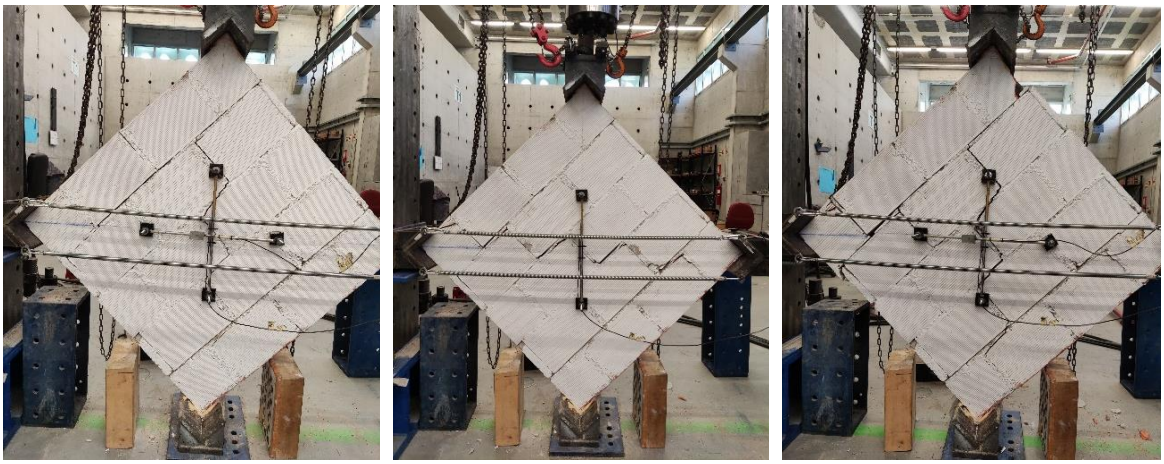
Figure V.14: Stress vs strain responses obtained for the biaxial cyclic diagonal tests of specimen FRM - 03: vertical (V1 to V7)) and horizontal (H1 to H7) strains vs stress obtained for loading cycles 1 to 7.

4.2.1 Crack patterns and failure modes

In the case of unreinforced specimens, the cracking patterns were clearly visible to the naked eye. In the case of reinforced specimens, the cracking process tends to be more controlled by the reinforcement and is therefore more complex and more interesting to analyse, helping to understand the efficiency of the strengthening system. For this reason, in the case of the strengthened specimens, COM and FRM, it was decided to use the 2D-DIC system to evaluate the evolution of cracking on the surface of the specimens. To do this, the stochastic pattern was applied, and the test sequences were photographed, then the images were reconstructed and processed in order to visualise the deformations and the evolution of the cracking processes.

The observed crack patterns clearly differ among the different types of specimens. The most common pattern for URM specimens comprised the development of one diagonal crack, in the direction of the load, following the path of the masonry joints, see **Figure V.15a)**. The same type of pattern developed when the horizontal cycle was applied, **Figure V.15b)**. At a later stage of the test, 6th vertical cycle, it was possible to observe the level of damage as a result of the imposed deformation **Figure V.15c)**. The specimens where one layer of rendering mortar was applied, URMR, showed different crack patterns, see **Figure V.16a)**, where cracks were not strictly following the mortar joints but presenting some straight segments. Nonetheless, for higher levels of damage the pattern tended to follow the mortar joints, as shown in **Figure V.16b)**. The strengthened specimens, COM and FRM, show an even more evident influence of the addition of layers of strengthening materials to the original masonry, with the crack pattern originally following the mortar joint being unidentifiable. Instead, as shown in **Figure V.17** and **Figure V.18**, the main crack formed in the specimens presents a straight-line shaped pattern. In the case of FRM-02 specimen, the crack pattern obtained when the peak load of the vertical monotonic loading cycle is reached (see point a in **Figure V.9**) presents multiple parallel straight open cracks, as shown in **Figure V.14a)**. These cracks tend to close once the horizontal loading cycle is started and point b in **Figure V.9** is reached. **Figure V.14b)** shows the crack pattern obtained at this stage using DIC. At a later phase of the horizontal loading cycle the horizontal load gradually increases until the peak load is reached, see point c in **Figure V.9**. During this stage the diagonal cracks initiate and grow in the horizontal diagonal of the specimen, see **Figure V.14c)**.

When the COM strengthening system is analysed, an essentially similar crack pattern is obtained, as shown in **Figure V.15**. When the maximum displacement of the 5th vertical cycle is reached, represented by point a in **Figure V.10**, it is possible to observe a straight crack fully formed and connecting the vertical supports, as shown in **Figure V.15a)**. This crack closes when unloading occurs and the 5th horizontal cycle starts. At this stage a new crack forms and completely connects the horizontal supports when the peak load of the corresponding cycle is attained, see point b in **Figure V.10** and **Figure V.15b)**. At the peak of the last vertical cycle, represented by point c in **Figure V.10**, the vertical cracks open again and further extend, revealing a higher level of damage, as shown in **Figure V.15c)**.



a) b) c)

Figure V.15: Cracking evolution at the surface of URM-01: crack pattern after 5th vertical loading cycle; b) crack pattern after 5th horizontal loading cycle; c) crack pattern after 6th and last vertical loading cycle.



a) b)

Figure V.16: Cracking evolution at the surface of URMR specimen: crack pattern at peak load of 5th vertical loading cycle; b) pattern at the peak load of the 5th horizontal loading cycle.

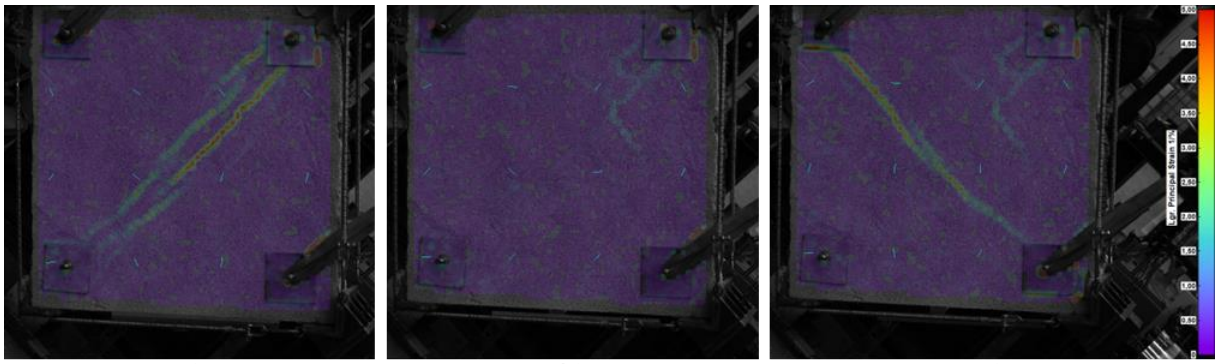


Figure V.17: Evolution of the crack pattern of FRM-02 specimen: a) pattern at the peak load of the vertical monotonic solicitation; b) pattern at the onset of the monotonic horizontal loading cycle; c) pattern at the peak load of the horizontal loading cycle.

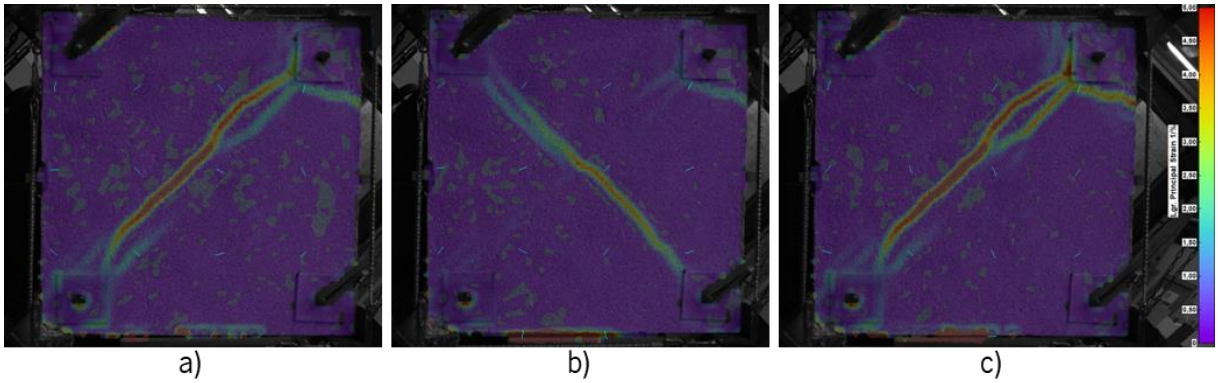


Figure V.18: Evolution of the crack pattern of COM-03 specimen obtained with DIC: a) crack pattern at the peak load of the 5th vertical loading cycle; b) crack pattern at the peak load of the 5th horizontal loading cycle; c) crack pattern at the peak load of the 6th vertical loading cycle.

In general the main failure mode observed for plain masonry, URM, and for the rendered masonry specimens, URMR, was determined by the diagonal tensile stresses exceeding the diagonal tensile strength of the masonry with or without rendering. For the URM specimens the failure occurred between supports, and the failure tensile crack followed the brick joints. In the case of URMR specimens the failure occurred in a similar fashion, despite the contribution of the rendering for increasing the stiffness of the specimens. The influence of the strengthening systems was clearly visible when observing the failure modes of COM and FRM specimens. First some crushing of the masonry units occurred next to the supports, due to the higher stiffness and strength conferred by the strengthening systems and consequently the higher loads reached. At a later stage failure was reached

due to excessive diagonal tensile stresses at the middle of the specimens, and finally due to the development of severe damage of the bricks at inner part of the specimens.

4.2.2 Evolution of crack opening

The evolution of the crack opening was evaluated for both types of strengthening solutions, COM and FRM, using the data obtained from the 2D-DIC analysis. The crack opening evolution vs timestep for the monotonic tests is shown in **Figure V.19** and **Figure V.20**. Each step represents a time interval of 10 s. In the monotonic tests, compressive deformation starts to be imposed in the vertical direction at a displacement rate of 0.01 mm/s. Initially the crack opening (crack_v1) is not evolving, but once it initiates the opening increases at a fast pace, until the maximum vertical load is reach (Fv_max) and unloading takes place. In a second stage, compressive deformation starts to be imposed in the horizontal direction at a displacement rate of 0.01 mm/s. First the deformation imposed to the specimen is translated into the closing of the vertical crack. Once this process is finished, compressive load starts to increase and a few stages later the horizontal crack (crack_h1) initiates and opens fast, until the maximum horizontal load is reached (Fh_max) and unloading initiates. Representative results of the last cycles of the biaxial tests performed in COM-03 and FRM-03 are shown in **Figure V.21** and **Figure V.22**, respectively. Given the cyclic nature of the imposed displacement, the behaviour obtained in the monotonic test was emulated, however bigger crack openings were observed only after several cycles.

In all cases the step at which the maximum load for vertical and horizontal cycles was reached is identified, and the obtained values are compiled in **Table V.4**. The crack opening values at maximum load obtained for COM system varied between 0.41 and 1.48 mm, while for FRM system it varied between 0.02 and 0.67 mm. When analysing the results obtained for the monotonic tests, a lower difference can be observed between the crack opening responses of the vertical and horizontal loading cycles, when comparing to the cyclic test results. This effect can be explained by the accumulated damage occurring during the previous loading cycles. For example, for specimen FRM-03 and during the horizontal cycle number 7, the crack opening reached 0.80 mm at a lower maximum load. The accumulation of damage translates into higher heterogeneity between the loading responses observed in both loading directions, since localization initiates earlier at lower loading levels.

Table V.4: Results from the biaxial cyclic diagonal compressive tests.

Specimen	Cycle	Crack_id	Vertical cycle Load (kN)	Vertical cycle Crack opening (mm)	Horizontal cycle Load (kN)	Horizontal cycle Crack opening (mm)
COM-01	1	Crack_h1	**139.70**	0.10	**148.00**	**0.59**
		Crack_v1		**0.41**		-0.03
FRM-01	1	Crack_h1	**182.30**	-0.03	**152.20**	**0.67**
		Crack_v1		**0.02**		0.01
		Crack_v2		**0.66**		0.01
COM-03	5	Crack_h1	110.90	-0.02	**65.00**	**0.80**
		Crack_v1		1.37		0.01
	6	Crack_h1	**159.40**	0.03	--	--
		Crack_v1		**1.48**	--	--
FRM-03	6	Crack_h1	115.10	-0.03	**79.80**	**0.04**
		Crack_v1		0.10		0.02
	7	Crack_h1	**126.90**	-0.04	64.40	0.80
		Crack_v1		**0.22**		-0.01

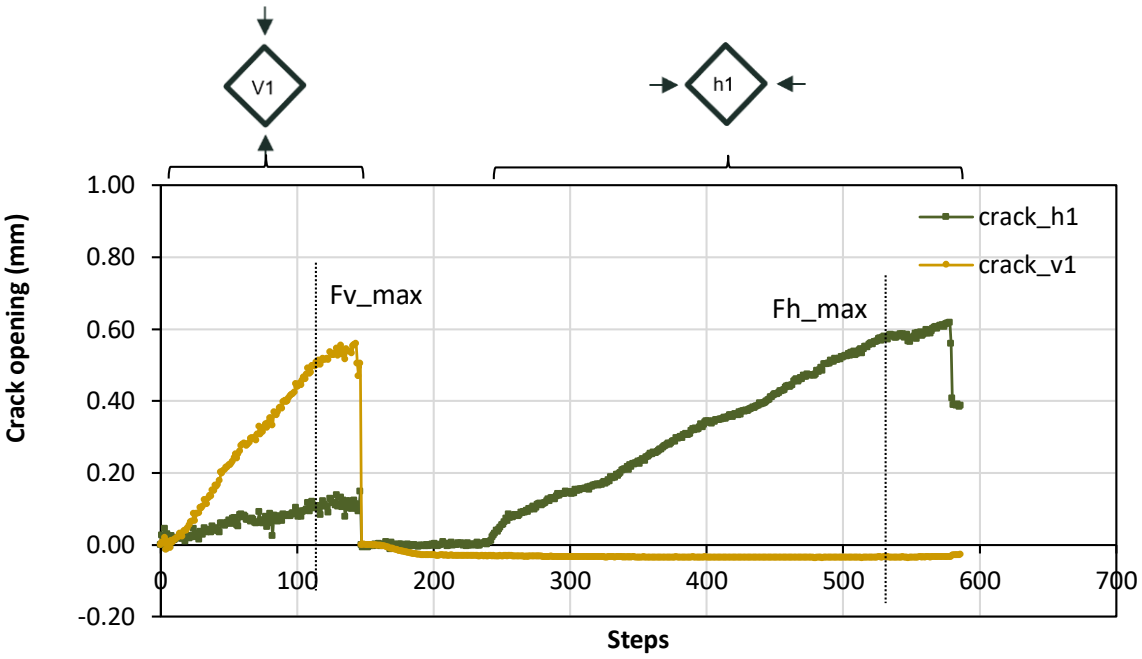


Figure V.19: Crack opening evolution from monotonic test to COM-01.

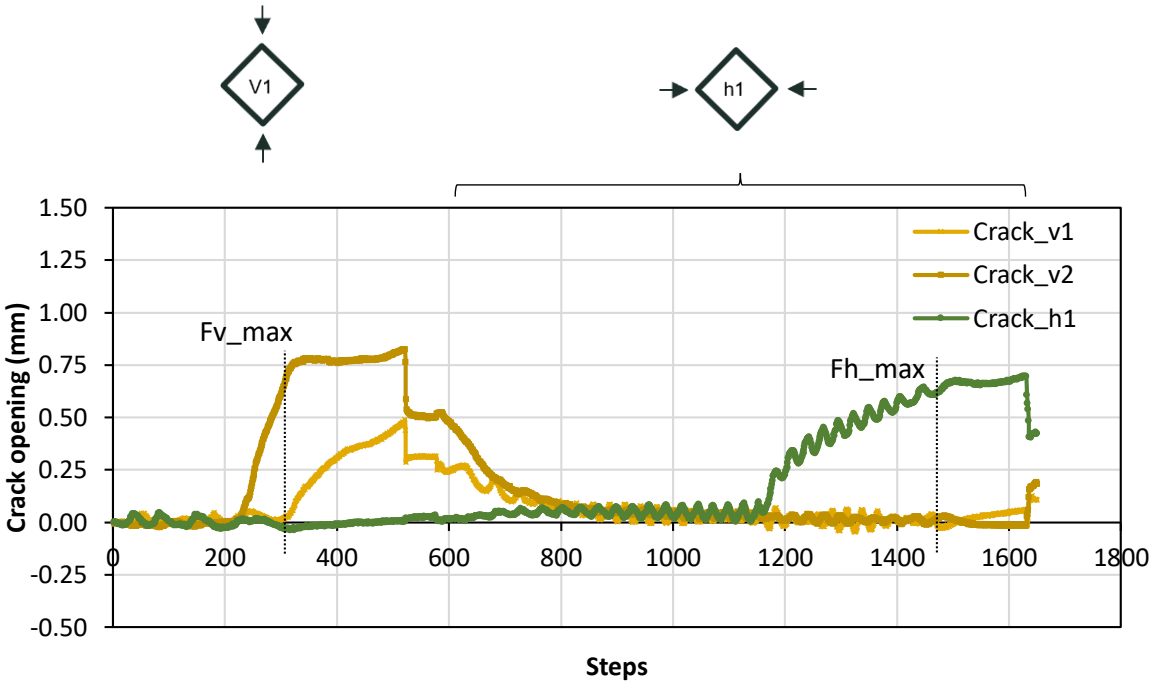


Figure V.20: Crack opening evolution from monotonic test to FRM-01.

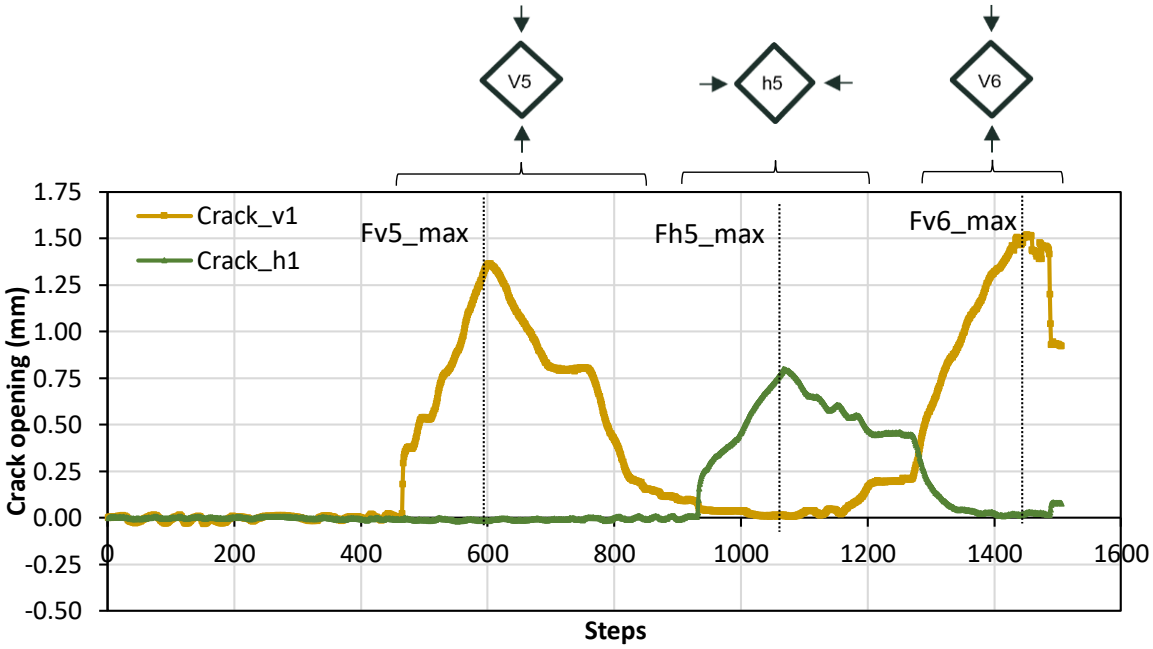


Figure V.21: Crack opening evolution from cyclic test to COM-03, only the last two vertical cycles and the last horizontal cycle are represented.

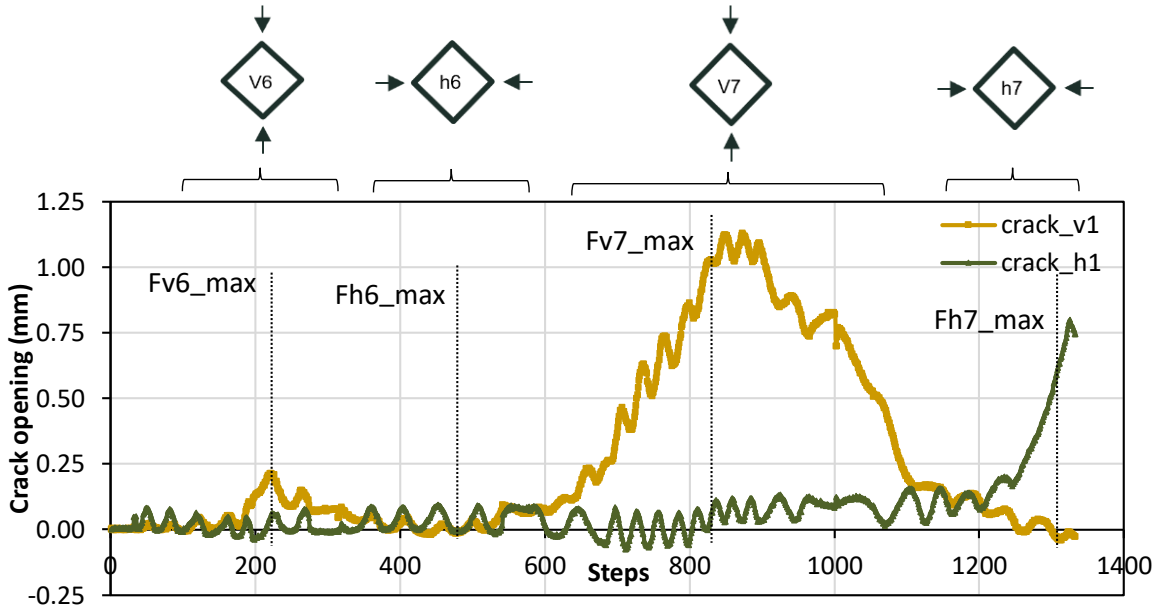


Figure V.22: Crack opening evolution from cyclic test to FRM-03, only the last two vertical and horizontal cycles are represented.

5 CONCLUSIONS

The mechanical performance and behaviour of masonry elements strengthened with externally applied fibre-reinforced mortar (FRM) overlays were evaluated using a biaxial diagonal tensile testing methodology. This experimental approach proved to be a practical and efficient means of characterizing masonry under loading conditions representative of those encountered in real-world scenarios. The study focused on the effects of cyclic loading applied along both diagonals, providing insight into the cumulative impact of multiaxial displacements on the degradation of structural capacity.

The investigation encompassed a comparative analysis of various masonry configurations, including unreinforced (plain) masonry, masonry with a render layer, and masonry strengthened with two different textile-reinforced mortar (TRM) systems—FRM and COM. The key findings from this work are as follows:

- Applying a render layer to plain masonry effectively doubled the compressive strength of the specimens, increasing it from 0.98 MPa to 1.92 MPa. Further enhancements were observed with the strengthening systems: FRM led to a 24% increase, while COM achieved a 59% increase in compressive strength relative to rendered masonry.

- The biaxial cyclic diagonal tensile test setup demonstrated its effectiveness in assessing the shear performance of masonry. The maximum shear capacity rose from 0.37 MPa in plain masonry to 0.97 MPa in rendered specimens. With the incorporation of strengthening systems, additional gains were recorded, 23% for COM and 18% for FRM.
- The use of Digital Image Correlation (DIC) provided a detailed visual record of crack evolution and failure mechanisms. Distinct differences were observed between unreinforced and strengthened specimens: cracks in plain masonry typically followed mortar joints, whereas strengthened elements exhibited more linear, vertical or diagonal crack paths indicative of altered stress distribution and improved confinement.

Future research should focus on enhancing the test setup to ensure more uniform stiffness along both loading directions. One potential improvement involves the use of a Dywidag bar system placed along both diagonals to connect actuators with fixed supports. This configuration would allow for better control of the loading regime and provide a stable platform to impose asymmetrical cyclic displacements. Such refinements would enable a more precise evaluation of multiaxial failure surfaces and further our understanding of TRM system behaviour under complex loading conditions. Ultimately, these improvements would enhance the robustness and applicability of this experimental approach in the seismic assessment and strengthening of masonry structures.

References

[1] S. De Santis, P. Casadei, G. De Canio, G. De Felice, M. Malena, M. Mongelli, I. Roselli, Seismic performance of masonry walls retrofitted with steel reinforced grout, Earthquake Engng Struct. Dyn 45 (2016) 229–251. https://doi.org/10.1002/eqe.2625.

[2] G. Maddaloni, M. Di Ludovico, A. Balsamo, G. Maddaloni, A. Prota, Dynamic assessment of innovative retrofit techniques for masonry buildings, Compos B Eng 147 (2018). https://doi.org/10.1016/j.compositesb.2018.04.038.

[3] B. Ghiassi, Mechanics and durability of textile reinforced mortars: A review of recent advances and open issues, RILEM Technical Letters 4 (2019). https://doi.org/10.21809/rilemtechlett.2019.99.

[4] F. Akhoundi, G. Vasconcelos, P. Lourenço, L.M. Silva, F. Cunha, R. Fangueiro, In-plane behavior of cavity masonry infills and strengthening with textile reinforced mortar, Eng Struct 156 (2018) 145–160. https://doi.org/10.1016/j.engstruct.2017.11.002.

[5] J. Donnini, G. Maracchini, S. Lenci, V. Corinaldesi, E. Quagliarini, TRM reinforced tuff and fired clay brick masonry: Experimental and analytical investigation on their in-plane and out-of-plane behavior, Constr Build Mater 272 (2021). https://doi.org/10.1016/j.conbuildmat.2020.121643.

[6] T.D. Krevaikas, Experimental study on carbon fiber textile reinforced mortar system as a means for confinement of masonry columns, (2019). https://doi.org/10.1016/j.conbuildmat.2019.03.033.

[7] Z. Dong, M. Deng, J. Dai, P. Ma, Diagonal compressive behavior of unreinforced masonry walls strengthened with textile reinforced mortar added with short PVA fibers, Eng Struct 246 (2021). https://doi.org/10.1016/J.ENGSTRUCT.2021.113034.

[8] E. Bertolesi, G. Milani, Diagonal Compressive Tests on Double Wythe Brick Ancient Masonry Panels Unreinforced and Reinforced with Innovative Cement Based Materials: Advanced FE Simulations, RILEM Bookseries 18 (2019) 1000–1008. https://doi.org/10.1007/978-3-319-99441-3_108.

[9] A. Bustos-García, E. Moreno-Fernández, R. Zavalis, J. Valivonis, Diagonal compression tests on masonry wallets coated with mortars reinforced with glass fibers, Materials and Structures/Materiaux et Constructions 52 (2019). https://doi.org/10.1617/s11527-019-1360-y.

[10] S.S. Lucchini, L. Facconi, F. Minelli, G. Plizzari, Retrofitting unreinforced masonry by steel fiber reinforced mortar coating: uniaxial and diagonal compression tests, Materials and Structures/Materiaux et Constructions 53 (2020) 1–22. https://doi.org/10.1617/S11527-020-01574-W/FIGURES/12.

[11] P.E. Mezrea, M. Ispir, I.A. Balci, I.E. Bal, A. Ilki, Diagonal tensile tests on historical brick masonry wallets strengthened with fabric reinforced cementitious mortar, Structures 33 (2021) 935–946. https://doi.org/10.1016/J.ISTRUC.2021.04.076.

[12] N. Gattesco, I. Boem, A. Dudine, Diagonal compression tests on masonry walls strengthened with a GFRP mesh reinforced mortar coating, Bulletin of Earthquake Engineering (2014) 1–24. https://doi.org/10.1007/s10518-014-9684-z.

[13] A. Borri, G. Castori, M. Corradi, E. Speranzini, Shear behavior of unreinforced and reinforced masonry panels subjected to in situ diagonal compression tests, Constr Build Mater 25 (2011) 4403–4414. https://doi.org/10.1016/j.conbuildmat.2011.01.009.

[14] G. Ferrara, C. Caggegi, E. Martinelli, A. Gabor, Shear capacity of masonry walls externally strengthened using Flax-TRM composite systems: experimental tests and comparative assessment, Constr Build Mater 261 (2020). https://doi.org/10.1016/J.CONBUILDMAT.2020.120490.

[15] F.F.S. Pinho, V.J.G. Lúcio, M.F.C. Baião, Rubble stone masonry walls in Portugal strengthened with reinforced micro-concrete layers, Bulletin of Earthquake Engineering 10 (2011) 161–180. https://doi.org/10.1007/s10518-011-9280-4.

[16] C.G. Papanicolaou, T.C. Triantafillou, K. Karlos, M. Papathanasiou, Textile-reinforced mortar (TRM) versus FRP as strengthening material of URM walls : in-plane cyclic loading, Mater Struct 40 (2007) 1081–1097. https://doi.org/10.1617/s11527-006-9207-8.

[17] L. Garcia-Ramonda, L. Pelà, P. Roca, G. Camata, Experimental and numerical insights on the in-plane behaviour of unreinforced and TRM/SRG retrofitted brick masonry walls by diagonal compression and shear-compression testing, Constr Build Mater 402 (2023) 132997. https://doi.org/10.1016/J.CONBUILDMAT.2023.132997.

[18] P. Meriggi, C. Caggegi, A. Gabor, G. de Felice, Shear-compression tests on stone masonry walls strengthened with basalt textile reinforced mortar (TRM), Constr Build Mater 316 (2022) 125804. https://doi.org/10.1016/J.CONBUILDMAT.2021.125804.

[19] M. Ponte, A. Penna, R. Bento, In-plane cyclic tests of strengthened rubble stone masonry, Materials and Structures/Materiaux et Constructions 56 (2023) 1–18. https://doi.org/10.1617/S11527-023-02126-8/TABLES/5.

[20] B. Silva, M. Dalla Benetta, F. da Porto, C. Modena, Experimental assessment of in-plane behaviour of three-leaf stone masonry walls, Constr Build Mater 53 (2014) 149–161. https://doi.org/10.1016/j.conbuildmat.2013.11.084.

[21] J. Milosevic, A.S. Gago, M. Lopes, R. Bento, Experimental assessment of shear strength parameters on rubble stone masonry specimens, Constr Build Mater 47 (2013) 1372–1380. https://doi.org/10.1016/j.conbuildmat.2013.06.036.

[22] A. Brignola, S. Frumento, S. Lagomarsino, S. Podestà, Identification of Shear Parameters of Masonry Panels Through the In-Situ Diagonal Compression Test, International Journal of Architectural Heritage 3 (2008) 52–73. https://doi.org/10.1080/15583050802138634.

[23] A. Dehghani, G. Fischer, F. Alahi, Strengthening masonry infill panels using engineered cementitious composites, Mater Struct (2013). https://doi.org/10.1617/s11527-013-0176-4.

[24] J. Almeida, E. Pereira, J. Barros, Performance assessment of overlay strengthened masonry under cyclic loading using the diagonal tensile test, in: 9th International Masonry Conference, July 7, 8, 9; Guimarães, Guimarães, 2014: pp. 1–12.

[25] A. Dalalbashi, B. Ghiassi, D. V. Oliveira, In-Plane Behavior of Clay Brick Masonry Wallets Strengthened by TRM System, in: RILEM Bookseries, 2022: pp. 143–151. https://doi.org/10.1007/978-3-030-76465-4_13.

[26] M. Angiolilli, A. Gregori, S. Cattari, Performance of Fiber Reinforced Mortar coating for irregular stone masonry: Experimental and analytical investigations, Constr Build Mater 294 (2021). https://doi.org/10.1016/J.CONBUILDMAT.2021.123508.

[27] H. Santa-Maria, G. Duarte, A. Garib, Experimental Investigation of masonry panels externally strengthened with CFRPlaminates and fabric subjected to in-plane shear load, in: 13th World Conference on Earthquake Engineering, Vancouver, B.C., Canada, 2004.

[28] J.A.P.P. Almeida, E.B. Pereira, J.A.O. Barros, Assessment of overlay masonry strengthening system under in-plane monotonic and cyclic loading using the diagonal tensile test, Constr Build Mater 94 (2015) 851–865. https://doi.org/10.1016/J.CONBUILDMAT.2015.07.040.

[29] G. Vasconcelos, P.B. Lourenço, Experimental characterization of stone masonry in shear and compression, Constr Build Mater 23 (2009) 3337–3345. https://doi.org/10.1016/j.conbuildmat.2009.06.045.

[30] A. Furtado, H. Rodrigues, A. Arêde, H. Varum, Influence of the In-Plane and Out-of-Plane Masonry Infill Walls' Interaction in the Structural Response of RC Buildings, Procedia Eng 114 (2015) 722–729. https://doi.org/10.1016/J.PROENG.2015.08.016.

[31] A. Furtado, H. Rodrigues, A. Arêde, H. Varum, Experimental evaluation of out-of-plane capacity of masonry infill walls, Eng Struct 111 (2016) 48–63. https://doi.org/10.1016/j.engstruct.2015.12.013.

[32] G. Brandonisio, E. Mele, A. De Luca, Some considerations on out-of-plane collapse modes of masonry walls, (2008) 565–573.

[33] T.T. Bui, A. Limam, Out-of-plane behaviour of hollow concrete block masonry walls unstrengthened and strengthened with CFRP composite, Compos B Eng 67 (2014) 527–542. https://doi.org/10.1016/J.COMPOSITESB.2014.08.006.

[34] M. Di Domenico, P. Ricci, G.M. Verderame, Experimental Assessment of the Influence of Boundary Conditions on the Out-of-Plane Response of Unreinforced Masonry Infill Walls, Journal of Earthquake Engineering 24 (2020) 881–919. https://doi.org/10.1080/13632469.2018.1453411.

[35] F. Anić, D. Penava, L. Abrahamczyk, V. Sarhosis, A review of experimental and analytical studies on the out-of-plane behaviour of masonry infilled frames, 18 (2020) 2191–2246. https://doi.org/10.1007/s10518-019-00771-5.

[36] L. Sorrentino, D. D'Ayala, G. de Felice, M.C. Griffith, S. Lagomarsino, G. Magenes, Review of Out-of-Plane Seismic Assessment Techniques Applied To Existing Masonry Buildings, International Journal of Architectural Heritage 11 (2017) 2–21. https://doi.org/10.1080/15583058.2016.1237586.

[37] M.R. Valluzzi, F. da Porto, E. Garbin, M. Panizza, Out-of-plane behaviour of infill masonry panels strengthened with composite materials, Mater Struct 47 (2014) 2131–2145. https://doi.org/10.1617/s11527-014-0384-6.

[38] H. Derakhshan, D.Y. Dizhur, M.C. Griffith, J.M. Ingham, Seismic assessment of out-of-plane loaded unreinforced masonry walls in multi-storey buildings, Bulletin of the New Zealand Society for Earthquake Engineering 47 (2014) 119–138. https://doi.org/10.5459/bnzsee.47.2.119-138.

[39] Comité Européen de Normalisation, EN 772-1:2000 Methods of test for masonry units. Determination of compressive strength, (2000) 14.

[40] J.A.P.P. Almeida, E.N.B. Pereira, J.A.O. Barros, Hybrid Fibre Reinforced Mortar for masonry strengthening overlay, 2024.

[41] CEN, EN 1052-1 Methods of test for masonry - Part 1: Determination of compressive strength, (1998).

[42] American Society for Testing and Materials, E 519 – 02: Test Method for Diagonal Tension (Shear) in Masonry Assemblages, (2022). https://doi.org/10.1520/E0519_E0519M-22.

[43] M. Sutton, W. Wolters, W. Peters, W. Ranson, S. McNeill, Determination of displacements using an improved digital correlation method, Image Vis Comput 1 (1983) 133–139. https://doi.org/10.1016/0262-8856(83)90064-1.

[44] J. Holmes, S. Sommacal, R. Das, Z. Stachurski, P. Compston, Digital image and volume correlation for deformation and damage characterisation of fibre-reinforced composites: A review, Compos Struct 315 (2023) 116994. https://doi.org/10.1016/J.COMPSTRUCT.2023.116994.

[45] B. Torres, F.B. Varona, F.J. Baeza, D. Bru, S. Ivorra, Study on Retrofitted Masonry Elements under Shear Using Digital Image Correlation, Sensors 20 (2020) 2122. https://doi.org/10.3390/s20072122.